VOLUME 77 FEBRUARY 1, 1973 NUMBER 3

JPCHAx

THE JOURNAL OF PHYSICAL CHEMISTRY

PUBLISHED BIWEEKLY BY THE AMERICAN CHEMICAL SOCIETY

THE JOURNAL OF

PHYSICAL CHEMISTRY

BRYCE CRAWFORD, Jr., *Editor*
STEPHEN PRAGER, *Associate Editor*
ROBERT W. CARR, Jr., FREDERIC A. VAN-CATLEDGE, *Assistant Editors*

EDITORIAL BOARD: A. O. ALLEN (1970–1974), C. A. ANGELL (1973–1977), J. R. BOLTON (1971–1975), F. S. DAINTON (1972–1976), M. FIXMAN (1970–1974), H. S. FRANK (1970–1974), R. R. HENTZ (1972–1976), J. R. HUIZENGA (1969–1973), W. J. KAUZMANN (1969–1973), R. L. KAY (1972–1976), W. R. KRIGBAUM (1969–1973), W. J. MOORE (1969–1973), R. M. NOYES (1973–1977), J. A. POPLE (1971–1975), B. S. RABINOVITCH (1971–1975), H. REISS (1970–1974), S. A. RICE (1969–1975), F. S. ROWLAND (1973–1977), R. L. SCOTT (1973–1977); W. A. ZISMAN (1972–1976)

AMERICAN CHEMICAL SOCIETY, *1155 Sixteenth St., N.W., Washington, D. C. 20036*

Books and Journals Division

JOHN K CRUM *Director*
RUTH REYNARD *Assistant to the Director*

CHARLES R. BERTSCH *Head, Editorial Processing Department*
D. H. MICHAEL BOWEN *Head, Journals Department*
BACIL GUILEY *Head, Graphics and Production Department*
SELDON W. TERRANT *Head, Research and Development Department*

©Copyright, 1973, by the American Chemical Society. Published biweekly by the American Chemical Society at 20th and Northampton Sts., Easton, Pa. 18042. Second-class postage paid at Washington, D. C., and at additional mailing offices.

All manuscripts should be sent to *The Journal of Physical Chemistry*, Department of Chemistry, University of Minnesota, Minneapolis, Minn. 55455.

Additions and Corrections are published once yearly in the final issue. See Volume 76, Number 26 for the proper form.

Extensive or unusual alterations in an article after it has been set in type are made at the author's expense, and it is understood that by requesting such alterations the author agrees to defray the cost thereof.

The American Chemical Society and the Editor of *The Journal of Physical Chemistry* assume no responsibility for the statements and opinions advanced by contributors.

Correspondence regarding accepted copy, proofs, and reprints should be directed to Editorial Processing Department, American Chemical Society, 20th and Northampton Sts., Easton, Pa. 18042. Head: CHARLES R. BERTSCH. Assistant Editor: EDWARD A. BORGER. Editorial Assistant: JOSEPH E. YURVATI.

Advertising Office: Centcom, Ltd., 142 East Avenue, Norwalk, Conn. 06851.

Business and Subscription Information

Remittances and orders for subscriptions and for single copies, notices of changes of address and new professional connections, and claims for missing numbers should be sent to the Subscription Service Department, American Chemical Society, 1155 Sixteenth St., N.W., Washington, D. C. 20036. Allow 4 weeks for change of address. Please include an old address label with the notification.

Claims for missing numbers will not be allowed (1) if received more than sixty days from date of issue, (2) if loss was due to failure of notice of change of address to be received before the date specified in the preceding paragraph, or (3) if the reason for the claim is "missing from files."

Subscription rates (1973): members of the American Chemical Society, $20.00 for 1 year; to nonmembers, $60.00 for 1 year. Those interested in becoming members should write to the Admissions Department, American Chemical Society, 1155 Sixteenth St., N.W., Washington, D. C. 20036. Postage to Canada and countries in the Pan-American Union, $5.00; all other countries, $6.00. Single copies for current year: $3.00. Rates for back issues from Volume 56 to date are available from the Special Issues Sales Department, 1155 Sixteenth St., N.W., Washington, D. C. 20036.

This publication and the other ACS periodical publications are now available on microfilm. For information write to MICROFILM, Special Issues Sales Department, 1155 Sixteenth St., N.W., Washington, D. C. 20036.

Notice to Authors last printed in the issue of November 23, 1972

THE JOURNAL OF
PHYSICAL CHEMISTRY

Volume 77, Number 3 February 1, 1973

JPCHAx 77(3) 301–426 (1973)

ห้องสมุด กรมวิทยาศาสตร์
23 มี.ค. 2516

COMMUNICATIONS TO THE EDITOR

AUTHOR INDEX

In papers with more than one author the name of the author to whom inquiries about the paper should be addressed is marked with an asterisk in the by-line.

THE JOURNAL OF
PHYSICAL CHEMISTRY

Registered in U. S. Patent Office © *Copyright, 1973, by the American Chemical Society*

VOLUME 77, NUMBER 3 FEBRUARY 1, 1973

Hydrogen Atom Abstraction by Fluorine Atoms[1]

Ronald L. Williams and F. S. Rowland*

Department of Chemistry, University of California, Irvine, California 92664 *(Received August 4, 1972)*
Publication costs assisted by the Division of Research, U.S. Atomic Energy Commission

The relative rates of abstraction of hydrogen atoms by ^{18}F atoms have been measured for H_2, D_2, CH_4, CD_4, C_2H_6, CH_3CF_3, H_2S, and HI *vs.* the rate of addition to acetylene. The measurements have involved the competitive diminution in yield of $CH_2{=}CH^{18}F$ (from $CH^{18}F{=}CH$ + HI) *vs.* RH(or RD)/C_2H_2 ratio. The samples contained excess SF_6 which served both as the target for formation of ^{18}F by the $^{19}F(n,2n)^{18}F$ nuclear reaction, and as the moderator for the excess recoil energy of these ^{18}F atoms. The relative rates per H or D atom varied from 0.018 ± 0.004 for CH_3CF_3 to 0.65 ± 0.05 for H_2S. The abstraction of H was favored over D for both isotopic pairs of molecules: for H_2/D_2 and for CH_4/CD_4. No reaction was observed for ^{18}F with xenon.

Introduction

Macroscopic studies of hydrogen atom abstraction by fluorine atoms have only infrequently been attempted, and have been complicated by several difficult experimental problems, including the high rates of reaction of fluorine atoms with many substrates, the great exothermicity of HF-forming reactions, the chemical reactivity of HF, and of many potential fluorine atom sources, such as F_2, UF_6, etc.[2-12] Some of these problems can be avoided or ameliorated by experiments at tracer levels utilizing radioactive ^{18}F atoms, as described in our earlier communication about this work,[13] and in related work by Root and Parks.[14] We describe here the experimental details and more extensive conclusions from the data briefly summarized earlier.[13]

In our experiments, ^{18}F atoms are formed at very high energies ($\sim 10^5$ eV) by the fast neutron induced nuclear reaction, $^{19}F(n,2n)^{18}F$, in gaseous SF_6.[15-19] These energetic ^{18}F atoms are then moderated to near-thermal energies by multiple collisions with SF_6, and finally react with minor components in the gaseous mixture by paths characteristic of thermal fluorine atoms. Approximately 1% of the ^{18}F atoms react while still translationally hot by substitution into SF_6 with the formation of $SF_5{}^{18}F$, while other ^{18}F atoms also react while hot with the other components. The hot reactions with these other molecules are roughly proportional in yield to the mole fraction of the substrate mixed with SF_6, and can be effectively minimized in yield by performing experiments in a substantial excess of SF_6. As discussed later, almost all of the abstraction reactions occurring in 95% SF_6 are initiated by essentially thermal ^{18}F atoms.

(1) This research was supported by A.E.C. Contract No. AT-(04-3)-34, Agreement No. 126.
(2) G. C. Fettis and J. H. Knox, *Progr. Reaction Kinet.*, **2**, 1 (1964).
(3) P. D. Mercer and H. O. Pritchard, *J. Phys. Chem.*, **63**, 1468 (1959).
(4) G. C. Fettis, J. H. Knox, and A. F. Trotman-Dickenson, *J. Chem. Soc.*, 1064 (1960).
(5) R. Foon and N. A. McAskill, *Trans. Faraday Soc.*, **65**, 3005 (1969).
(6) R. Foon and G. P. Reid, *Trans. Faraday Soc.*, **67**, 3513 (1971).
(7) K. H. Homann, W. C. Solomon, J. Warnatz, H. G. Wagner, and C. Zetzch, *Ber. Bunsenges. Phys. Chem.*, **74**, 585 (1970).
(8) H. G. Wagner, J. Warnatz, and C. Zetzch, *An. Assoc. Quim. Argent.*, **59**, 169 (1971).
(9) J. B. Levy and B. K. W. Copeland, *J. Phys. Chem.*, **67**, 2156 (1963).
(10) J. B. Levy and B. K. W. Copeland, *J. Phys. Chem.*, **69**, 408 (1965).
(11) J. B. Levy and B. K. W. Copeland, *J. Phys. Chem.*, **72**, 3168 (1968).
(12) G. A. Kapralova, A. L. Margolin, and H. M. Chaikin, *Kinet. Katal.*, **11**, 669 (1970).
(13) R. L. Williams and F. S. Rowland, *J. Phys. Chem.*, **75**, 2709 (1971).
(14) N. J. Parks and J. W. Root, presented at the 161st National Meeting of the American Chemical Society, Los Angeles, Calif., March 1971.
(15) T. Smail and F. S. Rowland, *J. Phys. Chem.*, **74**, 1866 (1970).
(16) T. Smail, G. Miller, and F. S. Rowland, *J. Phys. Chem.*, **74**, 3464 (1970).
(17) T. Smail, R. S. Iyer, and F. S. Rowland, *J. Amer. Chem. Soc.*, **94**, 1041 (1972).
(18) R. L. Williams and F. S. Rowland, *J. Amer. Chem. Soc.*, **94**, 1047 (1972).
(19) R. L. Williams and F. S. Rowland, *J. Phys. Chem.*, **76**, 3509 (1972).

When acetylene is included as a minor component in SF_6, two reactions account for >95% of the ^{18}F atoms formed,[18] abstraction from acetylene, as in (1), and addition to it, as in (2). The excited $CH^{18}F{=}CH^*$ radical is

$$^{18}F + C_2H_2 \longrightarrow H^{18}F + C_2H \quad (1)$$

$$^{18}F + C_2H_2 \longrightarrow CH^{18}F{=}CH^* \quad (2)$$

then stabilized by collision with SF_6, and can be converted into $CH_2{=}CH^{18}F$ by reaction with a hydrogen-donating scavenger such as HI, as in (3), or H_2S. The inclusion of the scavenger permits another reaction path for ^{18}F, abstraction from HI, as in (4). The relative rate of (4) *vs.*

$$CH^{18}F{=}CH + HI \longrightarrow CH_2{=}CH^{18}F + I \quad (3)$$

$$^{18}F + HI \longrightarrow H^{18}F + I \quad (4)$$

(1) plus (2) should be proportional to the HI/C_2H_2 ratio in an experiment if the three reactions are directly competing for the same pool of ^{18}F atoms. If and when this system is well behaved, the inclusion of a fourth component, RH, permits additional reactions, including especially abstraction from this additional substrate, as in

$$^{18}F + RH\,(\text{or RD}) \longrightarrow H^{18}F\,(\text{or } D^{18}F) + R \quad (5)$$

We have carried out such competitive measurements *vs.* acetylene with several hydrogen-containing molecules, including H_2S, CH_4, CD_4, H_2, D_2, C_2H_6, and CH_3CF_3. Several experiments with Xe are also reported. Most of these experiments have been conducted at pressures between 2500 and 3000 Torr to maximize the number of fluorine atoms as targets in the fast neutron flux, and therefore the total yield of ^{18}F. At such pressures, there is no evidence for decomposition of $CH^{18}F{=}CH^*$ before stabilization.[18]

Experimental Section

Fluorine-18 atoms were formed by the nuclear reaction $^{19}F(n,2n)^{18}F$ occurring in SF_6 exposed to the fast neutron flux from a Kaman A711 neutron generator. Most samples contained >90% SF_6 as well as C_2H_2, HI, and usually one other minor component in a 15-ml bulb at about 3000 Torr total pressure. After irradiation, the gaseous contents were analyzed by radio gas chromatography. The experimental details are essentially the same as those described in a detailed study of ^{18}F reactions with acetylene itself.[18]

No direct analysis was usually performed for the $H^{18}F$ molecules formed by abstraction reactions 1, 4, or 5. Instead, the summed yield of such reactions was indirectly estimated from the diminution in $CH_2{=}CH^{18}F$ yield, the other major fate for near-thermal ^{18}F atoms in these systems. The indirect measurement procedure was adopted because we are able to obtain much better reproducibility for the determination of product compounds which are both volatile and relatively nonreactive, such as $CH_2{=}CH^{18}F$, than we are for reactive species such as $H^{18}F$. One consequence of this technique, however, is that we are unable to distinguish among reaction paths that do not produce a readily identifiable ^{18}F-containing species. Among such uncertainties are the possible reactions 6 and 7,[20] whose products might not pass through our normal gas chromatographic analytical procedure, even if otherwise nonreactive under our experimental conditions. The substitution of ^{18}F for H in hydrocarbons as in (8), although usually also exothermic, has been shown experimentally not to be important by the negligible yields (in 95% SF_6) of the corresponding $R^{18}F$ product. (With lower SF_6 concentrations, appreciable yields of $R^{18}F$ molecules can be observed.) The abstraction of F from CH_3CF_3 is highly endothermic because of the weakness of the ^{18}F–F bond, and has a negligible yield in 95% SF_6 mixtures.

$$^{18}F + HI \longrightarrow {}^{18}FI + H \quad (6)$$

$$^{18}F + H_2S \longrightarrow HS^{18}F + H \quad (7)$$

$$^{18}F + RH \longrightarrow R^{18}F + H \quad (8)$$

The eventual accuracy of the quantitative evaluation of these experiments thus depends upon the reproducibility of absolute measurements of $CH_2{=}CH^{18}F$ yield. The most important error here involves the general monitoring of the total ^{18}F production in the system, estimated to be ±6–8% in these experiments. This error in the total production is proportionately smaller for yields less than 100%, *i.e.*, ±3–4% for yields of about 50%.

Most of the chemicals used in these experiments were Research grade (Matheson Co.): C_2H_2, H_2S, HI (96%), SF_6 (98%), CH_4, C_2H_6, D_2. The sources of the other gases were (CD_4) Merck Sharpe and Dohme, (CH_3CF_3) Peninsular Chem Research, and (Xe) Air Reduction Co.

Results and Discussion

Kinetic Competition in C_2H_2–HI Mixtures. After moderation of the initial extra kinetic energy, the ^{18}F atoms react competitively among the available reaction paths. With C_2H_2 as the only other component (in addition to SF_6), the distribution between $H^{18}F$ and $CH^{18}F{=}CH$ is in the ratio of the respective rate constants, k_1^*/k_2^*. (The rate constants have been marked with asterisks as a reminder that these "constants" are averaged over whatever energetic distribution is present in the particular experimental system. The similarity of these distributions to the Maxwell–Boltzmann distribution, and of k_1^*/k_2^* to k_1/k_2, the thermal rate constants, is discussed later.)

No direct measurement of the yield of (2) is possible until a hydrogen donor, usually HI, has been added and the ratio of yields of $H^{18}F$ to $CH_2{=}CH^{18}F$ is then given by (9), and the ratio of total available ^{18}F (*i.e.*, all ^{18}F atoms that did not, while still possessing extra kinetic energy, react to form a stable chemical bond) to the yield of $CH_2{=}CH^{18}F$ is given by (10). This equation predicts a straight line for a graph of $(Y(CH_2{=}CH^{18}F))^{-1}$ *vs.* $[HI]/[C_2H_2]$ with an intercept >1.0 and a slope reflecting the relative rates of reaction 4 *vs.* 2.

$$Y(H^{18}F)/Y(CH_2{=}CH^{18}F) = (k_1^*[C_2H_2] + k_4^*[HI])/k_2^*[C_2H_2] \quad (9)$$

$$Y(\text{total})/Y(CH_2{=}CH^{18}F) = \{(k_1^* + k_2^*)[C_2H_2] + k_4^*[HI]\}/k_2^*[C_2H_2] = \{(k_1^* + k_2^*)/k_2^*\} + k_4^*[HI]/k_2^*[C_2H_2] \quad (10)$$

The data for a series of C_2H_2/HI competition experiments are given in Table I. In each case, yields were also observed for $SF_5{}^{18}F$ (about 1%), $CH{\equiv}C^{18}F$ (<1%), and $CH_3{}^{18}F$ (<0.2%). The first two are formed by hot reactions of ^{18}F with SF_6 and C_2H_2, respectively, while the source of the small variable amounts of $CH_3{}^{18}F$ is uncertain. When the HI/C_2H_2 concentration ratio is ~0.1, the

(20) No thermodynamic measurements are available for HSF. Reaction 6 is approximately 4.5 kcal/mol endothermic from current data and is probably negligible in yield for that reason.

TABLE I: Absolute Yields of $CH_2{=}CH^{18}F$ from ^{18}F Reactions with C_2H_2 in SF_6–C_2H_2–HI Mixtures

Sample pressure, Torr			% yield of
SF_6	C_2H_2	HI	$CH_2{=}CH^{18}F$
1990	100	10	83.4
1440	86	43	75.0
3040	95	48	71.8
2580	95	48	68.8
2570	83	42	73.1
2870	45	23	76.6
2830	14	14	72.1
2830	14	43	44.8
2830	14	72	31.0
1070	223	4	67.6
1070	223	23	71.6
1070	223	46	79.3
1150	587	46	76.2
1150	338	46	77.1
370	107	17	75.7
930	186	186	54.3
730	144	260	40.4

$CH_2{=}CH^{18}F$ yield in Table I is as high as 83%, clearly indicating that addition to acetylene dominates over abstraction from acetylene by $\geq(83)/(15)$, assuming $\sim$2% total hot reaction, and $\leq$15% yield for $H^{18}F$ by difference (including $H^{18}F$ from reactions with HI). However, when the HI/C_2H_2 ratio is >1, the yield of $CH_2{=}CH^{18}F$ is substantially reduced, evidence that abstraction of H from HI is qualitatively quite competitive with addition to acetylene. Extrapolation of the data of Table I to zero concentration of HI, as in Figure 1, indicates that the ratio of abstraction to addition with C_2H_2 alone is about 0.14, corresponding to percentage yields of about 12 and 86%, respectively. The inclusion of HI or other possibly competitive reactant molecule can reduce both of these percentage yields.

If all of the measurements were made in an overwhelming excess of SF_6 (*e.g.*, 10^3 or 10^4 to 1), then the only important concentration ratio in these experiments would be that of C_2H_2 to HI, and their ratio to SF_6 or any other essentially inert component would have no effect on the distribution of ^{18}F atoms among possible reaction pathways. However, when the SF_6/C_2H_2 ratio is much smaller, as low as 2/1, hot reactions to form other products can be more significant and an additional fraction of ^{18}F atoms may well react while still hot by reactions 1, 2, 4, 5, or by other undetected paths. The ratio of rate constants may in general be dependent upon energy, and the apparent ratios of rate constants, k_i^*/k_j^*, may well vary with the composition ratio of SF_6 to other components.

In Figure 1, we have graphed all of the results of experiments from Table I in which the mole fraction of SF_6 exceeded 0.90. With SF_6 in such excess, each ^{18}F atom is >9 times more likely at each energy to make a nonreactive collision with SF_6 than to make a possibly reactive collision with C_2H_2 or HI. Under such conditions, most ^{18}F atoms are essentially thermal in kinetic energy at the time of reactive collision.[18,19] The straight line of Figure 1 is a reasonable fit to these data, leading to an estimate from its slope of 0.37 $\pm$ 0.05 for the ratio of the rate of abstraction from HI *vs.* addition to C_2H_2.

At an HI/C_2H_2 concentration ratio of 0.02, the observed yield of $CH_2{=}CH^{18}F$ is less than it is at higher ratios.

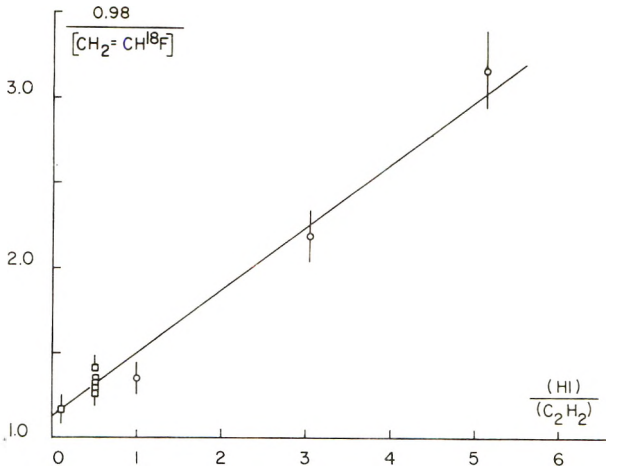

Figure 1. Decreasing yield of $CH_2{=}CH^{18}F$ from ^{18}F addition to acetylene as HI/C_2H_2 concentration increases: O, SF_6/C_2H_2 = 200; □, SF_6/C_2H_2 = 16 to 65.

The major contributor to this diminution in yield of $CH_2{=}CH^{18}F$ is probably the competition between reactions 3 and 11 for the newly formed fluorovinyl-^{18}F radical. The $C_4H_5{}^{18}F$ formed by reaction of the $C_4H_4{}^{18}F$ radicals from (11) with HI would probably not have been detected in our standard radio gas chromatographic procedures.

$$CH^{18}F{=}CH + C_2H_2 \longrightarrow C_4H_5{}^{18}F \qquad (11)$$

The evaluation of yields at low absolute concentrations of HI is also suspect because of irreproducibility in the handling and irradiation of such samples, and some very low concentration HI experiments in these and related systems[21] have shown exceptionally low "scavenged-radical" yields. In the succeeding tables, those experiments designated with asterisks have been disregarded in the accompanying figures as probably having incompletely scavenged radical yields.

The experiments listed in the lower part of Table I all involve SF_6 mole fractions less than 0.90, and the yields of $CH_2{=}CH^{18}F$ are somewhat lower than found at high SF_6 mole fractions for the same HI/C_2H_2 ratios. This trend suggests that the abstraction of H from C_2H_2 by energetic ^{18}F atoms has a higher yield relative to addition than the 0.14 measured for the nearly thermalized ^{18}F atoms of the 95% SF_6 systems.

Addition of RH (or RD) to SF_6–C_2H_2–HI Mixtures. With the addition of a fourth component (RH or RD) to the gaseous mixture, while still maintaining SF_6 in great excess, abstraction from RH or RD must also be included in the overall mechanism, and the resulting equation for the inverted ratio of yield of $CH_2{=}CH^{18}F$ to total "available" ^{18}F is given by

$$Y(\text{total})/Y(CH_2{=}CH^{18}F) = [(k_1^* + k_4^*)/k_2^*] + (k_4^*[HI]/k_2^*[C_2H_2]) + (k_5^*[RH]/k_2^*[C_2H_2]) \qquad (12)$$

Since a reasonable estimate of the value of $k_4^*[HI]/k_2^*[C_2H_2]$ can be calculated from the experiments on C_2H_2–HI mixtures without RH, this equation can be rewritten as (13), suggesting a linear graph of the left-hand

(21) R. L. Williams and F. S. Rowland, unpublished data.

TABLE II: Effect of Hydrogen on Absolute Percentage Yields of $CH_2{=}CH^{18}F$ from ^{18}F Reactions with C_2H_2 in SF_6–C_2H_2–HI Mixtures

Sample pressures, Torr					
SF_6[a]	C_2H_2	HI	H_2	D_2	% yield[b] of $CH_2{=}CH^{18}F$
2840	57	14	86		66.5, 69.1, 69.7, 70.8
2860	57	11	86		67.0
2840	57	14		86	68.9, 70.7, 71.5
3060	57	14		86	73.9
2840	24	14	119		46.8, 50.1
2840	24	14		119	53.6, 56.0, 60.1
2840	14	14	129		33.8, 35.3
2780	14	14	133		37.4
2680	14	14	133		36.7
2840	14	14		129	41.4, 41.5, 42.5, 49.0
2840	10	6	49		41.4, 48.2
2900	14	3	129		16.4*
2870	14	72	129		19.7

[a] The SF_6 pressures in duplicate samples all fell within ±15 Torr of the listed pressure. [b] Multiple entries represent the results of separate experiments under essentially identical initial conditions. Concentration of HI marked with an asterisk may have been insufficient to scavenge completely all $CH^{18}F{=}CH$ radicals.

function *vs.* $[RH]/[C_2H_2]$ with its slope providing an estimate of the relative rates for k_5^*/k_2^*.

$$(Y(\text{total})/Y(CH_2{=}CH^{18}F)) - (k_4^*[HI]/k_2^*[C_2H_2]) = [(k_1^* + k_2^*)/k_2^*] + (k_5^*[RH]/k_2^*[C_2H_2]) \quad (13)$$

The effects of H_2 and D_2 as additional components in reducing the observed yields of $CH_2{=}CH^{18}F$ are summarized in Table II. These data, after correction for reaction 4 by the appropriate $[HI]/[C_2H_2]$ ratio,[22] are graphed *vs.* H_2/C_2H_2 and D_2/C_2H_2 in Figure 2. Both sets of data give reasonable straight line fits consistent with equation 13, and clearly show an isotope effect favoring reaction 14 over 15. The respective slopes of these two lines correspond to relative reaction efficiencies (again, *vs.* addition to C_2H_2 as unity) of 0.14 ± 0.02 and 0.08 ± 0.02, for an isotope effect in relative reaction rate of about 1.8 (see below).

$$^{18}F + H_2 \longrightarrow H^{18}F + H \quad (14)$$

$$^{18}F + D_2 \longrightarrow D^{18}F + D \quad (15)$$

The single H_2 point measured at high HI concentration does not fit particularly well as plotted. If k_4^* for reaction with HI were assumed as 0.51 instead of 0.37 for this experiment, then the point would fall directly on the line. Such a value for k_4^* is, however, too high for the data of Figure 1. This discrepancy probably represents a reasonable estimate of the overall consistency of our procedures, including not only errors in accuracy and precision but also in the approximations involved in deriving equations 9, 10, 12, and 13. Comparisons of two molecules with similar reactivity under similar conditions should give ratios of reactivities with better precision. The points measured at consistent ratios of HI/C_2H_2 do give good straight lines in Figure 2, and indicate that this procedure for evaluating relative rates of fluorine atom reactions is quite valid, although not of high precision.

Many of the reactions of fluorine atoms occur with collision efficiencies in the 0.01 to 1.0 range, thereby making it

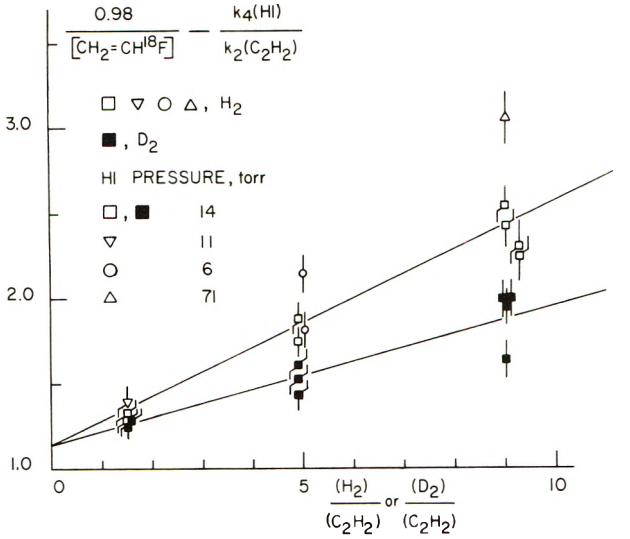

Figure 2. Decreasing yield of $CH_2{=}CH^{18}F$ from ^{18}F addition to acetylene with increasing ratio of H_2 or D_2 *vs.* C_2H_2.

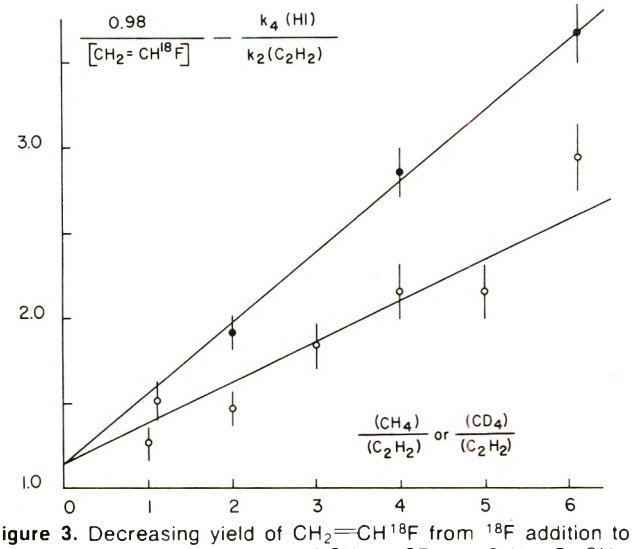

Figure 3. Decreasing yield of $CH_2{=}CH^{18}F$ from ^{18}F addition to acetylene with increasing ratio of CH_4 or CD_4 *vs.* C_2H_2: ●, CH_4; ○, CD_4.

very difficult to attain a true Boltzmann distribution in fluorine atom energies. It is possible that the characteristic distributions for ^{18}F atom energies are slightly different for variations in the components, especially when comparing highly reactive and nearly inert additives, or in comparisons of "high" *vs.* "low" HI samples or "high" *vs.* "low" H_2 samples, etc. The effects, probably small, of any such differences are included in the overall errors implied by the deviations from straight lines in Figures 1 and 2 and subsequently in Figures 3–5.

Similar sets of experimental data with CH_4 and CD_4 are given in Table III and Figure 3, providing estimates from the slopes of the lines of 0.41 ± 0.04 and 0.24 ± 0.04 for the relative rates of the abstraction reactions 16 and 17. The data for abstraction from C_2H_6 and CH_3CF_3 are given in Tables IV and V; both are graphed in Figure 4. Clearly, abstraction from C_2H_6 reduces the yield of $CH_2{=}CH^{18}F$ very much more than for an equivalent con-

(22) *E.g.* first line of Table II. Assume *Y*(total) = 98%. *Y*(total)/*Y*($CH_2{=}CH^{18}F$) = (0.98)/(0.665) = 1.43. Correction for reaction 4 = (0.37)(14)/(57) = 0.09. 1.43 − 0.09 = 1.34. Graphed as 1.34 at H_2/C_2H_2 = (86)/(57) = 1.5.

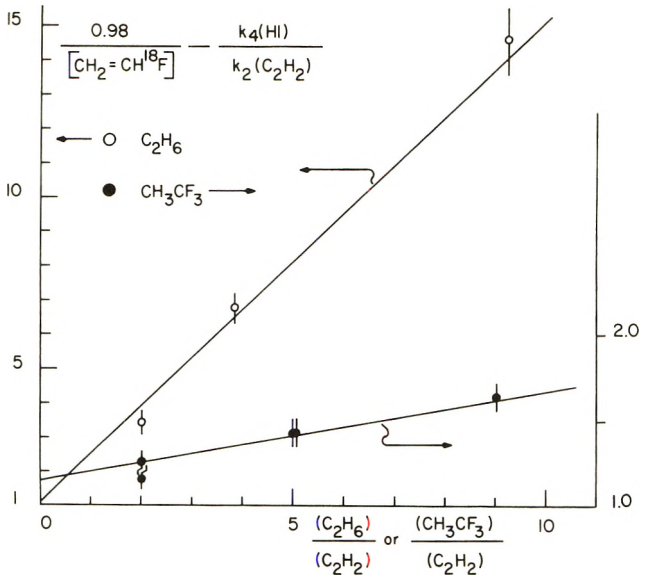

Figure 4. Decreasing yield of $CH_2{=}CH^{18}F$ from ^{18}F addition to acetylene with increasing ratio of C_2H_6 or CH_3CF_3 *vs.* C_2H_2.

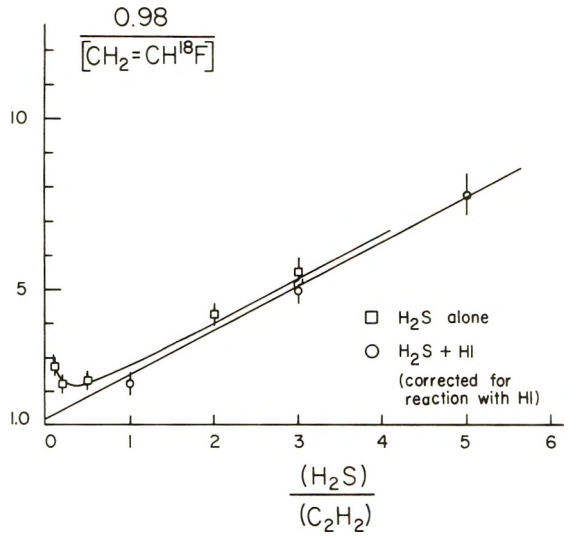

Figure 5. Decreasing yield of $CH_2{=}CH^{18}F$ from ^{18}F addition to acetylene with increasing ratio of H_2S to C_2H_2.

centration of CH_3CF_3. After allowing for the factor of 2 in number of hydrogen atoms, each H atom in C_2H_6 is about 13 ± 3 times as easy to abstract as the H atoms in CH_3CF_3.

$$^{18}F + CH_4 \longrightarrow H^{18}F + CH_3 \quad (16)$$

$$^{18}F + CD_4 \longrightarrow D^{18}F + CD_3 \quad (17)$$

$$^{18}F + C_2H_6 \longrightarrow H^{18}F + C_2H_5 \quad (18)$$

$$^{18}F + CH_3CF_3 \longrightarrow H^{18}F + CH_2CF_3 \quad (19)$$

$$^{18}F + H_2S \longrightarrow H^{18}F + SH \quad (20)$$

Addition of Xenon to SF_6-C_2H_2-HI Mixtures. A few experiments were performed with xenon as the added component, as summarized in Table VI. The $CH_2{=}CH^{18}F$ yields in the xenon systems were in excellent agreement with those expected for competition between C_2H_2 and HI as the only reactants, with xenon acting as an inert species.

TABLE III: Effect of Methane on Absolute Percentage Yields of $CH_2{=}CH^{18}F$ from ^{18}F Reactions with C_2H_2 in SF_6-C_2H_2-HI Mixtures

Sample pressures, Torr				% yield of $CH_2{=}CH^{18}F$[a]
SF_6	C_2H_2	HI	CH_4	
2840	47	24	92	46.5
2840	28	14	111	32.2
2840	20	11	120	25.4
2860	14	7	125	16.7*
			CD_4	
2840	70	35	70	66.8
2780	45	23	48	57.3
2850	47	23	92	59.1
2840	35	17	104	48.6
2840	28	15	111	41.8
2830	23	11	116	42.3
2810	20	10	119	31.5
2730	15	8	124	21.5*
2780	14	7	126	11.0*

[a] Concentration of HI marked with an asterisk may have been insufficient to scavenge completely all $CH^{18}F{=}CH$ radicals.

TABLE IV: Effect of C_2H_6 on Absolute Percentage Yields of $CH_2{=}CH^{18}F$ from ^{18}F Reactions with C_2H_2 in SF_6-C_2H_2-HI Mixtures

Sample pressures, Torr				% yield[b] of $CH_2{=}CH^{18}F$
SF_6	C_2H_2	HI	C_2H_6	
2850	47	23	92	26.8
2710	28	14	106	14.0
2830	14	7	125	6.6

TABLE V: Effect of CH_3CF_3 on Absolute Percentage Yields of $CH_2{=}CH^{18}F$ from ^{18}F Reactions with C_2H_2 in SF_6-C_2H_2-HI Mixtures

Sample pressures, Torr				% yield of $CH_2{=}CH^{18}F$
SF_6	C_2H_2	HI	CH_3CF_3	
2840	57	29	57	67.3, 72.8
2850	22	11	110	61.5, 61.5
2860	13	13	116	53.8
2280	116	58	580	51.4, 56.2

H_2S as a Reactant and Scavenger in SF_6-C_2H_2 Mixtures. Some additional experiments have also been performed which permit evaluation of the rate constant for reaction 20. Since H_2S is widely used as a free-radical scavenger, a three-component system SF_6-C_2H_2-H_2S can be used. However, as shown in Table VII and Figure 5, the $CH_2{=}CH^{18}F$ yields from these experiments do not extrapolate smoothly to the expected $(k_1^* + k_2^*)/(k_2^*)$ intercept, but instead display a maximum in yield and a minimum in the plot of reciprocal yield. When HI is added as a fourth component, and the usual correction for reactions with HI is made, a good straight line is obtained with a slope corresponding to a relative rate of 1.30 ± 0.10.

The difficulty with the SF_6-C_2H_2-H_2S system can be readily explained through competition between H_2S and C_2H_2 for the $C_2H_2{}^{18}F$ radicals, as in (21) and (11). If the

$$CH^{18}F{=}CH + H_2S \longrightarrow CH_2{=}CH^{18}F + SH \quad (21)$$

TABLE VI: Effect of Added Xenon on Absolute Percentage Yields of $CH_2{=}CH^{18}F$ from ^{18}F Reactions with C_2H_2 in SF_6–C_2H_2–HI Mixtures

Sample pressure, Torr				% yield of $CH_2{=}CH^{18}F$	
SF_6	C_2H_2	HI	Xe	Measured[a]	Estimated[b]
2830	24	14	119	72.1	72.2
2840	24	14	119	77.9	72.2
2850	14	14	129	65.2	65.0
2830	14	15	129	65.2	64.1

[a] Accuracy from statistical fluctuations alone, ±0.3%; estimated absolute accuracy, ±5%. [b] Estimated from straight line on Figure 1 for given HI/C_2H_2 ratio.

TABLE VII: Effect of H_2S on Yields of $CH_2{=}CH^{18}F$ from Reaction of ^{18}F with C_2H_2 in SF_6–C_2H_2 Mixtures

Sample pressure, Torr				% yield of $CH_2{=}CH^{18}F$
SF_6	C_2H_2	H_2S	HI	
2830	131	13	0	35.5
2830	120	24	0	43.5
2830	95	48	0	41.3
2840	48	95	0	22.6
2840	36	108	0	17.7
2830	58	58	29	40.4
2840	32	95	16	19.0
2840	22	110	11	12.3

rate constant for (21) is not overwhelmingly faster than for (11), then appreciable fractions of the $C_2H_2{}^{18}F$ radicals may fail to appear as $CH_2{=}CH^{18}F$ at low H_2S/C_2H_2 ratios. If the ratio of k_{21}^*/k_{11}^* is assumed to be 8.4, and k_{20}^*/k_2^* is taken as 1.30 ± 0.10 from the SF_6–C_2H_2–H_2S–HI experiments, then the calculated curve of Figure 5 is obtained. The fit to all of the data in Figure 5 is quite satisfactory; values of k_{21}^*/k_{11}^* in the range 8.4 ± 1.0 also give fits that are satisfactory within the accuracy of the data. The fate of $C_4H_4{}^{18}F$ radicals, if formed by (11), is not known; our chromatography would not have measured $C_4H_5{}^{18}F$ or higher polymers.

Relative Rate Constants for Reactions of ^{18}F. All of the relative rate constants from the tables and figures are collected in Table VIII.

Activation Energies for Hydrogen Abstraction. The activation energy for abstraction of hydrogen by fluorine atoms has often been assumed to be very low (of the order of 1 kcal/mol or less). The abstraction of H from C_2H_6 is 13 ± 3 times easier *per H atom* than from CH_3CF_3. Since the methyl geometries are quite similar in these two molecules, it is plausible that this difference in rate is primarily the result of differences in the energies of activation for these two reactions. At 283°K, an activation energy difference of 1.5 kcal/mol is required to create a factor of 13 difference in the rates of two thermal reactions. If there are small deviations in our system from Maxwellian energy distributions, these deviations would be in the direction tending to increase the number of ^{18}F atoms in the high-energy tail. Differences in relative rate constants in such a system would tend to be smaller than in true thermal systems. While such deviations from thermal distributions are believed to be rather small in 95% SF_6, the present experiments therefore suggest that abstraction

TABLE VIII: Relative Rates of Reaction of ^{18}F Atoms in 95% SF_6 Mixtures

		Rate constant	Rate constant per C–H or C–D bond
Addition to acetylene		k_2^*	
$^{18}F + C_2H_2 \rightarrow CH^{18}F{=}CH$		(1.00)	
Abstraction from acetylene		k_1^*	
$^{18}F + C_2H_2 \rightarrow H^{18}F + C_2H$		0.14 ± 0.07	0.07 ± 0.04
Abstraction from HI		k_4^*	
$^{18}F + HI \rightarrow H^{18}F + I$		0.37 ± 0.05[a]	0.37 ± 0.05
Abstraction from RH or RD		k_5^*	
$^{18}F + RH \rightarrow H^{18}F + R$			
$(+RD \rightarrow D^{18}F + R)$			
RH	RD		
H_2		0.14 ± 0.02	0.07 ± 0.01
	D_2	0.08 ± 0.02	0.04 ± 0.01
CH_4		0.41 ± 0.04	0.10 ± 0.01
	CD_4	0.24 ± 0.04	0.06 ± 0.01
C_2H_6		1.40 ± 0.12	0.23 ± 0.02
CH_3CF_3		0.053 ± 0.012	0.018 ± 0.004
Reaction with xenon		0.00 ± 0.01	
Abstraction from H_2S			
$^{18}F + H_2S \rightarrow H^{18}F + SH$		1.30 ± 0.10[b]	0.65 ± 0.05

[a] Includes any contribution from k_6, the thermal formation of ^{18}FI. [b] Includes any contribution from k_7, the thermal formation of $HS^{18}F$.

from CH_3CF_3 has an activation energy ≥1.5 kcal/mol larger than from C_2H_6. The energy of activation for abstraction from CH_3CF_3 has been estimated to be 2.1 ± 0.1 kcal/mol greater than that for addition to $CF_3CF{=}CF_2$ from recoil ^{18}F experiments by Root, *et al.*[23]

The relative yields for abstraction from the saturated C–H bonds in Table VIII fall into a smooth correlation of diminished yield from bonds with higher dissociation energies (in parentheses in kcal/mol): $C_2H_6(98)$[24] > $CH_4(104)$[24] > $CH_3CF_3(109)$.[25] The activation energy for H abstraction from C_2H_6 by fluorine atoms is generally assumed to be only 280 cal/mol[2] and the reaction is believed to occur on nearly every collision. While the formation of the 135 kcal/mol H–F bond makes all of these abstractions highly exothermic, the activation energy barrier apparently increases slowly for the very strong C–H bonds.

The abstraction of H from C_2H_2 is substantially greater than from CH_3CF_3, although estimates of the C_2H–H bond dissociation energy are all in excess of 109 kcal/mol, ranging from 114 kcal/mol[24] to the recent 128 kcal/mol.[26] The data are too sparse for a detailed evaluation of the relationship between abstraction yields and C–H bond dissociation energies.

Relative Rates in Thermal Systems. The relative rates of reaction in Table VIII[27] can be profitably compared with the relative rates of the same reactions measured in thermal systems. Such a comparison is made in Table IX. In general, the agreement is reasonable in view of the large experimental uncertainties involved in our determinations as well as in the comparison data. The only sub-

(23) N. Parks, K. A. Krohn, and J. W. Root, *J. Chem. Phys.*, **55**, 2690 (1971).
(24) J. Kerr, *Chem. Rev.*, **66**, 465 (1966).
(25) J. C. Amphlett and E. Whittle, *Trans. Faraday Soc.*, **64**, 2130 (1968).
(26) J. Wyatt and F. Stafford, *J. Phys. Chem.*, **76**, 1913 (1972).
(27) H. G. Wagner and C. Zetzch, private communication.

TABLE IX: Relative Rates of Formation of $H^{18}F$ (or $D^{18}F$) from Different Substrates

	This work	Thermal F atom systems[e]
$k[CH_4]/k[H_2]$	2.9 ± 0.5	4.8,[a] 2.5,[b] 4.5,[c] 12.5[d]
$k[C_2H_6]/k[CH_4]$	3.4 ± 0.5	2.0,[a] 2.7[b]
$k[C_2H_6]/k[H_2]$	10 ± 2	9.6,[a] 6.9[b]
$k[H_2]/k[D_2]$	1.8 ± 0.4	1.6[d]

[a] References 2 and 4. [b] Reference 6. [c] References 7 and 8. [d] Reference 12. [e] Reference 27.

stantial discrepancy involves the comparison of the relative rates of reaction with CH_4 and H_2 *vs.* those of ref 12; in this case, the other three determinations are much closer to each other and to our value and in clear disagreement with that of ref 12. The reasonable agreement between our results and those from nonnuclear sources of fluorine atoms is quite consistent with our basic assumption that the ^{18}F atoms in 95% SF_6 mixtures are reacting with the other components while possessing essentially thermal energies.

The relative rates of reaction with the pairs of isotopic molecules each show a definite preference for abstraction of H by a factor between 1.5 and 2.0. Two recent trajectory calculations have indicated a preference for reaction with H_2 *vs.* D_2 by similar factors: 1.59 ± 0.24[28] and 1.65.[29] The scatter of our measurements at high concentrations of H_2 or D_2 is sufficiently large to make our relative rate data of low accuracy, but consistent with both the earlier experimental measurement and the trajectory simulations.

No experimental measurements of the isotope effect in abstraction from methane appear to have been carried out. In both isotopic comparisons, the small preference for abstraction of H *vs.* D is a quite reasonable consequence of the different zero-point energies plus the overall rapid rates.

Acknowledgment. The authors wish to thank Professor H. G. Wagner for comments on the relative rates of thermal fluorine atom reactions.

(28) J. Muckerman, *J. Chem. Phys.*, **54**, 1155 (1971).
(29) R. L. Jaffee and J. B. Anderson, *J. Chem. Phys.*, **54**, 2224 (1971); **56**, 682 (1972).

Kinetic Isotope Effects in the Dehydrofluorination of Chemically Activated 1,1,1-Trifluoroethane

B. D. Neely[1] and Halbert Carmichael*

Department of Chemistry, North Carolina State University, Raleigh, North Carolina 27607 *(Received July 10, 1972)*

Hexafluoroacetone was cophotolyzed with acetone and with acetone-d_6, and the rate of the unimolecular dehydrofluorination of the 1,1,1-trifluoroethanes formed from combination of CF_3 and CH_3 or CD_3 radicals was determined from the difluoroethene/trifluoroethane ratio. This ratio was found to depend on the extent of conversion because of secondary reactions. Extrapolations to zero conversion corrected for this effect. The measured kinetic isotope effect was found to be 2.84 ± 0.07. Values of the isotope effect and rate constants predicted by applying RRKM theory to two different models of the activated complex show that both models predict results similar to observations.

Introduction

Since the unimolecular dehydrohalogenation of chemically activated partially halogenated alkanes was first recognized by Pritchard, Venugopalan, and Graham,[2] this type reaction has been one of the most useful methods for testing theories of unimolecular reactions. Alcock and Whittle showed that HF is eliminated from the chemically activated trifluoroethane formed by the combination of methyl and trifluoromethyl radicals,[3] and Giles and Whittle further showed that rate constants for the unimolecular reaction could be extracted from the CF_2CH_2/CF_3CH_3 ratio.[4] They also pointed out that secondary radical reactions with the olefin product could cause inaccuracies in this measurement. A large body of experimental data on reactions of this type has been built up.[5,6] Most of this work has taken no account of the secondary reactions other than to keep the conversion of starting materials to a minimum.

Several different models for the transition state for this class of unimolecular dehydrohalogenations have been proposed[5,7-9] and the RRKM theory has been used to test

(1) Abstracted in part from the thesis submitted by B. D. Neely in partial fulfillment of requirements for the Ph.D. Degree.
(2) G. O. Pritchard, M. Venugopalan, and T. F. Graham, *J. Phys. Chem.*, **68**, 1786 (1964).
(3) W. G. Alcock and E. Whittle, *Trans. Faraday Soc.*, **61**, 244 (1965).
(4) R. D. Giles and E. Whittle, *Trans. Faraday Soc.*, **61**, 1425 (1965).
(5) A. Maccoll, *Chem. Rev.*, **69**, 33 (1969).
(6) (a) H. W. Chang and D. W. Setser, *J. Amer. Chem. Soc.*, **91**, 7648 (1969); (b) G. O. Pritchard and M. J. Perona, *J. Phys. Chem.*, **73**, 2944 (1969); (c) J. A. Kerr and D. M. Timlin, *Trans. Faraday Soc.*, **67**, 1376 (1971).
(7) C. K. Ingold, *Proc. Chem. Soc., London*, 279 (1957).
(8) S. W. Benson and A. N. Bose, *J. Chem. Phys.*, **39**, 3463 (1963).
(9) A. Maccoll and P. J. Thomas, *Progr. React. Kinet.*, **4**, 119 (1967).

these models.[10,11] The models range from a four-centered ring structure to one with only bond stretching prior to the activated complex. Neither model can be eliminated solely on the basis of the values calculated for observable quantities in pyrolysis reactions,[10] but the possibility exists that chemical activation together with kinetic isotope effects will allow a discrimination between these models. The kinetic isotope effect has been measured for the dehydrohalogenation of several chlorine compounds[12] and for chemically activated 1,1,1-trifluoroethane.[13,14] Trends in the reactivities of different haloalkanes have also been used to argue in favor of a highly polar transition state.[9]

This investigation has a dual purpose. The effect of secondary reactions on the experimental quantity related to the rate constant for the unimolecular dehydrofluorination of 1,1,1-trifluoroethane was eliminated, and the sensitivity of the RRKM theory to the choice of activated complex model was tested. This test was made by comparing the predicted values of the kinetic isotope effect for two distinctly different models with each other and with experimental values.

Experimental Section

The hexafluoroacetone used was obtained in a cylinder from Allied Chemical Co. The acetone-d_6 used was obtained from Mallinckrodt Chemical Works and had a specified minimum isotopic purity of 99.5%. All gases were degassed at −196° and stored behind stopcocks. No sample of acetone was stored for more than 2 days prior to use. Photolysis mixtures were prepared by measuring the hexafluoroacetone pressure in the photolysis cell, then filling to a measured total pressure with acetone. All pressures were measured on a Zimmerli gauge connected to the vacuum line. The mixture was then allowed to stand in the cell from 1 to 2 hr to permit mixing.

The photolysis cell was a cylindrical quartz cell approximately 10 cm in length and 5 cm in diameter with plane quartz windows. The total volume of this cell was 195 cc. To increase the amount of radiation absorbed, the rear window of the cell was silver plated. The photolysis cell was isolated from the rest of the vacuum line by a Fisher-Porter Teflon needle valve. Located between the Teflon needle valve and the photolysis cell and outside the furnace was a U-trap which was maintained at approximately 100° by a water bath to prevent condensation of materials from the photolysis cell. The total volume outside the furnace was approximately 15 cc.

The light source used was a high-pressure mercury lamp (Osram HVB200W). The lamp was allowed to warm up for approximately 0.5 hr before a photolysis was run. Photolyses were started and stopped by means of a shutter. The radiation from the lamp was passed through a quartz collimating lens to give as uniform illumination of the cell as possible. In a typical run where the hexafluoroacetone pressure in the cell was 10.0 Torr at 468°K approximately 4×10^{16} quanta/sec were absorbed by the hexafluoroacetone in 180 cc. The quartz photolysis cell was located on the axis of a cylindrical aluminum block furnace, which was regulated by means of a relay unit controlled by a thermistor probe located in the body of the furnace. Temperatures were measured by means of an iron–constantan thermocouple attached to the photolysis cell and were constant within 0.2° during any one run.

After the hexafluoroacetone–acetone mixtures had been photolyzed, the products were passed through a liquid nitrogen trap. The CO and CH_4 were thus removed from the rest of the products and discarded since they gave no information relevant to the reaction being studied. The condensed material in the trap was then taken to a gas chromatograph for analysis. The column used was a combination of a 6-ft silica gel column followed by a 2-ft alumina column in 0.25-in. copper tubing. The detector was a flame ionization detector. After a large number of analyses, it was necessary to prepare new columns of the same materials, since separation of the peaks eventually could not be achieved on old columns.

The products were injected onto the column by freezing into an evacuated Pyrex sample loop, which was then warmed to room temperature and the products injected onto the column. Products observed were C_2H_6, CF_2CH_2, CF_3H, and CF_3CH_3. C_2F_6 could not be determined by the flame ionization detector and the quantities of material were too small to obtain results using a thermal conductivity detector. The column remained at room temperature until the C_2H_6 and CF_2CH_2 had passed through the column. The column temperature was then programmed at a rate of 2.9°/min until the CF_3H and CF_3CH_3 had passed through the column. The unknown peaks in the photolysis mixture were qualitatively determined by comparison of retention times with known standards of C_2H_6, CF_2CH_2, CF_3H, and CF_3CH_3. Their relative retention times with the previously described method of temperature programming were C_2H_6 (1), CF_2CH_2 (2), CF_3H (2.8), and CF_3CH_3 (4.5). Quantitative analysis of the photolysis products was made by comparison of peak area for an unknown quantity of material to the peak area for a known quantity of material.

Results

Table I shows the results from one series of photolyses. It is obvious that the CF_2CH_2/CF_3CH_3 ratio decreases with increasing length of photolysis. The 600- and 15-sec photolyses in this series represent the highest conversion and lowest conversions of any runs in any series. At 33% conversion tertiary as well as secondary reactions are occuring and the equations to be derived for secondary reactions no longer satisfactorily describe the results. At 0.58% conversion the amounts of products are so small that analytical errors become significant. Some photolyses at lower temperatures were much longer because of the decrease in quantum yield for both ketones at lower temperatures. The fraction converted was always within the range given by the example in Table I. Table I lists the time of photolysis as well as the fraction of the hexafluoroacetone converted. This fraction converted was determined by measuring the sum of the CF_3 units contained in the measured CF_3H, C_2F_6, CF_3CH_3, and CF_2CH_2. While these products do not account for all the trifluoromethyl radicals generated, it was assumed that they account for a constant fraction of the total. The C_2F_6 was usually not measured directly but was found from the relationship

(10) B. Noble, H. Carmichael, and C. L. Bumgardner, *J. Phys. Chem.*, **76**, 1680 (1972).
(11) P. N. Clough, J. C. Polanyi, and R. T. Taguchi, *Can. J. Chem.*, **48**, 2919 (1970).
(12) (a) A. T. Blades, P. W. Gilderson, and M. G. H. Wallbridge, *Can. J. Chem.*, **40**, 1526 (1964); (b) K. Dees and D. W. Setser, *J. Chem. Phys.*, **49**, 1193 (1968).
(13) G. O. Pritchard and M. J. Perona, *Int. J. Chem. Kinet.*, **2**, 281 (1970).
(14) H. W. Chang, N. L. Craig, and D. W. Setser, *J. Phys. Chem.*, **76**, 954 (1972).

$$[CF_3CH_3 + CH_2CF_2]^2/[C_2F_6][C_2H_6] = 4 \quad (I)$$

To account for the trends seen in Table I, one should look at the reactions occurring after the photochemical generation of methyl and trifluoromethyl radicals

$$CF_3 + CF_3 \longrightarrow C_2F_6 \quad (1)$$

$$CH_3 + CH_3 \longrightarrow C_2H_6 \quad (2)$$

$$CF_3 + CH_3 \longrightarrow CF_3CH_3^* \quad (3)$$

$$CF_3CH_3^* \longrightarrow CF_2CH_2 + HF \quad (4)$$

$$CF_3CH_3^* + M \longrightarrow CF_3CH_3 + M \quad (5)$$

Errors in the determination of k_4/k_5M will occur if the olefin product is lost by radical addition reactions, such as

$$CF_3 + CF_2CH_2 \longrightarrow CF_3CH_2CF_2 \quad (6)$$

$$CH_3 + CF_2CH_2 \longrightarrow CH_3CH_2CF_2 \quad (7)$$

Reactions 6 and 7 cannot be measured by measuring the products, because the radical products of (6) and (7) react to form several different stable species.

We have corrected for reactions 6 and 7 using the following expressions. The equation for the formation of CF_2CH_2 is

$$d[CF_2CH_2]/dt = k_4[CF_3CH_3^*] - k_6[CF_3][CF_2CH_2] - k_7[CH_3][CF_2CH_2] \quad (II)$$

For relatively small conversions $[CF_2CH_2]$ is the only variable, so this is an equation of the form

$$d[CF_2CH_2]/dt = a - b[CF_2CH_2] \quad (III)$$

where $a = k_4[CF_3CH_3^*]$ and $b = k_6[CF_3] + k_7[CH_3]$. Integration of III gives

$$[CF_2CH_2] = (a/b)(1 - e^{-bt}) \quad (IV)$$

Eliminating time by dividing III by the expression for the rate formation of CF_3CH_3 gives

$$d[CF_2CH_2]/d[CF_3CH_3] = (a - b[CF_2CH_2])/k_5[CF_3CH_3^*][M] \quad (V)$$

Substitution from eq IV gives

$$d[CF_2CH_2]/d[CF_3CH_3] = (a - a + ae^{-bt})/k_5[CF_3CH_3^*][M] = k_4e^{-bt}/k_5[M] \quad (VI)$$

If the rates are constant, the ratio $[CF_2CH_2]/[CF_3CH_3]$ can be used for the left-hand side of VI and the data extrapolated to zero time. Better extrapolations are obtained from the linear form of the equation

$$\log([CF_2CH_2]/[CF_3CH_3]) = \log(k_4/k_5[M]) - (bt/2.303) \quad (VII)$$

Figure 1 shows the plot for two series with identical conditions except for deuteration. For each series of photolyses $\log[CF_2CH_2]/[CF_3CH_3]$ was plotted against time and against the fraction of hexafluoroacetone converted. Due to small changes in the lamp intensity from photolysis to photolysis, better linearily was obtained from the latter series of plots. The data for VII were treated by least squares to obtain a slope and intercept. These zero conversion intercepts are shown in Table II as $[CF_2CH_2/CF_3CH_3]_0$ and are direct measures of $k_4/k_5[M]$. Series 1-5 vary only the total pressure, and plotting $[CF_2CH_2]/[CF_3CH_3]_0$ *vs.* $1/P$ for these series gives a linear plot confirming the mechanism through step 5. Series 6-10 repeat the variation of pressure but with the acetone to hexafluoroacetone ratio equal to 8.0. The slope of this plot is 0.0985 atm compared to 0.0852 atm for the series with acetone to hexafluoroacetone ratio being 2.5. Solving for the relative efficiencies for the two ketones as deactivators in step 5 shows that the efficiency for acetone is 0.5 times as

TABLE I: Photolysis of HFA-Acetone Mixtures at 468°K[a]

t, min	HFA reacted, μmol	Fraction of HFA converted	$[CF_2CH_2]$, μmol	CF_2CH_2/CF_3CH_3
10.00	79.3	0.335	4.20	0.173
7.00	38.6	0.163	2.36	0.202
5.00	30.4	0.131	2.31	0.267
3.00	17.9	0.076	1.52	0.354
2.00	13.2	0.055	1.28	0.397
1.00	9.6	0.040	0.833	0.433
0.5	3.8	0.016	0.443	0.490
0.25	1.4	0.0058	0.111	0.536

[a] Acetone:HFA = 5.2, total pressure = 110 Torr, $(HFA)_0 = 2.37 \times 10^{-4}$ mol, run 3 in Table II.

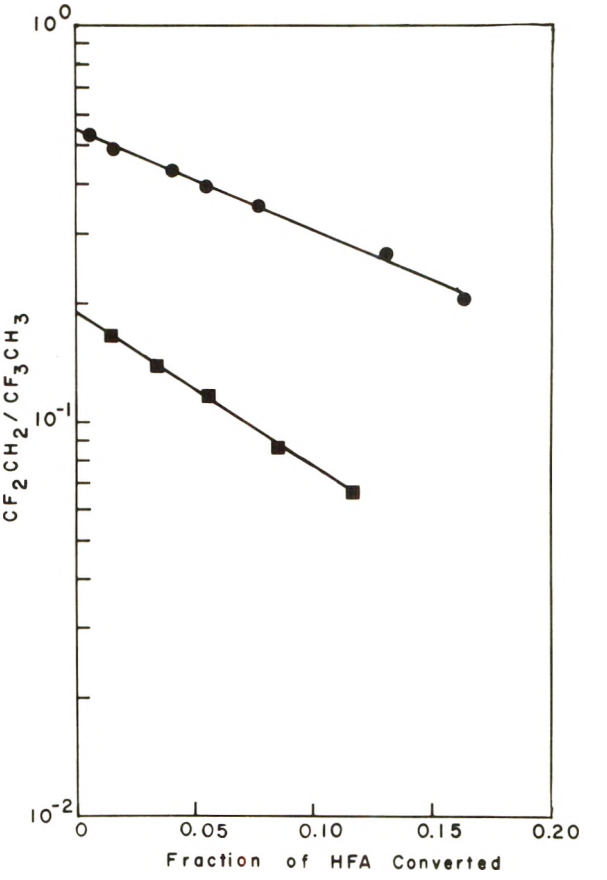

Figure 1. Difluoroethylene/trifluoroethane ratio *vs.* fraction of hexafluoroacetone photolyzed in the cophotolysis of hexafluoroacetone and acetone at 468°K and 110 Torr total pressure: acetone/hexafluoroacetone = 2.5; ● CF_2CH_2/CF_3CH_3; ■ CF_2CD_2/CF_3CD_3.

TABLE II: Results for CH_2CF_2/CH_3CF_3 Ratio from Photolysis of Acetone–Hexafluoroacetone Mixtures[a]

Run	P_{total}, Torr	Acetone/HFA	T, °K	$[CF_2CH_2]/[CF_3CH_3]^0$	b, min^{-1}
1	55.5	2.5	468	1.46	0.057
1D	55.5	2.5	468	0.510	0.061
2	110	2.5	468	0.541	0.057
2D	110	2.5	468	0.188	0.105
3	175	2.5	468	0.427	0.118
3D	175	2.5	468	0.149	0.132
4	75.0	2.5	468	0.857	0.054
5	129	2.5	468	0.518	0.079
6	90.0	8.1	468	0.855	0.072
7	110	8.0	468	0.607	0.033
8	135	8.0	468	0.621	0.068
9	155	8.1	468	0.482	0.055
10	175	8.0	468	0.426	0.049
11	99.0	2.5	413	0.505	0.048
11D	99.0	2.5	413	0.184	0.036
12	88.5	2.5	373	0.431	0.031
12D	88.5	2.5	373	0.152	0.032
13	78.2	2.5	333	0.352	0.020
13D	78.2	2.5	333	0.121	0.047

[a] Acetone-d_6 used in runs 1D, 2D, etc.

large as that for hexafluoroacetone. This is consistent with the report of Giles and Whittle who found acetone to be 0.6 times as effective as hexafluoroacetone.[4] Series 2, 11, 12, and 13 show the temperature dependence of k_4. k_4 was calculated from our data assuming $k_5 = \lambda Z$, where $\lambda = 1$ for hexafluoroacetone and 0.6 for acetone, and Z is the collision frequency using 5-Å collision diameters.

The pairs of series 1 and 1D, 2 and 2D, and 3 and 3D give three different measurements of the kinetic isotope effect for reaction 4

$$CF_3CH_3^* \longrightarrow CF_2CH_2 + HF \qquad (4H)$$

$$CF_3CD_3^* \longrightarrow CF_2CD_2 + DF \qquad (4D)$$

k_{4H}/k_{4D} is 2.86 ± 0.01 at 468°K. Series 11–13D give the information necessary to obtain isotope effects at four different temperatures. The pressures for these series were chosen so that [M] is the same in all these runs as it was in series 2 and 2D. Table III summarizes the kinetic isotope effects. While there is some scatter in the data, it is obvious that there is no significant temperature dependence in the isotope effect.

Discussion

Figure 2 compares our k_4's calculated from extrapolated CF_2CH_2/CF_3CH_3 ratios with those calculated from the data of previous workers.[4,13] Two things are apparent: k_4 is measurably higher than previously reported but is still of the same order of magnitude, and the new data still show a measurable temperature dependence of the same size as that seen before. This variation with temperature is also of the same size as the conversion dependence, so that it is possible to confuse conversion dependence and temperature dependence. The kinetic isotope effects for the dehydrofluorination of chemically activated 1,1,1-trifluoroethane reported in Table III are all lower than the 3.1 reported by Pritchard and Perona.[9] This difference is due to the fact that these workers did not correct for secondary reactions, and in every case the correction is more

TABLE III: Observed and Calculated Kinetic Isotope Effects for Dehydrofluorination of 1,1,1-Trifluorethane

		k_{4H}/k_{4D}		
			Calculated	
T, °K	P, Torr	Observed	Heterolytic	Homolytic
468	55.0	2.86		
468	110.0	2.87	2.34	2.99
468	175.0	2.85		
413	99.0	2.74	2.34	2.87
373	88.5	2.84	2.41	3.08
333	78.2	2.91	2.42	3.10

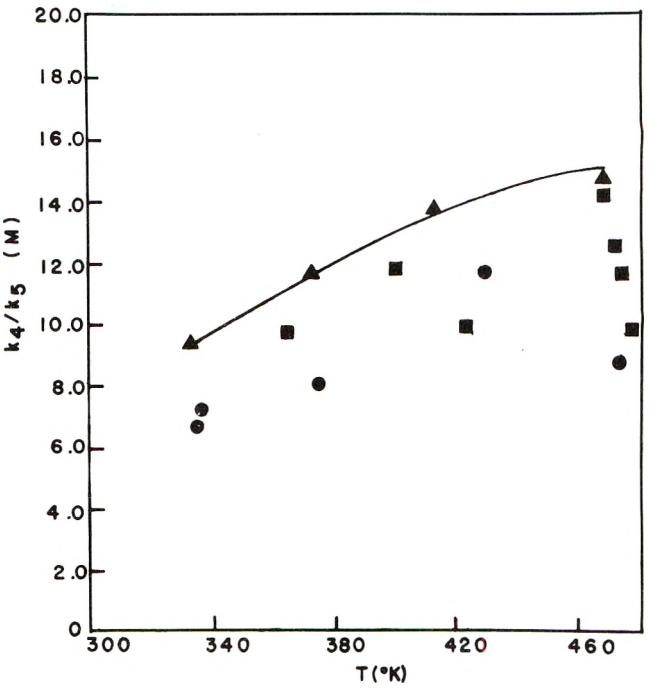

Figure 2. Apparent rate constants for the unimolecular dehydrofluorination of chemically activated CF_3CH_3: ▲, extrapolated values from this work; ●, ref 4; ■, ref 14.

severe for the deuterated molecules than for the nondeuterated molecules.

It should be possible to extract values for k_6 and k_7, the rate constants for radical addition to CH_2CF_2, from the data in the last column of Table II. Since there are two unknown rate constants and two radical concentrations to be indirectly calculated, a great deal of consistent data is required to calculate these rate constants with any precision. The variation of the b factors in Table II is sufficiently large and erratic to make detailed calculations meaningless. However, an order of magnitude calculation can be made to test the reasonableness of our explanation of the variation in the CH_2CH_2/CH_3CF_3 ratio with time. Two assumptions are made: that k_6 and k_7 are equal and that the CF_3 and CH_3 concentrations are equal. The second assumption can be checked against the product yields and appears to be correct to within less than a factor of 2 for the experiments with acetone/HFA = 2.5.

Calculating the radical concentrations from the rates of C_2H_6 and C_2F_6 formation and using the rate constants for radical combination,[15,16] we find that the rate constant

(15) A. Shepp, *J. Chem. Phys.*, **24**, 939 (1956).
(16) P. B. Ayscough, *J. Chem. Phys.*, **24**, 944 (1956).

for radical addition required to explain the loss of CH_2CF_2 is 8.7×10^8 cm^3 mol^{-1} sec^{-1}. This is to be compared with the rate constants measured for

$$CH_3 + CH_2CH_2 \longrightarrow CH_3CH_2CH_2 \quad (8)$$

$$CF_3 + CH_2CH_2 \longrightarrow CF_3CH_2CH_2 \quad (9)$$

$$CH_3 + CF_2CF_2 \longrightarrow CH_3CF_2CF_2 \quad (10)$$

These are 8×10^7, 1.9×10^9, 1.9×10^{10}, respectively.[17-19] The rate constant necessary to explain our result is intermediate between the independently measured rate constants tor similar reactions at 468°K.

The ultimate purpose of this work is to examine the possibility of distinguishing between two models of the activated complex for this general type of unimolecular reaction by comparing the predictions of RRKM theory for the two models with experimental observations of kinetic isotope effects for the dehydrofluorination of chemically activated CH_3CF_3. To do this it is necessary to derive expressions for the particular quantities that are being observed. The apparent first-order rate constant, k, for the reaction of molecules with a distribution of energies would be

$$\text{rate} = k_4[CH_3CF_3^*] \quad \text{(VIII)}$$

$$k_4 = \sum_0^\infty P(E)k(E)\ \exp(-E/RT)/\sum_0^\infty P(E)\ \exp(-E/RT) \quad \text{(IX)}$$

where $k(E)$ is the unimolecular rate constant for energy level E; E is the thermal energy contained in the colliding radicals above the minimum energy E_{min}; T is the temperature of the overall system at which the radicals are assumed to be thermalized, and $P(E)$ is the degeneracy of the energy level E. Appendix I details the models used for the system of colliding radicals and explains the calculation of $P(E)$.

The rate constant, $k(E)$, is calculated from the RRKM theory

$$k(E) = \sigma\left(Q_r^\ddagger \sum_0^E P^\ddagger(E^\ddagger)/Q_r^* h N^*(E^*)\right) \quad \text{(X)}$$

where σ is the reaction path degeneracy, Q_r the rotational partition function, $P^\ddagger(E^\ddagger)$ the degeneracy of a vibrational level, E the unfixed energy, and $N^*(E^*)$ the energy density.

The superscripts distinguish between properties of the energized molecule (*) and the activated complex (‡).

The appropriate matching of thermal energy in the radicals, E, the unfixed energy of the energized molecule, E^*, and the unfixed energy of the activated complex, $E^\ddagger$, is obtained from the following relationships

$$E^* = E + E_{min} = E^\ddagger + E_0 \quad \text{(XI)}$$

Clough, *et al.*, show that E_{min} is equivalent to 98 kcal/mol.[11] The average of three different pyrolytic determinations of the activation energy, E_a, is 71.1 kcal/mol.[20-22] From activated complex theory one can derive the following equation which relates E_a to the critical energy, E_0

$$E_0 = E_a - RT - E_{th}^\ddagger + E_{th}^* \quad \text{(XII)}$$

where E_{th} is the thermal energy of the molecule or complex at the temperature of the experimental determination. For both models of the activated complex, $E_{th}^* - E_{th}^\ddagger$ can be calculated to be 2.2 kcal/mol; so that the experimental E_a of 71.1 kcal/mol corresponds to E_0 = 68.9 kcal/mol. The two figures match because the vibrations which differ between the models are of such high frequency that they make little contribution to $E_{th}^\ddagger$.

From this E_0 a potential energy of activation was obtained by subtracting the zero-point energy of the activated complex and adding the zero-point energy of the molecule. To this potential energy of activation (71.1 kcal/mol for the heterolytic complex and 72.3 kcal/mol for the homolytic complex) was added the zero-point energies for the deuterated molecules and complexes in order to obtain the appropriate E_0's for the reaction of these species. E_{min} was unchanged by isotopic substitution because the zero-point energies of the radicals cancelled against the zero-point energies of the molecules.

This method for calculating the apparent first-order rate constant was applied to two models of the activated complex similar to those used in a previous paper.[10] The heterolytic model involves only stretching of the C-F

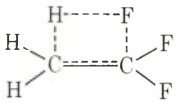

homolytic model

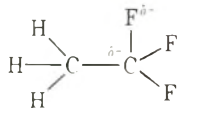

heterolytic model

bond. The homolytic or four-centered model involves simultaneous formation of the H-F bond and breaking of the C-H and C-F bonds. While these are reasonable approximations of the complexes that involve charge separation and lack of charge separation, respectively, the names may be misleading because the only significant feature affecting these calculations is the fact that the homolytic model changes the frequency of the C-H bonds, while the heterolytic model does not. It is this difference that should be reflected in the kinetic isotope effect.

The models used in this paper all have bond orders half-way between the bond orders in the reactant molecule and the bond orders in the final products. This differs from the choice taken by Chang, Craig, and Setser[14] but is no more arbitrary. As later calculations show, this choice seems to have little effect on the final result. All bond lengths were found using Pauling's rule. The $Q_r^\ddagger/Q_r^*$ ratios for all the different models were very nearly the same: 1.28 ± 0.02. The reaction path degeneracy is taken as 3 for the heterolytic model and 6 for the homolytic model. As discussed in a previous paper, these assignments are subject to some uncertainty.[10]

The vibration frequencies, which are listed in Tables IV and V, were approximated using Badger's rule[23] and bond orders. In the heterolytic model a C-F stretch is taken as the reaction coordinate, and two C-C-F or F-C-F bends are decreased in going to the activated complex. In the

(17) L. Endrenyi and D. J. LeRoy, *J. Chem. Phys.*, **71**, 1334 (1967).
(18) J. M. Sangster and J. C. J. Thynne, *J. Chem. Phys.*, **73**, 2746 (1969).
(19) J. M. Sangster and J. C. J. Thynne, *Int. J. Chem. Kinet.*, **1**, 571 (1969).
(20) D. Sianesi, G. Nelli, and R. Fontanelli, *Chim. Ind. (Milan)*, **40**, 619 (1968).
(21) P. Cadman, M. Day, A. W. Kirk, and A. F. Trotman-Dickenson, *Chem. Commun.*, 203 (1970).
(22) E. Tschuikow-Roux and W. J. Quiring, *J. Phys. Chem.*, **75**, 295 (1971).
(23) H. S. Johnston, "Gas Phase Reaction Rate Theory," Ronald Press, New York, N.Y., 1966, p 72.

TABLE IV: Vibration Frequencies and Degeneracies for CH_3CF_3 and Its Activated Complexes

Frequencies, cm^{-1}			Degeneracies	
Observed[a]	Model	Molecule	Heterolytic complex	Homolytic complex
3075(2)	3000	3	3	2
2975				
1443(2)	1400	6	5	5
1408				
1280				
1233(2)				
970(2)	800	5	3	6
830				
602				
541(2)				
365(2)	400	3	5	3
196	200	1	1	1

[a] Doubly degenerate frequencies are identified by (2).

TABLE V: Vibration Frequencies and Degeneracies for CD_3CF_3 and Its Activated Complexes

Frequencies, cm^{-1}			Degeneracies	
Observed[a]	Model	Molecule	Heterolytic complex	Homolytic complex
2284(2)	2200	3	3	2
2172				
1323	1200	6	5	5
1202(2)				
1069				
1043(2)				
812	800	4	2	5
798(2)				
569				
523(2)	400	4	6	4
333(2)				
150	200	1	1	1

[a] Doubly degenerate frequencies are identified by (2).

homolytic model a C-C-H bend is taken as the reaction coordinate, and a C-H stretch, a C-F stretch, and a C-C-F bend are taken as decreasing. The C-C stretch is increased to account for the incipient formation of the double bond. The vibration analysis of trifluoroethane clearly shows that most of the normal modes of this molecule are so thoroughly mixed that the motions listed above cannot be simply identified with the observed vibrations.[24] Our models assume that one out of a set of frequencies to which a motion contributes will be changed on going to the activated complex without drastically changing the remaining members of that set of frequencies. The significant difference between the heterolytic and homolytic models is that only in the homolytic model are the frequencies which change on deuteration changed in going to the activated complex.

To simplify calculation of the degeneracies of the energy levels of the activated complex, $P^{\ddagger}(E^{\ddagger})$, and the energy densities of the energized molecule, $N^*(E^*)$, the following simplifications were made. All molecular vibration frequencies[24] were grouped in five degenerate sets each of which had frequencies corresponding to integral multiples of 200 cm^{-1}.

$P(E)$ is found from the expression

$$P(E) = \sum_{a=0}^{a_m} P_a \left(\sum_{b=0}^{b_m} P_b \left\{ \sum_{c=0}^{c_m} P_c \left[\sum_{d=0}^{d_m} P_d \left(\sum_{e=0}^{e_m} P_e \right) \right] \right\} \right) \quad \text{(XIII)}$$

where the letters, a, b, c, d, and e refer to the number of units of energy available to the various oscillators of one of the five classes. The degeneracy due to the distribution of n_x units of energy among the g_x different oscillators of class n is given by

$$P_x = (n_x + g_x - 1)!/n_x!(g_x - 1)! \quad \text{(XIV)}$$

A program to calculate these sums was written for a Hewlett-Packard 9100B computer. $N(E) = P(E)/\Delta E$, where ΔE is the size of the energy interval between levels for which the $P(E)$ are calculated.

The degeneracies and energy densities were then substituted into eq X to calculate $k(E)$ for each E from E_{min} to E_{min} + 4000 cm^{-1}. These $k(E)$ values are then substituted into IX along with the appropriate $P(E)$ values. One may then calculate k's from eq IX or take ratios to obtain kinetic isotope effects. Table III shows the kinetic isotope effects calculated for the two models described in Tables IV and V for four different temperatures and compares them with the observed isotope effects. The kinetic isotope effect cancels out many of the necessary assumptions about the models used in the calculation. The four-centered model very slightly over estimates the isotope effect; the heterolytic model under estimates it. This is surprising since the isotope effect in the heterolytic model is as large as it is, for this model this is a secondary isotope effect; all the C-H frequencies are unchanged in going from the molecule to the complex.

To test for the possibility of artificial effects being introduced into the RRKM calculations by the simplifications necessary to make the solution for $P^{\ddagger}(E^{\ddagger})$ and $N^*(E^*)$ practical by the method used here, all calculations were duplicated using the Whitten-Rabinovitch method for evaluating $\Sigma P^{\ddagger}(E^{\ddagger})$ and $N^*(E^*)$.[25] Equation X was used to calculate $k(E)$, and the same distribution of colliding radicals was used. This calculation was now applied to the models described in Tables IV and V; new models in which the full frequencies of the original molecule were used and then reduced by arbitrary ratios as shown in Table VI; and finally the model used by Chang, Craig, and Setser in their recent paper on this reaction.[14] For each type of molecular model, a heterolytic and homolytic set of activated complex frequencies was chosen for CH_3CF_3 and CD_3CF_3, and rate constants and kinetic isotope effects were calculated for 468°K. These are summarized and compared with experimental observations in Table VII. All the calculated rate constants are larger than the observed value. The different calculated rate constants vary by as much as a factor of 3, indicating that this much variation can be caused by relatively small changes in the model. The most interesting thing about Table VII is that the isotope effects do not change markedly. Therefore, the values reported in Table III are not caused by arbitrary choices in the model, nor are they seriously affected by the approximations necessary for this calculation.

(24) B. Lafon and J. R. Nielson, *J. Mol. Spectrosc.*, **21**, 175 (1966).
(25) G. Z. Whitten and B. S. Rabinovitch, *J. Chem. Phys.*, **38**, 2466 (1963).

TABLE VI: Molecular and Activated Complex Frequencies Used in Full-Frequency Models of the Activated Complexes for Dehydrofluorination of 1,1,1-Trifluoroethane

CH_3CF_3			CD_3CF_3		
	Complex			Complex	
Molecule	Heterolytic	Homolytic	Molecule	Heterolytic	Homolytic
3035(2)	3035(2)	3035(2)	2284(2)	2284(2)	2284(2)
2975	2997	2110	2172	2172	1540
1443(2)	1443	1443	1323	1323	1323(2)
1408	1408	1000	1202(2)	1202	856
1280	1280	908	1069	1069	757
1233(2)	1233(2)	1233(2)	1043(2)	1043(2)	1043
970(2)	970(2)	1183	812	812	1000
830	830	830(2)	798(2)	798(2)	798(2)
602	602	602	569	404	404
541(2)	384(2)	384(2)	523(2)	371(2)	371(2)
365(2)	365(2)	365(2)	333(2)	333(2)	333(2)
196	196	196	150	150	150

TABLE VII: Rate Constants and Kinetic Isotope Effects for Different Models and Modes of Calculation for the Dehydrofluorination of 1,1,1-Trifluoroethane at 468°K

	σ	$10^{-8}k$, sec^{-1}	k_H/k_D
Observed		4.76	2.86
Equation XIII			
Heterolytic, Tables IV and V	3	11.6	2.36
Homolytic, Tables IV and V	6	12.3	2.99
Whitten–Rabinovitch method			
Heterolytic, Tables II and V	3	8.0	2.30
Homolytic, Tables IV and V	6	16.0	2.56
Heterolytic, Table VII	3	7.47	2.68
Homolytic, Table VII	6	25.0	2.66
Chang, Craig, and Setzer[23]	6	9.09	2.59

Conclusion

It has been shown that corrections for secondary reactions are necessary to obtain accurate rate constants for the unimolecular dehydrohalogenations of chemically activated alkanes. The RRKM calculations show that the calculated rate constant is more sensitive to details of the activated complex model than is the calculated kinetic isotope effect. In the kinetic isotope effect calculations many of the necessary assumptions cancel. While the calculated rate constants for a number of different models matched the experimentally determined value within the accuracy of some of the necessary assumptions, the fact that two rather crude but distinctly different models gave similar kinetic isotope effects shows that this quantity does not depend on the model in such a way as to allow subtle distinctions to be drawn or to warrant great effort to obtain an "exact" model for use in calculations. It appears that the comparison of accurately measured pyrolysis rate constants and isotope effects with calculated results will be necessary to clearly distinguish between the two types of activated complex models discussed here. In pyrolysis, quantum mechanical tunnelling should become important in the four-centered complex and be unimportant in complexes that do not directly involve the hydrogen atoms. Chemical activation produces the activated reactant in such high energy levels that this effect would be unimportant.

TABLE VIII: Vibration Frequencies for Colliding Radicals

Frequency cm^{-1}	Degeneracies		
	CF_3	CH_3	CD_3
3000		3	
2200			3
1400	1	3	
1200	2		3
600	2		
400	1		

Appendix I

For a system of two colliding radicals the degeneracy of an energy level, $P(E)$, was calculated as follows. The degeneracy contributed by 12 vibrations, 6 rotations, and the relative translation along the line of centers was included. Vibrations were all assumed to have frequencies equal to integral multiples of 200 cm^{-1}, and the degeneracies of the other degrees of freedom were summed over similar intervals before combining them into the total. Vibrational degeneracies were found by simple state counting for the models shown in Table VIII. The translational degeneracy for each energy interval was found on a purely relative basis. Since the energy density for a translation is inversely proportional to $\sqrt{E}$, $P_{tr}(E)$ for an interval was taken as proportional to the inverse square root of the energy in the middle of the interval.

Rotational degeneracies for each energy interval were found by summing over the degeneracies of all possible combinations of rotational quantum numbers whose energies from eq XV fall within that interval. The rotational

$$E_{rot} = BJ(J + 1) + CK^2 \qquad \text{(XV)}$$

constants B and C were evaluated for CF_3 assuming C_{3v} symmetry with tetrahedral angles and 1.39 Å C–F bond lengths and for CH_3 assuming planar structure with C–H bond lengths of 1.09 Å.

The four classes of degeneracy (total vibration, translation, CF_3 rotation, and CH_3 rotation) were combined by the equation

$$P(E) = \sum_0^E P_r(E_r)\left(\sum_0^{E_{r'}} P_{r'}(E_{r'})\left\{\sum_0^{E_{tr'}} P_{tr}(E_{tr})\right)\left[\sum_0^{E_{v'}} P_v(E_v)\right]\right\}\Bigg) \qquad \text{(XVI)}$$

The results of these calculations can be fitted by the equation

$$\log P(E) = d\sqrt{E} + f \qquad \text{(XVII)}$$

where E is given in cm^{-1}. For both isotopic forms d = 1.23 $cm^{1/2}$. For $CH_3 + CF_3$, f = 5.09; for $CD_3 + CF_3$, f = 5.67. This approximation underestimates $P(E)$ for E = 0 but is good to within less than 5% for all other E's up to 4000 cm^{-1}.

π Electronic Structure of Aqueous Squaric Acid and Its Anions

Lowell M. Schwartz* and Leland O. Howard

Department of Chemistry, University of Massachusetts, Boston, Massachusetts 02116 *(Received June 19, 1972)*

The spectra of aqueous squaric acid and its anions, bisquarate and squarate ion, have been determined in the near ultraviolet. Because of incomplete dissociation of the acid and the monoanion, the individual spectra were found by recording spectra of the equilibrium mixture at varying pH and utilizing the known dissociation constants of the acid to calculate the contribution of each species. The spectra were also calculated theoretically by the Pariser–Parr molecular orbital method. A comparison of the experimental and theoretical transition energies indicated that the ten π electron molecular orbital treatment serves as a valid model for understanding the spectra in the near ultraviolet.

Squaric acid (1,2-dihydroxycyclobutenedione) is a member of a series of oxocarbonic ring systems[1,2] with unusually strong acidic properties. It has been suggested[3,4] that the high acidities could be explained by extra stability of the anions due to π electron delocalization. This is supported by infrared spectral evidence that bands attributed to the C=O and C=C groups in the crystalline parent acids disappear in the spectra of the crystalline dianion salts.[3,5] On the other hand, however, a recent study[6] of the aqueous dissociation of squaric acid has shown through a thermodynamic analysis that the high degree of dissociation is due not to an excessive decrease in enthalpy upon dissociation but to an unusually low decrease in entropy. The high acid strength, therefore, must apparently be interpreted in terms of the nature of the structure of the solvent water. The entropy change on dissociation is small either because the water is greatly structured both around the undissociated acid and the ions (perhaps the neutral species resembles an ion pair) or because the water is relatively unstructured around both (perhaps charge delocalization in the anion imparts a low degree of structuring to the water). These experiments call for a comparison of the structures of squaric acid and its anions in the crystal and in solution. The structure of the squarate ion in the potassium monohydrate crystal has been well established by X-ray[7] and vibrational spectroscopic[8] methods, but the structures of crystalline bisquarate and squaric acid are unknown exactly although a vibrational study of squaric acid has been reported.[9] In solution the structure of squarate ion has been studied[8] but not the others, and this paper begins to attempt to do so.

Spectroscopic Measurement and Calculation

In order to probe the π electron character of squaric acid and its anions, we have undertaken a comparison of the ultraviolet absorption spectra of the three aqueous species: squarate ion (Sq^{2-}), bisquarate ion (HSq^-), and undissociated squaric acid (H_2Sq). Because of the relative acidity constants of the two dissociations, $pK_1 = 0.52$[6] and $pK_2 = 3.48$[10] at 25°, it is relatively simple to measure the Sq^{2-} spectrum at high pH values but spectra of the other two species cannot be obtained without interference. The method we used was first to buffer the solution so that only HSq^- and Sq^{2-} were present and to subtract the contribution due to squarate ion absorption and second to subtract the bisquarate absorption from a mixture of H_2Sq and HSq^-.

The three recorded spectra are shown in Figure 1. The Sq^{2-} spectrum is of a solution 1.82×10^{-5} F in squaric acid and 8.63×10^{-5} F in NaOH. The HSq^- and Sq^{2-} mixed spectrum was taken of 1.82×10^{-5} F squaric acid in acetic acid–acetate buffer (pH 4.11) and also in acetic acid (pH 3.39). The H_2Sq–HSq^- spectrum was of 3.68×10^{-5} F squaric acid in hydrochloric acid (pH 1.10). All the spectra were obtained with a Cary 14 spectrophotometer in 10-mm silica cells using the appropriate buffer as a reference solution.

In order to determine the spectrum of each species, it was necessary to know the concentrations of the individual species in the different solutions. These were calculated from the equilibrium expressions knowing the dissociation constants and estimating the ionic activity coefficients using the Davies equation.[11] The calculations were necessarily iterative and were done on a digital computer. The resulting spectra of the individual species are shown in Figure 2. The spectra of HSq^- derived from the buffers (pH 4.11 and 3.39) were identical within experimental error.

We estimate that experimental and theoretical uncertainties propagated to the molar absorptivities yield maximum uncertainties of 1.5, 5, and 32% of the peak values of the Sq^{2-}, HSq^-, and H_2Sq spectra, respectively. Each of the three appears to be composed of two overlapping peaks which shift slightly to longer wavelength in the sequence H_2Sq, HSq^-, and Sq^{2-} and which increase slightly in intensity in this same order.

π Electron Molecular Orbital Treatment

It is of interest to relate these spectra to a molecular orbital description of the π electrons. We are unaware of molecular orbital studies of H_2Sq or HSq^- but several

(1) R. West, H. Y. Niu, D. L. Powell, and M. V. Evans, *J. Amer. Chem. Soc.*, **82**, 6204 (1960).
(2) R. West and D. L. Powell, *J. Amer. Chem. Soc.*, **85**, 2577 (1963).
(3) S. Cohen, J. R. Lacher, and J. D. Park, *J. Amer. Chem. Soc.*, **81**, 3480 (1959).
(4) E. Patton and R. West, *J. Phys. Chem.*, **74**, 2512 (1970).
(5) K. Yamada, N. Mizumo, and Y. Hirata, *Bull. Chem. Soc. Jap.*, **31**, 543 (1958).
(6) L. M. Schwartz and L. O. Howard, *J. Phys. Chem.*, **75**, 1798 (1971).
(7) W. M. MacIntyre and M. S. Werkema, *J. Chem. Phys.*, **40**, 3563 (1964).
(8) M. Ito and R. West, *J. Amer. Chem. Soc.*, **85**, 2580 (1963).
(9) F. G. Baglin and C. B. Rose, *Spectrochim. Acta, Part A*, **26**, 2293 (1970).
(10) L. M. Schwartz and L. O. Howard, *J. Phys. Chem.*, **74**, 4374 (1970).
(11) C. W. Davies, "Ion Association," Butterworths, London, 1962, p 41.

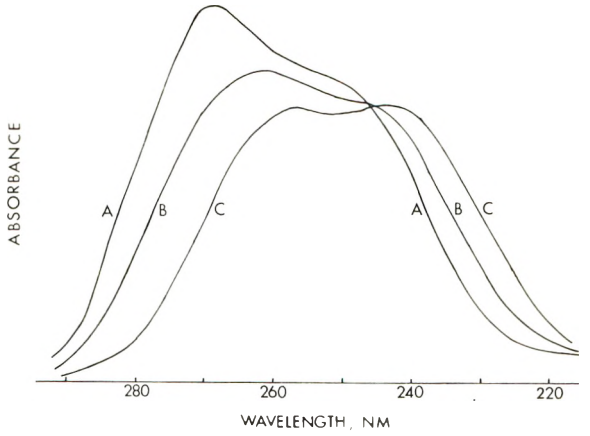

Figure 1. Squaric acid solution spectra in different pH media: 1.82×10^{-5} *F* squaric acid in 8.63×10^{-5} *F* NaOH (A); 1.82×10^{-5} *F* squaric acid in pH 3.39 acetate (B); 3.68×10^{-5} *F* squaric acid in 0.1 *M* HCl (absorbance normalized to 1.82×10^{-5} *F* squaric acid) (C).

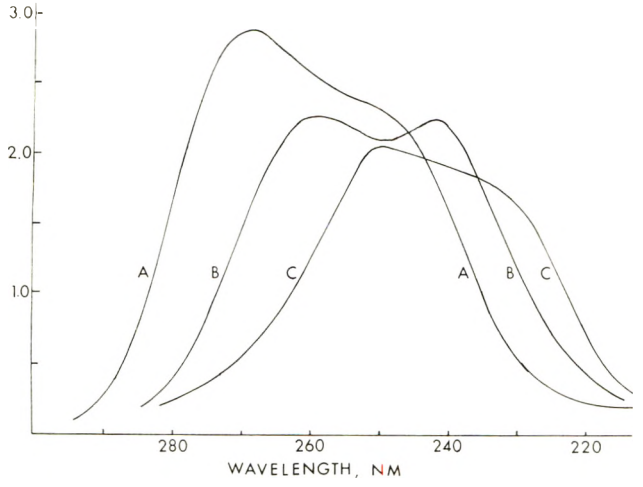

Figure 2. Spectra of aqueous Sq^{2-} (A), HSq^{-} (B), and H_2Sq (C). The ordinate scale is the molar absorptivity $\times 10^{-4}$ in (cm *M*)$^{-1}$.

calculations of this sort have been reported for the series of $(C_nO_n)^{-m}$ ions which includes the squarate ion. West and Powell[2] used the simple LCAO Hückel method, which generally is unsatisfactory for spectral predictions, but Bery[12] and Sakamoto and I'Haya[13] carried out more extensive calculations. We shall calculate spectral transition energies by the semiempirical Pariser-Parr (PP) method[14] which has been used successfully to describe electronic spectra in a wide variety of molecules.[15] The method will not be described except for values and sources of parameters used and the notation will follow that of Suzuki[15] whose summary of the method is particularly clear.

Since in this paper we are limited in dealing with the spectra in Figure 2 only, and since the absorption intensity of these is rather high ($\epsilon_{max} \approx 2.9 \times 10^4$), we assume that these bands correspond to symmetry-allowed transitions and so omit from consideration triplet state transitions from the singlet ground and also transitions involving nonbonded electrons on the oxygen atoms (n-π^* transitions) both types of which are forbidden and so would be expected to be weak at best. As stated earlier, the geometries of squaric acid species are unknown in solution and only squarate ion in the crystal has been well defined.

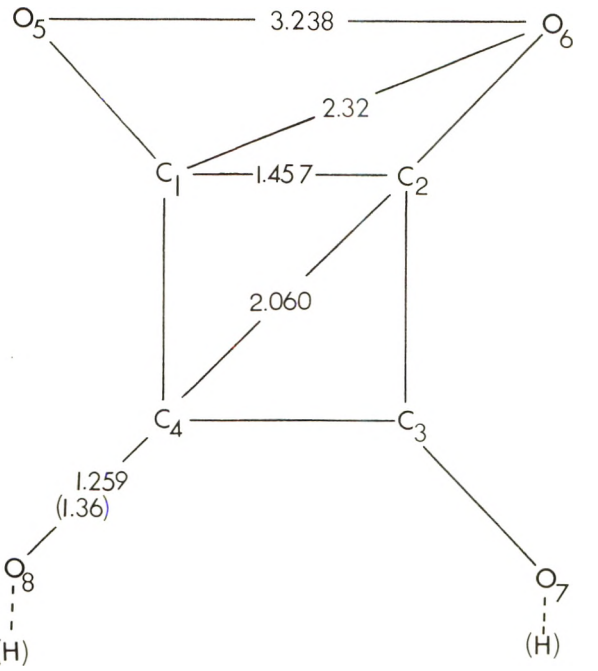

Figure 3. Atomic framework assumed for squaric acid species. The subscripts are atomic orbital indices and the values indicated between atoms are distances in Å. Parentheses indicate the structure when protonated.

Since geometrical parameters are required for the PP method, we will base the calculation on squarate ion only and will assume without justification that the geometry of the ion in the crystal carries over to dilute aqueous solution.

Squarate ion is a planar species whose symmetry corresponds to the point group D_{4h}.[7,8] The atomic framework of the ion is shown in Figure 3 where subscripts on each atom refer to the numbered index of atomic orbitals, *i.e.*, no. 1 through 4 are carbon and 5 through 8 are oxygen atomic orbitals. In the absence of structural information about the bisquarate ion, we will assume that this species differs from squarate ion in the bonding of a proton to oxygen no. 8 in Figure 3 and the lengthening of the C_4–O_8 distance to reflect its essential single bond character. Similarly H_2Sq will be assumed to have protons bonded to both O_8 and O_7. The addition of these protons lowers the symmetry of the framework and if the protons affect only the C–O groups to which they are attached, the π electron system of both HSq^- and H_2Sq would be characterized by C_{2v} symmetry. In HSq^- the C_2 axis would coincide with the C_4–O_8 bond, and in H_2Sq it would bisect the C_1–C_2 and C_3–C_4 bonds.

The internuclear distances in Sq^{2-} are also shown in Figure 3 between the corresponding atoms. These are from the X-ray analysis of MacIntyre and Werkema[7] and each distance is the average of two slightly differing values measured. In HSq^- and H_2Sq the length of the C–O bonds to which hydrogens bond will be assumed to increase to about 1.36 Å which is characteristic of phenols.

Sets of starting LCAO molecular orbitals of the form $\phi_i = \Sigma_i C_{ij}\chi_j$ were written based on the symmetry of the

(12) J. C. Bery, *J. Chim. Phys. Physicochim. Biol.*, **67**, 586 (1970).
(13) K. Sakamoto and Y. J. I'Haya, *J. Amer. Chem. Soc.*, **92**, 2636 (1970).
(14) R. Pariser and R. G. Parr, *J. Chem. Phys.*, **21**, 466, 767 (1953).
(15) H. Suzuki, "Electronic Absorption Spectra and Geometry of Organic Molecules," Academic Press, New York, N. Y., 1967.

TABLE I: Starting LCAO Molecular Orbitals

Molecular symmetry species	Orbital energy index	Atomic orbital coefficients							
		C_{i1}	C_{i2}	C_{i3}	C_{i4}	C_{i5}	C_{i6}	C_{i7}	C_{i8}
					Sq^{2-} (D_4h)				
a_{2u}	ϕ_1	0.4254	C_{11}	C_{11}	C_{11}	0.2627	C_{15}	C_{15}	C_{15}
e_g	ϕ_2	0.3456	0	$-C_{21}$	0	0.6169	0	$-C_{25}$	0
e_g	ϕ_3	0	C_{21}	0	$-C_{21}$	0	C_{25}	0	$-C_{25}$
b_{1u}	ϕ_4	0.1298	$-C_{41}$	C_{41}	$-C_{41}$	0.4828	$-C_{45}$	C_{45}	$-C_{45}$
a_{2u}	ϕ_5	C_{15}	C_{15}	C_{15}	C_{15}	$-C_{11}$	$-C_{11}$	$-C_{11}$	$-C_{11}$
e_g	ϕ_6	C_{25}	0	$-C_{25}$	0	$-C_{21}$	0	C_{21}	0
e_g	ϕ_7	0	C_{25}	0	$-C_{25}$	0	$-C_{21}$	0	C_{21}
b_{1u}	ϕ_8	C_{45}	$-C_{45}$	C_{45}	$-C_{45}$	$-C_{41}$	C_{41}	$-C_{41}$	C_{41}
					HSq^- (C_{2v})				
b_2	ϕ_1	0.3927	0.3868	C_{11}	0.4227	0.2352	0.2316	C_{15}	0.4462
a_2	ϕ_2	0.2116	0	$-C_{21}$	0	0.6747	0	$-C_{25}$	0
b_2	ϕ_3	−0.1885	−0.2595	C_{31}	0.0650	−0.1958	−0.2695	C_{35}	0.8415
b_2	ϕ_4	−0.1249	0.2427	C_{41}	−0.0614	−0.3945	0.7665	C_{45}	0.0855
b_2	ϕ_5	−0.2350	−0.2102	C_{51}	−0.3790	0.4827	0.4317	C_{55}	0.2221
b_2	ϕ_6	0.0378	0.6546	C_{61}	−0.6761	−0.1650	−0.2853	C_{65}	0.1720
a_2	ϕ_7	−0.6747	0	$-C_{71}$	0	0.2116	0	$-C_{75}$	0
b_2	ϕ_8	0.4879	−0.5015	C_{81}	−0.4610	−0.1321	0.1358	C_{85}	0.0816
					H_2Sq (C_{2v})				
b_2	ϕ_1	0.3840	C_{11}	0.4070	C_{13}	0.2155	C_{15}	0.3748	C_{17}
a_2	ϕ_2	0.0398	$-C_{21}$	−0.1550	$-C_{23}$	0.0367	$-C_{25}$	−0.6878	$-C_{27}$
b_2	ϕ_3	−0.2970	C_{31}	−0.0310	C_{33}	−0.3481	C_{35}	0.5382	C_{37}
a_2	ϕ_4	−0.2276	$-C_{41}$	0.0396	$-C_{43}$	−0.6658	$-C_{45}$	−0.0577	$-C_{47}$
b_2	ϕ_5	−0.1618	C_{51}	−0.3536	C_{53}	0.5398	C_{55}	0.2395	C_{57}
a_2	ϕ_6	−0.4349	$-C_{61}$	0.5079	$-C_{63}$	0.1901	$-C_{65}$	−0.1294	$-C_{67}$
b_2	ϕ_7	0.4880	C_{71}	−0.4565	C_{73}	−0.2024	C_{75}	0.1120	C_{77}
a_2	ϕ_8	0.5074	$-C_{81}$	0.4652	$-C_{83}$	−0.1386	$-C_{85}$	−0.0829	$-C_{87}$

species. The χ_j represent 2p π atomic orbitals at site j corresponding to the subscripts in Figure 3, and the coefficients C_{ij} were determined by a Hückel calculation using the following parameters suggested mainly in Chapter 9 of ref 15. For the parameter $\beta_{ij} = k_{ij}\beta$, k_{ij} is 0.89 for adjacent carbons at 1.457 Å, 0.30 for diagonal carbons at 2.060 Å, 0.80 for the C–O bonds at 1.260 Å, and 0.65 for the C–O bonds at 1.36 Å. For the parameter $\alpha_i = \alpha + h_i\beta$, h_i is zero for the carbons assumed trigonally hybridized, 1.28 for the essentially double bonded oxygens assumed digonally hybridized, and 2.0 for the essentially single bonded oxygens. The resulting sets of coefficients are shown in Table I for each of the three squaric acid species. The molecular orbitals are indexed in order of increasing energy as given by the Hückel calculation.

Since ten electrons participate in the π network of each species, the five lowest energy orbitals are each doubly occupied in the ground state (denoted by V_0) which belongs to the representation A_1 of the group C_{2v} or A_{1g} of D_{4h}. Considering all the possible singly-excited configurations V^{kr}, that is, states corresponding to the transfer of a single electron from an occupied molecular orbital k in the ground to an unoccupied molecular orbital r, one finds in the squarate ion configurations belonging to A_{1g}, A_{2g}, B_{1g}, B_{2g}, and E_u representations but only the E_u states can yield a nonzero transition moment with the A_{1g} ground and so only transitions to these states are symmetry-allowed and are likely to correspond to intense absorptions. In HSq^- and H_2Sq transitions from the ground to

TABLE II: Singly-Excited Configurations Yielding Allowed Transitions to the Ground V_0

Sq^{2-}	E_u:	$\{V^{56}, V^{57}\}$,[a] $\{V^{46}, V^{47}\}$, $\{V^{16}, V^{17}\}$, $\{V^{28}, V^{38}\}$
HSq^-	A_1:	$V^{56}, V^{58}, V^{46}, V^{48}, V^{36}, V^{38}, V^{27}, V^{16}, V^{18}$
	B_1:	$V^{57}, V^{47}, V^{37}, V^{26}, V^{28}, V^{17}$
H_2Sq	A_1:	$V^{57}, V^{46}, V^{48}, V^{37}, V^{26}, V^{28}, V^{17}$
	B_1:	$V^{56}, V^{58}, V^{47}, V^{36}, V^{38}, V^{27}, V^{16}, V^{18}$

[a] $\{$ denotes degenerate pair.

all the single-excited configurations are allowed and these are listed in Table II. In the PP method these configurations are expressed as antisymmetrized products of molecular orbitals and the actual molecular states are linear combinations of these with coefficients determined by a secular equation expressing the interaction among configurations of the same symmetry species. We have limited this interaction to singlet singly-excited configurations and have omitted doubly-excited configurations. This is an approximation which is taken to reduce the extent of the calculation but which introduces inaccuracies especially in the higher energy states.

Parameters needed for the PP calculations were chosen as follows. (1) Core Coulomb integrals $\alpha_p{}^c = -I_p - \Sigma_{q \neq p}(pp|qq)$ which in effect neglects penetration integrals. Valence state ionization energies I_p are given in Table III. It has been assumed in this model that the proximity of protons to oxygens in the HSq^- and H_2Sq

TABLE III: Parameters Chosen for the PP Calculation Valance State Ionization Energies I_p and Electron Affinities A_p[a]

	I_p, eV	A_p, eV
C tr tr tr π	11.16	0.03
O di²di π² π	17.91	2.71
O⁺ tr²tr tr π	34.08	15.30

Core Resonance Integrals, eV

β_{CC}^c (adjacent)	β_{CC}^c (diagonal)	β_{CO}^c	β_{COH}^c
−1.76	−0.088	−2.36	−1.9

Two-Center Coulomb Repulsion Integrals, eV

$(C_1C_1\|C_2C_2)$	7.297	$(C_4C_4\|O_8^HO_8^H)$	8.810
$(C_1C_1\|C_3C_3)$	6.032	$(O_5O_5\|O_6O_6)$	4.346
$(C_1C_1\|O_5O_5)$	8.539	$(O_5O_5\|O_7O_7)$	3.106
$(C_1C_1\|O_6O_6)$	5.714	$(O_5O_5\|O_7^HO_7^H)$	3.044
$(C_1C_1\|O_7O_7)$	4.200	$(O_5O_5\|O_8^HO_8^H)$	4.260
$(C_1C_1\|O_7^HO_7^H)$	4.090	$(O_7^HO_7^H\|O_8^HO_8^H)$	4.181
$(C_1C_1\|O_8^HO_8^H)$	5.617		

[a] Reference 17.

TABLE IV: Predicted Transitional Energies Relative to the Ground

Energy, eV	Principal configuration	Energy, eV	Principal configuration
	Sq^{2-} E_u States		Sq^{2-} E_u States
4.31	(0.9842) V^{56} or V^{57}	8.47	(0.9284) V^{16} or V^{17}
7.30	(0.8912) V^{46} or V^{47}	11.69	(0.9579) V^{28} or V^{38}
	HSq^- A_1 States		HSq^- B_1 States
0	(0.8825) V_0	5.49	(0.9490) V^{57}
4.98	(0.9767) V^{56}	7.10	(0.8197) V^{26}
6.51	(0.8400) V^{46}	7.37	(0.8334) V^{47}
7.98	(0.6639) V^{27}	11.12	(0.7758) V^{28}
8.69	(0.8277) V^{58}	12.19	(0.8262) V^{17}
10.55	(0.7412) V^{16}	13.49	(0.9820) V^{37}
10.85	(0.8998) V^{48}		
12.20	(0.7458) V^{36}		
14.83	(0.9504) V^{15}		
16.92	(0.9464) V^{38}		
	H_2Sq A_1 States		H_2Sq B_1 States
0	(0.8332) V_0	5.20	(0.9889) V^{56}
5.47	(0.9044) V^{46}	5.74	(0.9689) V^{47}
7.70	(0.7292) V^{57}	8.31	(0.9433) V^{58}
9.47	(0.9036) V^{48}	10.20	(0.9380) V^{36}
10.90	(0.9293) V^{37}	11.18	(0.9466) V^{16}
12.18	(0.8963) V^{17}	13.50	(0.8173) V^{27}
13.18	(0.9288) V^{26}	14.44	(0.7432) V^{38}
17.84	(0.9661) V^{28}	15.75	(0.7905) V^{18}

species changes the hydridization of oxygen from digonal to trigonal and that a full positive charge appears on the oxygen. This assumption leads to large differences in oxygen I_p values depending on the presence or absence of protons and also to differences of total positive charge on the σ cores of the three species. This practice has been questioned by a reviewer who suggests an alternative procedure of setting the oxygen I_p's in Sq^{2-} equal to the average of those in H_2Sq. We acknowledge this as a possibility but feel that it in effect puts too much positive charge into the Sq^{2-} core system. Perhaps our procedure puts in too little and we leave this question open. (2) Core resonance integrals β_{pq}^c are assigned empirical values. For the carbonyls $\beta_{CO}^c = -2.36$ eV, a value found to be satisfactory in similar calculation on quinones by Leibovici and Deschamps.[16] $\beta_{COH} = -1.9$ eV which value is estimated from β_{CO}^c assuming proportionality with respect to atomic overlap integrals[15] taken at 1.36 and 1.26 Å. We also adopt the empirical expression used in ref 16 for carbon–carbon core resonance integrals. (3) Coulomb repulsion integrals over atomic orbitals are estimated by Pariser and Parr's method[14] including the zero-differential overlap approximation. The one-center integrals (pp|pp) are taken as $I_p - A_p$ and valence state electron affinities A_p are listed in Table III.[17] The two-center integrals (pp|qq) are calculated from the tangent-sphere model for nuclei separated by more than 2.80 Å and from an interpolation formula which varies quadratically with interatomic distance at lesser values. All nonzero Coulomb repulsion integrals are given in Table III.

The PP calculations with configuration interaction yield the energy values shown in Table IV. Each value represents the energy of a π electron state comprising a linear combination of configurations of the same symmetry and is relative to the ground or lowest such state. These are the predicted energies of the spectral bands in this approximation. Although the configuration interaction precludes the assignment of these transition energies to particular singly-excited transitions V^{kr}, we have listed that V^{kr}, together with its normalized mixing coefficient, which is the principal contributor to the linear combination.

Discussion

The three spectral bands shown in Figure 2 each appear to be composed of two overlapping peaks. A resolution of the Sq^{2-} band into two Gaussian components by a least-squares method[18] yields peaks of unequal height and width centered at 272 (4.55 eV) and 252 nm (4.90 eV). Similarly, component peaks resolved from the HSq^- spectrum are at 264 (4.80 eV) and 244 nm (5.07 eV). The high degree of uncertainty associated with the H_2Sq spectrum in Figure 2 makes a resolution into components meaningless although the band position is clearly shifted about 0.2 eV higher than HSq^- and the shape implies two components with peaks separated by a fraction of an electron volt.

The π electron molecular orbital calculation summarized in Table IV predicts that several transitions should occur between 4 and 6 eV corresponding to the spectral range of Figure 2. In Sq^{2-} there is predicted a transition at 4.3 eV, in HSq^- at 5.0 and 5.4 eV, and in H_2Sq at 5.2, 5.5, and 5.7 eV. The experimental spectrum implies two transitions for each species with each transition rather intense, *i.e.*, having oscillator strength values roughly in the range 0.2–0.7. Approximate theoretical calculations of the oscillator strengths of these transitions indicate that all are sufficiently intense except for the 5.5-eV transition in H_2Sq. It seems reasonable then to conclude that the H_2Sq spectrum corresponds to the calculated transitions at 5.20 and 5.74 eV and that the HSq^- spectrum corresponds to the calculated transitions at 4.98 and 5.49 eV. The Sq^{2-}

(16) C. Leibovici and J. Deschamps, *Theor. Chim. Acta*, **4**, 321 (1966).
(17) J. Hinze and H. H. Jaffé, *J. Amer. Chem. Soc.*, **84**, 540 (1962); *J. Phys. Chem.*, **67**, 1501 (1963).
(18) L. M. Schwartz, *Anal. Chem.*, **43**, 1336 (1971).

spectrum corresponds to the transition from the ground to the double-degenerate E_u excited state at 4.31 eV in which perhaps the degeneracy has been destroyed.

The absolute energy values of the spectra do not correspond exactly to the calculated transitional energies. This could be attributed to the approximations in the theory such as the neglect of doubly-excited states in the configuration interaction or to the effect of inherent uncertainties such as the unknown geometries of the aqueous species and the estimated values of the empirical parameters employed. The inclusion of doubly-excited configurations would lead to a relative lowering of the singly-excited states which would tend to reduce the discrepancies of HSq^- and H_2Sq. In Sq^{2-}, however, the theoretical value of 4.3 eV is too low and two other calculations[12,13] have both shown already that inclusion of doubly-excited configurations lowers the predicted value still further.

Acknowledgment. We are deeply appreciative of the helpful discussions offered by Professor Robert I. Gelb in the course of the experimental part of this work and also to the National Institute of Dental Research, N. I. H., Bethesda, Md., for permission to use their digital computation facilities.

On the Properties of Certain Four-Phase Oil–Water–Solid–Vapor Configurations. I. Comments on the Stability of a Four-Phase Contact Line

M. P. Aronson, A. C. Zettlemoyer,* and M. C. Wilkinson

Center for Surface and Coatings Research, Lehigh University, Bethlehem, Pennsylvania 18015 *(Received May 8, 1972)*

An oil drop resting on a solid surface and partially submerged in a film of water represents a four-phase configuration common to certain situations in detergency, in lubrication, in the flushing of pigments from water to oil phase, in the flotation of minerals, and in secondary oil recovery. With depletion of the water film, a four-phase oil–water–solid–vapor line of contact can develop. A thermodynamic analysis, which is an extension of the methods used by Gibbs when all phases are fluid, indicates that this configuration can either be stable or unstable. Criteria for the stability of the contact line in terms of the solid–fluid contact angles are determined and then applied to several systems.

Introduction

An oil drop resting on a solid surface and partially submerged in a film of water represents a four-phase configuration common to several technologies. These include certain situations in detergency, in lubrication, in flushing of pigments from water to oil phase, and in the flotation of minerals. Notwithstanding its practical importance, the configuration of a partially submerged drop has received little attention and has usually been discussed in conjunction with other phenomena.[1-3]

Another example of a four-phase configuration is that shown in Figure 1a and has the interesting feature of possessing a four-phase contact line. This configuration has been proposed as a limiting state reached from a partially submerged drop by water film drainage[3] or surface tension fluctuations.[1,2] Although it is well known that four intersecting soap film lamella constitute an unstable configuration,[4,5] it is not so generally appreciated that a four-phase (or more) contact line can be stable under appropriate conditions. Gibbs[6] considered the case of four intersecting fluids phases and determined criteria for the stability of such contact lines.

One goal of this paper is to extend the Gibbsian formulation to obtain criteria for the stability of the four-phase contact line when one of the phases is solid. Following this, a discussion of the use of the stability criteria for predicting the domain of equilibrium states of the four-phase contact line is given.

In a subsequent article the static profiles of partially submerged drops and the four-phase contact line state are extensively discussed.

Contact Angle Criteria for the Stability of the Four-Phase Contact Line. In calculating the stability of any thermodynamic system, the type of change to which the stability refers is first specified. These changes may include the formation of a new phase or interface in, on, or at the intersection of preexisting phases or interfaces. The conditions for equilibrium without regard to stability, subject to continuous changes, are first calculated. Relationships which must be obeyed for the stability of this equilibrium are then sought. The equilibrium calculation involves conditions which render the first variation in en-

(1) E. J. Clayfield, D. J. Dean, J. B. Mathews, and T. V. Withen, *Int. Congr. Surface Activity, 2nd*, **3**, 165 (1957).
(2) J. T. Davies, and E. K. Rideal, "Interfacial Phenomena," Academic Press, New York, N. Y., 1961.
(3) A. C. Zettlemoyer, M. P. Aronson, and J. A. Lavelle, *J. Colloid Interface Sci.*, **34**, 545 (1970).
(4) C. V. Boys, "Soap Bubbles Their Colors and Forces which Mold Them," Dover Publications, New York, N. Y.
(5) A. W. Adamson, "Physical Chemistry of Surfaces," Interscience, New York, N. Y., p 524.
(6) J. W. Gibbs, "Thermodynamics," Vol. 1, Dover Publications, New York, N. Y., p 287.

tropy zero, while the stability calculation involves relationships which render the entropy an actual maximum, *i.e.*, the second variation of entropy must be negative. The conditions among the state variables so obtained will be both *necessary* and *sufficient* for stable equilibrium.

It is evident that a complete stability analysis (including configurational stability) as described above for the system shown in Figure 1a subject to even a limited number of changes might be formidable. However, if only certain necessary conditions for stability are sought (leaving the sufficiency questionable), the problem becomes much simpler. In many instances, these conditions will be satisfactory for determining whether stability of the four-phase configuration is precluded.

The discussion will be limited to the relationships among the contact angles defined in Figure 1a which are necessary for stability subject to changes which are now described. These changes include the continuous increase or decrease of the solid-fluid contact areas (Figure 1b); the formation of a new interface, solid-vapor, at the intersection of the four phases (Figure 1c); and the formation of a new interface, oil-water, at the intersection of the four phases (Figure 1d).

In all that follows the solid will be regarded as smooth, planar, homogeneous, and rigid. Thus, the state of strain of the solid is assured constant and unaffected by the pressure distribution within the fluids, and their surface tensions. Furthermore, it is assumed that passive resistances to change are absent. The criteria thus obtained are strictly valid for ideal systems of the type studied by Zisman and others.[7,8]

A Necessary Contact Angle Condition for Equilibrium of the Four-Phase Configuration Subject to Continuous Change in Interfacial Area. It has been shown[9] that a necessary relationship for equilibrium of the four-phase configuration subject to the type of variation shown in Figure 1b is

$$\gamma_{S/O} + \gamma_{O/V} \cos \theta_o = \gamma_{S/W} + \gamma_{W/V} \cos \theta_W \qquad (1)$$

where $\gamma_{S/O}$, $\gamma_{O/V}$, $\gamma_{S/W}$, and $\gamma_{W/V}$ are the interfacial tensions at the solid-oil, oil-vapor, solid-water, and water-vapor interfaces, respectively. θ_o and θ_W are the contact angles defined in Figure 1a. Equation 1 can be obtained by a procedure analogous to that used by Gibbs[10] when all phases were fluid (energy formulation) or an extension of the method used by Johnson[11] to derive the Young equation[12] for a three-phase solid-liquid-fluid contact line in a gravity field.

It should be noted that eq 1 was derived for the configuration in a gravity field but contains no terms for the so-called "hydrostatic force contribution to the resolution of forces at the contact line" as earlier supposed.[1-3] Since eq 1 is necessary for equilibrium, it is obviously also necessary for stable equilibrium.

Since the Young equation[11-13] is obeyed at equilibrium for an oil drop, submerged in water, in contact with a solid surface

$$\gamma_{S/V} - \gamma_{S/O} = \gamma_{O/W} \cos \theta_{O/W}^{eq} \qquad (2)$$

where $\gamma_{O/W}$ is the oil-water interfacial tension and $\theta_{O/W}^{eq}$ is the equilibrium contact angle at the oil-water-solid intersection, measured through the oil phase, eq 1 may be rewritten as

$$\gamma_{O/V} \cos \theta_o = \gamma_{O/W} \cos \theta_{O/W}^{eq} + \gamma_{W/V} \cos \theta_W \qquad (3)$$

Thus, if all fluid tensions are known and $\theta_{O/W}^{eq}$ is determined, pairs of angles, θ_o and θ_W, satisfying eq 1 can be calculated. It appears from eq 1 or 3 that, for the four-phase contact line, the two angles θ_o and θ_W are both not uniquely determined by the interfacial tensions of the system.

Contact Angle Conditions for Stability to the Formation of a Solid-Vapor Interface. Assume that the initial state of the system is at stable equilibrium with respect to continuous changes in area. The variation now considered is the formation of a solid-vapor interface of infinitesimal area as shown in Figure 1c. A necessary condition regarding the contact angles which render the unvaried state stable to this change will now be determined.

To demonstrate that the initial state is stable to such a variation, it is necessary to show that the energy of this state is less than the energy of any other state which contains a solid-vapor interface of infinitesimal extent (providing the entropy is fixed). However, the infinitesimally varied state of least energy will necessarily be that of a state in which the solid-vapor interface created subsists, in equilibrium, with the rest of the system. Thus, conditions which cause the energy of the initial state to be less than the energy of the proposed equilibrium state also cause the initial state to have less energy than all such states produced by infinitesimal variations.

For the varied state containing the increment of solid-vapor interface to subsist at equilibrium, it is necessary that the two contact lines, solid-oil-vapor and solid-water-vapor, be also at equilibrium. This requires that the Young equation be obeyed

$$\gamma_{S/V} = \gamma_{S/O} + \gamma_{O/V} \cos \theta_o' = \gamma_{S/O} + \gamma_{O/V} \cos \theta_o$$

and (4)

$$\gamma_{S/V} = \gamma_{S/W} + \gamma_{W/V} \cos \theta_W' = \gamma_{S/W} + \gamma_{W/V} \cos \theta_W$$

where $\gamma_{S/V}$ is the equilibrium surface tension of the solid-vapor interface in which the solid is in the same state of strain and is in equilibrium with a vapor *saturated* with oil and water components. Since the variation is infinitesimal, θ_W' and θ_o' differ infinitely little from θ_o and θ_W.

If however

$$\gamma_{S/V} > \gamma_{S/O} + \gamma_{O/V} \cos \theta_o$$

and (5)

$$\gamma_{S/V} > \gamma_{S/W} + \gamma_{W/V} \cos \theta_W$$

then the initial state will be stable to the formation of an increment of solid-vapor interface. To see this, we observe that for the varied state containing the new interface and satisfying the above inequality to come to a new equilibrium requires θ_o and θ_W to diminish (cos θ's to increase). This requires movement of the two contact lines (solid-oil-vapor and solid-water-vapor) toward the position occupied by the four-phase contact line in the initial state. But since the displacement is infinitesimal, the four-phase contact line will be re-formed before the two three-phase contact lines could achieve positions such that their angles would satisfy the Young conditions.

(7) W. A. Zisman, "Contact Angle, Wettability, and Adhesion," American Chemical Society, Washington, D. C., pp 1-51.
(8) A. W. Neumann, G. Haage, and D. J. Renzow, *J. Colloid Interface Sci.*, **35**, 379 (1971).
(9) M. P. Aronson, Ph.D. Thesis, Lehigh University, 1973.
(10) Reference 6, p 276.
(11) R. E. Johnson, *J. Phys. Chem.*, **63**, 1655 (1959).
(12) T. Young, "Miscellaneous Works," Vol. 1, G. Peacock, Ed., J. Murray, London, 1855, p 418.
(13) Reference 6, p 326.

ห้องสมุด กรมวิทยาศาสตร์

If, on the other hand

$$\gamma_{S/V} < \gamma_{S/O} + \gamma_{O/V} \cos \Theta_o$$

and (6)

$$\gamma_{S/V} < \gamma_{S/W} + \gamma_{W/V} \cos \Theta_w$$

then equilibrium of the two three-phase contact lines in the varied state can be achieved by motion in a direction away from the initial state (corresponding to a decrease in cos Θ's). In this case, motion of the varied state would be away from the initial state and the four-phase configuration would be unstable. The necessary contact angle requirement for stability of the four-phase configuration can be reexpressed using Young's equation

$$\gamma_{S/V} - \gamma_{S/O} = \gamma_{O/V} \cos \Theta_o^{eq}$$

and (7)

$$\gamma_{S/V} - \gamma_{S/W} = \gamma_{W/V} \cos \Theta_w^{eq}$$

where Θ_o^{eq} and Θ_w^{eq} are the equilibrium contact angles at the oil-solid-vapor and water-solid-vapor intersections for mutually saturated liquid oil and water, respectively, in the presence of a vapor saturated with oil and water. The combination of eq 7 with the conditions given by eq 4 and 5 give

$$\Theta_o \geqq \Theta_o^{eq}$$

and (8)

$$\Theta_w \geqq \Theta_w^{eq}$$

Contact Angle Conditions for Stability to the Formation of an Oil-Water Interface. Again assume that the initial state is at stable equilibrium with respect to continuous changes in area. The variation now considered is the creation of an oil-water interface which is vanishingly small. Proceeding as above, we note that the distinguishing case of stability *vs.* instability of the four-phase contact line occurs when the created increment of oil-water interface can just subsist, at equilibrium, with the rest of the system. For this varied state we may write

$$\gamma_{O/W}^2 = \gamma_{O/V}^2 - \gamma_{W/V}^2 - 2\gamma_{O/V}\gamma_{W/V} \cos (180 - \alpha') = \gamma_{O/V}^2 + \gamma_{W/V}^2 - 2\gamma_{O/V}\gamma_{W/V} \cos (180 - \alpha) \quad (9)$$

and

$$\gamma_{O/W} \cos \Theta_{O/W} = \gamma_{S/W} - \gamma_{S/O} \quad (10)$$

Equation 9 is a formulation of Neumann's Triangle[14] (using the law of cosines) for the oil-water-vapor intersection, while eq 10 is the Young equation.

Since the variation is indefinitely small, α' differs infinitesimally from $\alpha (= 180 - \Theta_o - \Theta_w)$ in the initial state. However, the angle $\Theta_{O/W}$ is somewhat arbitrary. Let us assume that there exists some angle $\Theta_{O/W}$ which satisfies eq 10 and then investigate the conditions in α which are necessary to render the initial state stable.

Suppose that $\gamma_{O/W}$ and α are such that

$$\gamma_{O/W}^2 > \gamma_{O/V}^2 + \gamma_{W/V}^2 - 2\gamma_{O/V}\gamma_{W/V} \cos (180 - \alpha) \quad (11)$$

then no equilibrium of the three-phase oil-water-vapor contact line can be achieved by motion in the direction away from the solid surface. This situation holds because such motion would only increase α and, therefore, would increase the inequality in eq 11, *i.e.*, drive the system away from possible equilibrium as expressed by a condition analogous to eq 9. Thus the system will move toward equilibrium in a direction which creates the four-phase contact line. Since the displacement is infinitesimal, the initial state will be stable and will be re-formed.

If however

$$\gamma_{O/W}^2 < \gamma_{O/V}^2 + \gamma_{W/V}^2 - 2\gamma_{O/V}\gamma_{W/V} \cos (180 - \alpha) \quad (12)$$

then an equilibrium state for the three-phase line of contact lies in a direction away from the initial state. Hence, spontaneous motion away from the four-phase state would commence and this state would be unstable to the change.

From Neumann's law of triangles and the law of cosines

$$\gamma_{O/W}^2 = \gamma_{O/V}^2 + \gamma_{W/V}^2 - 2\gamma_{O/V}\gamma_{W/V} \cos (180 - \alpha^{eq}) \quad (13)$$

where α^{eq} is the equilibrium angle between the oil-vapor and water-vapor interfaces for an oil lense. We may then write that a necessary condition for at least marginal stability of the four-phase configuration subject to the formation of an oil-water interface is

$$\begin{gathered} -\cos (180 - \alpha^{eq}) \geqq -\cos (180 - \alpha) \\ \cos \alpha^{eq} \geqq \cos \alpha \end{gathered} \quad (14)$$

or

$$\alpha = 180 - \Theta_o - \Theta_w \geqq \alpha^{eq} \quad (15)$$

In summary, the necessary contact angle conditions for the four-phase oil-water-solid-vapor intersection to be stable with respect to continuous changes in area, or to separating to form two three-phase intersections are

$$\gamma_{S/O} + \gamma_{O/V} \cos \Theta_o = \gamma_{S/W} + \gamma_{W/V} \cos \Theta_w \quad (1)$$

or

$$\gamma_{O/V} \cos \Theta_o = \gamma_{O/W} \cos \Theta_{O/W}^{eq} + \gamma_{W/V} \cos \Theta_w \quad (3)$$

$$\begin{gathered} \Theta_o \geqq \Theta_{O/V}^{eq} \\ \Theta_w \geqq \Theta_{W/V}^{eq} \end{gathered} \quad (8)$$

$$180 - (\Theta_w + \Theta_o) \geqq \alpha^{eq} \quad (15)$$

From the above conditions, some obvious cases in which instability of the four-phase oil-water-solid-vapor contact line is either probable or certain are (1) spontaneous spreading of the oil on the water phase or the water on the oil phase; (2) spontaneous spreading of the oil on the water-covered solid surface; (3) high values for Θ_o^{eq} of Θ_w^{eq}, *i.e.*, very hydrophobic or oleophobic solids. Circumstances which would enhance the chances for a stable contact line are (1) spontaneous spreading of water at the water-solid-vapor intersection with low Θ_o^{eq}, and (2) large oil-water interfacial tension.

Finally, it should be mentioned that the necessary conditions for stability of the four-phase contact line have been determined for a symmetric example. However, such criteria would also hold for less symmetric examples such as oil films coating flat plates which are partially immersed vertically in water.

Use of the Criteria to Determine the Equilibrium Domain of the Four-Phase Contact Line. The equations which can be used to describe the shape or configurations of the system shown in Figure 1 are the well-known Laplace[15]–Young[16] equations coupled with eq 3

(14) F. Neumann, "Vorlesungen uber die Theorie der Capillaritat," Teubner, Leipzig, 1894.
(15) P. S. De Laplace, "Mecanique Celeste," Suppl. Vol. 10, 1806.
(16) P. R. Pujado, C. Huh, and L. E. Scriven, *J. Colloid Interface Sci.*, **38**, 662 (1972).

$$P_o - P_v = \gamma_{O/V}(1/R_{1(O/V)} + 1/R_{2(O/V)}) \quad (16)$$

$$P_w - P_v = \gamma_{W/V}(1/R_{1(W/V)} + 1/R_{2(W/V)}) \quad (17)$$

and

$$\gamma_{O/V} \cos \Theta_o = \gamma_{O/W} \cos \Theta_{O/W}^{eq} + \gamma_{W/V} \cos \Theta_w \quad (3)$$

The left members of eq 16 and 17 represent the pressure difference across the curved fluid interface and γ's are interfacial tensions. The $(1/R)$'s are principle curvatures given positive sign if their centers are in the phase given by the subscript of the leading pressure term. Equations 16 and 17 embody the usual assumptions regarding the neglect of the contribution of bending and torsional motion to the superficial energy of the particular dividing surface[17,18] and the influence of gravity on the interfacial tensions.[19]

For the axisymmetric configuration, eq 16 and 17 can be transformed in the usual manner[20] by substituting for the pressure at any position, the pressure at an appropriate reference position plus the hydrostatic pressure term, and replacing the curvatures by the well-known expressions from analytical geometry. With reference to Figure 2, this gives the set of second-order nonlinear differential equations

$$[y''/(1 + (y')^2)^{3/2}] + [y'/X(1 + (y')^2)^{1/2} = (y/a_{O/V}^2) - (K/\gamma_{O/V}) \quad (18)$$

and

$$[V''/(1 + (V')^2)^{3/2}] + [V'/X(1 + (V')^2)^{1/2}] = (V/a_{W/V}^2) - (h_\infty/a_{W/V}^2) \quad (19)$$

where $y(x)$, $v(x)$, and h_∞ are shown in Figure 2, a's are the capillary constants, $a_{i/J} = (\gamma_{i/J}/g\Delta\rho_{iJ})^{1/2}$, and K is defined as

$$K = 2(\gamma_{O/V}/b) + \lambda g \Delta\rho_{O/V} \quad (20)$$

where $1/b$ is the limiting curvature at the apex of the drop, *i.e.*, at $x = 0$, $y = \lambda$.

Equations 18 and 19 have the boundary conditions

$$y'(o) = 0 \quad (21)$$

$$y'(d) = \tan(180 - \Theta_o) \quad (22)$$

$$y(d) = 0 \quad (23)$$

$$V(d) = 0 \quad (24)$$

$$V'(d) = \tan\Theta_w \quad (25)$$

and

$$V' \to 0 \text{ as } x \to \infty \quad (26)$$

The volume of the oil phase is given by

$$V_o = 2\pi \int_0^d y(x)x\,dx \quad (27)$$

Suppose that all the fluid tensions, densities and $\Theta_{O/W}^{eq}$ are known. It appears from eq 3 and 18–26 that, for a given volume of oil, V_o, there are an infinite number of values of h_∞ (within limits which are discussed below) which simultaneously satisfy eq 3, 16, and 17. This can be seen through the following argument. $y(x)$ is uniquely determined through eq 18 once Θ_o and V_o are known. However, there are an infinite number of Θ_o's which satisfy eq 3 and, therefore, a family of $y(x)$ functions which simultaneously satisfy eq 18, the volume constraint (eq 27), and

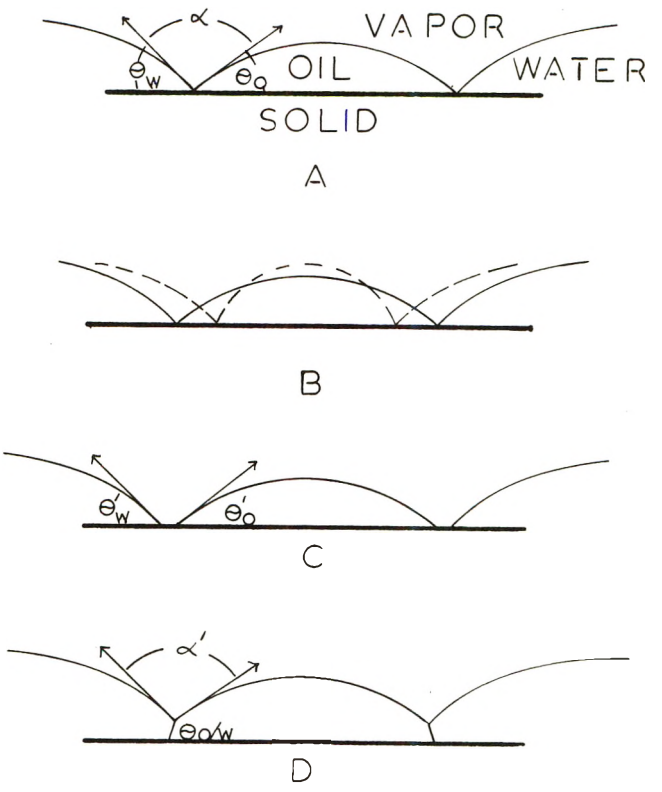

Figure 1. (a) Oil–water–vapor–solid system containing a four-phase intersection; (b) variation of state in which no new interface is formed; (c) formation of solid–vapor interface; (d) formation of an oil–water interface.

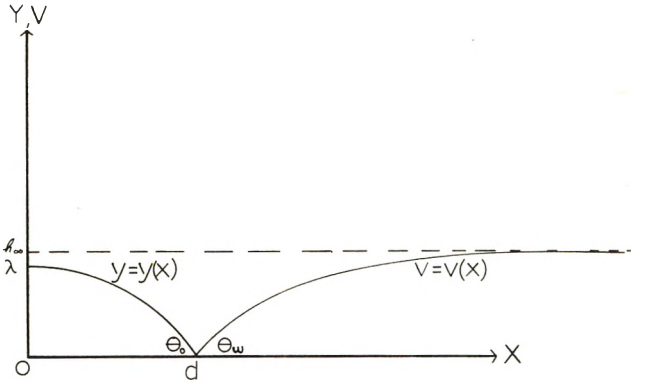

Figure 2. Coordinate system and nomenclature for the calculation of the profile of the four-phase contact line configurations.

the boundary conditions in eq 21 and 22. This is also physically obvious since it is well known that two oil drops of identical volumes, in contact with different solids, will have different base radii (d) provided that the two contact angles are different.

If an arbitrary value of Θ_o, Θ_o*, satisfying the criteria of eq 8 is chosen, this will uniquely fix the value of d (V_o is considered specified). However, for this value of Θ_o*, Θ_w* will also be uniquely determined from eq 3. Once, d and Θ_w* are fixed a unique $V(x)$ and h_∞ which simultaneously satisfy the boundary conditions (eq 24–26) and eq 19 will

(17) J. C. Melrose, *Ind. Eng. Chem.*, **60**, 53 (1968).
(18) C. Huh, Ph.D. Thesis, Department of Chemical Engineering, University of Minnesota, 1969, p B1–11.
(19) Reference 6, p 281.
(20) H. M. Princin, "Surface and Colloid Science," Vol. 2, E. Matijevic, Ed., Wiley-Interscience, New York, N. Y.

result as shown in an elegant article by Huh and Scriven.[21] Thus for any value of Θ_o* a particular water film thickness results. However, Θ_o* was chosen arbitrarily and thus, for a given system, having a particular oil volume, there are a family of solutions of the configuration, each determined uniquely by a particular water film thickness, h_∞.

The criteria expressed in eq 3, 8, and 15 enable the calculation of the minimum and maximum oil drop radii (and the accompanying water film thickness) in which a particular oil volume can remain in the configuration containing a four-phase contact line. The minimum radius and accompanying height can be calculated in the following way. (1) From eq 3 it is observed that as Θ_o increases so does Θ_w and *vice versa*. The maximum stable angles Θ_o^{max} and Θ_w^{max} will be those in which

$$180 - \Theta_o^{max} - \Theta_w^{max} = \alpha^{eq} \quad (28)$$

where α^{eq} can be calculated from eq 13. (2) Once Θ_o^{max} is calculated d_{min} can be calculated from the solution to eq 18 which satisfy the boundary conditions in eq 21-23 and the volume constraint given in eq 27. (3) From the values of d_{min} and Θ_w^{max} the accompanying value of h_∞ can be calculated from the solution to eq 19 with the boundary conditions (eq 24-26).

Values of d_{max} and h_∞ can be calculated in a similar manner, in this case using the criteria given in eq 8.

In a subsequent article detailed numerical calculations of the profile of four-phase contact line configurations and partially submerged drops will be presented.

Examples

Suppose that the oil phase is a white mineral oil such as Drakeol-10 (Pennsylvania Refining Co.) whose surface and interfacial tension with water are 30.4 and 52.0 dyn cm^{-1}, respectively. The value of α^{eq} calculated from these tensions and eq 13 is 141°. For stability of a four-phase contact line in a system containing water and this oil, the sum of the contact angles Θ_w and Θ_o on the particular solids of interest cannot exceed 39°, subject to eq 3 and 8. Table I contains values of the various contact angles for the solids polytetrafluoroethylene (Teflon), polyethylene, polymethylmethacrylate (Plexiglas G), and glass.

TABLE I: Values of the Contact Angles on Several Solid Surfaces (Oil Phase–White Mineral Oil)

Solids	$\Theta_{O/V}^{eq}$, deg	$\Theta_{W/V}^{eq}$, deg	$\Theta_{O/W}^{eq}$, deg
Polytetrafluoroethylene	52	108	37
Polyethylene	0	91	56
Polymethylmethacrylate	0	74	89
Glass	0 (<2)	0	144

For the low-energy solids Teflon, polyethylene, and Plexiglas the stability conditions (eq 3, 8, and 15) cannot be simultaneously met. Thus, the four-phase contact line, if formed, will not be stable. Exactly which final state would be formed from the four-phase contact line depends on the initial values of the contact angles Θ_o, Θ_w, and α. If α were greater than or equal to 141°, then the final state would be as shown in Figure 1c. This particular example has application in film dewetting processes initiated by oil droplets as described in ref 3. Conversely, if Θ_o and Θ_w satisfied eq 8, the final state would contain an oil-water interface. This final state may be as shown in Figure 1d or it might consist of a submerged drop.

For the glass-Drakeol-10-water-air system the contact angles listed in Table I do not preclude the existence of a stable four-phase contact line. Such a configuration has been observed in this laboratory. However, in such a state a quantitative measurement of the contact angles is difficult to obtain because of edge and meniscus effects. A variety of angles Θ_o and Θ_w satisfying eq 3, 8, and 15 are possible depending on the water film thickness and oil volume used. Estimated ranges of Θ_o and Θ_w are 2-15 and 10-25°, respectively.

Acknowledgment. The authors wish to acknowledge the helpful comments made by Dr. James C. Melrose of Mobil Research and Development Corp. and Dr. Rulon E. Johnson, Jr., of E. I. duPont. Very helpful discussions were held with Professor Dominic Edelen of the Center for the Application of Mathematics at Lehigh University.

10-25°, respectively.

(21) C. Huh and L. E. Scriven, *J. Colloid Interface Sci.*, **30**, 323 (1969).

On the Absorption Spectra of Alkali Metal–Amine Solutions

K. Bar-Eli* and G. Gabor

Department of Chemistry, Tel-Aviv University, Tel-Aviv, Israel *(Received March 3, 1972)*

We have investigated very carefully the temperature dependence, solvent dependence, and decay rates of the spectra of alkali metals in solutions in methylamine and ethylamine. Results confirm earlier assumptions that the M band is associated with the negative metal ion. The decay rates of these solutions confirm the equilibrium between the metal anions and the solvated electrons. This equilibrium is shifted toward the metal negative ions on cooling. The existence of a new, hitherto unreported, absorption band at 440 nm in solutions of lithium is reported.

Introduction

The absorption spectra of solutions of alkali metals in various amines and in ammonia have been studied extensively.[1] The existence of two bands has been established:[2] an M band which peaks between 660 and 1000 nm depending on the metal, and an S band which is metal independent and peaks at 1400 nm.[3] The temperature dependence of the M band was investigated, and used as a clue in the identification of the chemical species associated with it. Also various other properties were reexamined, such as the solvent dependence, decay rates, etc., in order to shed more light on the behavior of these solutions.

Experimental Section

Solutions were prepared from alkali metals of highest available purity, Koch Light 99.9%, which were distilled into the reaction vessel as described earlier.[1f,2b] The amines from the Matheson Co., Inc., were distilled from blue potassium solution onto the purified alkali metals. After being in contact with the metal for a few minutes, the solution was transferred through sintered quartz (in order to avoid the introduction of metal particles) into the spectroscopic cell. As was indicated earlier,[1g,2] the whole vessel, apart from the Fischer and Porter Co. Pyrex–Teflon needle valve, was made of quartz.

Since the surface area of the vessel probably has great influence on the solutions, all vessels went through a careful and uniform cleaning procedure as follows: (1) washing in boiling solution of Alconox detergent, (2) washing the Alconox with distilled water, (3) boiling in distilled water, (4) washing twice in triple distilled water, (5) drying in an oven overnight at 500°, and (6) warming to 300° under vacuum for 24 hr.

In spite of the uniformity of the cleaning procedure, there were variations in the stability of the solutions, although the general patterns of behavior were always reproducible.

The cell was located in a dewar flask equipped with optical windows. The dewar was cooled by dry nitrogen as described earlier.[4] The measurements were done in a Cary 14 spectrophotometer. The optical path in all experiments was 1 cm. The position of the maximum was found as follows: a few horizontal lines were drawn near the band maximum. The intersection of the midpoint line and the band was taken as λ_{max}.[1c] The spectra for these measurements were taken on an expanded wavelength scale in order to obtain greater accuracy. All the measurements of temperature dependence were done by increasing the temperature slowly from −80°, in order to avoid complications arising from the faster decay rates at high temperatures.

Results and Discussion

In Figure 1 typical spectra of potassium are shown in both solvents. It is seen that changing the solvent from ethylamine to methylamine causes a small red shift in the M band, and the S band is greatly increased. In the case of Li–methylamine and Cs–methylamine solutions, the S band was so large that the M band was not observed at the beginning. In lithium solutions it appeared later, as the decay rate of the S band is faster than that of the M band (see following paragraphs).

On lowering the temperature, the M band is blue shifted. The extent of the blue shift depends on the alkali metal (Figure 2) and on the solvent (Figure 3). The results are summarized in Table I.

Following Stein and Treinin[5] we plot the values of the slopes of Figure 3, namely, $d\bar{\nu}/dT$ *vs.* the peak absorption at 20°. A straight line for this plot is a test for a CTTS absorption. Indeed a straight line is obtained (Figure 4) in agreement with the results of others[6,7] that the species associated with the M band is the metal negative ion.

The CTTS mechanism for the absorption involves the solvation shell of the negative ion. The thermal vibrations of this shell decrease on lowering the temperature, and will cause narrowing of the band, together with absorbance increase, in order to preserve the oscillator strength.[8]

(1) (a) H. Blades and W. Hodgins, *Can. J. Chem.*, **33**, 411 (1955); (b) L. R. Dalton, J. D. Rynbrandt, E. M. Hansen, and J. L. Dye, *J. Chem. Phys.*, **44**, 3969 (1966); (c) M. Gold and W. L. Jolly, *Inorg. Chem.*, **1**, 818 (1962); (d) R. C. Douthit and J. L. Dye, *J. Amer. Chem. Soc.*, **82**, 4472 (1960); (e) D. F. Burrow and J. J. Lagowski, *Advan. Chem. Ser.*, **No. 50**, 125 (1965); (f) M. Ottolenghi, K. Bar-Eli, A. Linschitz, and T. R. Tuttle, Jr., *J. Chem. Phys.*, **40**, 3729 (1964); (g) G. Gabor and K. Bar-Eli, *J. Phys. Chem.*, **75**, 286 (1971).

(2) (a) I. Hurley, T. R. Tuttle, Jr., and S. Golden, *J. Chem. Phys.*, **48**, 2818 (1968); (b) *Pure Appl. Chem., Suppl.*, **449**, 503 (1969).

(3) One has to be careful when working in quartz vessels to eliminate as far as possible the leaching of sodium from the walls.[2]

(4) M. Ottolenghi, K. Bar-Eli, and H. Linschitz, *J. Chem. Phys.*, **43**, 206 (1965).

(5) G. Stein and A. Treinin, *Trans. Faraday Soc.*, **55**, 1086, 1091 (1959).

(6) (a) S. Matalon, S. Golden, and M. Ottolenghi, *J. Phys. Chem.*, **73**, 3098 (1969); (b) D. Huppert and K. H. Bar-Eli, *ibid.*, **74**, 3285 (1970).

(7) M. G. DeBacker and J. L. Dye, *J. Phys. Chem.*, **75**, 3092 (1971).

(8) (a) G. E. Gibson and N. S. Bayliss, *Phys. Rev.*, **44**, 188 (1933); (b) G. E. Gibson, O. K. Rice, and N. S. Bayliss, *ibid.*, **44**, 193 (1933); (c) C. N. R. Rao, "Ultraviolet and Visible Spectroscopy," Butterworths, London, 1961, p 142.

TABLE I: Spectral Data on Solutions of Alkali Metals in Methylamine–Ethylamine Mixtures

Mole fraction of $MeNH_2$		1				0.98				0.54				0.365		0.368[a]		0.0			
Solute		K		Rb		K		K		Rb		K		K		Na[c]	K	Rb	Cs
Band		M	S	M	S	M	S	M	S	M	S	M	S	M	S	M	M	M	M
Absorbance	+20°	1.9	1.9	1.11	0.7	1.9	1.6	1.85	0.58	1.8	0.43	1.13	0.32	3.67	0.56	1.34[d]	0.32	0.53	1.02[d]
	−80°	2.9	1.1	1.7	0.38	3.05	1.2	2.56	0.51	2.7	0.45	1.63	0.19	3.25	0.1	0.74	0.46	0.81	0.98
Ratio M/S	+20°	1.0		1.58		1.19		3.2		4.2		3.52		6.55					
	−80°	2.64		4.48		2.5		5.0		6.0		8.6		3.25[b]					
Width at half-intensity[e]	+20°	4100		3450												3450	3600	4100	3600
	−80°	2700		3000												2750	2550	3200	2630
$-d\tilde{\nu}/dT$, $cm^{-1}\ deg^{-1}$		10.8 ±0.3		11.8 ±1.2				9.8 ±0.2		10.8 ±0.5						8.9 ±1.1	8.2 ±0.6	9.4 ±0.5	13.9 ±1.1

[a] Solution saturated with KCl. [b] At low temperatures split spectrum is obtained (ref 1g). [c] Measured in lithium solutions. [d] Absorbance results are doubtful because of fast decay rate. [e] Error is approximately ±100 cm^{-1}

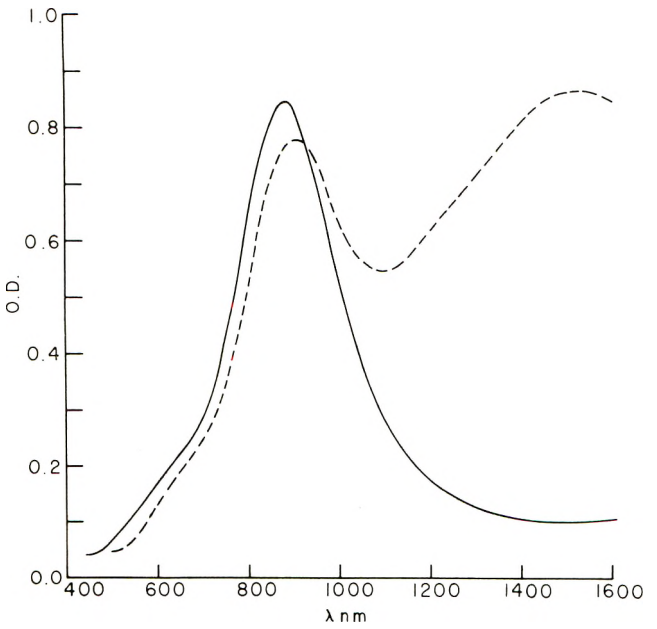

Figure 1. Spectra of potassium in (——) ethylamine and (- - - -) methylamine.

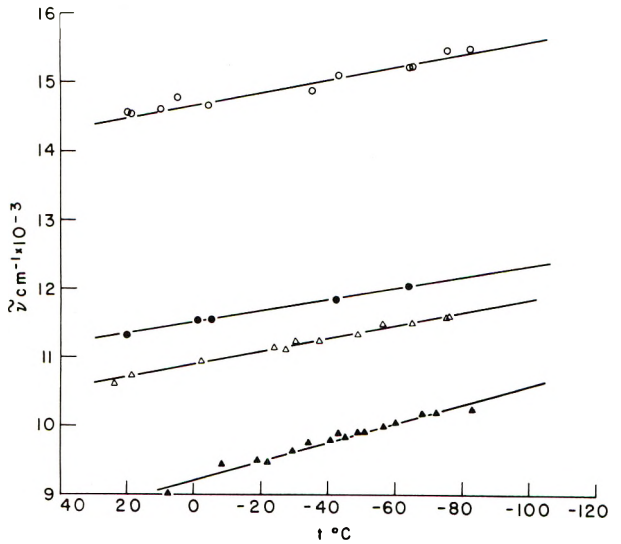

Figure 2. M band *vs.* temperature in solutions of alkali metals in ethylamine: O, Na (see footnote c, Table I); ●, K; △, Rb; ▲, Cs.

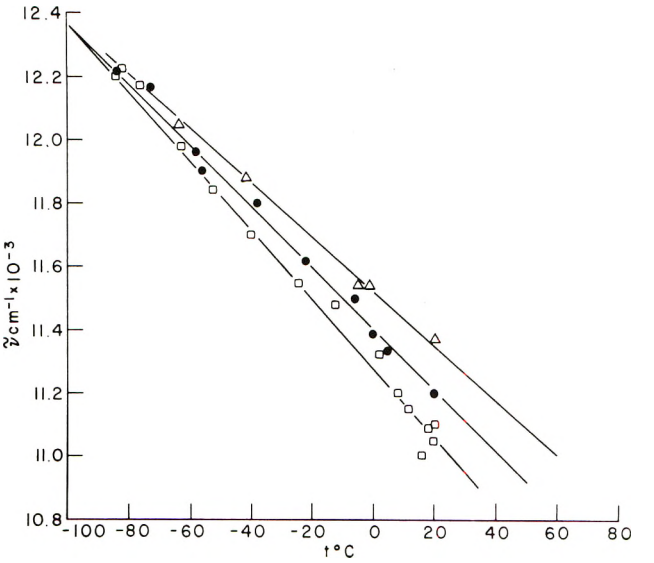

Figure 3. M band maximum *vs.* temperature in solution of potassium in □, methylamine; ●, methylamine–ethylamine mixture ≈1:1; and △, ethylamine.

This is indeed borne out by experiment, as can be seen from Table I.

In solutions where the S band is significant, the ratio M/S increases with the ethylamine mole fraction and with temperature decrease, as seen from Table I.

One expects the S band to be stabilized by methylamine, since in pure ethylamine this band is hardly seen. The temperature influence is twofold: (a) the increase, described in Table I, of the M band, due to the freezing of the solvation shell, and (b) the decrease of the S band, due to the shift of equilibrium in (1) to the left on lowering the temperature. This deduction is given further support by adding potassium chloride; the ratio M/S is further increased as is expected from the above equilibrium (see Table I).

$$M \rightleftarrows M^+ + 2e^- \qquad (1)$$

The decay of both M and S bands, follows first-order law;[9] the M band decays twice as fast as the S band. This result conforms with the fact that equilibrium 1 is fast.[4,6b] Taking logarithms and the derivative with respect to time of equilibrium 1, one obtains

(9) J. L. Dye, *Accounts Chem. Res.*, **1**, 306 (1968).

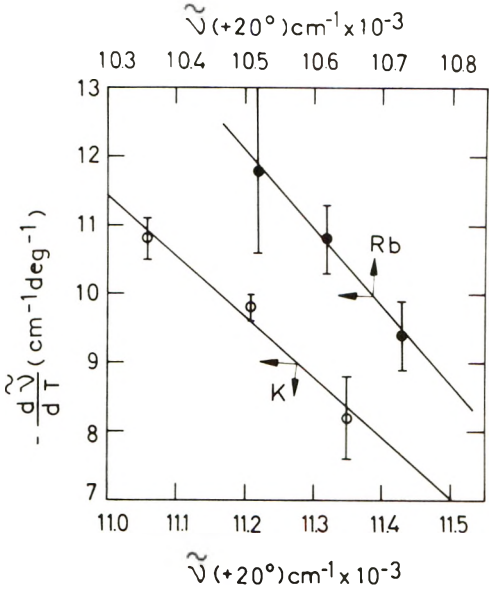

Figure 4. "Blue shift" of M band *vs.* M band maximum at room temperature.

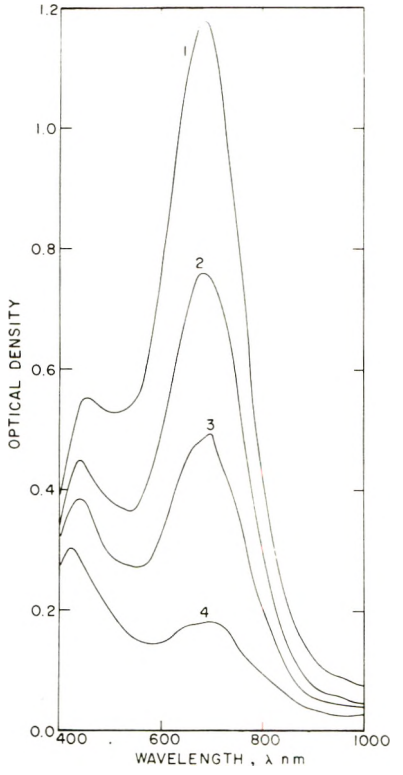

Figure 5. Visible part of spectrum of solution of lithium in ethylamine. Notice the fast decay of 690-nm band (5 min between each plot). This spectrum is recorded after the complete decay of the S band.

$$R = (\mathrm{d}\ln[\mathrm{M}^-]/\mathrm{d}t)/(\mathrm{d}\ln[\mathrm{e}]/\mathrm{d}t) = 2 + (\mathrm{d}\ln[\mathrm{M}\ ]/\mathrm{d}t)/(\mathrm{d}\ln[\mathrm{e}]/\mathrm{d}t) \quad (2)$$

Since [e] and [M$^-$] decrease with time, and it is reasonable to assume that [M$^+$] does not, then the ratio of the

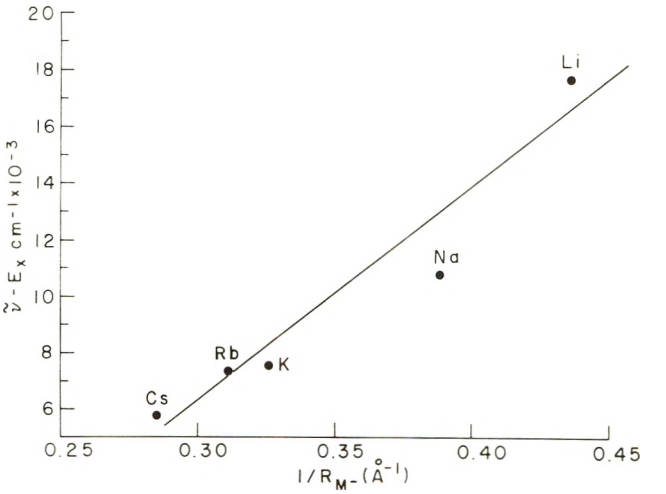

Figure 6. Difference between M band maximum (room temperature) and electron affinity *vs.* reciprocal of anion radii of the various alkali metals (the 440-nm band is assumed to be associated with lithium and the 690-nm band with sodium).

rates is $0 \leq R \leq 2$. The upper value is obtained in the case of potassium and rubidium in methylamine; the lower ratios are obtained for lithium in ethylamine. In the latter case one obtains an intense S band which decays very fast, leaving a band at 690 nm which decays more slowly; also, in a freshly prepared solution, we obtained a hitherto unreported band at 440 nm which decays slower than the 690-nm band (Figure 5). After its decay this 440-nm band does not reappear even when the solution contacts the metal again, while the S and the 690-nm bands do reappear.

Other reports on lithium solutions in ethylamine show only an S band.[1,2] However, Hurley, *et al.*,[2] report that in very concentrated lithium solutions, a 690-nm band exists and starts to decay only after there is no more S band; they do not report the existence of a 440-nm band. Similar results were obtained in ethylenediamine by Dewald and Dye.[10]

It is possible to associate the 690-nm band with the Li^- ion, *i.e.*, an M band, and the 440-nm band with an unidentified unstable organic species. Another possible explanation is to associate the 690-nm band with Na^- which is leached by lithium from the vessel walls (quartz contains $\approx 0.1\%$ of sodium), and the 440-nm band with Li^-, so that both bands are M bands of the respective metals.

Support for the latter conjecture can be obtained by the plot of the difference between the absorption energy and the electron affinity[11] *vs.* the reciprocal of the anion radii of the various alkali metals according to Stein and Treinin.[5] The assumption that the 440- and 690-nm bands are associated with lithium and sodium, respectively, will put all the alkali metals on one straight line (Figure 6).

In spite of the feasibility of each of the above explanations, it is impossible to definitely associate the bands with any particular species, until a stable solution of lithium is prepared and a method to dissolve sodium is found.

(10) N. R. Dewald and J. L. Dye, *J. Phys. Chem.*, **68**, 121 (1964).
(11) (a) A. W. Weiss, *Phys. Rev.*, **166**, 70 (1968); (b) B. Yaakobi, *Phys. Lett.*, **23**, 655 (1966).

Vibrational Spectra of Liquid Crystals. V. Far-Infrared Study of Intermolecular Modes in 4,4′-Azoxydianisole and 4-Methoxybenzylidene-4′-*n*-butylaniline

Bernard J. Bulkin* and Wai Bong Lok

Hunter College of the City University of New York, New York, New York 10021 *(Received August 22, 1972)*

Publication costs assisted by the U.S. Army Research Office—Durham

The far-infrared spectra of crystal, nematic, isotropic, and solution phase 4,4′-azoxydianisole (PAA), and nematic, isotropic, and solution phase 4-methoxybenzylidene-4′-*n*-butylaniline (MBBA) have been studied. Intermolecular modes are observed which are distinct from those seen in the Raman spectrum. The modes persist in the isotropic liquid, but disappear in dilute CCl_4 solution. Spectra of homogeneous and homeotropically aligned nematic MBBA do not show measurable difference in the intensity of the intermolecular mode. The results are discussed in comparison with Raman data and far-infrared data for polar liquids.

The low-frequency, intermolecular vibrations of liquid crystals[1-3] and polar liquids[4-7] yield information about intermolecular interactions in these phases. For polar liquids considerable research has been reported in the far-infrared region but few Raman spectra have been reported. For liquid crystals, just the reverse situation is true. The low-frequency Raman spectra of 4,4′-azoxydianisole (PAA) and 4-methoxybenzylidene-4′-*n*-butylaniline (MBBA) in crystal, nematic, and isotropic phases have been obtained but no far-infrared data have appeared.

The need for far-infrared spectra is readily seen when one compares such data as are available. Crystalline PAA has factor group symmetry C_{2h}^5, which imposes a mutual exclusion rule on the lattice vibrations. Depending on the force constants for intermolecular coupling of lattice vibrations, nine lattice modes are expected in the far-infrared spectrum of PAA, all distinct from the twelve modes seen in the Raman spectrum. As will be shown later, this expectation is partially realized in the far-infrared spectrum of crystalline PAA. These data are necessary for analysis of intermolecular forces in the crystal.

In previous Raman spectroscopic studies of liquid crystals,[1-3] bands were observed in the low-frequency spectra of the nematic phase which disappeared in the isotropic liquid. No intermolecular modes have been seen in the Raman spectra of isotropic phases of any nematogenic materials. Compare this to the situation for polar liquids such as dimethyl sulfoxide (DMSO) and acetonitrile. These do not show any low-frequency Raman bands[8] but do exhibit intense far-infrared absorption below 100 cm^{-1} which is of intermolecular origin.[4-7] These results indicate that the Raman and far-infrared spectra yield different information about intermolecular vibrations. They suggest that the longer-range order is seen in the Raman effect (bands in liquid crystalline but not isotropic phase) while short-range interactions appear in the far infrared. The study of far-infrared spectra of two liquid crystals reported lends additional weight to this proposal.

In this paper we report far-infrared spectra of crystal, nematic, isotropic, and solution phase PAA, as well as the spectra of nematic, isotropic, and solution phase MBBA. In an attempt to assign the low-frequency modes observed, the spectrum of nematic MBBA in which the molecules have been aligned parallel (homogeneous) and perpendicular (homeotropic) to the cell windows are reported.

Results and Discussion

Crystal Phase Spectra. When the Raman spectrum of crystalline PAA was examined in the lattice vibration region[1] evidence was obtained which supported earlier near-infrared results[9] concerning the crystal–nematic (c–n) phase transition. These results indicated that there were considerable pretransition effects in the crystalline phase as one approached the phase transition. These effects have been interpreted as being indicative of disorder in the crystalline phase. X-Ray data have also lent some support for this view,[10] as has the theoretical work by Kobayashi.[11]

In light of the earlier work, a first goal of the far-infrared studies was an answer to the question of whether such pretransition effects would again manifest themselves.

The results are shown in Figure 1. Figure 1a shows the far-infrared spectrum of PAA in the lattice vibration region at 25°. A number of clear absorption minima are seen. Their frequencies are listed in Table I, along with Raman data from ref 1 for comparison. The results indicate that certain bands are near coincident, whereas other modes are unique to one spectrum or the other. This is not surprising. For a very anisotropic molecule such as PAA, some intermolecular forces are strong while others are quite weak. For strong coupling, the splitting of symmetric (Raman) and asymmetric (far ir) vibrational

(1) B. J. Bulkin and F. T. Prochaska, *J. Chem. Phys.*, **54**, 635 (1971).
(2) N. M. Amer, Y. R. Shen, and H. Rosen, *Phys. Rev. Lett.*, **24**, 718 (1970).
(3) W. J. Borer, S. S. Mitra, and C. W. Brown, *Phys. Rev. Lett.*, **27**, 379 (1971).
(4) E. Constant, Y. Leroy, and L. Raczy, *C. R. Acad. Sci.*, **261**, 4687 (1965).
(5) B. J. Bulkin, *Helv. Chim. Acta*, **52**, 1348 (1969).
(6) R. J. Jakobsen and J. Brasch, *J. Amer. Chem. Soc.*, **86**, 3571 (1964).
(7) S. G. Kroon and J. Van der Elsken, *Chem. Phys. Lett.*, **1**, 285 (1967).
(8) B. J. Bulkin, unpublished work.
(9) B. J. Bulkin, D. Grunbaum, and A. Santoro, *J. Chem. Phys.*, **51**, 1602 (1969).
(10) C. H. Carlisle and C. H. Smith, *Acta Crystallogr., Sect. A*, **25**, 547 (1969).
(11) K. K. Kobayashi, *Mol. Cryst. Liquid Cryst.*, **13**, 137 (1971).

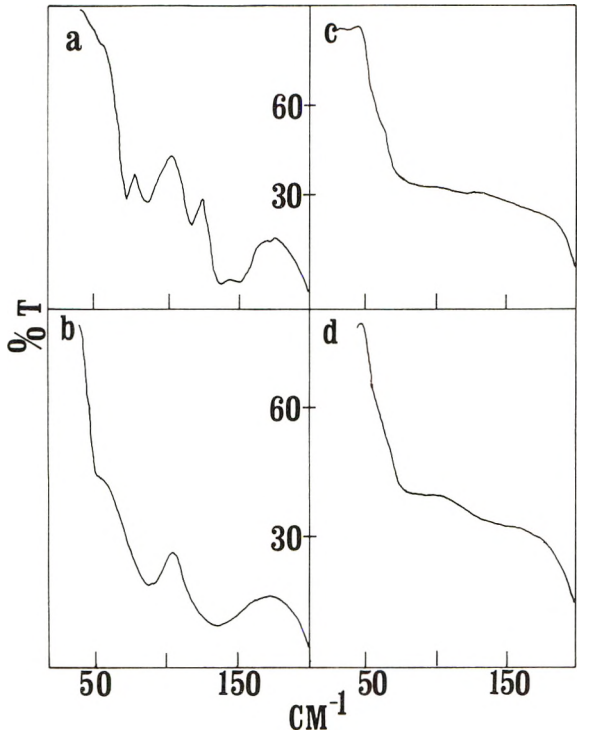

Figure 1. Far-infrared spectrum of crystalline PAA as a function of temperature: (a) 25, (b) 90, (c) 116, and (d) 117°.

TABLE I: Comparison of Far-Infrared and Raman Frequencies (cm^{-1}) of Poly Crystalline PAA[a]

Far infrared	Raman	Far infrared	Raman
	16	84	94
	30	115	
	38	135	
50	52	150	
70	72 (broad)		

[a] Single crystal values for Raman bands available in ref 1. All values taken at 25°.

frequencies will be great. When the particular force constant is small, near coincidence is seen. Of particular note are the strong absorptions between 100 and 150 cm^{-1} in the far infrared which have no correspondence in the Raman. While no quantitative explanation or assignment is yet possible, these data should be useful in obtaining a better understanding of the intermolecular forces.

Up to 110° (Figure 1b), only a moderate broadening of all lattice vibration bands is seen; this is no more than one expects at higher temperatures. As the temperature approaches the c–n transition, however, there is a considerable loss of definite absorption features in the spectrum (Figures 1c and 1d). Indeed, no distinct minimum can be observed. The spectra are somewhat distorted by light scattering from the polycrystalline sample, as well as by the presence of a strong internal vibration (not shown) near 180 cm^{-1}. Nonetheless, the results clearly show an abnormal broadening of the lattice vibration absorptions in the crystalline phase. The internal mode occurring at 180 cm^{-1} shows no such change in bandwidth.

This result is consistent with our previous near-infrared and Raman studies. In the infrared work, bands which had been assigned as sum or difference modes between

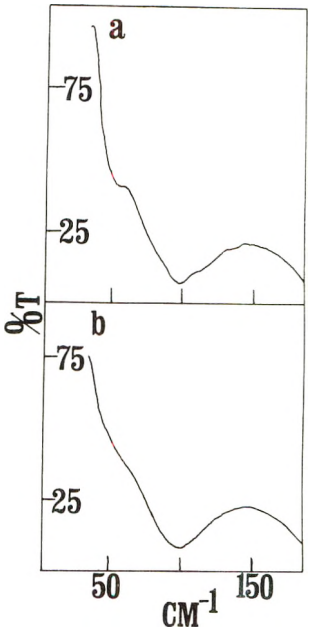

Figure 2. Far-infrared spectra of PAA: (a) nematic phase at 122° and (b) isotropic liquid at 140°.

lattice and internal vibrations showed a gradually decreasing peak intensity as the c–n phase transition was approached. This can now be understood as a broadening of these sum/difference modes which manifests itself as a decrease in intensity. The broadening in the near infrared is itself a consequence of the broadening in the far infrared shown in Figure 1. The analysis of this effect in terms of an order–disorder transition has been outlined in the previous papers.[1,9]

Nematic Phase Spectra. Figure 2a shows the spectrum of nematic PAA and Figure 3a nematic MBBA. One notes first that the absorption of PAA has once again become well defined. The PAA spectrum shows a strong band near 100 cm^{-1} with a shoulder near 55 cm^{-1}. The shoulder is coincident with a Raman band of nematic PAA, the higher-frequency mode is not. Clearly, it is this 100-cm^{-1} mode which gives the strongest absorption in the far infrared. In this case the far-infrared and Raman spectra are substantially different in the nematic phase.

MBBA also shows strong far-infrared absorption in the nematic phase, with the main peak centered at *ca.* 135 cm^{-1}. Again, this is higher in frequency than the main mode observed by Borer, *et al.*,[3] in the Raman spectrum. There does appear to be a weaker Raman mode at this frequency, however, it is not discussed in ref 3. The assignment of these far-infrared modes is considered further in the following sections.

Isotropic Phase Spectra. Perhaps the most interesting contrast between the far-infrared and Raman spectra comes in the isotropic phase. While both MBBA and PAA yield no low-frequency Raman bands in the isotropic phase, Figures 2b and 3b show that the far-infrared absorption is virtually identical with that in the nematic phase, after one takes account of broadening due to the higher temperatures. This persistence of the absorption clearly shows that it is a different mode from the intermolecular Raman scattering.

When one views the far-infrared spectra of isotropic PAA and MBBA in contrast with the spectra of other polar liquids, the results are not surprising. For example,

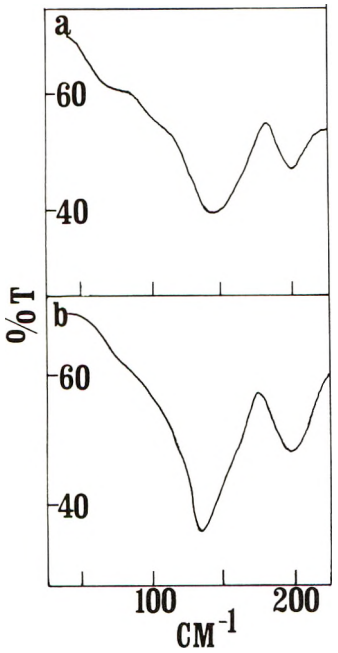

Figure 3. Far-infrared spectra MBBA: (a) nematic phase at 30° and (b) isotropic liquid at 55°.

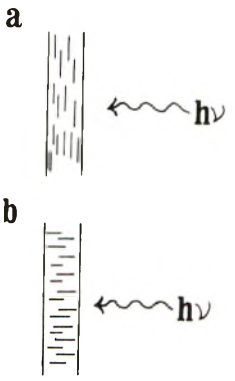

Figure 4. Sampling geometry for (a) parallel (homogeneous) and (b) perpendicular (homeotropic) alignments. Sample thickness was approximately 25 μ.

DMSO shows a far-infrared intermolecular absorption band of 60 cm^{-1} half-width, absorption maximum at 83 cm^{-1}, which is totally absorbing in a 50-μ thick film of the pure liquid.[5] Most other polar liquids examined show absorption bands of similar intensity, frequency, and breadth. It is interesting that the nematogenic materials show the absorption maxima at higher frequency than those of most polar liquids, if the origin of the absorption is indeed the same. The molecular weights of PAA and MBBA are, of course, much greater than that of DMSO, for example. If the vibration is a hindered translation its frequency should be inversely proportional to the mass. This is clearly not the case. A hindered rotation would have a frequency approximately inversely proportional to the square root of the moment of inertia. If this rotational mode occurs about the long axis of the nematogenic molecule, I is small. The smallest principal moment of PAA is approximately twice as large as the largest DMSO moment of inertia and greater than the smallest DMSO value by a factor of 3.5. However, taking into account the square root proportionality to frequency, and the strong intermolecular forces believed operative in liquid crystals, a difference in force constant could account for the

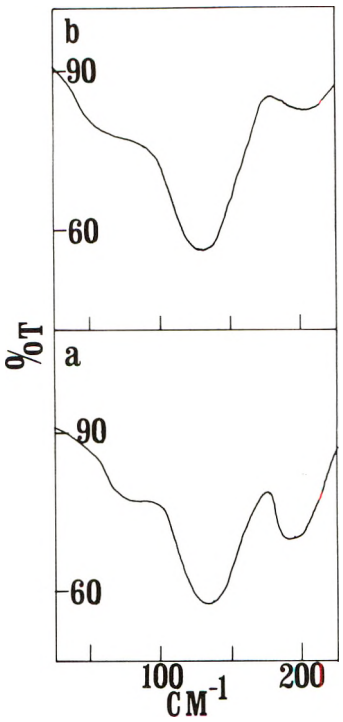

Figure 5. Far-infrared spectra of MBBA for (a) parallel and (b) perpendicular alignments.

frequencies observed. Kroon and Van der Elsken[7] have previously favored an assignment of a hindered rotatory mode for the low-frequency infrared modes of polar liquids and these data lend some support for this view.

Aligned Nematics. Additional evidence concerning the assignment of the intermolecular modes comes from experiments in which the nematic phase has been aligned either parallel (homogeneous) or perpendicular (homeotropic) to the cell windows. Methods for doing this are discussed in the Experimental Section. As seen in Figure 4, this alignment changes the orientation of the long molecular axes with respect to the direction of propagation of the incident light. Figure 5 shows the result obtained for the spectrum of nematic MBBA in the parallel and perpendicular orientations. The internal mode at 175 cm^{-1} decreases markedly in intensity in the perpendicular orientation, while the intermolecular mode at 100 cm^{-1} does not. Complete infrared spectra (4000–100 cm^{-1}) of MBBA, and its ethyloxy analog EBBA, in the two orientations have been obtained as well and yield information about order in these phases. These results will be published separately. Because of difficulties in preparing PAA oriented films at higher temperatures, it has not been possible to obtain reliable spectra of it in the aligned state.

The significance of the oriented spectra is that the intense band at 135 cm^{-1} in MBBA is not due to a hindered translation along the long axes of the molecules. Such a mode would show a considerable attenuation of its intensity in the homeotropic alignment. It does not rule out other hindered translation or rotation. These must be considered in light of the other evidence already discussed.

Solution Spectra. Finally, we report a set of experiments on PAA and MBBA designed to shed light on the strength of the intermolecular interactions responsible for the far-infrared bands. These experiments also make it clear that these bands could not have an intramolecular origin. For

brevity, only the PAA spectra are shown and discussed. A parallel set of data exists for MBBA. When PAA is dissolved in CCl_4, the spectrum shown in Figure 6a is obtained. The 55-cm^{-1} band seems to have disappeared, but the 100-cm^{-1} band is still present. After taking account of concentration, path length, and absorbance for this solution, one finds that the peak absorbance per mole of PAA present has decreased by 20 ± 5%. As CCl_4 has no absorption maximum in the spectral region (there is a very broad, weak absorption which is easily compensated for in the double-beam system) the saturated solution can be diluted 20-fold and the spectra obtained with a path length longer by a factor of 20. This yields the spectrum shown in Figure 6b. As can be seen, the 100-cm^{-1} band has effectively disappeared. Either (1) the concentration of absorbers has greatly decreased, (2) the band has become extremely broad, or (3) the band has shifted to very low frequency.

We believe that a likely explanation is that this band originated from a hindered rotation involving a pair of PAA molecules. There is an equilibrium constant for the association, which leads to a lower dimer concentration at higher dilution. Straightforward monomer-dimer equilibrium calculations show that an association constant of 100 would be necessary to yield the concentration behavior observed here. While this is a simple explanation, the results do not in any way rule out other possibilities such as larger clusters.

Broadening of the absorption band, and/or shifts to much lower frequencies, are only superficially different descriptions of the observation. If one has a hindered motion which becomes free the vibrational frequency shifts toward zero frequency. Similarly, if the amplitudes and time scales of the vibration are changing during this process the bandwidth will change. In short, if a dimeric species is dissociating, absorption bands characteristic of its vibrational modes will disappear. The manner in which they disappear depends upon the fate of the degrees of freedom involved.

To further elucidate the manner in which the band disappears, spectra were run in solutions of five- and tenfold dilution from the saturated solution, with a corresponding increase in path length. These indicated the presence of a weaker absorption band from that found in the saturated solution, but with unshifted (within ±5 cm^{-1}) absorption position maximum. Because of the poor signal-to-noise ratio in the wings of the weak absorption bands, it is not possible to determine the extent of broadening, if any, at the intermediate concentrations.

It should be pointed out that the solution behavior of the low-frequency modes is the most conclusive evidence that they are of intermolecular rather than intramolecular origin. Other evidence for this in PAA is the lack of coincidence with a Raman band, and the absence of a corresponding band in the far-infrared spectrum of the crystal.

Conclusions

This work points up an important similarity between nematogenic materials and polar liquids. The short-range intermolecular forces in each case are probably quite similar. The larger number of strong dipoles in the nematogenic materials likely results in somewhat stronger interactions. Many materials thus have the correct intermolecular electronic interactions (particularly dipolar) to form a liquid crystal but they lack the anisotropic shape.

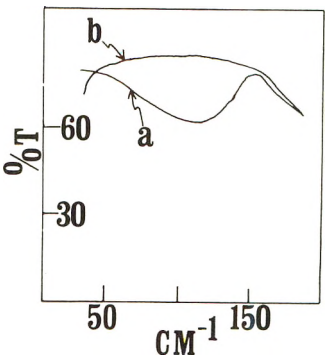

Figure 6. (a) Saturated solution of PAA in CCl_4 (0.035 *M*) run in a 0.5-mm pathlength cell; (b) 20-fold dilution of saturated solution run in 10-mm cell.

The contrast with Raman spectra of the same materials indicates that Raman and far-infrared yield different intermolecular data. It appears that the Raman bands are more sensitive to long-range order, while the far infrared reflects the nearest neighbor intermolecular coupling. More work is needed to elucidate this point in a more quantitative fashion.

Experimental Section

Far-infrared spectra were obtained using a Digilab FTS-14 interferometer.[12] In all spectra, the transformed interferogram of the sample was ratioed against a stored background spectrum of the cell windows. To prevent interference fringes, this background spectrum was taken with a film of nonabsorbing mineral oil between the windows, except for solution spectra where the pure solvent served as the reference. The instrument was run at a retardation sufficient to yield 2-cm^{-1} resolution.

Cell windows were crystal quartz, *ca.* 1 mm thick and wedged to minimize interference fringes. They were purchased from P. R. Hoffman Co., Carlisle, Pa.

Variable temperature measurements were carried out using either a Barnes Engineering Model VTC-1 variable temperature chamber, or an RIIC VLT cell modified for far-infrared operation. The cell temperature was stable within ±0.1°.

The zone-refined PAA used in these experiments was purchased from Princeton Organics, Princeton, N. J. MBBA was purchased from Eastman Organics and purified as described in the literature.[13]

A number of methods have been described in the literature for obtaining homeotropic alignments. We have used chemical rather than electric field techniques because of convenience in constructing infrared cells. Two methods were employed in this work. In one the windows are sprayed with $(CH_3)_2SiCl_2$. In the other, they were rubbed with vegetable lecithin as described by Dreyer.[14] We found the latter method to be extremely simple and reliable. Further, the lecithin film does not have any absorption bands in the far-infrared region. The techniques were refined on glass plates and the results checked using a polarizing microscope. This was not possible with quartz due to its optical activity. However, monitoring attenuation of internal modes gave good indication that homeotropic

(12) Digilab, Inc., Cambridge, Mass. 02139.
(13) See, for example, L. Verbit, *J. Chem. Educ.*, **49**, 36 (1972).
(14) J. Dreyer, presented at 3rd International Symposium on Liquid Crystals, Berlin, 1970.

alignment had been achieved. Good homogeneous alignment was achieved by rubbing plates with cat's fur. Again, the polarizing microscope was used to check alignment.

Acknowledgments. This work was supported in part by a grant from the U. S. Army Research Office—Durham. The Digilab interferometer was purchased under a grant from the National Science Foundation.

Aromatic Hydroxylation Catalyzed by Fenton's Reagent. An Electron Paramagnetic Resonance Study. II. Benzoic Acids

Takeshi Shiga,* Tomomi Kishimoto, and Etsuro Tomita

Department of Physicochemical Physiology, Medical School, Osaka University, 33 Joancho, Kitaku, Osaka, Japan

(Received June 12, 1972)

Unstable free radical intermediates of benzoic acid derivatives (*p*-fluoro-, *p*-chloro-, *p*-bromo-, *p*-hydroxy-, *p*-methoxy-, and *p*-, *m*-, and *o*-nitrobenzoic acids, and 2-, 3-, and 4-pyridinecarboxylic acids) produced by Fenton's reagent (Fe(II) + H_2O_2) were observed by electron paramagnetic resonance, using a continuous flow system. The observed hyperfine structures were analyzed and the molecular structures were assigned on the basis of HMO calculations with the McLachlan modification. All free radicals were the hydroxycyclohexadienyl derivatives, except for a phenoxy radical from *p*-hydroxybenzoic acid. A set of empirical Hückel parameters is introduced for the calculations (*i.e.*, the Coulomb integral for sp^3 carbon is $\alpha + 2.5\beta$, and for its neighboring carbons $\alpha - 0.2\beta$), and the observed hyperfine coupling constants and calculated spin densities agree well with few exceptions. In addition, it is recognized that the attack in hydroxylation occurs at the position(s) possessing minimal localization energy against radical attack and maximal free valence, with few exceptions. The reactive species involved in Fenton's reagent is probably free radical in nature.

Introduction

The reaction mechanism of Fenton's reagent, in particular the nature of the reactive species, has been studied extensively. Electron paramagnetic resonance (epr) studies combined with continuous flow systems certainly have made an epoch in this field. Since the first observation of aliphatic free radicals produced by Fenton's reagent,[1] numerous epr studies have been oriented to the analysis of intermediates[2,3] or to the reaction kinetics,[4-13] comparing them with other oxidation systems (*e.g.*, Ti(III) + H_2O_2).[14] At first sight, Fenton's reagent seemed to be quite different in nature from other oxidation systems, because the observed aliphatic and alicyclic free radicals are dissimilar to those produced by other systems or by the OH radical.[1-3] However, later studies[15-20] have shown that the annihilation of some free radicals by ferric iron must be taken into account for the explanation of our previous results.[1-3] At the same time, we have found that both Fenton's reagent and the Ti(III) + H_2O_2 system produce the same free radicals from furan derivatives.[21] In addition, it is shown that the hydroxylation of furans takes place at the position possessing maximal free valence.[21] On the other hand, some aromatic free radicals produced by the OH radical have been recently reported.[22,23] It is thought that the comparison of the intermediate radicals should be extended to aromatic compounds, therefore, we decided to continue the analysis of the aromatic intermediate free radicals produced by Fenton's reagent.

This paper, thus, primarily concerns itself with the determination of the intermediate free radicals of benzoic acid derivatives produced by Fenton's reagent. In order to assign the observed hyperfine structures to the molecular structures of the hydroxycyclohexadienyl radical, Mc-

(1) T. Shiga, *J. Phys. Chem.*, **69**, 3805 (1965).
(2) T. Shiga, A. Boukhors, and P. Douzou, *J. Phys. Chem.*, **71**, 3559 (1967).
(3) T. Shiga, A. Boukhors, and P. Douzou, *J. Phys. Chem.*, **71**, 4264 (1967).
(4) L. H. Piette, G. Bulow, and K. Loeffler, *Amer. Chem. Soc., Div. Petrol. Chem., Prepr.*, **9,2-c,** c-9 (1964).
(5) Y. S. Chiang, J. Craddock, D. Mickewich, and J. Turkevich, *J. Phys. Chem.*, **70**, 3509 (1966).
(6) H. Fischer, *Chem. Ber.*, **71**, 685 (1967).
(7) K. Takakura and B. Ranby, *J. Phys. Chem.*, **72**, 164 (1968).
(8) R. E. Florin, F. Sicilio, and L. A. Wall, *J. Phys. Chem.*, **72**, 3154 (1968).
(9) H. Taniguchi, K. Fukui, S. Ohnishi, H. Hatano, H. Hasegawa, and T. Maruyama, *J. Phys. Chem.*, **72**, 1926 (1968).
(10) R. E. James and F. Sicilio, *J. Phys. Chem.*, **74**, 1166 (1970).
(11) C. E. Burchill, *J. Phys. Chem.*, **75**, 167 (1971).
(12) R. E. James and F. Sicilio, *J. Phys. Chem.*, **75**, 1326 (1971).
(13) Y. Shimizu, T. Shiga, and K. Kuwata, *J. Phys. Chem.*, **74**, 2929 (1970).
(14) W. T. Dixon and R. O. C. Norman, *J. Chem. Soc.*, 3119 (1963).
(15) R. O. C. Norman and P. R. West, *J. Chem Soc. B*, 389 (1969).
(16) G. Czapski, H. Levanon, and A. Samuni, *Isr. J. Chem.*, **7**, 375 (1969).
(17) W. A. Armstrong, *Can. J. Chem.*, **47**, 3737 (1969).
(18) G. Czapski, *J. Phys. Chem.*, **75**, 2957 (1971).
(19) G. Czapski, A. Samuni, and D. Meisel, *J. Phys. Chem.*, **75**, 3271 (1971).
(20) G. Czapski, *Annu. Rev. Phys. Chem.*, **22**, 171 (1971).
(21) T. Shiga and A. Isomoto, *J. Phys. Chem.*, **73**, 1139 (1969).
(22) K. Eiben and R. W. Fessenden, *J. Phys. Chem.*, **75**, 1186 (1971).
(23) P. Neta, M. Z. Hoffman, and M. Simic, *J. Phys. Chem.*, **76**, 847 (1972).

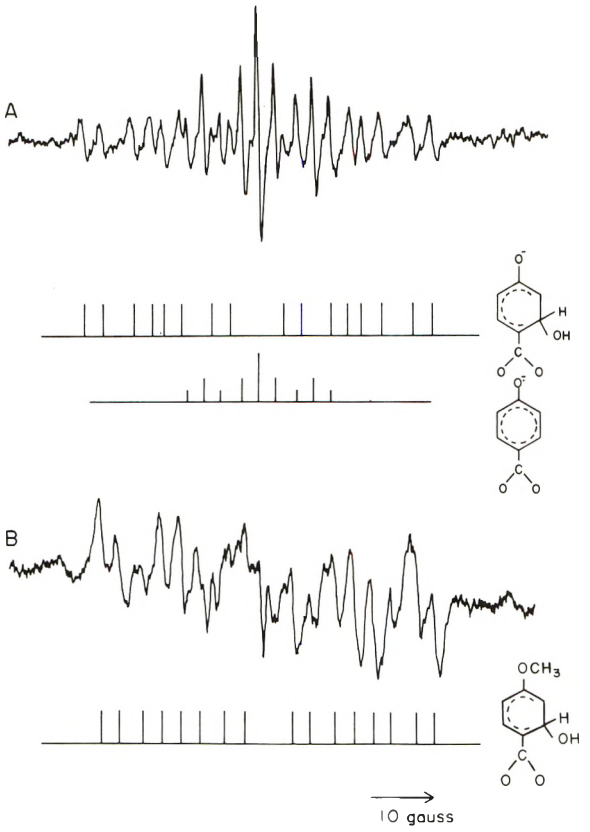

Figure 1. Epr spectra of (A) *p*-hydroxy- and (B) *p*-methoxybenzoic acid radicals. Conditions: (A), modulation 100 kHz, 0.63 G, time constant 0.3 sec, scanning speed 100 G/2 min; and (B), modulation 100 kHz, 1.0 G, time constant 1 sec, scanning speed 100 g/4 min. The arrow at the bottom indicates the direction of the magnetic field strength, and its length corresponds to 10 G.

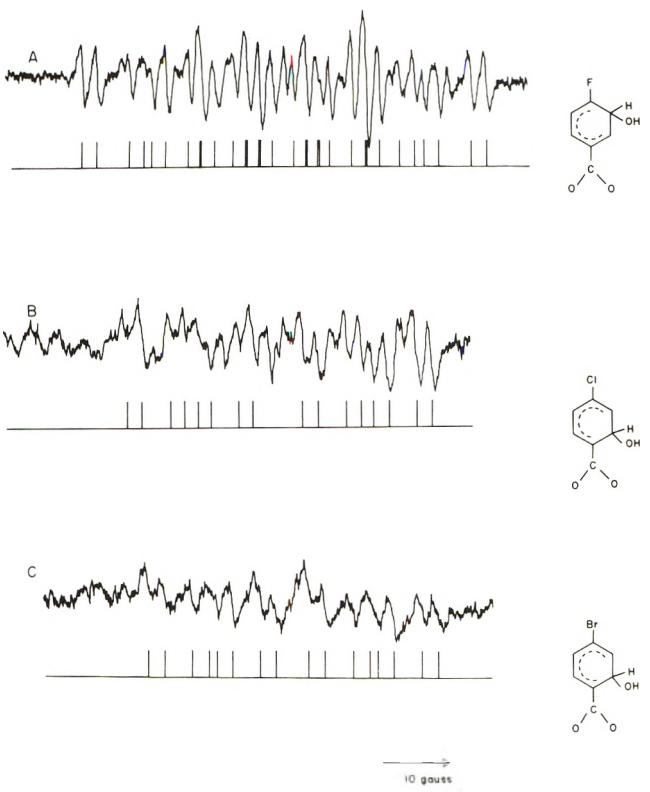

Figure 2. Epr spectra of (A) *p*-fluoro-, (B) *p*-chloro-, and (C) *p*-bromobenzoic acid radicals. Conditions: (A) and (C), modulation 100 kHz, 1.0 G, time constant 0.3 sec, scanning speed 100 G/4 min; and (B), modulation 100 kHz, 0.8 G, time constant 0.3 sec, scanning speed 100 G/4 min. The arrow at the bottom indicates the direction of the magnetic field strength, and its length corresponds to 10 G.

Lachlan calculations were carried out, using a set of empirical Hückel parameters. Finally, the relation between the position of attack and the reactive indices is discussed.

Materials and Methods

Apparatus. A Varian E-12 epr spectrometer was used. The design and characteristics of the continuous flow system have been described previously.[1,24] The pH of the solutions was adjusted by means of a Hitachi F-5 pH meter. All the reagents were of reagent grade and were not purified further.

Methods. The solvent was 0.1 *M* phosphate buffer, pH 7.0. The solution of Fe(II) (5 m*M* of ferrous sulfate)–ethylenediaminetetraacetic acid (5 m*M*) and the solution of H_2O_2 (0.1%) and benzoic acid derivatives (5–10 m*M*, depending on their solubilities) were mixed in the flow cell. Both solutions were bubbled with nitrogen gas in order to remove the dissolved oxygen. The epr spectra were recorded under continuous flow, 7–30 msec after the mixing of the two solutions. The hyperfine coupling constants and *g* values were measured by comparison with the signal of Fremy's salt, which was sealed in a capillary and inserted beside the flow cell. The *g* values of the observed free radicals were 2.003. The errors in the coupling constant measurements were within 0.3 G in most cases. The 100-kHz modulation amplitude could not be reduced below 0.25 G, because of poor signal-to-noise ratio. All experiments were carried out at room temperature (23°).

Calculations. A NEAC 2200-500 or a Hitac-10 digital computer was used for theoretical calculations.

Results

Epr Spectra. The epr spectra of *p*-hydroxy- and *p*-methoxybenzoic acid free radicals are shown in Figure 1. The latter spectrum mainly consists of 16 lines of equal intensity, and the former spectrum is composed of two signals: one is 16 lines of equal intensity and the other is 9 lines (with an intensity ratio of 1:2:1:2:4:2:1:2:1). The signals of 16 lines originate from four proton couplings, among which one proton splitting constant is as large as some 30 G, similar to that of the hydroxycyclohexadienyl radical from benzene[22,25] and from benzoic acid.[22] The signal of 9 lines from *p*-hydroxybenzoic acid is the same signal as that of the phenoxy radical reported by Stone and Waters.[26]

The epr spectra of *p*-fluoro-, *p*-chloro-, and *p*-bromobenzoic acid free radicals are shown in Figure 2. The spectra of *p*-Cl and *p*-Br derivatives, again, consist of 16 lines. The spectrum of *p*-fluorobenzoic acid free radical is complicated, but 32 lines can be recognized to which four protons and one fluoride contribute.

The epr spectra of three nitro-substituted free radicals are shown in Figure 3. The spectra of *p*- and *o*-nitroben-

(24) T. Shiga, A. Boukhors, and P. Douzou, "Recent Development of Magnetic Resonance in Biology," S. Fujiwara and L. H. Piette, Ed., Hirokawa, Tokyo, 1968, p 146.
(25) W. T. Dixon and R. O. C. Norman, *J. Chem. Soc.*, 4857 (1964).
(26) T. J. Stone and W. A. Waters, *J. Chem. Soc.*, 213 (1964).

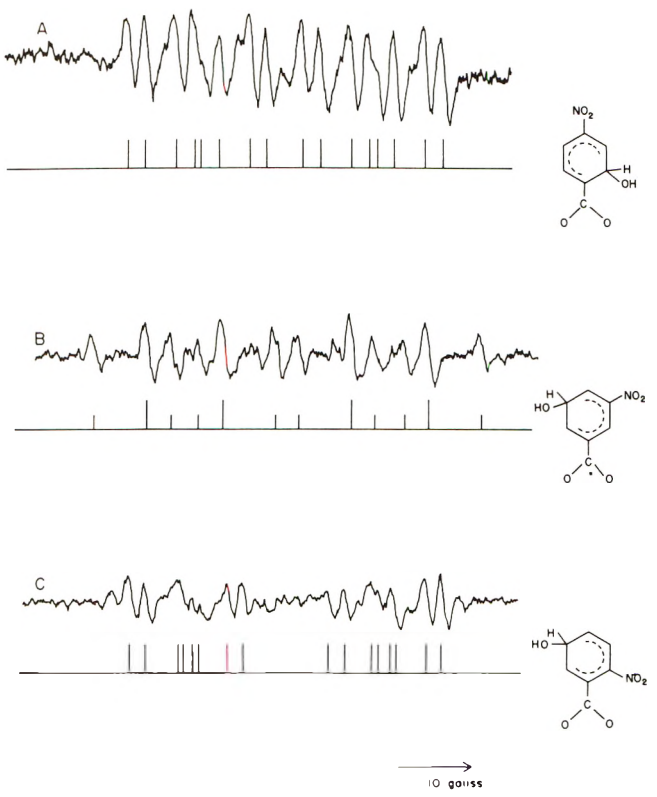

Figure 3. Epr spectra of (A) *p*-, (B) *m*-, and (C) o-nitrobenzoic acid radicals. Conditions: (A) and (B), modulation 100 kHz, 1.0 G, time constant 1.0 sec, scanning speed 100 G/4 min; and (C), modulation 100 kHz, 0.5 G, time constant 1.0 sec, scanning speed 100 G/4 min. The arrow at the bottom indicates the direction of the magnetic field strength, and its length corresponds to 10 G.

zoic acid free radicals consist of 16 lines, and the spectrum of *m*-nitro derivative of 12 lines which arise from 1H-1H-2H couplings.

The epr spectra of three kinds of pyridinecarboxylic acid are shown in Figure 4. The spectra of 4- and 2-substituted free radicals can easily be analyzed; the former, of isonicotinic acid free radical, consists of 26 lines originating from either 1H-1H-1N-2H or 1H-1H-1H-1H-1N couplings, and the latter, of picolic acid free radical, probably consists of 18 lines due to 1H-2H-1N couplings and other small lines. The spectrum of nicotinic acid free radical is too complicated, but may be, at best, analyzed to 48 lines as shown in the figure.

The spectrum of benzoic acid free radical is also complicated, and cannot be analyzed except for a signal of *p*-hydroxycyclohexadienyl radical, which consists of 18 lines due to 1H-2H-2H couplings. The other signals probably of meta and ortho derivatives as reported by Eiben and Fessenden,[22] cannot be separated. In addition, the shape of the spectrum did not alter with change in flow rate, *i.e.*, the ratios of the radical concentrations were the same during the 7–30 msec after mixing the solution.

In general, the signals of 16 lines can be assigned to one of the hydroxycyclohexadienyl radicals, either I or II. The large splitting of some 30 G arises from a proton attached to the sp^3 carbon of the hydroxylated position, as previously found with similar free radicals from benzene,[22,25] phenols,[27,28] benzoic acid,[22] and furans.[21] Such a large coupling constant originates from hyperconjugation with the neighboring p orbitals, but the coupling constant

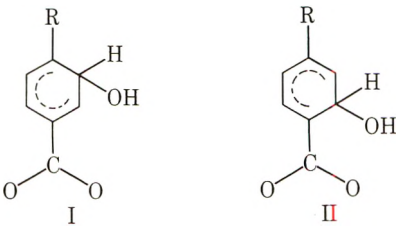

values of these radicals are smaller than that of the cyclohexadienyl free radical reported by Fischer[29] and others.[22,30]

Comparing the hyperfine coupling constants of the benzoic acid free radicals with those of reported hydroxycyclohexadienyl radicals from benzene,[25,22] the following assignments are possible: an approximately 13-G splitting from the para proton, a *ca.* 9-G splitting from the ortho proton, and the small splitting, less than 3 G, from the meta proton (para, meta, and ortho positions with respect to the hydroxylated sp^3 carbon).

Since the fluoride hyperfine coupling is about twice as large as that of a proton, the free radical from *p*-fluorobenzoic acid (Figure 2A) is assigned structure I. The free radical from *m*-nitrobenzoic acid (Figure 4B) is a hydroxylated adduct to the meta position (with respect to

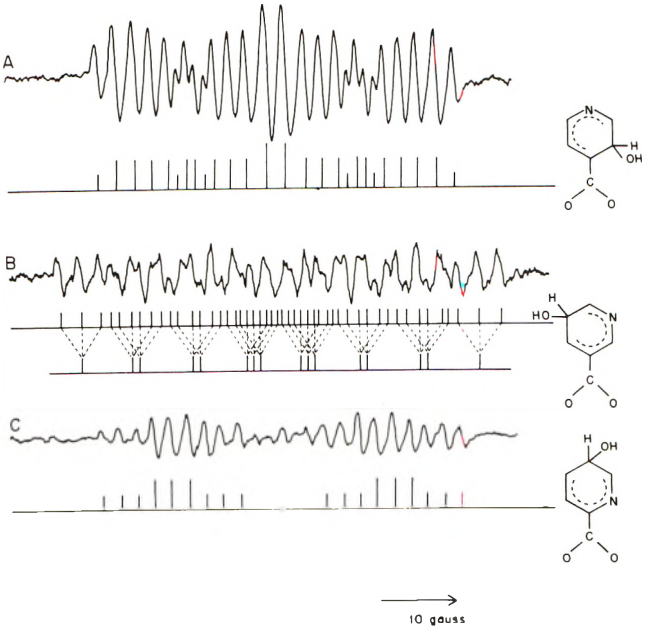

Figure 4. Epr spectra of pyridine- (A) 4-, (B) 5-, and (C) 6-carboxylic acid radicals. Conditions: (A) and (B), modulation 100 kHz, 0.5 G, time constant 1.0 sec, scanning speed 100 g/4 min; and (C), modulation 100 kHz, 0.5 G, time constant 1.0 sec, scanning speed 100 G/4 min. The arrow at the bottom indicates the direction of the magnetic field strength, and its length corresponds to 10 G.

the carboxylic group). Only these two radicals can be assigned structures, and the other radicals cannot be identified from the spectra without theoretical calculations.

(27) C. R. E. Jefcoate and R. O. C. Norman, *J. Chem. Soc. B*, 48 (1968).
(28) A. L. J. Beckwith and R. O. C. Norman, *J. Chem. Soc. B*, 403 (1969).
(29) H. Fischer, *J. Chem. Phys.*, **37**, 1094 (1962).
(30) R. W. Fessenden and R. H. Schuler, *J. Chem. Phys.*, **39**, 2147 (1963).

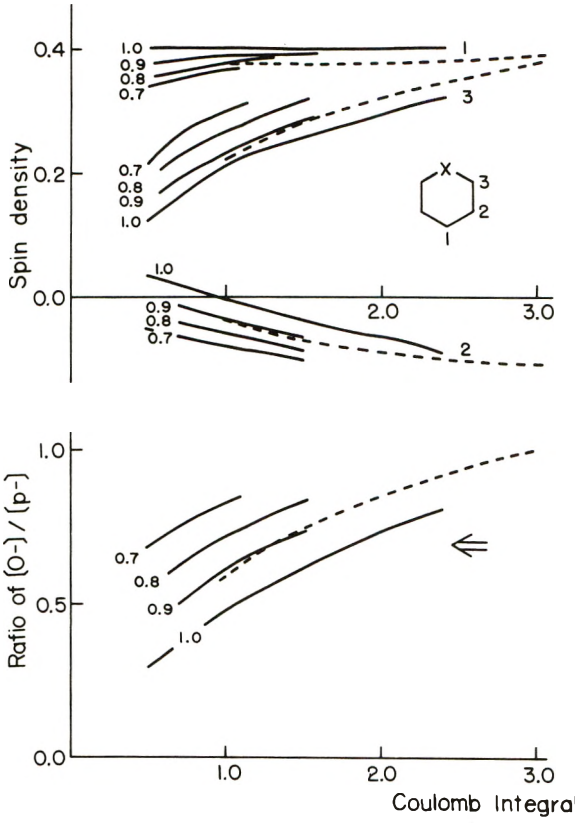

Figure 5. Plot of the Coulomb integral (δ(-CH(OH)-)) *vs.* the spin densities of the hydroxycyclohexadienyl radical: solid lines, $\delta(C') = -0.2$ and $\gamma(C\text{-}C') = 1.0$ is shown in the figure; broken lines, $\delta(C') = 0.0$ and $\gamma(C\text{-}C') = 1.0$.

Calculations

In order to assign the above hyperfine couplings to molecular structures, Hückel calculations for the molecular fragments, in which the sp^3 carbon is ignored, were carried out, since this approximation has been successfully applied to the free radicals from furan derivatives.[21] However, such a simple approximation failed to support the assignment of the above structures of the identified radicals (*p*-fluoro- and *m*-nitrobenzoic acid radicals), and also failed to predict the spin densities of hydroxycyclohexadienyl radical(s), *i.e.*, the calculated spin density on the p carbon becomes smaller than that on the ortho carbon (contradiction!). Therefore, it is necessary to introduce a new set of parameters for the sp^3 carbon; assuming a planar six-membered ring with a heteroatom, the McLachlan method[31] can then be applied in order to take into account the negative spin densities.

In order to find a suitable set of Hückel parameters, the hydroxycyclohexadienyl radical[22,25,30] is taken as an example. Three parameters are varied as follows: the Coulomb integral of the sp^3 carbon (heteroatom) was taken as $1.0 \leqq \delta(\text{-CH(OH)-}) \leqq 3.0$; that of the neighboring carbon, $0.0 \leqq \delta(\text{-C'-}) \leqq -0.3$; and the bond integral between them, $0.5 \leqq \gamma(C\text{-}C') \leqq 1.0$. These parameters are essentially analogous to those of a methyl group treated as a heteroatom. A part of the McLachlan calculations is shown in Figure 5, where the solid lines are the spin densities of three positions, varying δ(-CH(OH)-) and γ(C-C') with fixed δ(-C'-). As the best-fit parameters, δ(-CH(OH)-) = 2.5, $\delta(C') = -0.2$, and $\gamma(C\text{-}C') = 1.0$ are obtained.

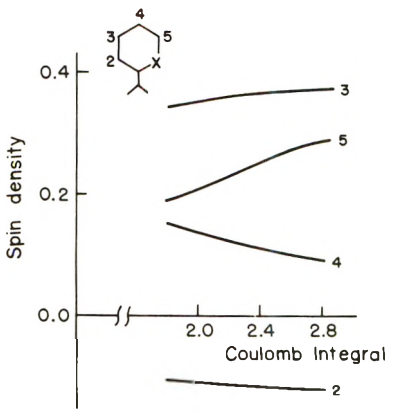

Figure 6. Plot of the Coulomb integral (δ(-CH(OH)-)) *vs.* the spin densities of the hydroxycyclohexadienyl radical from benzoic acid (ortho isomer): $\delta(C') = -0.2$ and $\gamma(C\text{-}C') = 1.0$.

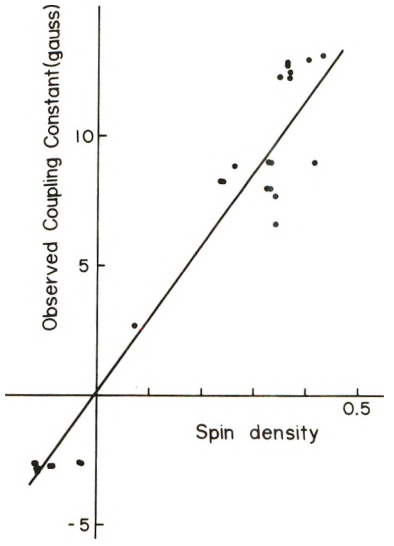

Figure 7. Plot of the calculated spin densities *vs.* observed hyperfine coupling constants.

TABLE I: Hückel Parameters[a]

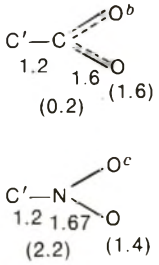

C'—F[d] 1.25 (0.21) (2.1)	C'—O[d] 0.9 (0.2) (2.0)	
C'—Cl[d] 0.8 (0.18) (1.8)	C'—O—C—H$_3$[e] 0.7 0.7 2.5 (2.0) (−0.1) (−0.2)	
C'—Br[d] 0.8 (0.16) (1.6)	C'—N—C'[f] 1.0 1.0 (0.64)	

[a] Numbers in parentheses are Coulomb Integrals, and numbers under the bond are bond integrals. [b] Slightly modified values of C. M. Moser, *J. Chem. Soc.*, 1073 (1953); and A. R. Buick, T. J. Kemp, G. T. Neal, and J. T. Stone, *J. Chem. Soc. A*, 2227 (1970). [c] Values found in ref 39. [d] Suggested values in T. Yonezawa, *et al.*, "Introduction to Quantum Chemistry," Vol. I, Kagaku-Dojin, Kyoto, 1964, p 55. [e] Values found in ref 21. [f] Values found in ref 40, which are smaller than those of C. L. Talcott and R. J. Myers, *J. Amer. Chem. Soc.*, **87**, 1651 (1965); J. C. M. Henning, *J. Chem. Phys.*, **44**, 2139 (1966); and M. D. Sevilla, *J. Phys. Chem.*, **74**, 805 (1970).

In order to obtain fine adjustment of the parameters, the calculations on hydroxycyclohexadienyl radical from benzoic acid (ortho hydroxylated)[22] were carried out. As shown in Figure 6, the spin densities are sensitive to the

(31) A. D. McLachlan, *Mol. Phys.*, **3**, 233 (1960).

TABLE II: Hyperfine Coupling Constants and Calculated Spin Densities[a]

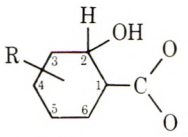

R	Position attacked	CH(OH)	Para	Ortho	Meta
4-F	(3)	30.0(3)	13.1(6)	9.0(2), 19.9(4-F)	2.7(5)
		0.084	*0.431*	*0.413, 0.110*	*0.072*
4-Cl	(2)	32.8(2)	12.9(5)	8.0(3)	2.6(6)
		0.112	*0.357*	*0.330*	*−0.115*
4-Br	(2)	29.9(2)	12.8(5)	8.0(3)	2.8(6)
		0.112	*0.357*	*0.325*	*−0.114*
4-OH	(2)	29.0(2)	12.3(5)	7.7(3)	2.9(6)
		0.113	*0.355*	*0.309*	*−0.114*
4-OCH_3	(2)	29.5(2)	12.5(5)	6.6(3)	2.8(6)
		0.109	*0.364*	*0.342*	*−0.115*
4-NO_2[b]	(2)	29.8(2)	12.8(5)	8.0(3)	3.3(6)
5-NO_2[b]	(3)	34.7(3)	12.9(6)	9.0, 9.0(2,4)	
6-NO_2[b]	(4)	34.2(4)		8.5, 7.5(3,5)	2.7(2)
4-(N)[b,c]	(2)	27.6(2)	13.0(5)	8.8(3)	3.2(6),3.2(4-N)
5-(N)[b,c]	(3)	28.0(3)	20.1(6)	10.0, 8.8(2,4)	3.4(5-N)
6-(N)[b,c]	(4)	36.2(4)		8.4, 8.4(3,5)	2.8(6-N)
Benzene[d]	(4)	34.34(4)	13.1(1)	9.0(3,5)	2.7(2,6)
		0.109	*0.402*	*0.329*	*−0.084*
Benzoate[e]	(4)	34.0(4)		8.25(3,5)	2.6(2,6)
		0.102		*0.280*	*−0.030*
	(2)	34.7(2)	12.3(5)	8.9(3)	2.6(4,6)
		0.110	*0.365*	*0.263*	*−0.117*

[a] Numbers in parentheses show the positions; the coupling constants are expressed in gauss. *Italicized* numbers are the calculated densities. [b] These radicals are tentatively assigned, and in some cases, two ortho positions cannot be assigned. [c] (N) is a nitrogen substitution of the benzene ring. [d] Data from ref 22, 29, and 30. [e] Data from ref 22, which we can barely confirm and give the proton coupling constant of CH(OH) proton of ortho isomer as 34.7 G.

value of δ(-CH(OH)-). Using the above parameters, the ratios between the spin densities fit well with those of the coupling constants. However, the Q value becomes slightly larger than usual.

All possible structures of the substituted benzoic acid free radicals are calculated, using the parameters shown in Table I. The assignments of the structures can easily be made, comparing the observed coupling constants and the calculated spin densities. The results are summarized in Table II. A few radicals containing nitrogen show a systematic discrepancy between the experimental and theoretical values (see Discussion). However, the assignment of the structures can still be made; the estimated structures are shown in Table II.

Among the halogen-substituted compounds, it is seen that the hydroxylated positions are not the same for *p*-F and *p*-Cl(Br) derivatives.

The relation between the observed hyperfine coupling constants and the calculated spin densities is shown in Figure 6, in which the radicals containing nitrogen are omitted but hydroxycyclohexadienyl radicals from benzene[22] and benzoic acid (para and ortho isomers, for which we can barely confirm the analysis of Eiben and Fessenden[22]) are added. The constants of the following equations[32] are determined by a least-squares fitting.

$$A = Q\rho \quad (1)$$

$$A = Q\rho + C \quad (2)$$

The constants obtained were $Q = -32.3$ ($\sigma = 2.4$) G for eq 1, and $Q = -28.5$, $C = 0.1$ ($\sigma = 2.2$) G for eq 2. The Q values of various organic compounds are $-22.5 \sim -30$ G,[33] therefore the present value is within the reasonable range.

Discussion

Configuration of Intermediate Free Radicals. Generally the oxidation of benzoic acids by Fenton's reagent yields hydroxycyclohexadienyl radicals, which are the precursors of the reaction products: phenols, etc.[27,34-36] The difficulty in the structure determination from epr spectra arises from the fact that every possible structure possesses the same number of nuclei giving the hyperfine splittings. Therefore, the assignments of the structures may be ambiguous without theoretical calculations. As described in the preceding section, the assignments of the structures can be successfully made by introducing a set of new parameters for the sp^3 carbon (treated as a heteroatom).

The steric configurations of these radicals are not known. For similar molecules, the Meisenheimer salt is shown to be a planar ring; the carbon atom attached to two methoxy groups is in the usual sp^3 configuration and the distance between the sp^2 carbon and the sp^3 carbon is

(32) H. M. McConnell, *J. Chem. Phys.*, **24**, 633, 764 (1956).
(33) A. Carrington, *Quart. Rev., Chem Soc.*, **17**, 67 (1963).
(34) J. R. Lindsay Smith and R. O. C. Norman, *J. Chem. Soc.*, 2897 (1963).
(35) A. J. Davidson and R. O. C. Norman, *J. Chem. Soc.*, 5404 (1964).
(36) C. R. E. Jefcoate, J. R. Lindsay Smith, and R. O. C. Norman, *J. Chem. Soc. B*, 1013 (1969).
(37) R. Destro, C. M. Gramaccioli, and M. Simonetta, *Nature (London)*, **215**, 289 (1967).

TABLE III: Reactive Indices

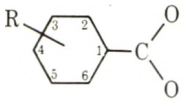

R	Position	q^a	FV[b]	L(E)[c]	L(R)[c]	L(N)[c]	Position attacked
4-F	(2)	1.0152	0.3934	1.8211	1.8211	1.8210	
	(3)	1.0340	*0.4419*	1.5912	*1.6603*	1.7295	×
4-Cl	(2)	0.9540	*0.4187*	1.7111	*1.6295*	1.5479	×
	(3)	1.0255	0.4137	1.5899	1.6444	1.6989	
4-Br	(2)	0.9696	*0.4160*	1.7384	*1.6568*	1.5753	×
	(3)	1.0360	0.4158	1.6025	1.6665	1.7306	
4-OH	(2)	0.9714	*0.4178*	1.6894	*1.6078*	1.5262	×
	(3)	1.0267	0.4171	1.5548	1.6181	1.6815	
4-OCH_3	(2)	0.9542	*0.4155*	1.6232	*1.5413*	1.4593	×
	(3)	1.0267	0.4106	1.5577	1.5727	1.5877	
4-NO_2	(2)	0.9590	0.4272	1.5870	1.5015	1.4161	×
	(3)	0.9555	*0.4481*	1.5343	*1.3556*	1.1769	
5-NO_2	(2)	0.9320	0.4436	1.6101	1.3759	1.1412	
	(3)	0.9987	0.4011	1.5314	1.5314	1.5315	×
	(4)	0.9298	0.4453	1.5910	1.3636	1.1361	
	(6)	0.9982	*0.4667*	1.5593	*1.3232*	1.0871	
6-NO_2	(2)	0.9537	0.4304	1.5704	1.4811	1.3919	
	(3)	0.9459	0.4218	1.5806	*1.3964*	1.2122	
	(4)	1.0160	0.3843	1.5854	1.5119	1.4384	×
	(5)	0.9341	*0.4606*	1.5775	1.4153	1.2530	
4-(N)	(2)	0.9779	*0.4203*	1.5526	*1.4690*	1.3854	×
	(3)	0.9041	0.4146	1.6999	1.4982	1.2965	
5-(N)	(2)	0.8635	0.4273	1.7455	1.4711	1.1967	
	(3)	1.0077	0.3926	1.4989	1.4988	1.4987	×
	(4)	0.8352	*0.4453*	1.8092	*1.4064*	1.0037	
	(6)	0.8126	0.4362	1.7490	1.5278	1.3066	
6-(N)	(2)	0.9099	*0.4599*	1.5704	*1.2419*	0.9134	
	(3)	0.9402	0.4023	1.6716	1.4497	1.2278	
	(4)	0.9331	0.4302	1.6491	1.3473	1.0476	×
	(5)	0.8878	0.4136	2.5520	2.5173	2.4826	

[a] q represent electron density. [b] FV = free valence. [c] L(E), L(R), and L(N) are the localization energies with respect to electrophilic, radical, and nucleophilic reagents.

about 1.5 Å.[37,38] Similarly, the cyclohexadienyl radical is considered to be planar, since two proton hyperfine coupling constants of the sp^3 carbon are the same (48.08 G).[22,25] Compared with the latter radical, the introduction of a hydroxy group to the sp^3 carbon, *i.e.*, in the case of the hydroxycyclohexadienyl radical from benzene,[22,25] decreases the proton coupling constant (34.34 G).

As shown in Table II, the radicals from benzoic acids have various coupling constants (29–34 G). Such variations are also observed with radicals from phenols (24–28 G),[27] and with radicals possessing aryl groups instead of the hydroxy group (28–35 G).[28] Introducing a hydroxy group to the sp^3 carbon, the proton coupling constant due to hyperconjugation tends to decrease.

Concerning the sp^3 carbon, the relation between the proton coupling constants and the spin densities are tested by a least-squares fitting to the following equations[21,39-44]

$$A = Q(\rho(C_1') + \rho(C_2'))$$

$$A = Q_1\rho(\text{-CH(OH)-}) + Q_2(\rho(C_1') + \rho(C_2'))$$

where $\rho(C_1')$ and $\rho(C_2')$ are the spin densities on the neighboring carbons to the sp^3 carbon. However, none of these equations gives acceptable results, mainly because the deviations are too large. The following factors may be considered in explaining the variation of the coupling constants: (i) the abnormal sp^3 configuration, (ii) the nonplanality of the ring, and (iii) the electron-withdrawing effect of the hydroxy group attached to an sp^3 carbon. At the present stage, the configuration around the sp^3 carbon of the hydroxycyclohexadienyl radical cannot be estimated.

Failure of the theoretical prediction of the spin densities occurs for the nitrobenzoic acids and the pyridinecarboxylic acids. However, the four coupling constants of these radicals (*i.e.*, *ca.* 30, 13, 9, and 3 G) coincided with those of the other radicals, so that a considerable modification of the entire configuration, such as a formation of intramolecular bonding, cannot be imagined and the assignments of the structures can be made as shown in Table II. For this reason, a complex formation between the radical and iron ion is also neglected. In order to solve the discrepancy between the observed and calculated

(38) H. Ueda, N. Sakabe, J. Tanaka, and A. Furusawa, *Nature (London)*, **215**, 956 (1967).
(39) P. H. Rieger and G. K. Fraenkel, *J. Chem. Phys.*, **39**, 609 (1963).
(40) T. Kubota, K. Nishikida, H. Miyazaki, K. Iwatani, and Y. Oishi, *J. Amer. Chem. Soc.*, **90**, 5080 (1968).
(41) C. Heller and H. M. McConnell, *J. Chem. Phys.*, **35**, 1535 (1960).
(42) M. Karplus and G. K. Fraenkel, *J. Chem. Phys.*, **35**, 1312 (1961).
(43) P. H. Rieger and G. K. Fraenkel, *J. Chem. Phys.*, **37**, 2811 (1962).
(44) E. G. Janzen and J. W. Happ, *J. Phys. Chem.*, **73**, 2335 (1969).

values, therefore, a further adjustment of the nitrogen parameters may be needed. However, our calculations are based on rough approximations, without knowledge of the real conformation. Thus a further adjustment may have no advantage. We leave this point as a future problem.

Reactive Indices and Positions of Attack. It was previously found that Fenton's reagent attacks the positions possessing maximal free valence of furan derivatives.[21] Similar tendencies are recognized with the benzoic acid derivatives. As shown in Table III, the position possessing maximal free valence and minimal localization energy against radical attack is hydroxylated, with a few exceptions. The present calculations predict the difference in position attacked between *p*-fluoro- and *p*-chloro (also bromo) benzoic acids.

In our experimental conditions, where the observations were made 7-30 msec after mixing the reactants, no change in the spectral shape was noticed within this time range with benzoic acid, which gave at least three kinds of free radicals. The whole kinetic behavior of the benzoic acid oxidation confirmed our previous description[1] of its similarity to methanol oxidation; *i.e.*, no evidence suggesting a selective annihilation of one radical and a persistence of the other[15-20] was observed in the present study. The results strongly suggest that the reactive species involved in Fenton's reagent has the character of a radical reagent.

In the cases of the nitrogen-containing compounds, in particular the pyridinecarboxylic acids, there is a possibility that the acid is complexed with the iron ion before it reacts with the reactive species. Then, the position of attack would change.

Acknowledgment. The authors wish to thank Drs. K. Kuwata and E. G. Janzen for their stimulating discussions.

Correlation between the n,π^* Triplet Energy of Some Ketones and Aldehydes and Their Electroreduction Potential[1]

Rafik O. Loutfy*

Division of Chemistry, National Research Council of Canada,[1] Ottawa K1A OR6, Ontario, Canada

and Raouf O. Loutfy

Department of Chemistry, University of Guelph, Guelph, Ontario, Canada *(Received May 22, 1972)*

Publication costs assisted by the National Research Council of Canada

The n,π^* triplet energies of some aliphatic and aromatic ketones and aldehydes were found to correlate linearly with the term ($E_I - E_{1/2}^{red.} + \Delta E_{soln}$). E_I (the ionization potential) was taken to correspond approximately to the energy of the n level, and $E_{1/2}^{red.}$ (the half-wave reduction potential), to that of the π^* level. It was found that a solvation energy term, ΔE_{soln}, should be included to correct for the differences in the solvation of the compounds investigated. This linear relation can be employed to determine the triplet energy, $\Delta E_{3(n,\pi^*)}$, of these carbonyl compounds whose $\Delta E_{3(n,\pi^*)}$ cannot be obtained spectroscopically. The n,π^* triplet energy of acetone was calculated to be 76.6 kcal/mol, which is in good agreement with the predicted value of 75–80 kcal/mol.

Introduction

The carbonyl functionality is one of the most widely studied groups in organic photochemistry because of its role in photochemical and photobiological reactions. Hence, the triplet states of carbonyl molecules are continuing to receive considerable attention from both the experimental and theoretical points of view. Phosphorescent emission and $S_0 \rightarrow T_1$ excitation spectroscopy are the most common techniques used to determine the triplet energy levels. However, the triplet energies of a large number of carbonyl compounds have not been reported. This is quite simply due to the fact that those compounds either do not emit, or that the emission is structureless, thereby rendering an estimate of the triplet energy difficult.

A linear relationship between the n,π^* triplet energies of some benzophenones, and thiobenzophenones, and the half-wave potentials ($E_{1/2}$) was found previously[2a] and an estimate made of the position of the n,π^* triplet energies of those compounds for which n,π^* triplet states could not be observed spectroscopically.

In this paper a systematic study of the effect of substituents on the relation between the energies of the n,π^* ex-

(1) National Research Council of Canada No. 13032.
(2) (a) R. O. Loutfy and R. O. Loutfy, *J. Phys. Chem.*, **76**, 1650 (1972); (b) W. R. Fawcett, P. A. Forte, R. O. Loutfy, and J. N. Prokipcak, *Can. J. Chem.*, **50**, 263 (1972).

cited state and half-wave potentials for a series of compounds containing the chromophore >C=O is reported. For the given series both the n and π* levels change upon substitution. The results are presented and discussed with respect to previous work.

Experimental Section

All experiments were carried out in acetonitrile (AN) containing 0.05 *M* tetraethylammonium perchlorate (TEAP). The solvent purification procedure is described in detail in ref 2b. The experimental technique and procedure are in all respects the same as described previously.[2a] Acetophenone, benzophenone, benzaldehyde, acrolein, and acetone were reagent grade chemicals used as supplied. Formaldehyde and acetaldehyde were introduced to the standard electrolyte in gaseous form by heating solid paraformaldehyde in the former case and by acid hydrolysis of paraldehyde in the latter. Table I shows the structures of the compounds investigated. The numbers in the table will be used to designate the above compounds throughout this paper.

Results and Discussion

All compounds gave well-characterized ac waves with a width at half-height of 90 ± 1 mV. This corresponds to a one-electron reduction to give the corresponding radical anion. Two ac waves were obtained for the acrolein in general agreement with the observed reduction of α,β-unsaturated carbonyl compounds as reported by Wawzonek, *et al.*, where two one-electrons steps to form the dianion were proposed.[3]

The half-wave potentials for all the compounds were obtained from cathodic and anodic sweeps of the ac wave in the usual manner. The $E_{1/2}$ values are shown in Table I.

Organic carbonyl molecules often possess a low-lying n,π* triplet state. These states are known to arise from the excitation of nonbonding (n) electrons into antibonding π orbitals. The correlation between the transition energies and the nature of the environment depends mainly on the fact that the transition energies are given by the difference of the n and π* orbital energies. The single configuration formula for the triplet excitation energy is given as[4]

$$\Delta E_{^3(n,\pi^*)} = \epsilon_n - \epsilon_{\pi^*} - J_{n,\pi^*} \quad (1)$$

where ϵ_n and ϵ_{π^*} are the energies of the n and π* levels, respectively, and J_{n,π^*} is the appropriate exchange integral. The substituent effects can be rationalized mainly in terms of raising or lowering the energies of the above orbitals.

The carbonyl compounds examined were chosen so that a systematic study of the effect of substituents on the n → π* transition of the parent compound, formaldehyde (**1**), could be investigated. There are mainly two effects associated with the σ or π donation of a substituents replacing H in **1**. The first and most direct effect is the increase of the π* orbital energy, which would correspond to an increase in the magnitude of the standard reduction potential (E^0), where the latter for practical purposes may be identified with the $E_{1/2}^{red.}$. The second effect is a consequence of the fact that σ or π donation of substituents may increase the negative charge on the carbonyl oxygen relative to HCHO **1**, and indirectly causes the oxygen lone-pair orbital to be less tightly bonded, due to lowering the effective nuclear charge. This effect corresponds approximately to the change observed in the ionization potential E_I.[5] Therefore, the terms ϵ_n and ϵ_{π^*} in eq 1 can be replaced by the E_I and $E_{1/2}^{red.}$, respectively, to give the lowest triplet transition $\Delta E_{^3(n,\pi^*)}$ in simple form

$$\Delta E_{^3(n,\pi^*)} = E_I - E_{1/2}^{red.} - \text{constant} \quad (2)$$

Accordingly, assuming the validity of all procedures leading to eq 2, a linear relation between $\Delta E_{^3(n,\pi^*)}$ and ($E_I - E_{1/2}^{red.}$) is anticipated. However, no correlation was found for the compounds under investigation, the scatter being particularly considerable for the small carbonyl molecules **1**, **2**, and **7**. This behavior could be due to a failure to consider changes in solvation energy. Peover[6] showed that a variation in solvation energy up to 1 eV can occur, in a series of dissimilar molecules thereby destroying a correlation such as that given by eq 2. Therefore, inclusion of a term to account for changes in solvation energy should allow the correlation to be made, eq 2 being rewritten as

$$\Delta E_{^3(n,\pi^*)} = E_I - E_{1/2}^{red.} + \Delta E_{soln} - \text{constant} \quad (3)$$

ΔE_{soln} is the difference in real solvation energy between the ion and the neutral molecule. An estimate of the magnitude of ΔE_{soln}, for anion and cation formation, can be made from the relations given by Peover[7]

$$E_{red}^{\circ} = E_A - \Delta E(R\cdot^-(s)) + C \quad (4)$$

$$E_{ox}^{\circ} = E_I + \Delta E(R\cdot^+(s)) + C \quad (5)$$

where $E_{red.}^{\circ}$ and E_{ox}° are the standard reduction and oxidation potentials, respectively, and $\Delta E(R\cdot^{\pm}(s))$ is the difference in real solvation energies of the ion $R\cdot^+$ or $R\cdot^-$ and the neutral molecule R. The value of *c* is known from the measured real potential of silver ion in acetonitrile[8] (*c* = −4.7 eV). The standard potentials can be replaced by the corresponding $E_{1/2}$, assuming that the activity and diffusion coefficients of the neutral molecule and the ions are equal.[8] Using the measured half-wave reduction potentials and the E_A[9] values measured or recalculated from measured E_I,[9] and employing eq 4 and 5, values for the solvation energy of the anions and cations of

TABLE I: Structure and Numbering of the Carbonyl Compounds Studied and the Half-Wave Reduction Potentials

Carbonyl compd	X-CO-Y		$-E_{1/2}^{red.}$, V
Formaldehyde (**1**)	H	H	2.03
Acetaldehyde (**2**)	CH_3	H	2.10
Acetone (**3**)	CH_3	CH_3	2.30
Benzaldehyde (**4**)	Ph	H	1.95
Benzophenone (**5**)	Ph	Ph	1.84
Acetophenone (**6**)	Ph	CH_3	2.12
Acrolein (**7**)	CH_2=CH	H	1.76

(3) S. Wawzonek and H. Gunderson, *J. Electrochem. Soc.*, 111, 324 (1964).
(4) R. Ditchfield, J. E. Del Bene, and J. A. Pople, *J. Amer. Chem. Soc.*, **94**, 703 (1972).
(5) R. O. Loutfy and R. O. Loutfy, to be submitted for publication.
(6) M. E. Peover, *Electrochim. Acta*, **13**, 1083 (1968).
(7) M. E. Peover, "Electroanalytic Chemistry," Vol. II, A. J. Bard, Ed., Marcel Dekker, New York, N. Y., 1967, Chapter 1.
(8) B. Case, N. S. Hush, R. Parsons, and M. E. Peover, *J. Electroanal. Chem.*, **10**, 360 (1965).
(9) L. G. Christophorus, "Atomic and Molecular Radiation Physics," J. B. Birks and S. P. McGlynn, Ed., Wiley-Interscience, New York, N. Y., 1971.

TABLE II: Ionization Potential, Electron Affinities, $E_{1/2}^{ox}$ and Solvation Energies of $R_2CO\cdot^-$ and $R_2CO\cdot^+$

Compd	E_I,[a] eV	E_A, eV	$E_{1/2}^{ox}$,[c] V	$-\Delta E(R_2CO\cdot^-(s))$,[d] V	$-\Delta E(R_2CO\cdot^+(s))$,[e] V
1	10.87	−0.87[b]	3.57	3.54	2.59
2	10.21	−0.21[b]	3.03	2.78	2.47
3	9.69	0.29[b]	2.59	2.10	2.41
4	9.60	0.45[a]	2.52	2.27	2.38
5	9.45	0.55[b]	2.37	2.31	2.38
6	9.65	0.33[a]	2.55	2.23	2.40
7	10.10	−0.10[b]	2.95	2.93	2.45

[a] Reference 9. [b] Calculated on the basis of the theoretical prediction that $E_I + E_A$ = constant. The constant was obtained from the known E_I and E_A for compound 4 and 6. For more detail see ref 10. [c] Calculated from the formula $E_{1/2}^{ox} = 0.89E_I - 6.04$, ref 11. [d] Calculated according to eq 4. [e] Calculated according to eq 5.

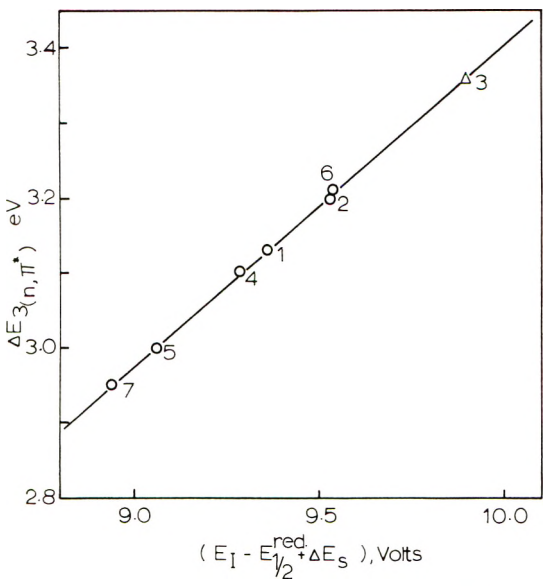

Figure 1. Relationship between the term $(E_I - E_{1/2} + \Delta E_{soln})$ of some carbonyl compounds and the n,π^* triplet energies.

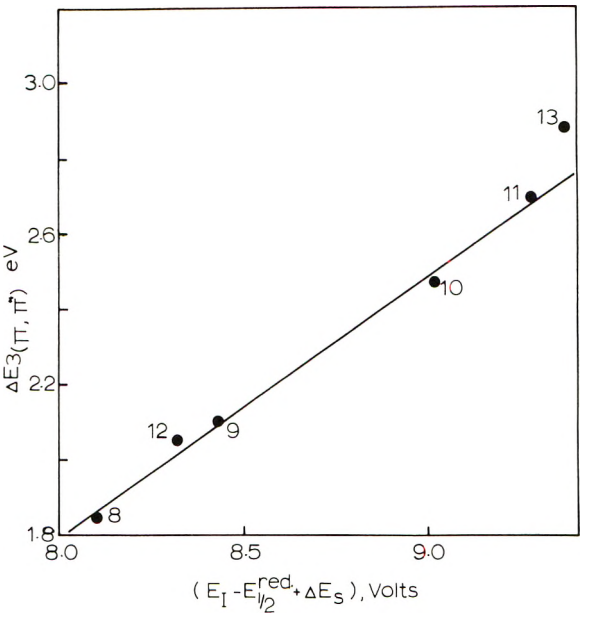

Figure 2. Relationship between the term $(E_I - E_{1/2} + \Delta E_{soln})$ of some aromatic hydrocarbons and their π,π^* triplet energies.

TABLE III: Triplet Energies and the Term $(E_I - E_{1/2}^{red.} + \Delta E_{soln})$ for the Carbonyl Compounds Studied

Compd	$\Delta E_{3(n,\pi^*)}$, eV	$(E_I - E_{1/2}^{red.} + \Delta E(R_2CO\cdot^-(s)))$
1	3.13[a]	9.36
2	3.20[a]	9.53
3	(3.26–3.47),[b] (3.36[c])	9.90
4	3.10[d]	9.28
5	2.99[d]	9.06
6	3.21[d]	9.54
7	2.95[d]	8.94

[a] Reference 14. [b] Reference 15. [c] Predicted from this work. [d] Reference 16.

the compounds investigated were calculated. The results are summarized in Table II.[10,11]

The magnitude of the solvation energies in Table II seems reasonable.[6,7,12] Furthermore, the values obtained for benzaldehyde and acetophenone are in very good agreement with values of 2.34 and 2.23 eV, respectively, reported by Peover.[5] It can be noted that $\Delta E(R_2CO\cdot^+(s))$ is almost constant throughout the series (see Table II); it is as anticipated from the linear relation between the $E_{1/2}^{ox}$ and E_I; for more detail see footnotes to Table II. However, $\Delta E(R_2CO\cdot^-(s))$ are not constant for the compounds investigated. This behavior is most likely due to the dependence of the degree of localization of the negative charge on the molecular size. The magnitudes of $\Delta E(R_2CO\cdot^-(s))$ obtained are, generally, in agreement with Hedges and Matsen's conclusion,[13] that a greater delocalization of charge in the molecule results in a lower value of ΔE_{soln}. Substituting $\Delta E(R_2CO\cdot^-(s))$ (Table II), in eq 3, the $(E_I - E_{1/2} + \Delta E_{soln})$ terms for the compounds investigated were calculated. The results are given in Table III[14-16] with the corresponding experimental values $\Delta E_{3(n,\pi^*)}$. Figure 1 shows an excellent linear correlation between the term $(E_I - E_{1/2} + \Delta E_{soln})$ and $\Delta E_{3(n,\pi^*)}$ for the compounds investigated; this result indicates the importance of including the solvation energy term. The slope of the linear correlation was found to be 0.82; while it is slightly less than the expected unity, obviously it is the right order of magnitude; also adding sup-

(10) N. S. Hush and J. A. Pople, *Trans. Faraday Soc.*, **51**, 600 (1955).
(11) L. L. Miller, G. D. Nordblom, and E. A. Mayed, *J. Org. Chem.*, **37**, 916 (1972).
(12) M. E. Peover, *Trans. Faraday Soc.*, **58**, 1656 (1962).
(13) R. M. Hedges and F. A. Matsen, *J. Chem. Phys.*, **28**, 1950 (1958).
(14) G. Herzberg, "Electronic Spectra and Electronic Structure of Polyatomic Molecules," Van Norstrand, Princeton, N. J., 1966.
(15) R. F. Borkman and D. R. Kearns, *J. Chem. Phys.*, **44**, 945 (1966).
(16) P. S. Egel and B. M. Monroe, *Advan. Photochem.*, **8**, 302 (1970).

TABLE IV: Correlation between $\Delta E_{3(\pi,\pi^*)}$ of Some Aromatic Hydrocarbon and the Term $(E_I - E_{1/2}^{red.} + \Delta E_{soln})$

Hydrocarbon	$\Delta E_{3(\pi,\pi^*)}$[a]	E_I,[b] eV	$-E_{1/2}^{red.}$,[c] V	$-\Delta E_{soln}$,[b] V	$(E_I - E_{1/2}^{red.} + \Delta E_{soln})$
Anthracene (**8**)	1.844	7.66	2.37	1.93	8.10
Pyrene (**9**)	2.10	7.72	2.49	1.78	8.43
Chrysene (**10**)	2.47	8.01	2.73	1.72	9.02
Phenanthrene (**11**)	2.69	8.06	2.88	1.66	9.28
1,2-Benzanthracene (**12**)	2.05	7.74	2.40	1.82	8.32
Triphenylene (**13**)	2.96	8.19	2.87	1.69	9.37

[a] Reference 15. [b] Reference 5. [c] Reference 7.

port to the development of eq 3. The deviation from the unity, however, could partly be due to the assumption that E_n and E_{π^*} are proportional to E_I and $E_{1/2}^{red.}$, respectively, with unity for the proportionality constant. However, a relation such as eq 3 is particularly of value with systems for which the solvation energy is constant and the symmetry properties of energy levels no longer hold.

In conclusion the correlation obtained between the n,π^* triplet energy of organic carbonyl molecules and the term $(E_I - E_{1/2} + \Delta E_{soln})$ indicates the existence of a direct and meaningful relation between the spectroscopic transition energies and the electrochemical and gas-phase properties of these molecules. Furthermore, it is anticipated that eq 3 is general and could be applied to other systems including those molecules which possess a π,π^* triplet state lowest energy transition, provided that E_I represents the ionization energy of the electron involved in the spectroscopic transition. Table IV verifies the prediction for a series of aromatic hydrocarbons where a similar correlation between $\Delta E_{3(n,\pi^*)}$ and the term $(E_I - E_{1/2} + \Delta E_{soln})$ was obtained (Figure 2 and Table IV) with a slope of 0.7. The latter is slightly different from the slope obtained previously, and also smaller than the expected unity, nevertheless, the linear relationship exists.

From Figure 1, and the electrochemistry and gas-phase data for acetone, an estimate of the $\Delta E_{3(n,\pi^*)}$ was obtained (Table III), which is in reasonable agreement with that predicted.[15]

Acknowledgment. The authors wish to express their appreciation to Dr. W. R. Fawcett of the Department of Chemistry, University of Guelph, Guelph, Ontario, Canada, for his encouragement and for making available the instrumentation used to determine the reduction potentials. The authors would also like to acknowledge Dr. W. R. Fawcett for the work reported in ref 1b. The National Research Council of Canada, Ottawa, Canada, and the Chemistry Department, University of Guelph, Guelph, Ontario are gratefully acknowledged.

A Comparison of Calculated and Experimental Energy Levels of the Rare Earths

R. C. Ropp and B. Carroll*

Chemistry Department, Rutgers, The State University, Newark, New Jersey 07102 *(Received September 18, 1972)*

The calculated free-ion energy levels of the rare earths, in the form of Grotrian diagrams, have been compared with the experimental values for the phosphates, borates, titanates, and oxides. Compounds were used in pure form. The resolution of the powder reflectance data was more than sufficient to resolve the Stark components. Crystal field effects, state broadening, and density of states illustrate the desirability of using calculated rather than the experimental (baricentered) free ion as a reference state. Our data indicate that the experimental baricenters usually observed are a function of crystal symmetry rather than of crystal field, and/or nephelauxetic effects, as is commonly held.

Historically, there have been a number of approaches to the determination of the trivalent energy levels of the rare earths. The first was the determination of experimental levels by fluorescence and absorption. Almost simultaneously, the "free-ion" levels were obtained by successive ionization of the metals in emission spectroscopy. Subsequently, calculations were developed from methods originated by Slater[1] and extended in considerable detail by Condon and Shortley.[2] The general method was then sys-

(1) J. C. Slater, *Phys. Rev.*, **34**, 1293 (1929).
(2) E. U. Condon and Shortley, "The Theory of Atomic Spectra," Cambridge University Press, New York, N.Y., 1963.

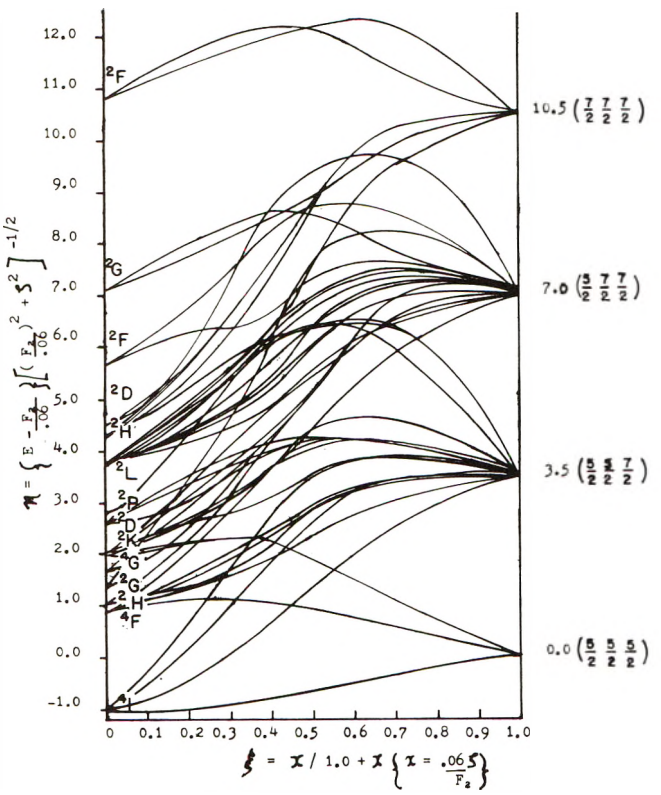

Figure 1. The complete free-ion f^3 intermediate coupling diagram according to Varga, *et al.*,[6] for an octahedral field. Energy on the ordinate is in terms of the Slater parameter, F_2, while the abscissa is in terms of the spin–orbit parameter, ζ. At the left is pure Russell–Saunders coupling while on the right is pure *j–j* coupling.

temized by Racah,[3] Judd,[4] and Wybourne,[5] to name a few. In an approach which has presently evolved, the energies are obtained in terms of a spin–orbit coupling factor, ζ, and are displayed as shown in Figure 1 for the f^3 ion.[6] What is done[7] is to adjust the spin–orbit parameter until the calculated levels agree with those of the experimentally determined baricenters as close as possible. These then are the free-ion levels.

Wybourne[8] has used a somewhat different approach and has published a self-consistent set of energy values which we have used to construct a set of Grotrian diagrams for each rare earth. After using these diagrams and attempting to correlate experimental Stark components of transitions with free-ion levels, we have come to the conclusion that it is better to employ a self-consistent set of levels rather than the adjusted set of free-ion levels. These conclusions are based upon new data on the spectral transitions of the rare earths as phosphates, borates, titanates, and oxides.

There are three factors involved in the interpretation of free-ion spectra. The first is the crystal field effect which is related to the spin–orbit parameter. The second is the nephelauxetic effect which arises due to orbital overlap of the bonding electrons of the host crystal with the shielded 4f states. It is related to the degree of covalency of the bonds in the crystal. The third is the symmetry effect which affects transition moments between Stark states of the levels in the crystal. It seems, from our data, that the apparent baricenter is shifted as a function of symmetry rather than as a function of the other two effects. The presence or absence of certain critical Stark components of a given transition has been sufficient to bring us to this conclusion.

Experimental Section

We have developed a method for measurement of reflectance of powders which gives resolutions of 1–2 Å. The full details have already given.[9] The basic instrument is the Cary-15 spectrophotometer, in which the source was replaced with a high-intensity Xe lamp in an enclosed housing so that nitrogen or argon atmosphere could be employed to eliminate oxygen absorption in the far uv. Matched reflectance spheres were employed, each coated with optical grade $BaSO_4$. $BaSO_4$ is stable and does not degrade under uv irradiation as does smoked MgO. A powder press was employed to give reproducible surfaces. The instrument as modified is easy to use and gives reproducible results. The resolution may be adjusted by control of the slit program and the speed of scanning. The latter is related to the response of the recorder. Since $BaSO_4$ has a reflectivity close to 99.7% clear across the spectrum, it is sufficient to adjust the system so that it reads 100% at all wavelengths. This corrects for all losses in the monochromator, the sensitivity decrease of the matched photomultipliers at the ends of the scanned spectrum, and losses in the reflectance heads. We obtained significant measurements through the range 1700–8000 Å.

Materials were prepared by precipitation from solution. The rare earth phosphates were prepared from phosphoric acid solution, the borates using boric acid, the titanates as coprecipitated oxalates, and the oxides as oxalates. By firing these raw materials at elevated temperatures, the desired rare earth compounds were obtained. Particle size distributions of the family of rare earth compounds were checked for reproducibility since this factor may affect the reflectance spectrum. All were nearly identical.

Basically, the instrument is very easy to operate. A powder surface is produced in the powder press and the sample placed in the sample position opposite a similar one of $BaSO_4$. The instrument is allowed to warm up and the Xe lamp is allowed to stabilize. Nitrogen atmosphere is circulated throughout the system for purge and is continued while the instrument is in operation. Generally, we ran a 30-ft chart in order to give good separation of the multiplets. Normally we ran $ErPO_4$ as a check upon resolution since there are several bands containing up to 15 components. Details are given in our prior report.[9]

Experimental Results and Discussion

Crystal Field Effects. In order to illustrate the utility of the calculated levels, we first compare the apparent shift in baricenter energy as a function of compound (crystal field effects). Perhaps the best lanthanide to work with

(3) G. Racah, *Phys. Rev.*, **61**, 186 (1942); **62**, 438 (1942); **63**, 367 (1942); **76**, 1352 (1949).
(4) B. R. Judd, *Proc. Phys. Soc., London*, **82**, 874 (1963); "Operator Techniques in Atomic Spectroscopy," McGraw-Hill, New York N. Y., 1963; *Physica*, **33**, 171 (1967); *Phys. Rev.*, **162**, 28 (1967); B. R. Judd, H. M. Crosswhite, and H. Crosswhite, *ibid.*, **169**, 13 (1968); B. R. Judd, *Advan. Chem. Phys.*, **14**, 1435 (1968).
(5) B. G. Wybourne, *J. Chem. Phys.*, **32**, 639 (1968); **34**, 279 (1961); **35**, 340 (1961); **36**, 2295 (1961); **36**, 2301 (1963); *J. Math. Phys.*, **4**, 354 (1963); *J. Chem. Phys.*, **40**, 1457 (1964); **43**, 4506 (1965); *J. Opt. Soc.*, **55**, 928 (1965).
(6) L. P. Varga, M. J. Reisfeld, and L. B. Asprey, *J. Chem. Phys.*, **53**, 250 (1970).
(7) R. L. Schwiesow, *J. Opt. Soc.*, **62**, 649 (1972).
(8) B. G. Wybourne, "Spectroscopic Properties of the Rare Earths," Interscience, New York, N. Y., 1965.
(9) R. C. Ropp, Ph.D. Thesis, Rutgers University, July 1971.

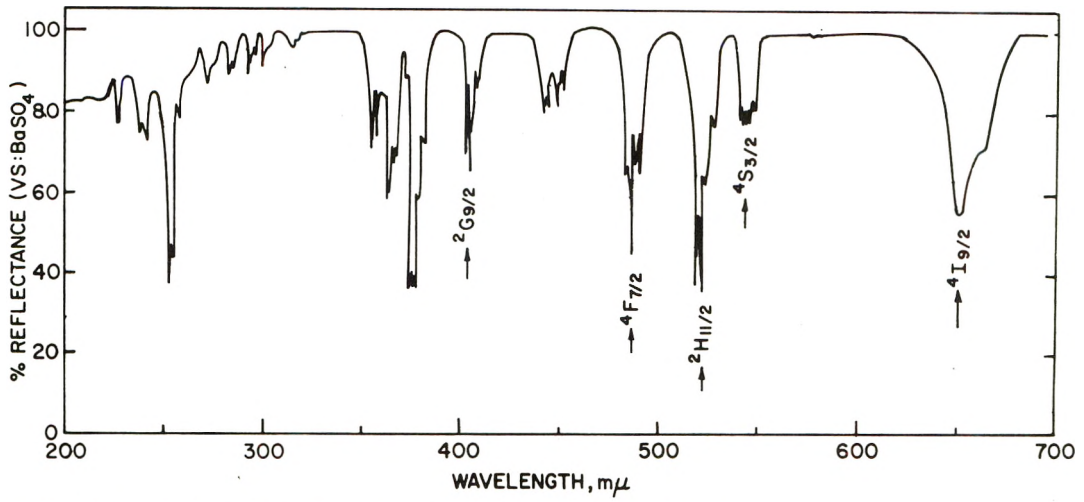

Figure 2. Powder reflectance spectrum for $ErPO_4$ reduced from 30-ft chart.

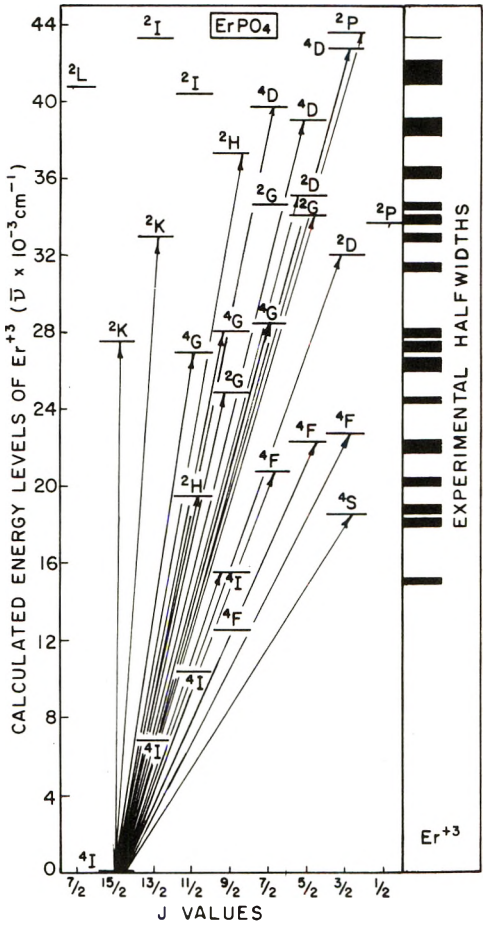

Figure 3. Comparison of experimental half-widths of reflectance bands of $ErPO_4$ as compared to Er^{3+} free-ion levels calculated on the basis of intermediate coupling.

this respect is Er^{3+} because its energy levels are separated sufficiently so that assignment of transitions can be made unambiguously. Figures 2–5 deal with the spectrum of $ErPO_4$; the latter two figures include additional erbium compounds for comparison purposes.

Figure 2 shows the powder reflectance spectrum, reduced from the original read-out chart 30 ft long. A few of the transitions in this figure are labeled. The intensities are compared to optical quality $BaSO_4$ whose reflectance

TABLE I: Apparent Shift, ΔE, in Baricenter of Er^{3+} Levels, $^4F_{7/2}$ and $^2G_{9/2}$, as Measured from Free-Ion Level[a]

	Baricenter, Å			
Compd	$^4F_{7/2}$	ΔE	$^2G_{9/2}$	ΔE
$ErBO_3$	4854	27	4070	53
$Er_2Ti_2O_7$	4892	65	4077	60
$ErPO_4$	4910	83	4083	66
Er_2O_3	4920	93	4101	84

[a] Data taken from Figures 4 and 5.

averages 99.7% throughout the visible and ultraviolet. In Figure 3, we indicate the apparent half-width of the various bands taken from the original data of Figure 2. These are plotted as ordinates alongside of the calculated free-ion levels. The assignment of the term symbols for the various bands in Figure 2 was made by inspection of the data in Figure 3. Note that in Figure 3 there appears to be a consistent downshift in energy for each band as compared to the free-ion level. This is the nephelauxetic effect as described by Jorgensen.[10]

Let us take a closer look at the $^4F_{7/2}$ transition at full resolution as shown in Figure 4 and the $^2G_{9/2}$ transition in Figure 5. Here we can see the Stark components of these transitions for a series of erbium compounds of various symmetries. The cation site symmetries for the various compounds are $ErPO_4$, D_{2d}; $ErBO_3$, D_{3d}; Er_2O_3, C_{2v}; and $Er_2Ti_2O_7$, O_h. The $^4F_{7/2}$ free-ion level lies at 4826.9 Å, while that for the $^2G_{9/2}$ lies at 4017.2 Å. Using the Stark components of greatest intensity for each spectrum, we determined the baricenters, as given in Table I. The energy shift from the free-ion value is expressed in the table as ΔE. These data indicate an apparent shift in energy over a range of 27–93 Å. We call attention to the fact that ΔE increases in the same manner for the two transitions as the nature of the compound changes, and that the direction is negative for Er^{3+}. This nephalauxetic effect is related to the covalency of bonding in the structures. All electronic Er^{3+} levels in a given compound appear to be shifted to about the same degree.

(10) C. K. Jorgensen, *Kgl. Dan. Vidensk. Selsk., Mat.-Fys. Medd.*, **30**, 22 (1956); see also, "Oxidation Numbers and Oxidation States," Springer-Verlag, Berlin, 1969.

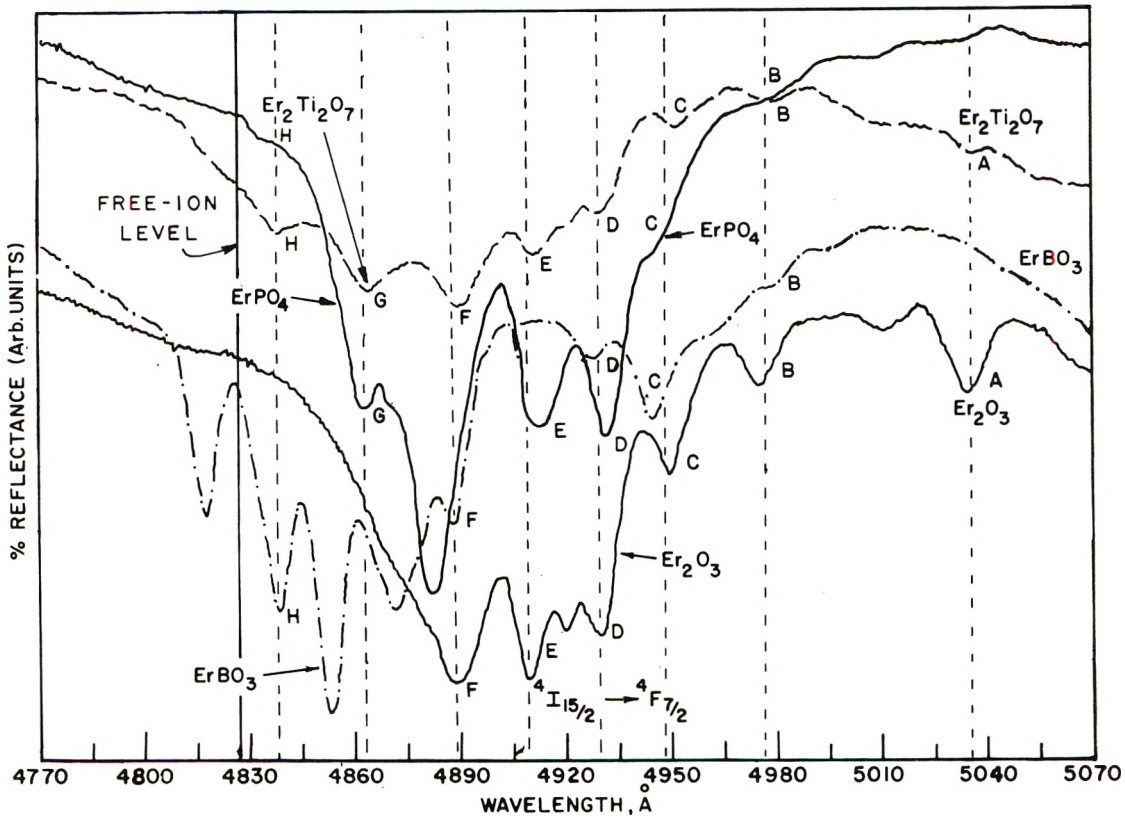

Figure 4. High-resolution reflectance spectra for $ErPO_4$, $ErBO_3$, Er_2O_3, and $Er_2Ti_2O_7$. The electronic transition is $^4I_{15/2} \rightarrow {}^4F_{7/2}$. The solid line indicates the free-ion value for intermediate coupling. The broken vertical lines indicate Stark components of matching wavelengths for the four compounds, wherever the letters A through H are shown.

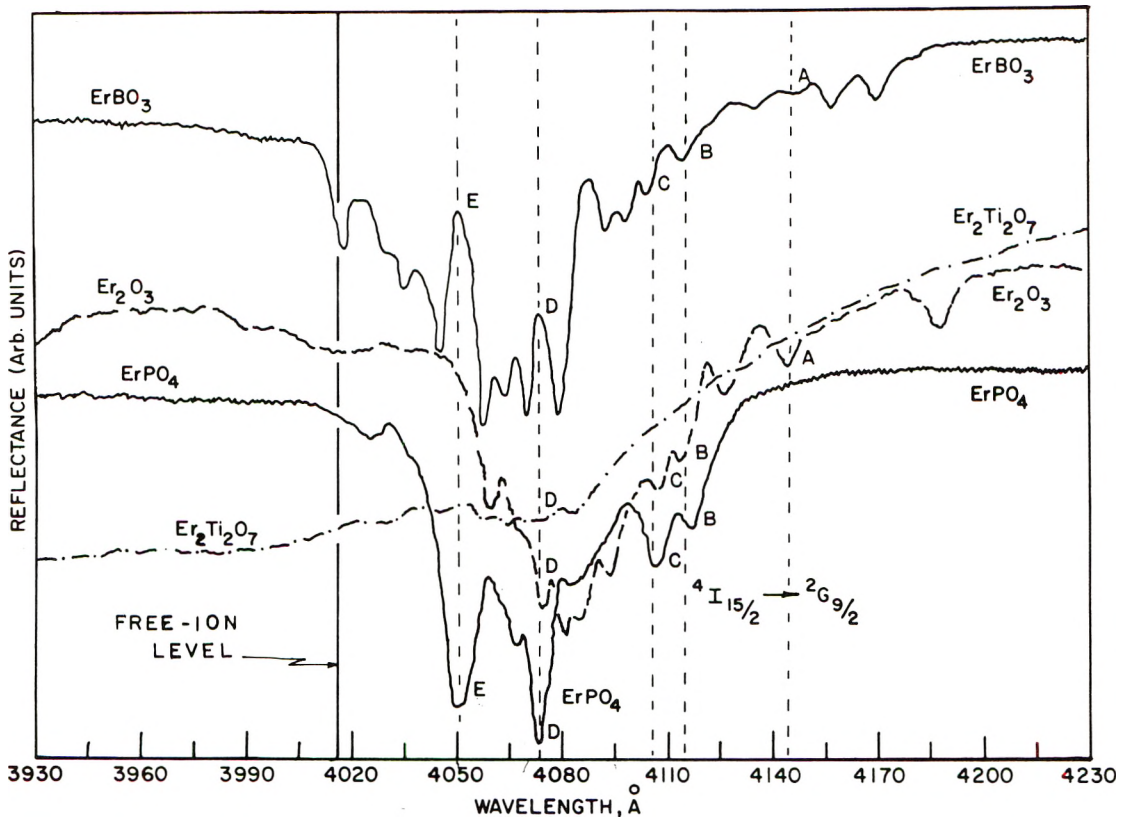

Figure 5. High-resolution reflectance spectra for the electronic transition, $^4I_{15/2} \rightarrow {}^2G_{9/2}$, for $ErPO_4$, $ErBO_3$, Er_2O_3, and $Er_2Ti_2O_7$. The solid line indicates the free-ion value for intermediate coupling. The broken vertical lines indicate Stark components of matching wavelengths for the four compounds. Those at A, B, and C indicate Stark lines of matching energy whereas those at D and E show matching Stark lines for $ErPO_4$, Er_2O_3, and $Er_2Ti_2O_7$, which are singularly absent in $ErBO_3$.

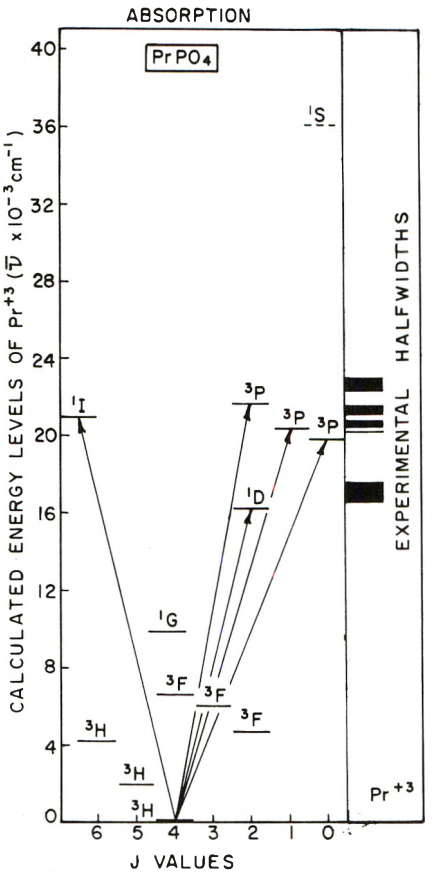

Figure 6. Reflectance spectrum of $PrPO_4$, a case of state broadening, for the ^3P_J states. A correlation of state broadening is noted as J changes from 0 to 2.

Because Er^{3+} is a Kramers ion, there are a total of 8 Stark states possible for the $^4I_{15/2}$ ground state, 4 Stark states for the $^4F_{7/2}$, and 5 Stark states for the $^2G_{9/2}$ state. This makes possible 32 Stark transitions for the former and 40 for the latter, if there were no symmetry restrictions. The spectral regions shown in Figure 4 and 5 were especially chosen because no other electronic transitions are possible. Thus all lines observed must arise from Stark states although some lines appear to be isolated from the main band.

Examining Figure 4, we find many matching Stark lines for the various compounds. To illustrate this, we have marked some of the corresponding Stark lines A, B, C, D, etc., for each compound. Note that in many cases there are four matching transitions as indicated by the broken paralled lines. In others, notably E and F, one line is missing but is present in the other compounds. We can find examples even more striking in the spectra of Figure 5 where at D and E, Stark lines are present in two or three of the spectra but notably absent in $ErBO_3$. It can be further noticed that the distance between neighboring Stark lines remains qualitatively the same for all four compounds. These observations imply that the strength of the crystal field has a minor effect on the energy separation of the Stark states and that the selection rules are governed by the symmetry of the crystal. Thus it appears that reported differences in baricenters for various compounds of a given rare earth are in fact dependent upon the number of Stark lines observed. We again call attention to the fact that up to 40 Stark lines are possible over the energy range shown in either Figure 4 or 5. Only a fraction of these appear, depending upon crystal symmetry. When they are present, they appear at the same energy, regardless of the nature of the anion. When they are

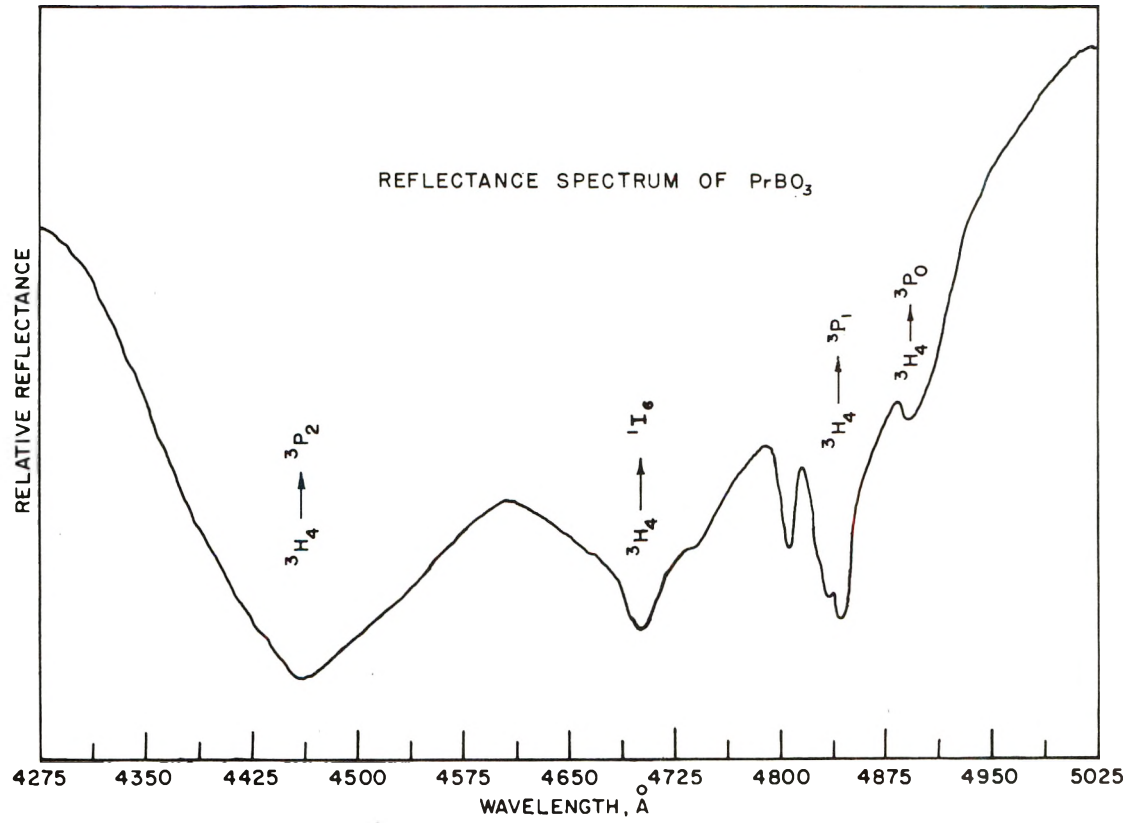

Figure 7. Reflectance spectrum of $PrBO_3$, illustrating the effect of state broadening. For the $^3P_0$ state, only one Stark component is expected and observed, whereas three Stark lines appear in the $^3P_1$ band. As $J \rightarrow 2$, all individual Stark lines are apparently smeared together.

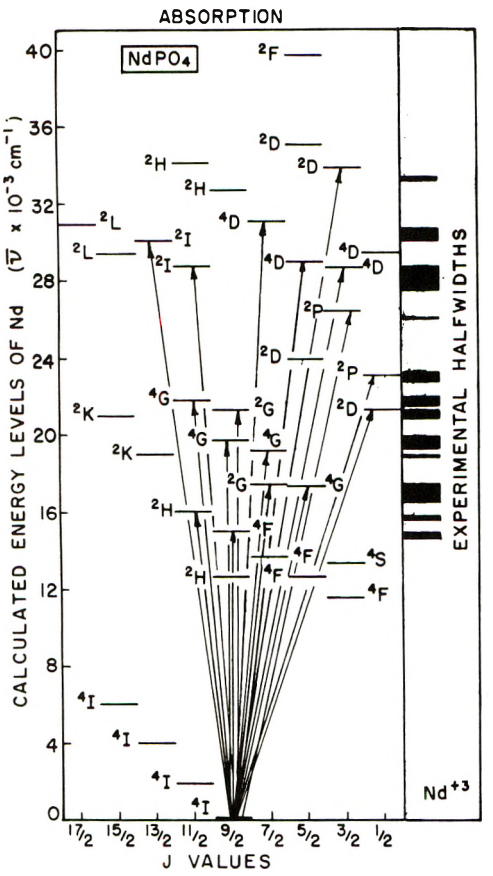

Figure 8. Comparison of experimental half-widths illustrating the factor, density of states. Choice of the proper label involves those of a given set of levels of multiplets, provided that at least one can be assigned unambiguously. The limit, $\Delta J < 6$, applies in all cases.

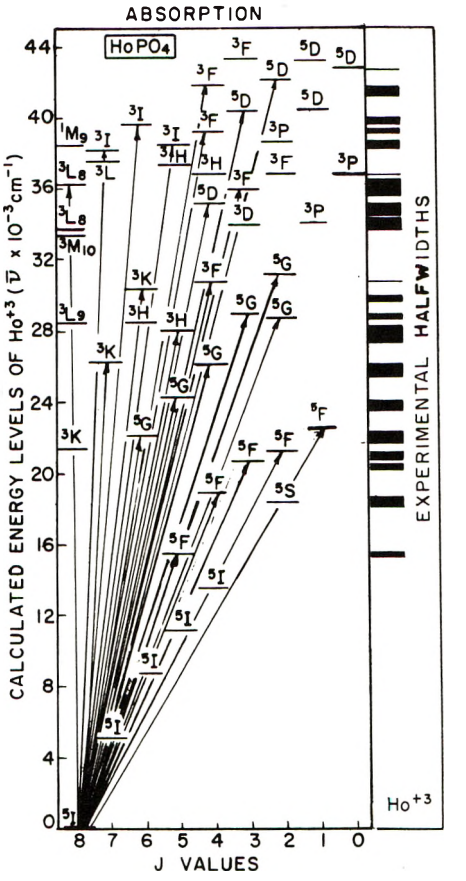

Figure 9. A further illustration of the density of states and the utility of labeling corresponding levels of a multiplet.

absent, the baricenter of the band is reported as shifted. Thus it would appear that the shift is not necessarily dependent upon crystal field strength as is commonly thought, but rather seems to be a symmetry effect.

For these reasons, it seems that the use of the calculated free-ion energy level provides a more desirable basis for the comparison of 4f multiplets rather than the widely used baricentered level.

It is interesting to note that the $^2G_{9/2}$ band as seen in Figure 3 for $Er_2Ti_2O_7$ is so weak that its presence is dubious whereas its $^4F_{7/2}$ band (Figure 1) is weak but clearly discernable. It is known that 4f transitions are strictly forbidden by the parity rule but that they do occur because of several reasons, as first given by Van Vleck.[11] These include mixing of orbitals of opposite symmetry and mixing brought about through the effect of odd lattice vibrations. These cause forced electric-dipole transitions. In a site with inversion symmetry, as is the case for $Er_2Ti_2O_7$, these transitions should not occur. In general, the 4f transitions in $Ln_2Ti_2O_7$ are significantly lower in intensity than those of the other compounds.

State Broadening. It is well known that the degree of broadening of an energy level is directly related to crystal field perturbation. Because of the uncertainty principle, all atomic states will have a finite line breadth. For the rare earths, where the 4f states are shielded by the outer $5s^25p^6$ electrons, the line breadths should be about 3-4 Å. We have observed that the heavy lanthanides (*i.e.*, greater than Gd^{3+}) show fairly narrow half-widths in crystals (about 8 Å) whereas the light lanthanides (up to Gd^{3+})

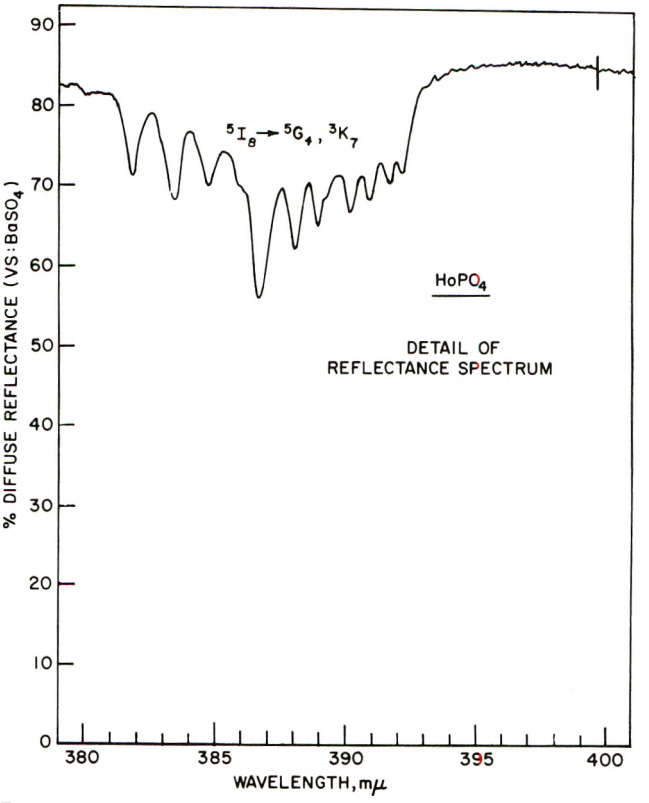

Figure 10. Detail of $HoPO_4$ reflectance spectrum. The Stark components are very narrow in contrast to those for other lanthanides such as Pr^{3+} (see Figure 7).

(11) J. H. Van Vleck, *J. Chem. Phys.*, **41**, 67 (1937).

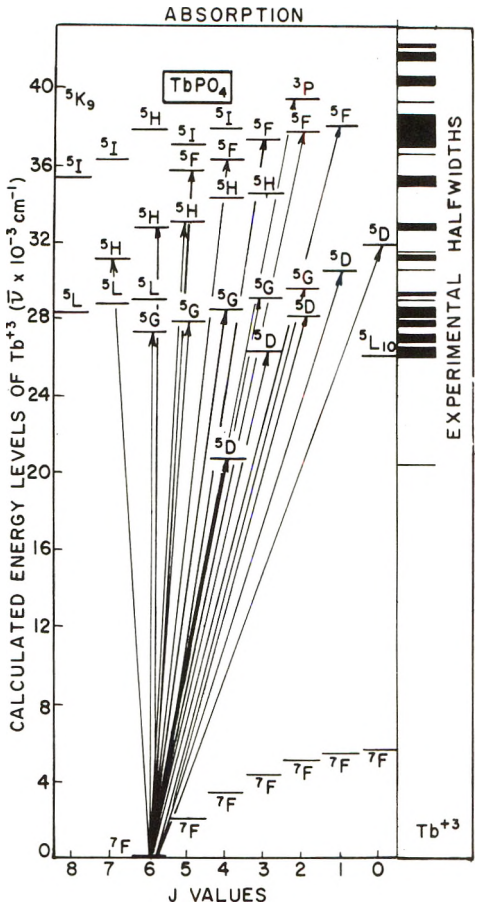

Figure 11. Reflectance spectrum of $TbPO_4$ further illustrating the utility of labeling corresponding levels of a multiplet. In this case, one of the levels of each multiplet is unquestionably present. It is easy to show that all of the component levels of the multiplet are present, even though they may be combined with other levels of another multiplet.

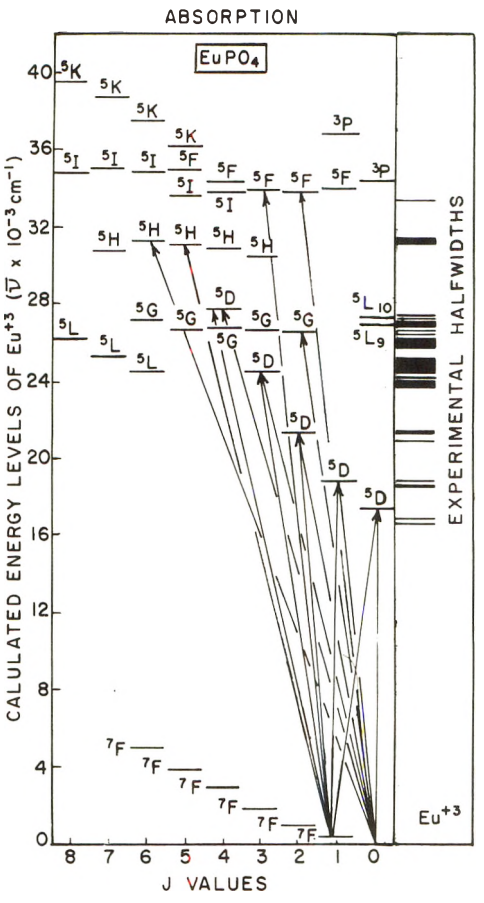

Figure 12. Reflectance spectrum of $EuPO_4$ showing further evidence of the utility of labeling of corresponding terms of a multiplet. Here doublets appear because the $^7F_1$ state is thermally populated at room temperature. This provides an unambiguous identification of the ^5D_J states. Those levels above about 32,000 cm^{-1} do not appear in the spectrum because of the charge transfer band of Eu^{3+}. Only the strongest appear as side bands on the broad CT band.

are broader.[9] For example, Nd^{3+} lines average closer to 15 Å in half-width, this being the half-width of the Stark components. However, the individual multiplets for a given ion can vary quite widely. For example, Pr^{3+} shows a marked broadening effect. This is shown in Figure 6 for $PrPO_4$. Note the $^1D_2$ state in this figure and the apparent half-width at the right of the figure. The ^3P_J states show a noticeable broadening as $J = 0 \rightarrow 2$. This is not a function of the compound but of the Pr^{3+} ion spectroscopic states. To substantiate this we present the Pr^{3+} spectrum for the $PrBO_3$ compound, as shown in Figure 7. The Stark components in this spectrum are 15–25 Å in half-width. The $^3P_0$ band is rather narrow, the $^3P_1$ band broader, and the $^3P_2$ band very broad, analogous to those shown in the previous figure for $PrPO_4$. It is interesting to note that for $J = 0$, one Stark component is expected, for $J = 1$, three components are expected, and for $J = 2$, five components are possible. Experimental results correspond for the first two bands but not the third. In the third band, individual Stark components are not apparent. This broadening effect indicates increased crystal field perturbation as J changes from 0 to 2. Thus we have a case where state broadening is associated with the total angular momentum quantum number, J. This illustrates the fact that not all spectroscopic states are shielded to the same degree by the outer electron shells.

Another example of state broadening can be seen in Figure 8 for $NdPO_4$. Here the $^2P_{1/2}$ band is rather broad whereas the $^2P_{3/2}$ is narrow. This is another case where two related terms of the multiplet are affected differently by the crystal field.

Density of States. The last factor we wish to consider is the density of states. For example, Figure 8 shows the experimental bands determined for $NdPO_4$. We show a lower limit of about 14,000 cm^{-1} because of instrumental limitations. Between 14,000 and 16,000 cm^{-1}, two bands appear, due to $^4F_{9/2}$ and $^2H_{11/2}$ transitions. Immediately above these is a broader band which may be due to both $^2G_{9/2}$ and $^4G_{5/2}$ transitions or to state broadening of either. As one compares experimental to calculated levels, it is readily apparent that correlation is difficult. There are a few levels which can be assigned unambiguously, notably $^2D_{3/2}$, $^2P_{3/2}$, $^2P_{1/2}$, $^2H_{11/2}$, and $^4F_{9/2}$, but a definite choice is difficult for many.

The utility of labeling corresponding levels in accordance with our recommended procedure can be illustrated further. Figure 9 displays the calculated and experimental levels of Ho^{3+} (as $HoPO_4$). The lowest energy band is $^5F_5$. The next is assigned as $^5F_4$, rather than $^5S_2$, because all of the other ^5F_J components are present. In a like manner,

(12) R. C. Ropp and B. Carroll, to be published.

the ^5G_J states can be assigned. We show the detail of the band at 26,000 cm^{-1} (388 μ) in Figure 10 with two transitions indicated. There are 11 Stark components whose widths vary between 5 and 8 Å in contrast to those of Figure 7 for Pr^{3+} where the half-widths were closer to 25 Å.

Up to this point we have accepted the concept of identifying corresponding terms of a given multiplet if one or more was unquestionably present.

Now we can take the opposite viewpoint and search to determine if all terms of a given multiplet can be found. To do this, we examine the data of Figure 11 for Tb^{3+} in $TbPO_4$. The lowest state is unquestionably $^5D_4$. The other ^5D_J states are apparent as are the ^5G_J states. By close inspection of Figure 11 we can also assign ^5H and ^5I transitions. The band at 38,000 cm^{-1} is very broad (about 90 Å in half-width). We have reason to assign it as a ^5F_J state and this will be the subject of a further communication.[12]

Another case where all of the terms of a multiplet are present in the spectrum is evident in Figure 12 for Eu^{3+} in $EuPO_4$. The $^7F_1$ state is thermally accessible at room temperature and is populated. Thus there appears in the spectrum what might at first glance seems to be doublets. These are lines for the ^5D states, one from the $^7F_0$ and the other from the $^7F_1$ term of the ground state. All of the terms can be correlated to line doublets in the spectrum. Not all of the ^5H terms appear to be present. This may be due to the fact that the 4f states above about 34,000 cm^{-1} are obscured by the charge transfer band of Eu^{3+}.[9]

Vibration-to-Rotation Energy Transfer in Water, Heavy Water, and Ammonia[1a]

Hyung Kyu Shin

Department of Chemistry,[1b] University of Nevada, Reno, Nevada 89507 *(Received August 10, 1972)*

Publication costs assisted by the Air Force Office of Scientific Research

Vibrational deexcitation in H_2O–H_2O, D_2O–D_2O, and NH_3–NH_3 in the temperature range 300–2000°K has been investigated on the basis of a vibration-to-rotation energy transfer mechanism. The deexcitation collision number for NH_3 is very small and changes slowly with temperature; it changes from 13 at 300°K to 5 at 2000°K. This result is in good agreement with ultrasonic absorption measurements over 300–773°K. For H_2O, the collision number is significantly larger: 197 at 300°K and 46 at 2000°K. The deexcitation is much less efficient in D_2O compared to H_2O, particularly at low temperatures: at 300°K it is 594 and decreases to 49 at 2000°K. D_2O rotates slower than H_2O, and is not as efficient as H_2O in deexciting the collision partner. In all collisions, the participation of translational motion as well as the effect of molecular attraction is explicitly considered. The model of vibration-to-translation energy transfer taking place at preferred dipole–dipole orientations lead to collision numbers which are seriously different from the above result; such energy transfer is not important in these systems. However, for SO_2–SO_2, the calculation indicates that the latter model is acceptable.

Introduction

Rates at which the vibrationally excited CH_4, SiH_4, and hydrogen halide molecules relax are known to be much faster than those predicted by conventional vibration-to-translation (V–T) energy transfer theories.[2,3] Recently, similar results have been reported for NH_3–NH_3[4] and HF–CO_2[5-8] collisions. Furthermore, the experimental studies[2,3,5,7,8h] show that the vibrationally excited molecules relax more rapidly than deuterated molecules, a trend which contradicts the predictions of V–T theories. Theoretical methods[2,9] have been developed to explain the vibrational relaxation of these molecules with the recognition of vibration-to-rotation (V–R) energy transfer. We have recently developed an approximate formulation of the V–R energy transfer theory in classical mechanics,[10] and applied it to the vibrational relaxation of hydrogen halide molecules with reasonable success both in calculating vibrational relaxation times and in predicting isotope effects.[10,11] The V–R energy transfer theory allows the major portion of the vibrational energy defect between initial and final states to be taken up by rotational motion of the colliding partner.

(1) (a) This work was supported by the Air Force Office of Scientific Research, Grant No. AFOSR-72-2231. Part of this work was reported at the Symposium on Molecular Energy Transfer, University of Mississippi, Oxford, Miss., April 13–14, 1972. (b) Theoretical Chemistry Group Contribution No. 1040.

(2) T. L. Cottrell and A. J. Matheson, *Trans. Faraday Soc.*, **58**, 2336 (1962).

(3) Also see related papers, (a) T. L. Cottrell and A. J. Matheson, *Proc. Chem. Soc., London*, 114 (1961); (b) T. L. Cottrell, R. C. Dobbie, J. McLain, and A. W. Read, *Trans. Faraday Soc.*, **60**, 241 (1964); (c) F. D. Shields and J. A. Burks, *J. Acoust. Soc. Amer.*, **43**, 510 (1968); (d) W. D. Breshears and P. F. Bird, *J. Chem. Phys.*, **50**, 333 (1969); **51**, 3660 (1969); **52**, 999 (1970).

(4) (a) H. E. Bass and T. G. Winter, *J. Chem. Phys.*, **56**, 3619 (1972); (b) H. E. Bass, Dissertation, Oklahoma State University, 1971.

(5) R. S. Chang, R. A. McFarlane, and G. J. Wolga, *J. Chem. Phys.*, **56**, 667 (1972).

(6) J. K. Hancock and W. H. Green, *J. Chem. Phys.*, **56**, 2474 (1972).

(7) R. R. Stephens and T. A. Cool, *J. Chem. Phys.*, **56**, 5863 (1972).

In the present paper we shall investigate the vibrational relaxation of H_2O and NH_3 molecules by use of the classical V-R energy transfer theory.[10] Since both molecules are strongly polar, we might expect dipole–dipole interaction energy,[12] as well as hydrogen-bond interaction,[7] to play an important role in the relaxation processess. In ref 12, we have attempted to calculate vibrational transition probabilities for these molecules in terms of the mechanism of V-T energy transfer taking place at preferred orientations. Since, in the V-R energy transfer model, the colliding molecules are assumed to rotate rapidly, the dipole–dipole interaction cannot play an important role. Furthermore, the molecules cannot maintain preferred orientations to form hydrogen bonds. The predictions of V-R energy transfer theory[10] and recent experimental results[4] of vibrational transition probabilities for these molecules are substantially different from those calculated by the V-T approach;[12] we shall discuss this aspect in detail. The interaction energy functions appropriate for the V-R energy transfer in H_2O–H_2O and NH_3–NH_3 are different from those for hydrogen halide collisions; we shall show the derivation of the function for H_2O–H_2O in the next section. Once the function is known, the V-R formulation reported in ref 10 can be readily applied.

Collision Model and Interaction Potential

For H_2O–H_2O, the collision model consists of a rotating oscillator $(H_2O)_v$ and a rigid rotator $(H_2O)_r$ which are in interaction with each other through the potential energy $U(r_1,r_2,r_3,r_4)$, where r_i's are the interaction distances between hydrogen atoms belonging to different molecules as shown in Figure 1. The angles that the O–H bonds of $(H_2O)_v$ and $(H_2O)_r$ make with the internuclear axis are represented by θ_1 and θ_2, respectively. Because the mass of oxygen atom, m_O, is very large compared with that of hydrogen atom, m_H, the distance between the centers of mass of $(H_2O)_v$ and $(H_2O)_r$ is essentially identical with that between two oxygen atoms. Since we are concerned with the removal of the vibrational energy associated with the bending mode of $(H_2O)_v$ by $(H_2O)_r$, it is necessary to set up the instantaneous collision coordinate system with the angle $\theta_1 + \delta$, where δ is the displacement from the equilibrium bond angle and it can take either positive or negative values. The equilibrium O–H bond distance, d, is $\sim$0.96 Å, and the equilibrium bond angle Θ is $\sim$105°. For the relative separation between two H_2O molecules significantly larger than d, we can approximate the distances r_1 and r_2 as

$$r_1 = r - qd\cos(\theta_1 + \delta) + qd\cos\theta_2 \quad (1a)$$

$$r_2 = r - qd\cos(\Theta - \theta_1 - \delta) + qd\cos\theta_2 \quad (1b)$$

where $q = m_O/(m_H + m_O)$. By use of simple trigonometric identities we obtain

$$r_1 = r - qd\cos\theta_1 + qd\cos\theta_2 + qd(\sin\theta_1)\delta \quad (2a)$$

$$r_2 = r - qd\cos\Theta\cos\theta_1 + qd\sin\Theta\sin\theta_1 + qd\cos\theta_2 + qd(\sin\Theta\cos\theta_1 + \cos\Theta\sin\theta_1)\delta \quad (2b)$$

in which the approximate relations $\cos\delta \simeq 1$ and $\sin\delta \simeq \delta$ have been introduced.

At interatomic distances for which eq 1 and 2 are valid, overlapping between electron clouds is not large so that the additivity of the interaction forces between the individual atoms belonging to different molecules can be applied.[13] Then, assuming a Morse-type exponential function, we write the overall interaction potential in the form

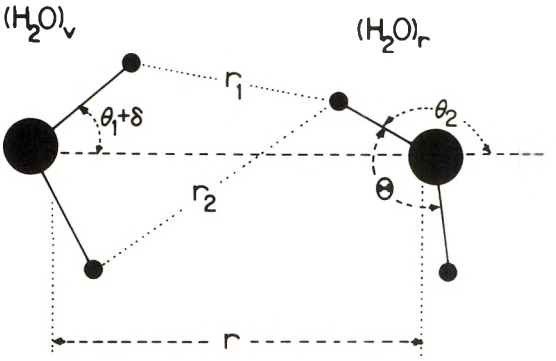

Figure 1. Collision model for the interaction of the bending mode of the rotating oscillator $(H_2O)_v$ with the rotator $(H_2O)_r$. δ is the displacement of the bending angle from the equilibrium value Θ.

$$U = \sum_{i=1}^{4} U(r_i) = D\sum_{i=1}^{4}[\exp(l - r_i/a) - 2\exp(l/2 - r_i/2a)] \quad (3)$$

where D, a, and l are potential parameters, and the second term is introduced to take into account the importance of the attractive forces which act between the colliding molecules. The constant D will be taken as the depth of the potential well, while the range parameters a and l can be determined by fitting the exponential potential to an empirical form such as the Lennard-Jones potential. However, l does not appear in the final expression. In the present model, both $(H_2O)_v$ and $(H_2O)_r$ are rotating so that we can determine the transition probability in terms of the interaction between a hydrogen atom of $(H_2O)_r$ and two hydrogen atoms of $(H_2O)_v$. In a certain range of θ_2, $U(r_1)$ is the dominate part of the overall interaction potential $\Sigma U(r_i)$, while at other ranges, $U(r_2)$, $U(r_3)$, or $U(r_4)$ is the most important. Since the hydrogen atoms are approaching each other in close range, the interaction between two oxygen atoms can be neglected. Furthermore, since the distance between the latter atoms is essentially equal to the relative separation r, the O–O interaction does not make any important contribution to the perturbation force which will be derived below. In eq 3, D is taken as the depth of the potential well between the colliding partners; then, it is obvious that if all atoms were at their equilibrium positions, the depth would be $4D$. To remove this physically unacceptable situation, we shall introduce a factor of $(1/4)^2$ in the derivation of the final expression of V-R energy transfer probability. In the following formulation we shall take $U(r_1)$ to be the most

(8) Also see related papers, (a) T. A. Cool, R. R. Stephens, and T. J. Falk, *Appl. Phys. Lett.*, **15**, 318 (1969); (b) T. A. Cool and R. R. Stephens, *J. Chem. Phys.*, **51**, 5175 (1969); (c) J. R. Airey and S. F. McKay, *Appl. Phys. Lett.*, **8**, 23 (1971); (d) J. F. Bott and N. Cohen, *J. Chem. Phys.*, **55**, 3698 (1971); (e) W. C. Solomon, J. A. Blauer, F. C. Jaye, and J. G. Hnat, *Int. J. Chem. Kinet.*, **3**, 215 (1971); (f) H. L. Chen and C. B. Moore, *J. Chem. Phys.*, **54**, 4072 (1971); (g) H. L. Chen, *ibid.*, **55**, 5551 (1971); (h) M. Y. D. Chen and H. L. Chen, *ibid.*, **56**, 3315 (1972).
(9) C. B. Moore, *J. Chem. Phys.*, **43**, 2979 (1965).
(10) H. Shin, *J. Phys. Chem.*, **75**, 1079 (1971).
(11) H. Shin, *Chem. Phys. Lett.*, **10**, 81 (1971).
(12) H. Shin, *J. Amer. Chem. Soc.*, **90**, 3029 (1968).
(13) L. Salem, *Proc. Roy. Soc., Ser. A*, **264**, 379 (1961).

important part of the overall interaction; obviously we could take any one term of $\Sigma U(r_i)$ to formulate the transition probability. We shall, however, include $U(r_2)$ in the formulation and show how it will affect vibrational transition probabilities in the numerical section.

By introducing the distances r_1 and r_2 into eq 3, we obtain

$$U(r,\theta_1,\theta_2,\delta) = D\exp[l - (r/a) - (qd/a)\cos\theta_2]\{\exp[(qd/a)\cos\theta_1] + \exp[(qd/a)\cos\Theta\cos\theta_1 - (qd/a)\sin\Theta\sin\theta_1]\} - 2D\exp[(l/2) - (r/2a) - (qd/2a)\cos\theta_2]\{\exp[(qd/a)\cos\theta_1] + \exp[(qd/2a)\cos\Theta\cos\theta_1 - (qd/2a)\sin\Theta\sin\theta_1]\} - (Dqd/a)\exp[l - (r/a) - (qd/a)\cos\theta_2]\{\exp[(qd/a)\cos\theta_1]\sin\theta_1 + \exp[(qd/a)\cos\Theta\cos\theta_1 - (qd/a)\sin\Theta\sin\theta_1][\sin\Theta\cos\theta_1 + \cos\Theta\sin\theta_1]\}\delta + (Dqd/a)\exp[(l/2) - (r/2a) - (qd/2a)\cos\theta_2]\{\exp[(qd/2a)\cos\theta_1]\sin\theta_1 + \exp[(qd/2a)\cos\Theta\cos\theta_1 - (qd/2a)\sin\Theta\sin\theta_1](\sin\Theta\cos\theta_1 + \cos\Theta\sin\theta_1)\}\delta \quad (4)$$

In the present model, the angle θ_2 which is associated with the rotational motion of $(H_2O)_r$ is directly responsible for the removal of vibrational energy from $(H_2O)_v$, but the rotational motion of $(H_2O)_v$ which is dependent on θ_1 has no direct contribution to the energy transfer. Therefore, we approximate the problem as the interaction of the rotation-averaged oscillator with the nonvibrating rotator. The θ_1 averaged potential can then be obtained as

$$U(r,\theta_2) = A\exp[l - (r/a) - (qd/a)\cos\theta_2][1 + (qd/a)I_0\ \mathrm{csch}\ (qd/a)] - B\exp[(l/2) - (r/2a) - (qd/2a)\cos\theta_2]\times[1 + (qd/2a)I_0'\ \mathrm{csch}\ (qd/2a)] - (Dqd/a)\{\exp[l - (r/a) - (qd/a)\cos\theta_2](I_1 + I_2) - \exp[(l/2) - (r/2a) - (qd/2a)\cos\theta_2](I_1' + I_2')\}\delta \equiv U(r,\theta_2) - [\mathfrak{F}(r,\theta_2)/d]\delta \quad (5)$$

where

$$A = (Da/qd)\sinh(qd/a), \qquad B = (4Da/qd)\sinh(qd/2a)$$

$$I_0 = 1/2\int_0^{\pi}\exp[(qd/a)\cos\Theta\cos\theta_1 - (qd/a)\sin\Theta\sin\theta_1]\sin\theta_1 d\theta_1$$

$$I_1 = 1/2\int_0^{\pi}\exp[(qd/a)\cos\theta_1]\sin^2\theta_1 d\theta_1$$

$$I_2 = 1/2\int_0^{\pi}\exp[(qd/a)\cos\Theta\cos\theta_1 - (qd/a)\sin\Theta\sin\theta_1](\sin\Theta\cos\theta_1 + \cos\Theta\sin\theta_1)\sin\theta_1 d\theta_1$$

The primed integrals take the identical forms as the unprimed expressions except that in the exponent a is now replaced by $2a$. We note that I_0, I_0', I_2, and I_2' are due to $U(r_2)$. These integrals as well as I_1, and I_1' cannot be integrated in analytical forms; we shall carry out integration numerically for given values of a.

Vibrational Transition Probability

The perturbation force can be parameterized in time through the trajectories $r(t)$ and $\theta_2(t)$, which are solutions of the classical equations of motion. With the time-dependent perturbation force, we can determine the amount of vibrational energy transferred to the rotating molecule $(H_2O)_r$ from the expression[14-16]

$$\Delta E = (1/2M)\left|\int_{-\infty}^{\infty}\mathfrak{F}[r(t),\theta_2(t)]\exp(i\omega t)dt\right|^2 \quad (6)$$

where M is the effective mass associated with the vibrational motion of $(H_2O)_v$. The procedure developed in ref 10 can now be used to determine the amount of energy transfer. Without showing all steps, we shall merely write the expression for ΔE as

$$\Delta E = (1/2M)[(q\pi\omega I/d)(1+\alpha)^2 I_1\ \mathrm{csch}\ (qd/a)]^2\times[1 - (t_r E_0/\omega\mu a^2)]^2\times\{1 - [B/4(2qIA)^{1/2}\alpha_0\omega](I_1'/I_1)\times[\sinh(qd/a)/\sinh(qd/2a)]\}^2\exp(-2\omega t_r) \quad (7)$$

where t_r is the collision time for V–R energy transfer,[10] E_0 is the relative translational energy, E_r is the rotational energy, μ is the reduced mass of the colliding partners, and $I = [m_H m_O/(m_H + m_O)]d^2$; α_0 and α are defined in ref 10.

In the classical model, the probability of vibrational transition $(1 \rightarrow 0)$ per collision can be expressed as $P_{10}(E_r,E_0) = \Delta E/\hbar\omega$ and its averaged value[10] over E_r and E_0 as

$$P_{10}(T) = (\omega/2\hbar M)[(q\pi I/d)(1+\alpha)^2 I_1\ \mathrm{csch}\ (qd/a)]^2\times Q_1Q_2(4\pi/3)^{1/2}(\chi/kT)^{1/2}\times\exp\{-(3\chi/kT) + (8/\pi)(a/qd)^{1/2}\times\{\sinh(qd/2a)/[\sinh(qd/a)]^{1/2}\}^2[(D\chi)^{1/2}/kT] + (64/3\pi^2)(a/qd)[\sinh^2(qd/2a)/\sinh(qd/a)]\times(D/kT) + (\Delta/2kT)\}. \quad (8)$$

where

$$Q_1 = \{1 - [B/4(2qIA)^{1/2}\alpha_0\omega](I_1'/I_1)\times[\sinh(qd/a)/\sinh(qd/2a)]\}^2$$

$$Q_2 = [1 - (2t_r^*kT/\omega\mu a^2) + 2(t_r^*kT/\omega\mu a^2)^2]$$

$$\chi = \{(I/2q)^{1/2}[\pi(1+\alpha)a\omega kT/d]\}^{2/3}$$

and t_r^* is the collision time evaluated as the "most probable rotational energy," E_r^*, for vibrational energy transfer.[10] In eq 8, Δ is the magnitude of the change in the oscillator's energy due to the transition. In this expression, Q_1 in the preexponential part represents the effect of molecular attraction while the factor Q_2 is due to the contribution of the translational motion of the colliding partners to the deexcitation of $(H_2O)_v$.

The number of collisions required to deexcite a quantum of vibrational energy can be defined as $Z_{10} = 1/$

(14) D. Rapp, *J. Chem. Phys.*, **32**, 735 (1960).
(15) K. Takayanagi, *Progr. Theor. Phys. Suppl. (Jap.)*, **25**, 1 (1963).
(16) H. Shin, *Chem. Phys. Lett.*, **5**, 137 (1970).

$P_{10}(T)$. Numerical results will be discussed in terms of the collision number of the following section.

Results and Discussion

For the H_2O–H_2O system we shall take the following potential parameters: D = 355°K, σ = 2.73 Å, the Lennard-Jones parameters, ν(= $\omega/2\pi$) = 1595 cm^{-1}, d_{OH} = 0.956 Å, and Θ = 104° 27′. As seen in eq 8, we need the values of the range parameter a, which are evaluated from the expression

$$a = (\sigma/\pi^{1/2})[\Gamma(7/12)/\Gamma(1/12)](4D/E_r^*)^{1/12}$$

In Table I we tabulate the calculated values of a for H_2O–H_2O for the temperature range 300–2000°K; the same values will be used for D_2O–D_2O collisions. We also list the values of a for NH_3–NH_3. The values vary only slightly with temperature, but such variation can still affect the temperature dependence of $P_{10}(T)$ substantially. The integrals I_1 and I_1' appearing in eq 8 were evaluated numerically on an XDS Sigma-7 computer for each temperature.

In Figure 2, we plot the collision number Z_{10} as a function of $T^{-1/3}$ on a semilogarithmic scale for H_2O–H_2O. The collision number slowly rises with temperature to a maximum value which occurs at ~400°K. Above this temperature, the collision number decreases slowly with increasing temperature. Over the entire temperature range 300–2000°K, the plot seriously deviates from the linear behavior of log Z_{10} *vs.* $T^{-1/3}$, which is often referred to as the Landau–Teller relation. The collision numbers are quite small and vary only by a factor of 4 over the temperature range; the change in Z_{10} is particularly very small below 600°K. The experimental data obtained by impact-tube[17] and ultrasonic absorption[18] techniques are also plotted. Since the data are widely scattered, no meaningful comparison can be made. It is important to mention that the present formulation includes the effect of translational motion Q_2 on the energy transfer, *i.e.*, the translational motion is not frozen at some distance during collision.

We also plot the values of Z_{10} calculated assuming vibration-to-translation energy transfer which takes place at preferred orientations; the detailed formulation has been given in ref 12, and the result in this reference is reproduced here. The dotted curve in the figure represents this calculation. The curve sharply rises to a maximum value at ~700°K as the temperature increases; the maximum value is ~300. Thereafter, the collision number rapidly decreases with rising temperature. This variation is in strong contrast with the V–R energy transfer in which Z_{10} changes only slightly. Because available experimental

TABLE I: Calculated Values of *a*

T, °K	H_2O–H_2O D_2O–D_2O	NH_3–NH_3
300	0.202	0.199
400	0.199	0.196
500	0.196	0.194
600	0.194	0.192
800	0.192	0.189
1000	0.189	0.187
1500	0.185	0.183
2000	0.182	0.180

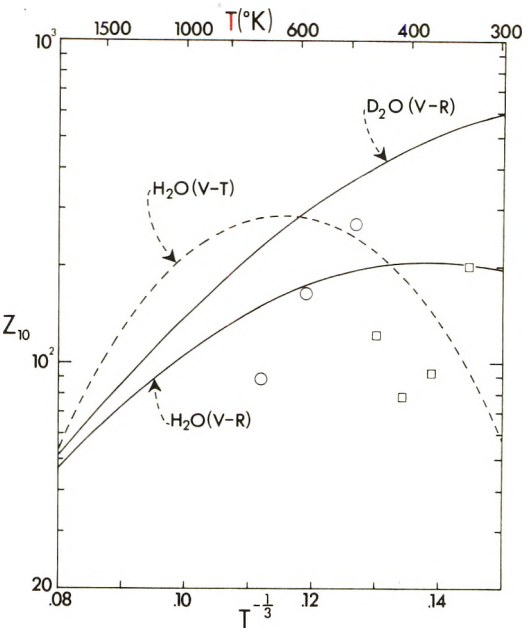

Figure 2. Plots of the collision numbers for H_2O–H_2O as a function of $T^{-1/3}$. The V–T curve is reproduced from ref 12, experimental data from (○) ref 17 and (□) ref 18.

data are widely scattered, it is difficult to conclude from the comparison which of these two mechanisms closely describes the vibrational energy transfer for H_2O–H_2O. However, since the molecule contains hydrogen atoms and rotates rapidly during the interaction to remove energy from $(H_2O)_v$, we believe that the V–R energy transfer is the dominant process operating in the system. We hope that accurate experimental data will become available so that a test of this prediction can be made.

The calculation of Z_{10} for D_2O–D_2O on the basis of V–R energy transfer is also shown in Figure 2. For this system we take ν = 1179 cm^{-1} and the same values of a given for H_2O–H_2O. The collision numbers are significantly larger than those of H_2O–H_2O at room temperature (by a factor of ~3) and rapidly decrease with rising temperature. Since D_2O rotates slower than H_2O, V–R energy transfer is not as efficient as in H_2O–H_2O. Above 1000°K, the difference between Z_{10} for D_2O–D_2O and H_2O–H_2O is not large; note that above this temperature the linear relation of log Z_{10} *vs.* $T^{-1/3}$ holds closely for D_2O–D_2O. The curve shows no sign of the appearance of a maximum value. For this system we did not carry out the V–T energy transfer calculated (at preferred orientation),[12] but we predict its temperature dependence to be similar to but stronger than that of H_2O–H_2O.

For NH_3–NH_3, we take the potential parameters as D = 320°K, σ = 2.6 Å, ν = 950 cm^{-1}, and d_{NH} = 1.014 Å. The values of the range parameter a are listed in Table I. For this system, recently the experimental data have become available[4a] for the temperature range 300–773°K, so a critical test of the present formulation of V–R energy transfer mechanism can be made. In Figure 3, we plot the collision numbers on a semilogarithmic scale as a function $T^{-1/3}$ along with the ultrasonic absorption data by Bass

(17) P. W. Huber and A. Kantrovitz, *J. Chem. Phys.*, **15**, 275 (1947).
(18) Y. Fujii, R. B. Lindsay, and K. Urushihara, *J. Acoust. Soc. Amer.*, **35**, 961 (1963).
(19) T. L. Cottrell and A. J. Matheson, *Trans. Faraday Soc.*, **59**, 824 (1963); J. D. Lambert and R. Salter, *Proc. Roy. Soc., Ser. A*, **253**, 277 (1959).

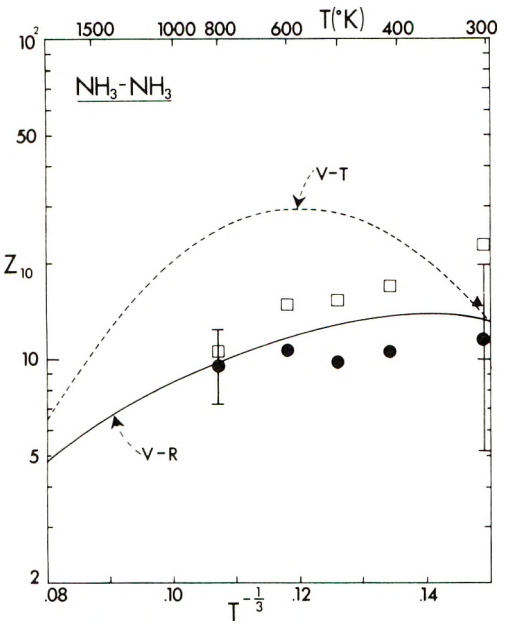

Figure 3. Plots of the collision numbers for NH_3–NH_3 as a function of $T^{-1/3}$. The V–T curve is reproduced from ref 12, experimental data from (●) hard-sphere model experimental points and (□) viscosity model experimental points by Bass and Winter (ref 4a), and from (▲) ref 19.

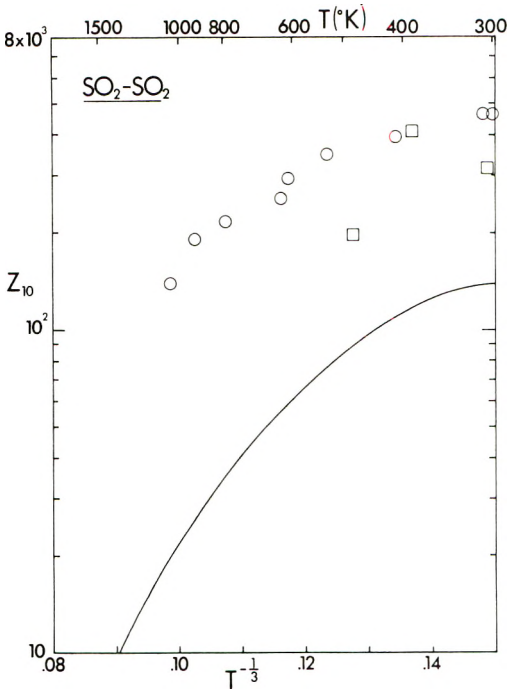

Figure 4. Plots of the collision numbers for SO_2–SO_2 as a function of $T^{-1/3}$. The V–T curve is reproduced from ref 12, experimental data from (○) ref 4b and (□) ref 20.

and Winter;[4a] the value at 303°K obtained by Cottrell and Matheson[19] is also shown. Here the agreement between the V–R calculation and experiment is excellent. For this system, the vibrational deexcitation is very efficient and the collision number is only 13 at 300°K; at 2000°K, it is as small as 5 indicating a weak temperature dependence of Z_{10}. Between 300 and 600°K, the change in the collision number is very slight, and the appearance of a maximum with slowly changing curvature at ~350°K is seen.

The V–T energy transfer probability assuming the model of preferred orientations is seriously different from the above results in both the magnitude and temperature dependence of Z_{10}. The calculation shows a strong inverse temperature dependence of Z_{10} with a sharp maximum value of about 30 at 600°K. By comparing the V–R and V–T calculation with experiment, we state that the deexcitation of vibrationally excited NH_3 molecules follows the mechanism of vibration-to-rotation energy transfer.

We now consider the SO_2–SO_2 system, for which experimental data are available[4b,20] in the temperature range 300–1000°K. In this system, all the atoms involved in collision are heavy and the V–R energy transfer is not expected to be an important process for the deexcitation of $(SO_2)_v$. Therefore, we only consider the mechanism of V–T energy transfer taking place at preferred orientations; in Figure 4, we reproduce Z_{10} calculated in ref 12 on the basis of V–T energy transfer. The figure shows that the collision numbers are smaller than experiment by a nearly constant factor of 3 in the temperature range 300–1000°K indicating the temperature dependence is in excellent agreement with experiment. We must note that the calculation shows that Z_{10} decreases by a factor of about 25 from 300 to 2000°K; above 800°K, Z_{10} rapidly decreases with rising temperature. The experimental values decrease by a factor of about 4 from 300 to 1000°K. Note that for H_2O–H_2O and NH_3–NH_3, for which we have concluded that the V–R energy transfer process is taking place, the collision numbers change by a factor of 1.5 or less over the same temperature range. The experimental Z_{10} for NH_3–NH_3 essentially remain unchanged over the temperature range 300–773°K.

We now note the importance of the terms in the potential function due to $U(r_2)$. The quantity $(qd/a)I_0$ csch (qd/a) in eq 5 is 9.71×10^{-3} at 300°K and 6.06×10^{-3} at 2000°K for H_2O–H_2O; both values are very small compared with unity. The quantity in the attractive term is also very small compared with unity. Note that these terms would appear in the exponential part of $P_{10}(T)$, but they are neglected in the above calculation. The ratio I_2/I_1 in $\mathfrak{F}(r_1\theta_2)$ takes the values of -1.31×10^{-2} and -9.63×10^{-3} at 300 and 2000°K, respectively, which are again very small compared to unity. We must note that the ratio I_2'/I_1' appearing in the attractive term is always significantly smaller than I_2/I_1. These terms contribute to the preexponential part of $P_{10}(T)$ and are neglected in numerical calculation. For NH_3–NH_3, we also find the terms due to $U(r_2)$ are similarly very small compared with unity. The integrals were evaluated numerically on an XDS Sigma-7 computer.

In the V–R energy transfer model,[10] the colliding molecules are assumed to rotate rapidly so that the effect of dipole–dipole interaction cannot be as important as in the model of V–T energy transfer taking place at preferred orientations. In the HF–HF collision system which has been previously investigated on the basis of V–R energy transfer,[11] there would be a strong hydrogen-bond interaction which can make the vibrational energy transfer efficient particularly at low temperatures. In ref 11, we treated the dipole–dipole interaction as mainly responsible for causing the rotating molecules to spend more time in those orientations for which the energy is small (*i.e.*, strong attraction). The effect of hydrogen-bond interac-

(20) J. D. Lambert and R. Salter, *Proc. Roy. Soc., Ser. A*, **243**, 78 (1957).

tion would be similar. Although we now feel that the hydrogen-bond interaction should have been considered in HF–HF collisions at low temperatures, the "effective dipole–dipole energy" obtained by including a Boltzmann distribution in averaging over all possible dipole orientation, gives energies which are comparable in magnitudes to the hydrogen-bond interaction; *e.g.*, the energy is ~3.1 kcal/mol at 400°K, ~1.8 kcal/mol at 600°K, and ~1.2 kcal/mol at 800°K.

For NH_3–NH_3 we find that the V–R energy transfer theory fits the experimental data very well and that it is not necessary to invoke dipole–dipole or hydrogen-bond interaction to explain the vibrational relaxation process. Such interactions are important in V–T energy transfer processes. Although there is no sufficient information available for H_2O–H_2O to make any meaningful comparison, we conclude that the system follows the V–R energy transfer mechanism as in NH_3–NH_3.

For the SO_2 molecule, the rotational motion is not expected to be as important as that in H_2O–H_2O or NH_3–NH_3, and the deexcitation of $(SO_2)_v$ is expected to go through the V–T energy transfer mechanism. For slowly rotating SO_2 molecules, the effect of dipole–dipole interaction can become important. The collision numbers calculated using the V–T energy transfer model with the inclusion of dipole–dipole interaction fit the experimental data with a nearly constant factor of 3 in the temperature range 300–1000°K.

Throughout this work on the V–R energy transfer we find that the second and third terms in the exponent of $P_{10}(T)$, which are due to the presence of attractive forces between the colliding molecules, make important contribution to the overall value of vibrational transition probabilities. For H_2O–H_2O, for example, at 300°K, the first three terms in the exponent take the values −14.4, 2.03, and 0.285; *i.e.*, the contribution of molecular attraction increases $P_{10}(T)$ by a factor of 10. At 1000°K, the three values are −9.12, 0.857, and 0.080, respectively, showing that the effect of molecular attraction is to increase the probability by a factor of 2.6. Since these two terms which originate from the molecular attraction are not large, we would expect an approximate linear behavior of log Z_{10} *vs.* $T^{-1/3}$ at higher temperatures, but the slope would be not as steep as in the V–T calculation since the leading term $3\chi/kT$ is significantly small for the V–R energy transfer mechanism. However, another important factor appearing in the exponent is $\Delta/2kT$, which takes the values of 3.82, 2.29, and 1.14, for example, for H_2O–H_2O at 300, 500, and 1000°K, respectively. Therefore, even if we completely neglected the effect of molecular attraction, there is an important factor in the exponent which is proportional to T^{-1}, so that such a linear behavior is not expected to hold unless the temperature is sufficiently high. Because of varying degrees of temperature dependence of the four terms in the exponent and because the leading term is negative while all others are positive, we find a very slow change in the overall magnitudes of the exponent in the V–R energy transfer mechanism. For example, for H_2O–H_2O, the sum of the four terms takes the values of −8.31, −8.02, −7.04, −6.36, and −5.87 at 300, 500, 1000, 1500, and 2000°K, respectively, the change being reflected in the slow variation of log Z_{10} shown in Figure 2. The appearance of a maximum value of Z_{10} in the plots for H_2O–H_2O and NH_3–NH_3 is due to the compensation of the negative leading term and the remaining three positive terms in the exponent and to an additional contribution from the preexponential part, which decreases slowly with rising temperature.

Conclusion

Vibrational deexcitation in NH_3–NH_3 and H_2O–H_2O is very fast, particularly in the former system, in the temperature range 300–2000°K which is attributed to energy transfer to the rotational motion of the collision partner under the influence of rotational and translational interaction at close range. Recent ultrasonic absorption measurements support this conclusion for NH_3–NH_3 in 300–773°K. A slowly varying inverse temperature dependence is found in 300–400°K for both collisions. D_2O–D_2O collisions are not as efficient as H_2O–H_2O in transferring vibrational energy to rotation particularly at temperatures below 600°K. In all collision systems, the effect of molecular attraction is found to be important. For H_2O, D_2O, and NH_3 it is shown that the participation of translational motion is not important.

Vibrational deexcitation in SO_2–SO_2 can be explained in terms of the mechanism of vibration-to-translation energy transfer which takes place at preferred dipole–dipole orientations.

Theoretical Gel Chromatographic Behavior of Irreversibly Isomerizing Systems Subject to Kinetic Control

S. M. A. Meggitt, L. W. Nichol,*[1] and D. J. Winzor

The Department of Applied Mathematics, School of General Studies, and The Department of Physical Biochemistry, John Curtin School of Medical Research, Australian National University, Canberra, A.C.T., 2601, Australia, and The Department of Biochemistry, University of Queensland, St. Lucia, Queensland, 4067, Australia *(Received July 10, 1972)*

Analytical expressions are obtained describing the migration behavior of a solute introduced by frontal gel chromatography into a new solvent where it undergoes a kinetically controlled and irreversible isomerization. The expressions are derived for migration in a one-phase system and adapted to the chromatographic situation involving two phases. Numerical examples are presented of plots of concentration *vs.* distance (for free migration) and of concentration *vs.* time (elution profiles) for the possibilities where the reactant is characterized by a velocity greater or less than that of the product. Features of the patterns are discussed in relation to their use in the detection of kinetic conversion and its characterization in terms of the rate constant.

Introduction

In a previous study,[2a] a differential technique of frontal gel chromatography was described in which a solution of a macromolecule was applied to a gel column preequilibrated with a different solvent system. This design permitted the comparison of the constituent velocities[2b] of the macromolecule ahead of and behind the migrating solvent front. With a suitable selection of gel type, these velocities will differ if the isomeric or polymeric state of the macromolecule is different in the two solvent environments. In the systems studied,[2a] the conformational change of bovine serum albumin and the change in the extent of association of β-lactoglobulin A were rapid, which facilitated the interpretation of the elution profiles in terms of the Johnston–Ogston equation[3] and two time-independent constituent velocities.

Several workers[4-7] have drawn attention to the complicated reaction boundaries which may arise in the mass migration of systems subject to kinetic control,[8] where constituent velocities are no longer time independent.[2b] Whereas these workers considered systems initially at equilibrium and in a fixed environment, the present theoretical treatment is concerned with the kinetic conversion between states of a solute inherent on its introduction into a new environment in a chromatographic experiment of differential design. An irreversible transition between two states of the solute is explored and it is suggested that the analytical solutions describing the forms of elution profiles may find application in the kinetic study of such phenomena as protein renaturation[9,10] and denaturation[11] when these interactions approximate to the selected two-state model.

Theory

The experiment is commenced by layering a large volume of solute A in one solvent (α region) over a large volume of a different solvent (β region). At time t the $\alpha\beta$ boundary will have migrated to a position $X = v_S t$, where v_S is the constant velocity of the solvent front. In the α region solute A is stable and moves with velocity v_A. Provided $v_A > v_S$, some A migrates across the $\alpha\beta$ boundary into the β region, where it undergoes a time-dependent conversion to the species B, governed by the rate constant k, *i.e.*

$$A \xrightarrow{k} B$$

Species A and B move independently in the β region with velocities v_A and v_B, respectively, the latter also being considered to be greater than v_S. The situation visualized, in fact, pertains to migration in a single-phase system; later, the theory will be adapted to meet the specific requirements of chromatography involving both mobile and stationary phases.

Migration in a Single-Phase System. Since the plateau of A alone at its original concentration ($\bar{c}^{\alpha}$) extends to the position $X = v_S t$, it is convenient to employ a frame of reference moving with the velocity of the $\alpha\beta$ boundary, v_S. Velocities of A and B relative to this frame of reference are denoted by v_A' and v_B', respectively, with distances denoted by x; clearly, $x = X - v_S t$. The boundary conditions become

$$c_A^{\beta} = \bar{c}^{\alpha} \quad x = 0,\ t > 0$$
$$= 0 \quad t = 0,\ x > 0$$

$$\bar{c}^{\beta} = c_A^{\beta} + c_B^{\beta} = \bar{c}^{\alpha} \quad x = 0,\ t > 0$$
$$= 0 \quad t = 0,\ x > 0$$

(1) Address correspondence to Department of Physical Biochemistry, The John Curtin School of Medical Research, Australian National University, Canberra City, A.C.T. 2601, Australia.
(2) (a) P. A. Baghurst, L. W. Nichol, R. J. Richards, and D. J. Winzor, *Nature (London)*, **234**, 299 (1971); (b) L. W. Nichol and A. G. Ogston, *Proc. Soc. Ser. B.*, **163**, 343 (1965).
(3) L. W. Nichol and A. G. Ogston, *J. Phys. Chem.*, **69**, 1754 (1965).
(4) J. R. Cann and H. R. Bailey, *Arch. Biochem. Biophys.*, **93**, 576 (1961).
(5) P. C. Scholten, *Arch. Biochem. Biophys.*, **93**, 568 (1961).
(6) K. E. Van Holde, *J. Chem. Phys.*, **37**, 1922 (1962).
(7) G. G. Belford and R. L. Belford, *J. Chem. Phys.*, **37**, 1926 (1962).
(8) L. G. Longsworth and D. A. MacInnes, *J. Gen. Physiol.*, **25**, 507 (1942).
(9) W. F. Harrington and P. H. Von Hippel, *Arch. Biochem. Biophys.*, **92**, 100 (1961).
(10) P. H. Von Hippel and K-Y. Wong, *Biochemistry*, **1**, 664 (1962).
(11) H. A. McKenzie and G. B. Ralston, *Experientia*, **27**, 617 (1971).

The statement of mass conservation during migration (for $x > 0$, $t > 0$) is given by

$$v_A'(\partial c_A^\beta/\partial x)_t + (\partial c_A^\beta/\partial t)_x = -kc_A^\beta. \quad (1a)$$

$$v_B'(\partial c_B^\beta/\partial x)_t + (\partial c_B^\beta/\partial t)_x = kc_A^\beta \quad (1b)$$

which neglects diffusional effects.[2b,12,13] Since A and B move independently, we first consider the distribution of A, which is obtained by solution of eq 1a using the corresponding Lagrange system of ordinary differential equations or Laplace transforms.[14]

$$c_A^\beta(x, t) = c_A^\beta(x - v_A't, 0) \exp(-kt) = 0; \; x > v_A't \quad (2)$$

$$c_A^\beta(x, t) = c_A^\beta(0, t - x/v_A') \exp(-kx/v_A') = \bar{c}^\alpha \exp(-kx/v_A'); \; x < v_A't \quad (3)$$

Equation 2 describes the solvent plateau or a region containing B alone ahead of the sharp boundary of A arising at v_At, while eq 3 expresses the exponential decay of A as a function of the distance travelled by A in the β region. In gas chromatographic studies of surface-catalyzed reactions,[14,15] incorporation of the catalytic microreactor into a conventional analytical column permits analysis of the emergent pulse in terms of reactant concentration, whereupon eq 3 allows evaluation of k. The success of this design of experiment relies on ability to freeze the reaction at a specified time by removal of the reaction mixture from the catalyst.

In contrast, the reactions presently being considered progress with time both on and off the column and thus it is necessary to obtain the distribution of total solute concentration in the β region, $\bar{c}^\beta$, which may be the only concentration available to the experimenter. Addition of eq 1a and 1b, and subsequent rearrangement, gives

$$v_B'(\partial \bar{c}^\beta/\partial x)_t + (\partial \bar{c}^\beta/\partial t)_x = (v_B' - v_A')(\partial c_A^\beta/\partial x)_t \quad (4)$$

The corresponding Lagrange system of ordinary differential equations may readily be written and integrated to yield

$$\bar{c}^\beta(x, t) - [(v_B' - v_A')/v_B']c_A^\beta(x, t) = \Phi(x - v_B't) \quad (5)$$

The function Φ is determined by use of the appropriate boundary conditions. Consider first the case $v_A' > v_B'$. For $x > v_A't$ and $x < v_B't$, the values of Φ are determined by setting $t = 0$ and $x = 0$, respectively, in eq 5. In the remaining region, $v_B't < x < v_A't$, the value of $c_A^\beta(x,t)$ is given by eq 3, the relevant values of x and t being $(x - v_B't)v_A'/(v_A' - v_B')$ and $(x - v_B't)/(v_A' - v_B')$, respectively; the latter denote intersections of the line $x = v_A't$ with lines parallel to $x = v_B't$, along which Φ has a constant value. The solutions of eq 5 become

$$\bar{c}^\beta(x,t) = 0; \; x > v_A't \quad (6a)$$

$$= (v_A'/v_B')\bar{c}^\alpha \exp[-k(x - v_B't)/(v_A' - v_B')] - [(v_A' - v_B')/v_B']\bar{c}^\alpha \exp(-kx/v_A'); \; v_B't < x < v_A't \quad (6b)$$

$$= (v_A'/v_B')\bar{c}^\alpha - [(v_A' - v_B')/v_B']\bar{c}^\alpha \exp(-kx/v_A'); \; x < v_B't \quad (6c)$$

Equations 6b and 6c describe surfaces in the space defined by the cartesian coordinates $(\bar{c}^\beta, x, t)$ and it may readily be shown that these surfaces intersect along the line $x = v_B't$. Thus, at constant time in the $(\bar{c}^\beta, x)$ plane, the curve exhibits a discontinuity of slope at $x = v_B't$. Also, in this plane the area under the curve is given by the sum of the integrals of eq 6b and 6c, which equals $\bar{c}^\alpha v_A't$, the total amount of original solute to have crossed the $\alpha\beta$ boundary in time t.

In the alternative situation, $v_B' > v_A'$, the solutions analogous to eq 6 are

$$\bar{c}^\beta(x,t) = 0; \; x > v_B't \quad (7a)$$

$$= (v_A'/v_B')\bar{c}^\alpha \{1 - \exp[-k(x - v_B't)/(v_A' - v_B')]\}; \; v_A't < x < v_B't \quad (7b)$$

$$= (v_A'/v_B')\bar{c}^\alpha - [(v_A' - v_B')/v_B']\bar{c}^\alpha \exp(-kx/v_A'); \; x < v_A't \quad (7c)$$

Migration in a Two-Phase System. In accordance with the preceding section, we again assign the reaction a single rate constant k, which implies identity of reaction rates in the mobile and stationary phases. Equations 6 and 7 describe concentration–distance distributions at a given time, whereas construction of an elution profile requires knowledge of the concentration–time profile at the exit plane located at a fixed distance X_F from the entry plane. The rewriting of eq 6 and 7 in appropriate form requires not only a conversion to a fixed frame of reference ($X = x + v_St$, $v_A = v_A' + v_S$, and $v_B = v_B' + v_S$), but also consideration of the partitioning of solute between the mobile and stationary phases on the column.[16] Thus, the total solute concentrations designated $\bar{c}^\alpha$ or $\bar{c}^\beta$ in the previous discussion must now be summed over both phases and are termed $\hat{c}^\alpha$ or $\hat{c}^\beta$. In the same connection, the velocities of the individual species and that of the $\alpha\beta$ boundary must be represented by $\bar{v}_A$, $\bar{v}_B$, and $\bar{v}_S$ to denote that they too are weighted averages over both phases. The procedure for converting eq 6 and 7 to forms describing elution profiles need only be illustrated for one relation and we choose eq 6c and 7c since it pertains to cases where A is either the slower or faster moving species and to regions where A and B coexist. It becomes

$$\hat{c}^\beta(X_F, t) = [(\bar{v}_A - \bar{v}_S)/(\bar{v}_B - \bar{v}_S)]\hat{c}^\alpha - [(\bar{v}_A - \bar{v}_B)/(\bar{v}_B - \bar{v}_S)]\bar{c}^\alpha \exp[-k(X_F - \bar{v}_St)/(\bar{v}_A - \bar{v}_S)] \quad (8)$$

and pertains to the region $X_F/\bar{v}_S > t > X_F/\bar{v}_B$ if $\bar{v}_A > \bar{v}_B$ or to the region $X_F/\bar{v}_S > t > X_F/\bar{v}_A$ if $\bar{v}_B > \bar{v}_A$. As noted earlier,[16] concentrations of solutes in the effluent from a column are identical with those in the mobile solution reaching the exit plane at that time, the relevant expression of mass conservation in the β region being

$$\dot{V}\bar{c}_e^\beta = \bar{v}\bar{c}^\beta(X_F, t) = \bar{v}_Ac_A^\beta(X_F, t) + \bar{v}_B\bar{c}_B^\beta(X_F, t) \quad (9)$$

where $\dot{V}$ is the volume rate of flow of the column and $\bar{c}_e^\beta$ is the total concentration of A and B in the β region in the eluate. Use of eq 9 requires specification of $\bar{c}_A^\beta(X_F,t)$ and

(12) G. A. Gilbert, *Proc. Roy. Soc., Ser. A*, **250**, 377 (1959).
(13) G. A. Gilbert and R. C. Ll. Jenkins, *Proc. Roy. Soc., Ser. A*, **253**, 420 (1959).
(14) S. H. Langer, J. Y. Yurchak, and J. E. Patton, *Ind. Eng. Chem.*, **61(4)**, 10 (1969).
(15) D. W. Bassett and H. W. Habgood, *J. Phys. Chem.*, **64**, 769 (1960).
(16) L. W. Nichol, A. G. Ogston, and D. J. Winzor, *J. Phys. Chem.*, **71**, 726 (1967).

$\bar{c}_B^{\beta}(X_F,t)$; the former is obtained directly from eq 3 and the latter by subtracting $\bar{c}_A^{\beta}(X_F,t)$ from $\hat{c}^{\beta}(X_F,t)$ given in eq 8. In these terms eq 9 becomes

$$\dot{V}\bar{c}_e^{\beta} = [\bar{v}_B(\bar{v}_A - \bar{v}_S)c^{\alpha}/(\bar{v}_B - \bar{v}_S)] - [\bar{v}_S(\bar{v}_A - \bar{v}_B)\hat{c}^{\alpha}/(\bar{v}_B - \bar{v}_S)] \exp[-k(X_F - \bar{v}_S t)/(\bar{v}_A - \bar{v}_S)] \quad (10)$$

Two more operations are required. The first involves the substitution in eq 10 of $\hat{c}^{\alpha} = V\bar{c}^{\alpha}/\bar{v}_A$ which expresses conservation of mass in the α region *cf.* eq 9). The second involves a change of variable from velocity to elution volume, effected by noting that $\bar{v}_A = X_F/t_A$ where $t_A = V_A/\dot{V}$, similar expressions defining the elution volumes V_B and V_S. Equation 10 written in these terms is

$$\bar{c}_e^{\beta} = [(V_S - V_A)/(V_S - V_B)]\bar{c}^{\alpha} - [(V_B - V_A)/(V_S - V_B)]\bar{c}^{\alpha} \exp[-kV_A(V_S - V)/\dot{V}(V_S - V_A)] \quad (11)$$

where the variable $V = \dot{V}t$.

Since eq 6b and 7b may be transformed in a similar manner, the general features of elution profiles may now be summarized. For $V_A < V_B$ ($v_A > v_B$), the solvent used to preequilibrate emerges initially at elution volumes less than V_A, at which value A begins to emerge. Thereafter between V_A and V_B both species coexist, the total concentration being given essentially by eq 6b, which in its transformed chromatographic form is

$$\bar{c}_e^{\beta} = [(V_S - V_A)/(V_S - V_B)]\bar{c}^{\alpha} \times \exp[-kV_A(V_B - V)/\dot{V}(V_B - V_A)] - [(V_B - V_A)/(V_S - V_B)]\bar{c}^{\alpha} \exp[-kV_A(V_S - V)/\dot{V}(V_S - V_A)] \quad (12)$$

At $V = V_B$ eq 12 reverts to eq 11, the latter describing the total emerging concentration until the solvent front ($\alpha\beta$ boundary) is eluted from the column at V_S; indeed at V_S eq 11 simplifies to $\bar{c}_e^{\beta} = \bar{c}^{\alpha}$, this being the onset of the emergence of a plateau of the originally applied solution.

For $V_B < V_A$ ($\bar{v}_B > \bar{v}_A$), the solvent plateau elutes first until B begins to emerge at V_B. Between V_B and V_A only B exists, the concentration being given by the transformed eq 7b

$$\bar{c}_e^{\beta} = [(V_S - V_A)/(V_S - V_B)]\bar{c}^{\alpha} \times \{1 - \exp[-kV_A(V_B - V)/\dot{V}(V_B - V_A)]\} \quad (13)$$

At $V = V_A$, A begins to emerge and thus at this elution volume the total concentration is a step function to be illustrated later, the lower limit being given by eq 13 and the upper by eq 11. Equation 11 continues to describe the profile until the emergence of the original solution with the solvent front at V_S.

Numerical Illustrations and Discussion

In the use of eq 6 and 7 to compute concentration distributions at fixed times for migration in a one-phase system, it is helpful to introduce certain reduced variables in order to give greater generality to numerical illustrations. Thus, the ordinate will be expressed relative to the applied concentration ($\bar{c}^{\beta}/\bar{c}^{\alpha}$), while the abscissa (distance) will be in terms of the solvent velocity v_S and the rate constant; time is also expressed relative to k. Illustrations will first be presented for cases where species A travels faster than species B.

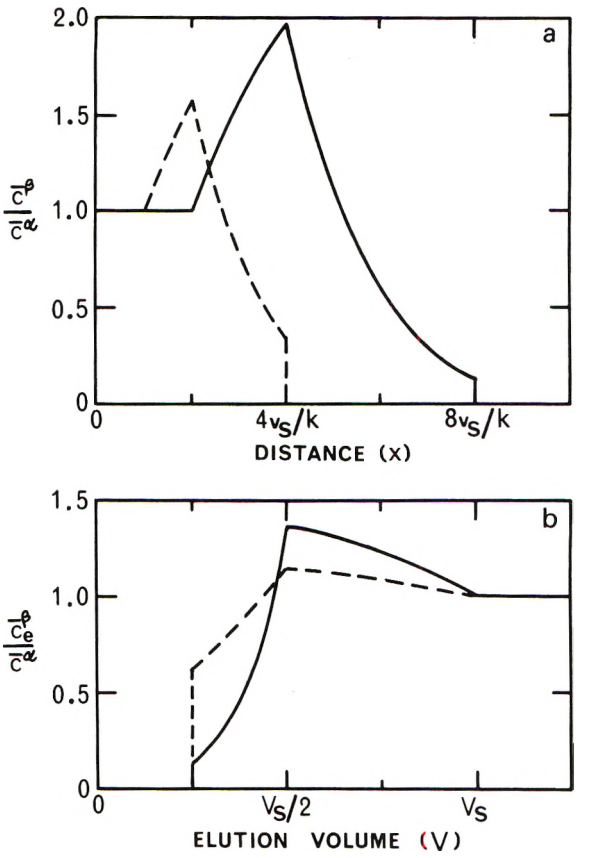

Figure 1. Computed concentration distributions for a system where reactant A travels faster than product B, both moving ahead of the solvent front S: (a) migration in a one-phase system with velocities $v_A = 2v_B = 4v_S$; broken line $t = 1/k$, solid line $t = 2/k$, time t being expressed in terms of rate constant k: (b) the corresponding elution profiles from two-phase chromatography, $V_S = 2V_B = 4V_A$; broken line $\dot{V}$ (flow rate) $= kV_S/2$, solid line (slower flow rate) $V = kV_S/8$.

Figure 1a presents concentration distributions at two fixed times, $t = 1/k$ and $2/k$, for a system in which the relative magnitudes of the velocities were arbitrarily selected as $v_A = 2v_B = 4v_S$. The interesting features in Figure 1a are that there is a maximal value of the ordinate (at the point of intersection $v_B t$) and that it increases with increasing time. Figure 1b refers to the corresponding situation ($V_S = 2V_B = 4V_A$) in chromatography calculated on the basis of eq 11 and 12. In this instance, the two patterns refer to different flow rates, $\dot{V}$, expressed in terms of V_S and k. These elution profiles are qualitatively similar to the concentration distributions shown in Figure 1a since a point of discontinuity occurs at V_A and the slope is discontinuous at V_S and V_B. Again, there is no evidence of a plateau in the β region, a maximum value of the ordinate, though less pronounced, being observed at V_B. The lack of a plateau in the β region may prove to be valuable in distinguishing kinetically controlled systems from those in which conversion is rapid ($k \rightarrow \infty$); for in the differential chromatography of the latter systems (equilibrium or irreversible) a plateau in the β region would be observed in accordance with the Johnston–Ogston equation.[2a,3] The advantage (in making such a distinction) of performing experiments at different flow rates is evident.

Figures 2a and 2b refer to situations in free migration and chromatography, respectively, where species B travels faster than species A ($v_B > v_A$ or $V_B < V_A$). Since both Figures 2a and 2b exhibit qualitatively similar features,

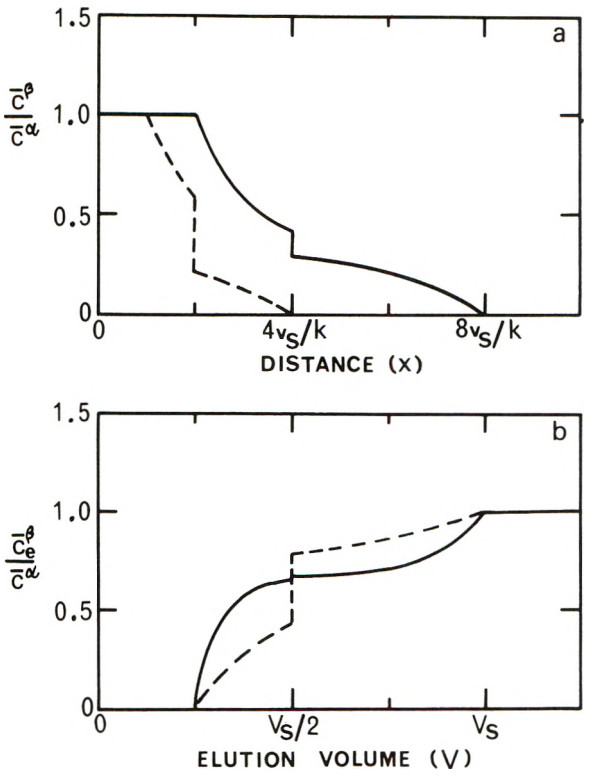

Figure 2. Computed concentration distributions for a system where reactant A travels slower than product B, but faster than the solvent front: (a) migration in a one-phase system with $v_B = 2v_A = 4v_S$; broken line $t = 1/k$, solid line $t = 2/k$: (b) the corresponding elution profiles from column chromatography, with $V_S = 2V_A = 4V_B$; broken line $V = kV_S/2$, solid line $V = kV_S/8$.

attention is directed to the chromatographic situation, Figure 2b, calculated on the basis of eq 11 and 13 with $V_S = 2V_A = 4V_B$ and flow rates as for Figure 1b. In contrast to the behavior observed in Figure 1b, the total concentration in the β region never exceeds the original concentration $\bar{c}^\alpha$. Again, the lack of a plateau in the β region may prove to be a valuable diagnostic test for kinetic conversion. However, it may be seen from Figure 2b that as the flow rate is decreased the step discontinuity at V_B becomes progressively smaller until the pattern gives the appearance of two plateaux separated by a concentration gradient near V_S, behavior also found in the study of a rapidly reacting system.[2a] Therefore, it would be advantageous to study the system at different flow rates, but in contrast to the earlier situation (Figure 1b) the difference between kinetic control and rapid conversion is accentuated at fast flow rates. In this case (broken line of Figure 2b), a derivative plot of $dc_e\beta/dV$ *vs.* V would exhibit trimodality with a sharp central region. Complicated reaction boundaries of this type have been discussed in relation to reversible kinetically controlled isomerizations examined in migration experiments of different design.[4-6]

It is noted that the main value of earlier theoretical studies[4-7] on the behavior of kinetically controlled systems in mass migration was also the recognition of such systems. Thus, quantitative measurement of thermodynamic and/or kinetic parameters describing the systems may well be more easily performed by means other than mass migration. For example, the rate constant governing the irreversible isomerization presently under discussion might be readily obtained by rapidly changing (say) the pH or ionic strength of the solution studied *in situ* and following the time dependence of a spectral or optical rotatory property. On the other hand, if the study is to involve a solvent in which the solid solute cannot rapidly be dissolved, the chromatographic method of differential design which effects a complete transfer of environment in the solution phase, may offer a unique method of elucidating the kinetics. For this purpose an analytical expression must be found involving k and experimentally determinable parameters. The values of V_A, V_B, and V_S may be found in separate experiments while $\dot{V}$ is readily measurable. For the case $V_A < V_B$, the simplest analytical expression involving these parameters and k is eq 11, the use of which would involve measurement from the elution profile of $\bar{c}_e{}^\beta/\bar{c}^\alpha$ at V_B. However, the value of $\bar{c}_e{}^\beta/\bar{c}^\alpha$ at V_B will be affected by diffusional spreading, of which eq 11 takes no account. An experimental measurement less affected by diffusion would appear to be the area under the pattern from the solvent plateau to V_B, which corresponds to the amount of solute in the eluate at that stage. If this experimentally determined area is termed Q, integration of eq 12 between the limits V_A and V_B leads to

$$Q = [\dot{V}(V_B - V_A)(V_S - V_A)\bar{c}^\alpha/kV_A(V_S - V_B)]\{1 - \exp[-kV_A(V_S - V_B)/\dot{V}(V_S - V_A)]\} \quad (14)$$

which may readily be solved for k. Two points require comment in relation to the choice of the limits of integration. First, the experimental measurement of Q should include the small amount of A which has diffused ahead of V_A to be consistent with the choice of V_A as the lower limit in the intergration of eq 12, as is apparent from Figure 1b. Second, it is recalled that integration from V_A to V_S leads to $c^\alpha(V_S - V_A)$, the condition for conservation of mass, and thus provides no information on k.

In the event that $V_B < V_A$, the value of Q obtained by integration of eq 13 between the limits V_B and V_A is

$$Q = [(V_S - V_A)(V_A - V_B)/(V_S - V_B)]c^\alpha[1 + (\dot{V}/kV_A)\exp(-kV_A/\dot{V}) - (\dot{V}/kV_A)] \quad (15)$$

The experimental measurement of Q in this case is subject to overestimation because of diffusional spreading if there is a pronounced step at V_A; in this regard, adjustment of the flow rate would be desirable to obtain a pattern such as shown by the solid line in Figure 2b.

In summary, it is hoped that the analytical expressions presented may prove useful in the detection from elution profiles of irreversibly isomerizing systems and be of use in the elucidation of kinetic parameters when more direct methods of study are precluded.

Surface Thermodynamics of Polymer Solutions

K. S. Siow and D. Patterson*

Chemistry Department, McGill University, Montreal, Canada *(Received May 16, 1972)*

Extending recent work by Gaines, the Prigogine–Maréchal theory has been used to predict the surface tension (γ), interfacial tension (γ) against a liquid or solid, and the adsorption of polymer solutions. Two cases are contrasted, corresponding to the pure polymer (2) having a larger or a smaller surface or interfacial tension than the pure solvent (1). When $\gamma_2 > \gamma_1$, corresponding to preferential solvent adsorption, there is little qualitative difference between the surface thermodynamics of a polymer solution and a mixture of spherical molecules. However, when $\gamma_2 < \gamma_1$, corresponding to preferential polymer adsorption, the surface or interfacial tension of the solution falls steeply at very low polymer concentration to almost the value for the pure polymer. Similarly, the polymer is strongly adsorbed at low concentration, the adsorption isotherm being very similar to that given by the Silberberg theory. The following experimental examples have been studied: the surface tension of dimethylsiloxane oligomers and the polymer in tetralin ($\gamma_2 < \gamma_1$) and interfacial tensions against water of the dimethylsiloxanes in cyclohexane ($\gamma_2 < \gamma_1$) and in benzene ($\gamma_2 > \gamma_1$), polyisobutylene in benzene ($\gamma_2 > \gamma_1$), and polystyrene in cyclohexane ($\gamma_2 < \gamma_1$). Except for the last system, the Prigogine–Maréchal theory gives good predictions with reasonable values of the adjustable χ parameter.

Some 20 years ago Prigogine and collaborators[1] presented a remarkably simple theory of the surface tension of polymer solutions. It is only recently, however, that extensive surface tension measurements have been made by Gaines,[2] who found the theory to be very successful in interpreting his results. In particular, it predicts a striking difference in the concentration dependence of the solution surface tension depending on whether the pure liquid polymer has a higher or a lower surface tension than the pure solvent. Thus, polyisobutylene (PIB) + *n*-heptane shows[2b] a slight lowering of the solution surface tension below a simple volume fraction average of the γ values of the pure components. Here the polymer has the higher surface tension, and the behavior of the solution surface tension is similar to that encountered for a mixture of equal-sized molecules. However, for a polymer of low surface tension, polydimethylsiloxane (PDMS), in a solvent of higher surface tension, toluene or tetrachloroethylene, there is a drastic drop of the surface tension of the solution[2a] even at very low polymer concentration. This corresponds to the known surfactant property of this polymer. Increasing the polymer concentration brings about a slow approach of γ to the value for the pure polymeric liquid. The drastic lowering of γ is related to the polymeric character of the solute, and does not occur with low molecular weight dimethylsiloxane oligomers.[2a] It is the surface tension counterpart of the following feature of the adsorption behavior of polymers. The adsorption of a polymer on a solid is associated with the polymeric liquid having a lower interfacial tension, γ_2, than the solvent, γ_1. Typically there is a large adsorption of the polymer on the solid at very low concentration, followed by little change with concentration.

Although the Prigogine theory refers specifically to the surface tension of polymer solutions, it should be equally applicable to the interfacial tension between a polymer solution and an immiscible liquid or a solid. It can also be used to predict the adsorption isotherm for polymer at any interface. The theory of polymer adsorption is an important, but still controversial subject. Earlier theories[3] focus attention on the configuration of the adsorbed macromolecule and conclude that only a small fraction of the segments are in actual contact with the surface. The Prigogine model[1] assumed the surface phase to correspond to a two-dimensional polymer solution with all polymer segments in contact with the surface. This would seem unrealistic in the light of the adsorption theories. However, more recent work by Silberberg[4] and by Hoeve[5] indicates that a large fraction, ~0.7, of the segments contact the surface. The adsorption isotherm implicit in the Prigogine theory has been examined by Ash, Everett, and Findenegg.[6] In the present work we lay emphasis on the isotherm in the high polymer range, and find that the theoretical predictions agree qualitatively, and almost quantitatively with those made by the more realistic, but much more complicated, Silberberg theory. The predictions of the Hoeve and Silberberg theories are qualitatively similar.[5] We confine our comparison to the Silberberg work where the effects of the various parameters are presented in detail.

Returning to surface tensions of polymer solutions we have extended the work of Gaines by studying another set of systems: short-chain dimethylsiloxane oligomers and PDMS (γ_2 = 20.0 dyn/cm at 30°) in tetralin (γ_1 = 34.8

(1) (a) I. Prigogine and J. Maréchal, *J. Colloid Sci.*, **7**, 122 (1952); (b) R. Defay, I. Prigogine, A. Bellemans, and D. H. Everett, "Surface Tension and Adsorption," Wiley, New York, N.Y., 1966, Chapter 13.
(2) (a) G. L. Gaines, Jr., *J. Phys. Chem.*, **73**, 3143 (1969); (b) *J. Polym. Sci., Part A-2*, **7**, 1379 (1969).
(3) (a) H. L. Frisch and R. Simha, *J. Chem. Phys.*, **24**, 652 (1956); (b) *ibid.*, **27**, 702 (1957).
(4) (a) A. Silberberg, *J. Phys. Chem.*, **66**, 1872 (1962); (b) *ibid.*, **66**, 1884 (1962); (c) *J. Chem. Phys.*, **46**, 1105 (1967); (d) *ibid.*, **48**, 2835 (1968); (e) Z. Priel and A. Silberberg, *Polym. Prepr., Amer. Chem. Soc., Div. Polym. Chem.*, **11**, 1405 (1970).
(5) (a) C. A. J. Hoeve, *J. Polym. Sci., Part C*, **30**, 361 (1970); (b) *ibid.*, **34**, 1 (1971).
(6) (a) S. G. Ash, D. H. Everett, and G. H. Findenegg, *Trans. Faraday Soc.*, **64**, 2639 (1968); (b) D. H. Everett, *ibid.*, **61**, 2478 (1965).

dyn/cm at 30°). This set of systems was chosen so that the solvent might have as large a surface tension as possible compared with that of the polymer. It is, however, difficult to find systems where $\gamma_1 > \gamma_2$. Polymeric liquids are usually denser, *i.e.*, have higher cohesive energy, than the typical organic "monomeric" solvents. Because of this, the surface tension of a polymeric liquid is usually higher than that of the solvent. However, *ipso facto*, the interfacial tension between polymer liquids and a solid or a highly cohesive liquid should be lower than the corresponding interfacial tension between an organic solvent and the solid or liquid. Although many studies of adsorption on solids have been made,[7] there is very little work on interfacial tensions between polymer solutions and other liquids. We have therefore investigated the interfacial tensions between several polymer solutions and water, and find the Prigogine-Maréchal theory to be successful in treating the results. We suggest that this theory constitutes a reasonable, approximate treatment of the surface tension and adsorption of polymer solutions, and that it merits more attention than it has received in the past.

The Prigogine-Maréchal Theory

We recall that the theory[1] assumes a quasicrystalline lattice in which sites may be occupied by a solvent molecule, or an r-mer segment. In the following, the equations are written to allow for solvent molecules which are chains occupying r_1 sites. Prigogine and collaborators considered[1b] the effect in the calculations of various assumptions concerning the nature of the surface phase. They concluded that realistic predictions could still be obtained neglecting any explicit effect of the surface in restricting the configurations of the macromolecules. This simplification is brought about by assuming the following model. The polymer molecules lie flat in the surface phase, the thickness of which corresponds to one lattice site. The surface and bulk phases are then described by the Flory-Huggins polymer solution thermodynamics. Equating the chemical potentials of the components in the phases, the following two equations are obtained for the solution or interfacial tension

$$(\gamma - \gamma_1)a/kT = \ln(\phi_1^s/\phi_1) + [(r-1)/r](\phi_2^s - \phi_2) + \chi[l(\phi_2^s)^2 - (l+m)\phi_2^2] \quad (1)$$

$$(\gamma - \gamma_2)a/kT = \ln(\phi_2^s/\phi_2)^{1/r} + [(r-1)/r](\phi_2^s - \phi_2) + \chi[l(\phi_1^s)^2 - (l+m)\phi_1^2] \quad (2)$$

By subtraction, eq 1 and 2 yield an equation for the composition of the surface phase, ϕ_2^s, *i.e.*, the adsorption isotherm

$$\ln(\phi_2^s/\phi_2)^{1/r}/(\phi_1^s/\phi_1) = [(\gamma_1 - \gamma_2)a/kT] + \chi(l+m)(\phi_1 - \phi_2) - \chi l(\phi_1^s - \phi_2^s) \quad (3)$$

Equations 1-3 correspond to eq 10-12 of ref 1a and to eq 13.24 in ref 1b. In the former paper, however, the solutions are athermal, *i.e.*, $\chi = 0$.

In the equations, the volume fractions in the bulk and surface phases are respectively ϕ and ϕ^s. The surface concentrations in terms of moles per unit area are

$$\Gamma_1 = \phi_1^s/aN_0; \Gamma_2 = \phi_2^s/raN_0 \quad (4a)$$

and the surface excess is

$$\Gamma_2^{(1)} = (\phi_2^s - \phi_2)/\phi_1 raN_0 \quad (4b)$$

The parameter r of the Flory-Huggins theory is the ratio of the molar volumes of the components, *i.e.*, $r_2/r_1 = V_2/V_1$. N_0 is Avogadro's number. The polymer-solvent interaction is characterized by the Flory-Huggins χ parameter

$$\chi = z\Delta w r_1/kT \quad (5)$$

Here Δw is the interchange energy or free energy expressed per segment of either polymer or solvent, and z is the lattice coordination number. In the model, the fraction of nearest neighbors in the same lattice plane is l and the corresponding fraction in each of the neighboring planes is m, so that $l + 2m = 1$. In the application[1] of the Prigogine theory, $m = 0.25$ and $l = 0.50$, as for a close-packed lattice. Other work[8] suggests that a choice of $m = 0.29$ may be superior. However, predictions of the theory are insensitive to this choice, and indeed χ itself may be set to zero (athermal case) without changing the main features of the predictions.

In the equations, a is the surface area occupied by a solvent molecule, whether spherical or chain like. If the solvent molecule is considered to be a chain of r_1 segments, each of volume v, then the area is given by the approximation $a = r_1^{2/3}$. All of the solvents used in the present work will be taken to correspond to single spherical segments, so that

$$a = v^{2/3} = (V/N_0)^{2/3} \quad (6)$$

where V is the molar volume. This means that the area of a polymer segment or element is also $v^{2/3}$, constituting a slightly different choice of area from that made[8] in dealing with the surface tension of pure polymer liquids. In the work of Prigogine, the γ referred to the surface tensions of the solution and the pure components. They may equally well be considered as interfacial tensions between the system and a solid or another liquid. In the case of a surface tension or interfacial tension against a liquid, the γ values are measurable. However, when they refer to interfacial tensions against a solid, the directly measurable quantity is ϕ_2^s, as given by adsorption eq 3. The parameter $(\gamma_1 - \gamma_2)a/kT$ is then an adjustable parameter, although in principle obtainable from contact angle measurements.

Referring now to adsorption eq 3, the left-hand side is positive or negative if there is preferential adsorption of respectively the polymer or the solvent. The first term on the right-hand side, $(\gamma_1 - \gamma_2)a/kT$, indicates the well-known tendency toward adsorption of the component of lower interfacial tension. This term corresponds to the adsorption parameter, χ_s of Silberberg[4d] or the parameter $\ln K$ of Ash, Everett, and Findenegg.[6] It involves interaction between the molecules of the pure components, as well as interactions with the solid or liquid adsorbent. These interactions involve the free energies, ϵ_{11}, ϵ_{22}, ϵ_{1a}, and ϵ_{2a}, required to break contacts of the following types: 1-1, 2-2, 1-adsorbent, and 2-adsorbent. Then

$$(\gamma_1 - \gamma_2)a/kT = (mz/kT)[1/2(\epsilon_{11} - \epsilon_{22}) + (\epsilon_{2a} - \epsilon_{1a})] \quad (7)$$

(7) J. J. Kipling, "Adsorption from Solutions of Non-electrolytes," Academic Press, New York, N.Y., 1965, Chapter 8.
(8) K. S. Siow and D. Patterson, *Macromolecules*, **4**, 26 (1971).

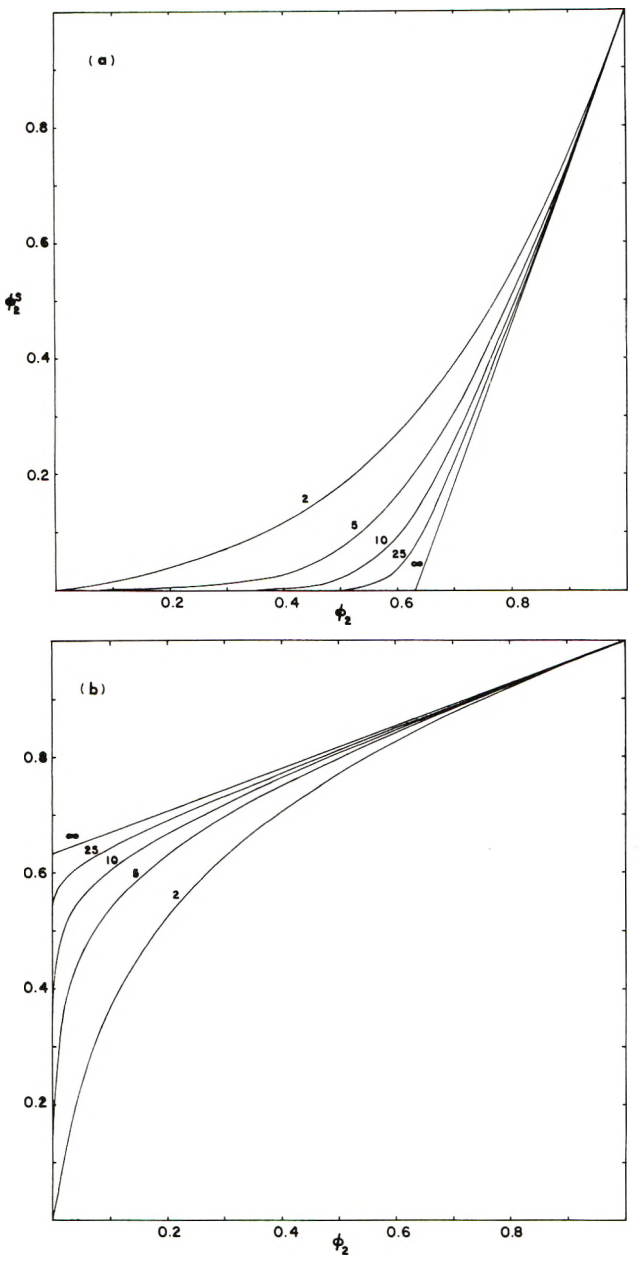

Figure 1. Adsorption isotherm from eq 3: surface volume fraction ϕ_2^s as a function of ϕ_2, for various values of r and with $\chi = 0$. The values taken for the $(\gamma_1 - \gamma_2)a/kT$ parameter are (a) -1, corresponding to preferential solvent adsorption; and (b) $+1$, corresponding to preferential polymer adsorption.

The parameter χ_s is identical with this if the ϵ are considered to be energies only. The first term of the expression, *i.e.*, $(mz/2kT)(\epsilon_{11} - \epsilon_{22})$ is merely the surface tension difference $(\gamma_1 - \gamma_2)a/kT$ measured against the vacuum in the absence of the adsorbent. The second term of expression 7 involves the interaction with the adsorbent, and is the parameter, x, of Silberberg.[4b]

Returning to eq 3 the second and third terms on the right-hand side indicate the effect on adsorption of the molecular interactions within the bulk and the surface phases, respectively. They depend on χ which is almost invariably positive corresponding to unfavorable polymer–solvent interactions. In case the polymer concentration is low in both phases, *i.e.*, $\phi_2 < \phi_1$ and $\phi_2^s < \phi_1^s$, the second term produces a positive effect, favoring polymer adsorption, and the third a negative effect, favoring desorption of the polymer. This corresponds to the well-known effect of unfavorable interactions in a mixture tending to eject from a phase whichever component is present in low concentration (*cf.* azeotropy). The molecular interactions can lead to a change of sign of the adsorption with change of concentration.

Predictions of the Prigogine–Maréchal Theory

Adsorption Isotherm. Equation 3 was solved analytically by Prigogine and Maréchal in the approximation that $(\gamma_1 - \gamma_2)a/kT \ll 1$. This requirement is not fulfilled, however, by most systems, and numerical methods must be used. In using the theory, Gaines[2a] has made the simplifying assumption that the surface layer is athermal, *i.e.*, $\chi = 0$ in the surface layer. The main simplification is in the adsorption isotherm since the surface concentrations are eliminated from the right-hand side. Since, however, numerical methods are still required, we prefer to keep the original equations, eq 1–3, and use for their solution a computer program written by J. M. Bardin of this laboratory.[9] Figure 1 shows ϕ_2^s as a function of ϕ_2 for $\chi = 0$ and with a number of values of the molecular size ratio, r. The parameter $(\gamma_1 - \gamma_2)a/kT$ represents an affinity of the surface for the second component relative to the first. It corresponds to χ_s in the Silberberg theory. (In that theory, however, χ_2 and χ, the Flory–Huggins parameter, are interpreted in terms of enthalpy only, whereas $(\gamma_1 - \gamma_2)a/kT$ is a free energy quantity.) Two values were taken for the parameter $(\gamma_1 - \gamma_2)a/kT$: -1, corresponding to preferential solvent adsorption, and $+1$, corresponding to preferential polymer adsorption. In the former case, for high r, the surface is almost entirely free of polymer until the bulk ϕ_2 reaches a very substantial value, in this case, 0.63. At this special value of ϕ_2, the surface concentration starts to rise steeply to unity. In the latter case of preferential polymer adsorption, ϕ_2^s has a substantial value, 0.63, even when the bulk is almost entirely free of polymer. An increase of ϕ_2 brings about a slow increase of ϕ_2^s to unity. In Figure 1, one sees that the adsorption isotherm hardly changes with molecular weight after $r = 25$, corresponding to a molecular weight of $\sim$2500. The limiting case when $r \to \infty$ should be representative of all molecular weights in the high polymer range. The adsorption eq 3 is easily solved analytically in this limiting case when $\chi = 0$ giving the following results for ϕ_2^s

Preferential Solvent Adsorption, $(\gamma_1 - \gamma_2)a/kT < 0$

$$\phi_2 \leq 1 - \exp\{(\gamma_1 - \gamma_2)a/kT\},\ \phi_2^s = 0$$

$$\phi_2 \geq 1 - \exp\{(\gamma_1 - \gamma_2)a/kT\}, \qquad (8)$$

$$\phi_2^s = 1 - (1 - \phi_2)\exp\{(\gamma_1 - \gamma_2)a/kT\}$$

Preferential Polymer Adsorption, $(\gamma_1 - \gamma_2)a/kT > 0$

$$\phi_2^s = 1 - (1 - \phi_2)\exp\{-(\gamma_1 - \gamma_2)a/kT\} \qquad (9)$$

Figure 2 employs a logarithmic scale to show the case of preferential polymer adsorption in greater detail. It is evident that the theory successfully predicts the observed features of polymer adsorption isotherms which have been summarized by Silberberg.[4b] For example, large adsorp-

(9) Program available from the authors and in A. K. Rastogi, Thesis, McGill University, 1969.

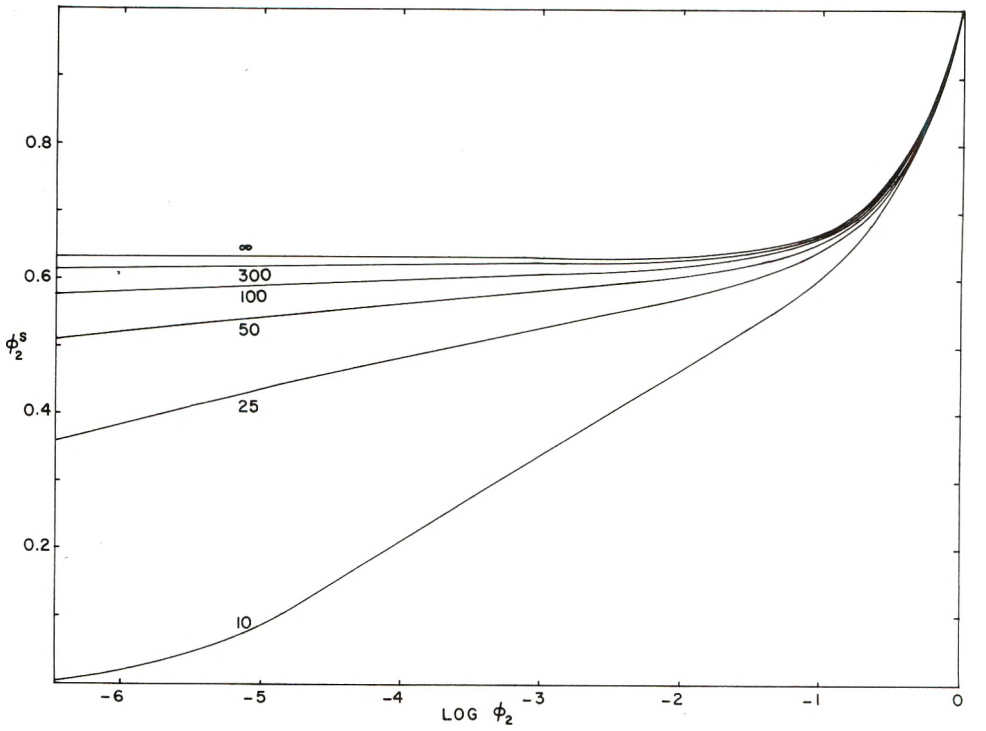

Figure 2. Adsorption isotherm from eq 3 for the case of preferential polymer adsorption, plotted as a function of log ϕ_2. Conditions used in the calculation same as for Figure 1b.

tion of polymer occurs at very low bulk concentration, and is followed by a plateau where there is little increase of adsorption with further increase of concentration. The amount adsorbed changes rapidly for lower molecular weights, attaining a limiting value for $r \to \infty$, which is given by eq 9. The behavior is almost identical with that shown in Figure 5 of Silberberg.[4b] (The quantity Γ used by Silberberg corresponds to the present ϕ_2^s.) The results of Silberberg were obtained with $\chi = 0$ and his parameter $x = 1$. Silberberg also assumed that $\epsilon_{11} = \epsilon_{22}$ so that $(\gamma_1 - \gamma_2)a/kT = \chi_s = x = 1$ as in our Figure 2.

Figure 3 shows the effect on the quantity of adsorbed polymer of increasing the $(\gamma_1 - \gamma_2)a/kT$ parameter. A high molecular weight corresponding to $r = 10^6$ was selected. The bulk concentration corresponds to the plateau region where ϕ_2^s is essentially independent of ϕ_2. Two values of χ have been used, and it is found that poor solvent quality enhances adsorption of the polymer, as observed experimentally. Again comparison may be made with Figure 7 of ref 4d of Silberberg where the same qualitative effect of χ_s may be seen. The effect of χ is, however, considerably greater than in the Silberberg theory. We conclude that the main features of polymer adsorption isotherms are predicted by the simple Prigogine-Maréchal theory in much the same manner as the Silberberg theory. It is of interest to note that the Prigogine-Maréchal theory, by neglecting the effect of the surface on polymer configurations, considers adsorption as a simple partitioning of the polymer between two phases, the bulk and the surface phase where the presence of the polymer is favored. It is well known that the efficiency of partitioning increases with molecular weight of the polymeric solute.[10] Thus, the strong effect of molecular weight on polymer adsorption finds a counterpart in other cases involving partitioning of polymer between two phases. For example, it is the basis of the usual polymer fractionation method.[10]

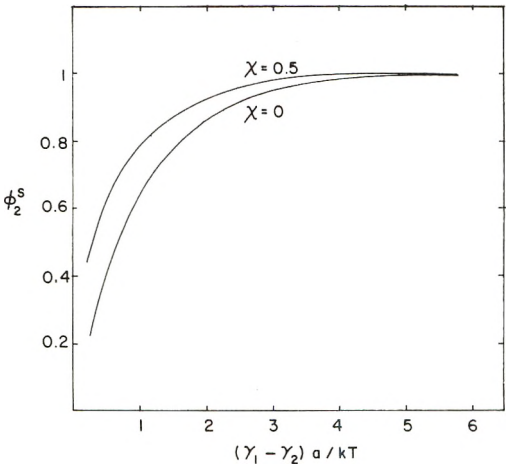

Figure 3. Dependence of adsorption of polymer on the $(\gamma_1 - \gamma_2)a/kT$ and χ parameters. The value of r used in the calculation is 10^6 and the bulk concentration corresponds to the plateau region of the adsorption isotherm.

Surface and Interfacial Tensions. The solution of eq 3 for ϕ_2^s is substituted into eq 1 or 2 to give the surface or interfacial tension of the mixture. Figures 4a and 4b give the surface and interfacial tension analogs of Figures 1a and 1b, using the same conditions. The surface tension increments $(\gamma - \gamma_1)a/kT$ and $(\gamma - \gamma_2)a/kT$ are given as functions of ϕ_2. In Figure 4a where $\gamma_1 < \gamma_2$ corresponding to preferential solvent adsorption, the polymeric character of the solute does not markedly change the concentration dependence of the solution surface tension. On the other hand, in Figure 4b where $\gamma_1 > \gamma_2$ corresponding to preferential polymer adsorption, the polymeric character of the solute causes a sharp decrease of the solution surface ten-

(10) H. Tompa, "Polymer Solutions," Butterworths, London, 1956, p 219.

sion at very low polymer concentration. The value of γ for the solution in the limit of $r \to \infty$ and $\chi = 0$ may be obtained from eq 8 and 9 used in eq 1 and 2. We again distinguish two cases corresponding to negative and positive values of $(\gamma_1 - \gamma_2)a/kT$, *i.e.*, preferential adsorption of the solvent or of the polymer.

Preferential Solvent Adsorption, $(\gamma_1 - \gamma_2)a/kT < 0$

$$\phi_2 \leq 1 - \exp\{(\gamma_1 - \gamma_2)a/kT\},$$

$$(\gamma - \gamma_1)a/kT = -\ln(1 - \phi_2) - \phi_2 \quad (10a)$$

$$\phi_2 \geq 1 - \exp\{(\gamma_1 - \gamma_2)a/kT\},$$

$$(\gamma - \gamma_1)a/kT = -[(\gamma_1 - \gamma_2)a/kT] + (1 - \phi_2)(1 - \exp\{-[(\gamma_1 - \gamma_2)a/kT]\}) \quad (10b)$$

or

$$(\gamma - \gamma_2)a/kT = (1 - \phi_2)(1 - \exp\{-[(\gamma_1 - \gamma_2)a/kT]\}) \quad (10c)$$

Preferential Polymer Adsorption, $(\gamma_1 - \gamma_2)a/kT > 0$

The surface tension is given by eq 10b or 10c throughout the concentration range.

Equation 10b shows that for $r \to \infty$, γ is a linear function of the volume fraction at high polymer concentration when $(\gamma_1 - \gamma_2)a/kT < 0$, and throughout the concentration range when $(\gamma_1 - \gamma_2)a/kT > 0$. Figure 5 shows the case of preferential polymer adsorption in greater detail at low concentration. It is evident that for high r, the surface tension of the solution remains essentially constant, down to extremely low concentration, at a value obtained from eq 10c by putting $\phi_2 = 0$. It is interesting that $(\gamma - \gamma_2)a/kT$ is numerically equal to ϕ_2^s when $r \to \infty$ and the concentration is low. The effects of χ and $(\gamma_1 - \gamma_2)a/kT$ follow from Figure 3. Larger values of χ and $(\gamma_1 - \gamma_2)a/kT$ corresponding to greater polymer adsorption, give lower values of $(\gamma - \gamma_2)a/kT$.

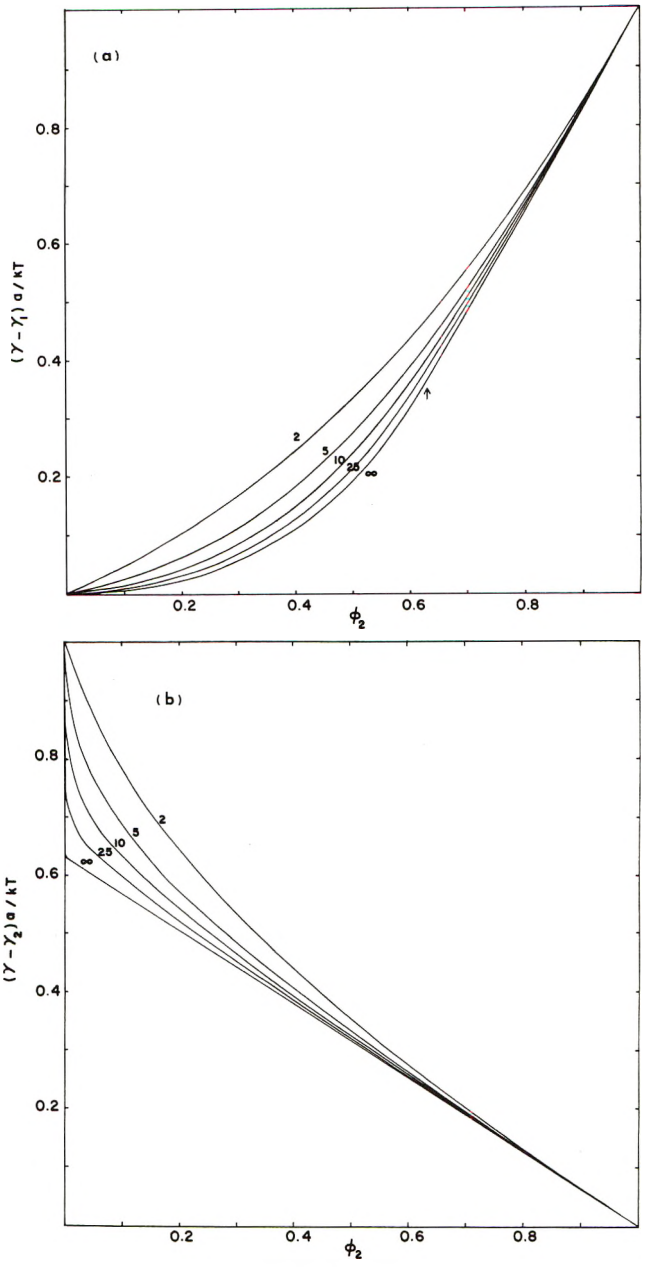

Figure 4. Calculated surface tension increment as a function of ϕ_2, for various values of r and with $\chi = 0$. The values taken for the $(\gamma_1 - \gamma_2)a/kT$ parameter are (a) -1, corresponding to preferential solvent adsorption; and (b) $+1$, corresponding to preferential polymer adsorption.

Experimental Section

The solvents used in preparing polymer solutions were obtained from Fisher Scientific Co. The tetralin was Purified grade and was freed of surface active contaminants by passage through columns of alumina and silica gel. The cyclohexane and benzene were Spectranalyzed grade and were used as received. The measured surface and interfacial tensions and densities of these solvents are given in Table I.

The polymers used in this study include polydimethylsiloxanes, polyisobutylenes, and polystyrene. The dimethylsiloxane oligomer, dodecamethylpentasiloxane (MD_3M), was a fractionally distilled sample obtained through the courtesy of Dr. O. K. Johansson of Dow Corning Co., Midland, Mich. The other PDMS samples were Dow Corning 200 fluids of various viscosity grades and were percolated through alumina–silica gel columns before use. Two PIB samples were obtained from Naphtachimie, Lavera, France (sample 2) and Polymer Corp., Sarnia, Ont. (sample 1). They were purified by first precipitating from benzene with methanol to eliminate the lowest molecular weights, then dissolving them in methylene chloride and passing the solutions through alumina–silica gel columns. The solvent was then removed by evacuation under high vacuum. The polystyrene PS ($M = 4000$) was a standard sample of narrow molecular weight distribution obtained from the Pressure Chemical Co., Pittsburgh, Pa., and was used as received. The number-average molecular weight of the polymers were determined by vapor pressure osmometry in benzene: the results are recorded in Table I, along with measured surface and interfacial tensions, and densities. These values are all consistent with comparable data in the literature.

The water used in interfacial tension measurements was triple distilled. The surface tension of the water was used as a measure of its purity; samples with values lower than 72.0 dyn/cm were not used.

All polymer solutions were prepared by weight. Solutions in cyclohexane and in benzene for interfacial tension

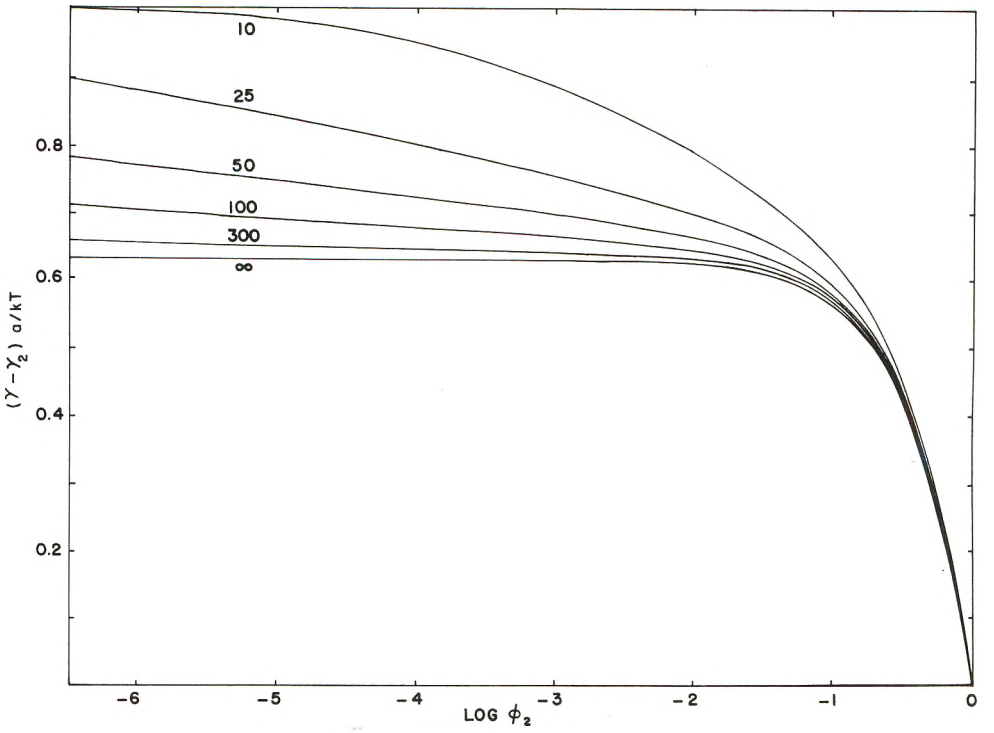

Figure 5. Calculated surface tension increment as a function of log ϕ_2 for the case of preferential polymer adsorption. Conditions used in the calculation same as for Figure 4b.

TABLE I: Properties of Solvents and Polymers

Substance	Density, g/ml 20°	Density, g/ml 30°	Surface tension, dyn/cm 20°	Surface tension, dyn/cm 30°	Interfacial tension against water at 20°, dyn/cm	$\bar{M}_n$
			Solvents			
Tetralin		0.9613		34.8		
Cyclohexane	0.7786		25.0		50.5	
Benzene	0.8792		28.7		34.8	
			Siloxanes			
MD_3M	0.8760	0.8654		17.6	41.0	400
5 cSt	0.9207	0.9112		18.5	40.9	684
10 cSt	0.9398	0.9304		19.1	42.4	1080
100 cSt	0.9700	0.9621		20.0	44.3	5390
			PIB			
Sample 1	0.8546		28.2		45.7	410
Sample 2	0.8967		32.2[a]			1400

[a] Measured by the pendant drop method.

measurements were prepared with the solvents having been saturated with water. Densities of solutions are required for converting weight concentrations to volume fractions, and also for correction of the surface tension measurements. These were calculated from the density values of the pure components, assuming volumes of mixing to be zero except for the polystyrene solutions the densities of which were measured directly.

Surface and interfacial tensions were measured with a Du Nouy tensiometer (Fisher Scientific Co.) using a 6-cm ring. The usual corrections[11] were applied in all cases. The temperatures at which the measurements were performed were controlled by a constant temperature circulating water bath and jacketed sample holder. The temperature of measurement for the polydimethylsiloxane–tetralin systems was set at 30°, since the polymer was not completely miscible with the solvent at lower temperatures. All other measurements were made at 20°. In every case, the solution in a small dish was kept in the sample holder for about 0.5 hr before the first measurement was made. During this period the ring was kept immersed in the solution, or in the water phase in the case of interfacial tension measurements. This length of time was found to be long enough for the solutions to reach the equilibrium value of the surface or interfacial tension, exept for those of PS and of PIB of the higher molecular weight sample. The latter solutions, due to their viscosity, were

(11) H. H. Zuidema and G. W. Waters, *Ind. Eng. Chem., Anal. Ed.*, **13**, 312 (1941).

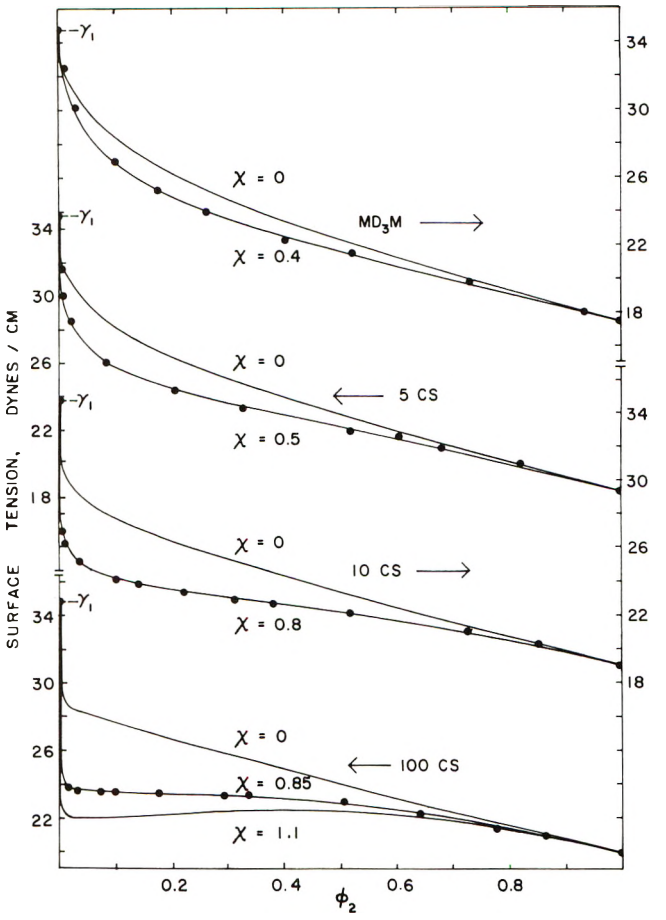

Figure 6. Surface tension of solutions of polydimethylsiloxanes in tetralin at 30°. Curves are calculated from eq 1-3 with $\chi = 0$ and with the values of χ chosen to fit the experimental points. The curve with $\chi = 1.1$ showing an inflection point is included for comparison. Values of γ_1 for the pure solvent indicated for each curve. Note shifts of ordinate axis.

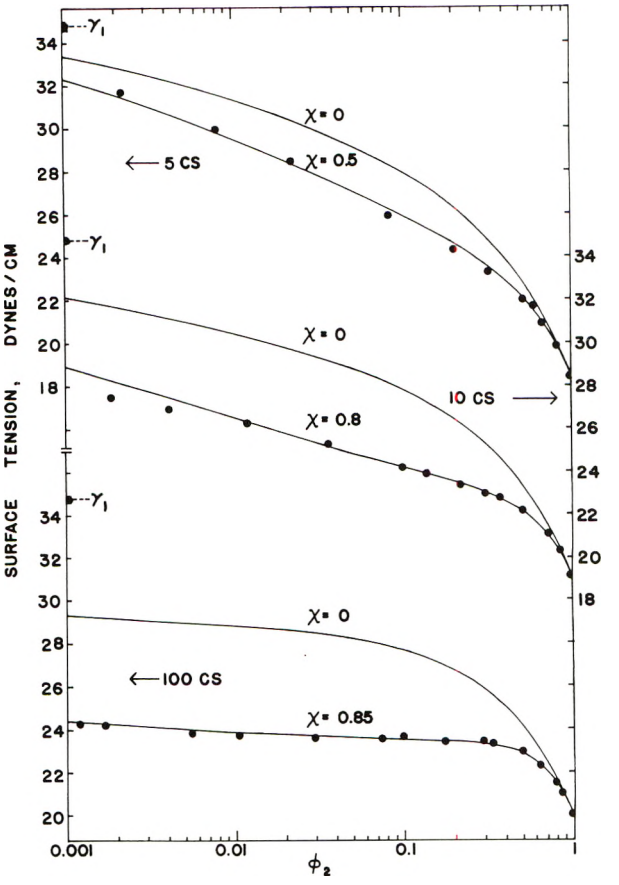

Figure 7. Surface tension of solutions of polydimethylsiloxanes in tetralin at 30° plotted on a logarithmic volume fraction scale. Note shifts of ordinate axis.

studied only up to relatively low concentrations of polymer, and it took up to several hours for them to reach the plateau values which were taken to be the values of their interfacial tension.

Results and Discussion

Surface Tension. Figure 6 shows the experimental values of γ for four dimethylsiloxane oligomers and polymers in tetralin. The accuracy is estimated to be ±0.1 dyn/cm. The figure also gives curves predicted by the theory with $\chi = 0$ (athermal case) and with values of χ chosen to give the best agreement with the experimental points. The shape of the curve is insensitive to the exact value of χ chosen. The other parameters required, *i.e.*, r and a, were obtained from the molar volumes as described above and are listed in Table II. The rather large values of χ are to be expected since the mixture of the 100-cSt sample with tetralin phase separates at room temperature. The Flory–Huggins theory would give a critical value of $\chi = 0.67$ for the molecular weight in question, valid at the relatively low critical polymer concentration. The χ parameter usually increases considerably with polymer concentration particularly when the solvent is poor. An average value of 0.85 as found here is reasonable for the 100-cSt sample. The increase of χ in passing from the oligomer of lowest molecular weight, MD_3M, to the polymer of 100-cSt viscosity seems rather large, but an increase of this type can be rationalized using contemporary theories of polymer–solvent interaction. As seen by comparison with the theoretical curves for the athermal case, $\chi = 0$, the net effect of the unfavorable polymer–solvent interaction in the bulk and surface phases is to increase polymer adsorption at low ϕ_2. This depresses the surface tension, and produces the characteristic flat region of the curve seen for the highest molecular weight of PDMS. Larger values of χ produce S-shaped curves, an example of which is shown in Figure 6. Figure 7 gives more experimental

TABLE II. Parameters for Fitting Eq 1-3

Solvents	V_1, ml	a, Å²
Tetralin	137.4	37.3
Cyclohexane	108.0	31.8
Benzene	88.8	27.9

	V_2, ml		$r = V_2/V_1$		
Polymers	20°	30°	Tetralin	Cyclohexane	Benzene
		Siloxanes			
MD_3M	439	444	3.23	4.06	
5 cSt	743	751	5.47	6.88	8.37
10 cSt	1149	1161	8.45	10.6	
100 cSt	5556	5601	40.8	51.4	62.6
		PIB			
Sample 1	480				5.41
Sample 2	1560				17.6

points in the region of low polymer concentration, showing the striking constancy of γ after the initial sharp drop at low ϕ_2. We have also used the equations developed by Gaines[2a] assuming an athermal surface layer. The fit to experiment is again good with χ values about 0.2 less than used with the Prigogine–Maréchal equations. This is to be expected since the Gaines approximation eliminates the unfavorable polymer–solvent interactions in the surface layer but not in the bulk. Hence for a chosen value of χ, the predicted adsorption and lowering of the surface tension will be greater when the Gaines approximation is used to solve the Prigogine–Maréchal equations (*cf.* eq 3).

The PDMS–tetralin system shows similar features to the PDMS–tetrachloroethylene and PDMS–toluene systems studied by Gaines,[2a] although they are enhanced by the greater $\gamma_1 - \gamma_2$ difference. Thus, in the tetralin system, and with the highest molecular weight of PDMS, the drop of γ at low ϕ_2 is 10 dyn/cm out of a total $\gamma_1 - \gamma_2$ difference of 15 dyn/cm. In the tetrachloroethylene and toluene systems the drops are 4.5 out of 10 dyn/cm and 3 out of 7.5 dyn/cm. Equation 10c shows that with decreasing $\gamma_1 - \gamma_2$ the relative magnitude of the drop decreases, as found experimentally.

Interfacial Tensions of Polymer Solutions Against Water. We have studied two solutions of PDMS against water: PDMS plus cyclohexane–water where preferential polymer adsorption is expected and PDMS plus benzene–water where preferential solvent adsorption is predicted. Two more systems, PIB plus benzene–water and PS plus cyclohexane–water were investigated. They show preferential adsorption of the solvent and of the polymer, respectively. Figure 8 shows that the interfacial tension of the PMDS plus cyclohexane–water system is qualitatively similar in its concentration dependence to the surface tension of PDMS plus tetralin, another case of preferential polymer adsorption (Figure 7). The sharp drop of interfacial tension at low polymer concentration appears and becomes more pronounced with increase of polymer molecular weight. The $\gamma_1 - \gamma_2$ value is, however, smaller in this system, 6.5 dyn/cm, with a correspondingly smaller drop of γ, 2 dyn/cm. The Prigogine–Maréchal theory is again successful in predicting the concentration dependence and the evolution of the γ curves with increasing molecular weight. The χ values which give the best fit to experiment are reasonable. For the 100-cSt sample the value of χ = 0.6 compares with values of about 0.5 found in vapor sorption studies on a high molecular weight sample in alkane solvents.[12] The polymer solutions are of course saturated with water. In the case of the cyclohexane solvent this corresponds[13] to a mole fraction of water $\sim 4 \times 10^{-4}$, which could in principle change the effective χ parameter for the interaction of the polymer with the solvent medium. However, in the present case, the effect would appear to be negligible. We should point out, however, that for the two systems PDMS (100 cSt) plus cyclohexane–water and PDMS (100 cSt) plus benzene–water, the density difference between the two phases becomes very small (less than 0.05 g/cm^3) at concentrations of the polymer higher than ϕ_2 = 0.7. Above this concentration the correction[11] applied to the measured surface tension is $\simeq$20%, attaining $\simeq$40% for pure PDMS (100 cSt)–water. The correction formula has not been sufficiently tested in this range. At the lower concentrations of this polymer, the accuracy is estimated to be ±0.5 compared with a reproducibility of ±0.2 dyn/cm. When the lower molecular weights of PDMS are used, the density differences between the two phases correspond to corrections less than 20% and the accuracy is thought to be better than that stated above. However, for the pure PDMS (100 cSt) against water at 23°, a value of 41.6 dyn/cm has been obtained[14] using the pendant drop method. This is considerably below the value, 44.3 dyn/cm, using the ring method and the correction. The pendant drop is also subject to error since the interfacial tension, as measured, depends directly on the small density difference between the two liquid phases. If the lower value is accepted, the Prigogine theory may again be fitted to the γ values for the pure components, again predicting the sharp drop of γ at low polymer concentration. However, γ values at intermediate concentrations predicted using reasonable χ values fall $\simeq$ 1 dyn/cm below the experimental values.

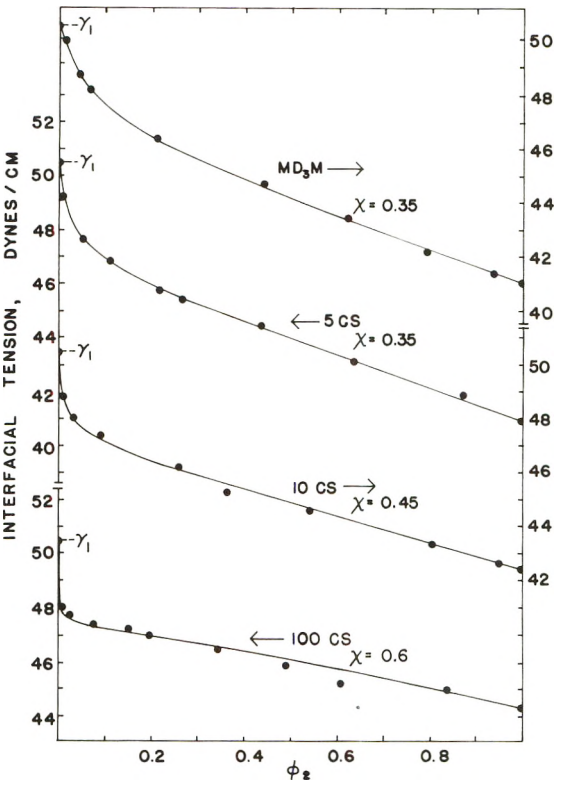

Figure 8. Interfacial tension against water of solutions of polydimethylsiloxanes in cyclohexane at 20°. The curves are calculated with the values of χ chosen to fit the experimental points. The value of γ_1 for the pure solvent is indicated for each curve. Note shifts of the ordinate axis.

Figures 9 and 10 show the interfacial tension of the PDMS plus benzene–water and PIB plus benzene–water systems. These are cases of preferential solvent adorption and have $\gamma(\phi_2)$ curves which are quite different from those for PDMS plus cyclohexane–water. The surface tension remains close to that of the pure solvent, then increases roughly linearly with concentration to reach the surface tension of the pure polymer. The values of γ are only slightly dependent on the molecular weight of the PDMS or PIB. This feature and the concentration dependences are well predicted by the Prigogine–Maréchal theory. In the case of the PDMS (100 cSt) plus benzene–water system, one might consider the pendant drop value

(12) W. P. Kao, R. S. Chahal, and D. Patterson, unpublished results.
(13) J. H. Hildebrand and R. L. Scott, "The Solubility of Nonelectrolytes," 3rd ed, Reinhold, New York, N.Y., 1950, p 266.
(14) A. Mar, unpublished results.

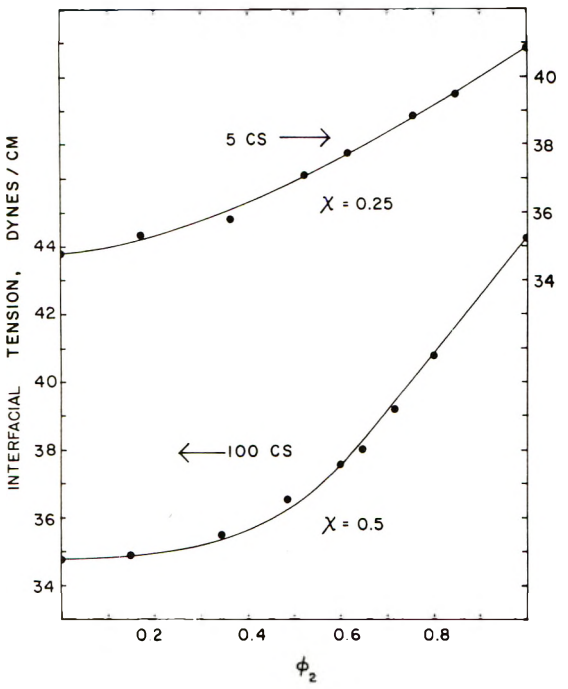

Figure 9. Interfacial tension against water of solutions of polydimethylsiloxanes in benzene at 20°. The curves are calculated with the values of χ chosen to fit the experimental points. Note shifts of ordinate axis.

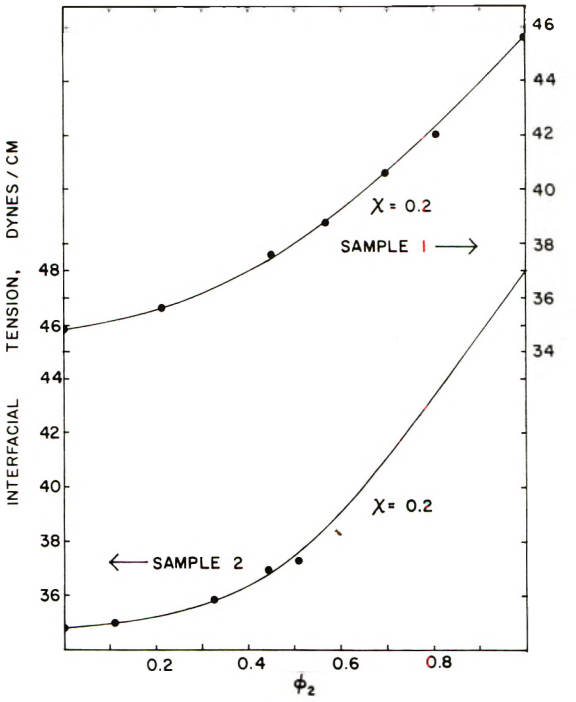

Figure 10. Interfacial tension against water of solutions of polyisobutylenes in benzene at 20°. The curves are calculated with the value of χ indicated. Note shifts of ordinate axis.

of 41.6 dyn/cm for PDMS (100 cSt)-water. Then, neglecting solution points for $\phi_2 > 0.7$, the Prigogine theory is able to predict the shape of the new $\gamma(\phi_2)$ curve using the same χ value of 0.5. In the case of the higher molecular weight PIB sample, the interfacial tension of the pure polymer could not be measured due to its high voscosity. The same χ value was used for the lower molecular weight and the value of γ_2 was fitted. Agreement between theory and experiment is obtained with reasonable values of the χ parameter. The solubility of water in benzene corresponds[13] to a mole fraction of 19×10^{-4} at 20° and is neglected. Values of the χ parameter are available for both of these polymer solutions,[12,15] but with high molecular weight samples only. In both cases they vary from $\simeq 0.5$ at low polymer concentration to $\simeq 0.8$ at high concentration. The lower molecular weight samples used here would presumably have rather lower χ values, but it seems clear that the fitted χ value of 0.2 for the PIB-benzene system is too low.

Results with the PS plus cyclohexane-water system are shown in Figure 11. They are of the preferential polymer adsorption type, but here the Prigogine-Marêchal theory is much less satisfactory than for the other systems. A difficulty is encountered in applying the theory since the pure polymer is a glass at room temperature, whose interfacial tension against water cannot be measured by the present method. However, if a value of $\gamma_2 = 21$ dyn/cm is assumed together with $\chi = 0.5$ the theory reproduces the γ values at the larger polymer concentrations, $\phi_2 \simeq 0.3$. Figure 11 shows that the drop of γ at low ϕ_2 is experimentally much less rapid than predicted. This is evident in the insert of Figure 11 where the shape of the experimental curve is different from those exhibited by the high molecular weight PDMS-tetralin system and by theory. Experimentally, therefore, the coverage of the surface by the polymer at low ϕ_2 is not as complete as predicted. It is

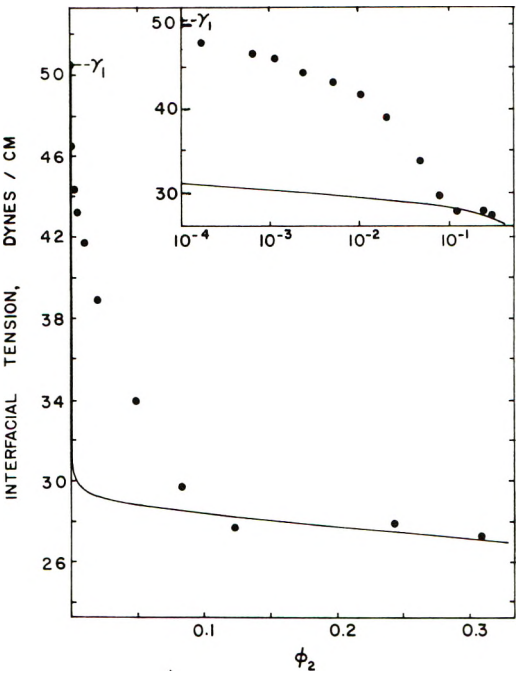

Figure 11. Interfacial tension against water of solutions of polystyrene in cyclohexane at 20°. The curve is calculated from eq 1-3. In the insert the results are plotted on a logarithmic volume fraction scale.

tempting to associate the less satisfactory results obtained in the PS case with the greater rigidity of this polymer compared with PDMS. Frisch and Al-Madfai[16] have shown that a configurational entropy effect is significant

(15) B. E. Eichinger and P. J. Flory, *Trans. Faraday Soc.*, **64**, 2053 (1968).
(16) H. L. Frisch and S. Al-Madfai, *J. Amer. Chem. Soc.*, **80**, 3561 (1958).

in the case of PS. It opposes the adsorption of the polymer due to energetic interactions. Our speculation is not supported, however, by the Silberberg theory which does consider the effect of the surface in restricting the configurations of the macromolecule. Figure 5 of ref 4d shows that decreasing the $\gamma_B\gamma_S$ parameter, which is a measure of chain flexibility, enhances the adsorption of the polymer and the surface tension depression. This is contrary to the change in the experimental data in passing from PDMS to PS.

In spite of the reservations to be made in the PS case, the Prigogine–Maréchal theory seems to be very successful. In fact, the good results are surprising in view of the extreme assumptions on which the theory is apparently based. At first sight, there might be two implications: first, the polymer molecules do lie entirely flat in the surface layer, as assumed, and secondly there is no explicit effect on the surface tension of a restriction of polymer configurations due to the presence of the surface. The predicted surface tension might be considered as the sum of three contributions: (1) the change in combinatorial entropy and free energy of the system as the polymer and solvent redistribute themselves between the surface and bulk phases in response to the adsorptive forces of the surface, (2) the free energy associated with the interaction of the surface with those solvent molecules and polymer segments which are in actual contact with it, and (3) the contribution which is not treated by the Prigogine theory, *viz.*, the lowering of the entropy of the surface-phase polymer molecules due to a restriction on their configurations. In our opinion virtually the same predictions of contributions 1 and 2 would have been obtained from a less restrictive model in which the surface phase could have been of a greater (and more realistic) thickness, with only a fraction of the segments of any one polymer molecule actually contacting the surface. The success of the Prigogine theory would thus not imply that the polymers really lie flat in the surface layer. The Prigogine model is only a convenient way of removing contribution 3 from explicit consideration. This seems to leave the conclusion that contribution 3 must indeed be negligible. However, this is not necessary. The theory makes no *a priori* calculation of the surface tension of the pure polymer, but uses the experimental γ_2 value. Thus, if contribution 3 is the same for polymer molecules in solution and in the pure liquid, the theory should give good results in spite of its lack of an explicit consideration of this contribution. The apparent error of the theory may in fact be an advantage over the more sophisticated theories, particularly at higher polymer concentrations. Some support for the idea of an unimportant contribution 3 may, however, come from a corresponding states correlation of surface tension data for pure monomeric and polymeric liquids.[17] The difference between the surface tensions of these two classes of liquids could be explained purely in terms of their differing degrees of thermal expansion. There was no apparent effect of a restriction on polymer configurations at the surface. (An alternative explanation of this would be that the bulk polymer melts are themselves ordered or restricted in their molecular configurations.)

We should emphasize that the Prigogine–Maréchal theory has in principle been superseded by the treatments of Silberberg and Hoeve. However, we believe that its extreme simplicity is useful at the present time and that it is an instructive basis for the interpretation of results in the areas of surface and interfacial tension and the adsorption of polymer solutions.

Acknowledgment. We acknowledge with gratitude the support of the National Research Council of Canada and the award of the Newell P. Beckwith Fellowship of the Paint Research Institute to K. S. S. We thank Mr. A. Mar of the Pulp and Paper Research Institute of Canada for his pendant drop work on the PDMS–water system, Mr. J. M. Bardin of this laboratory for developing the computer program for the solution of the Prigogine–Maréchal equations, and Dr. J. Pouchly of the Institute of Macromolecular Chemistry, Prague, for valuable discussion.

(17) D. Patterson and A. K. Rastogi, *J. Phys. Chem.*, **74**, 1067 (1970).

Transport Properties in Hydrogen Bonding Solvents. VII. The Conductance of Electrolytes in 1,1,1,3,3,3-Hexafluoro-2-propanol

Mary A. Matesich,*[1] Janice Knoefel,[2]

Department of Chemistry, Ohio Dominican College, Columbus, Ohio 43219

Howard Feldman,[3] and D. Fennell Evans

Department of Chemistry, Case Western Reserve University, Cleveland, Ohio 44106 *(Received July 24, 1972)*

Publication costs assisted by the Office of Saline Water, U.S. Department of the Interior

Precise conductance measurements are reported for the tetraalkylammonium salts Me_4NCl, Me_4NBr, Me_4NI, Me_4NClO_4, Et_4NBr, Pr_4NBr, Pr_4NI, Bu_4NCl, Bu_4NBr, Bu_4NI, Bu_4NClO_4, i-Am_3BuNI, and $Hept_4NI$ in 1,1,1,3,3,3-hexafluoro-2-propanol at 25°. Data have been analyzed using the 1957 Fuoss-Onsager equation and a modified version due to Justice. A surprisingly low degree of ionic association was found. Results are consistent with extensive solvation of anions and poor solvation of cations by the fluorinated alcohol.

Introduction

The polyfluorinated alcohols appear to be an interesting group of electrolyte solvents exhibiting properties distinct from other hydrogen-bonding solvents. Electrolyte conductance in 2,2,2-trifluoroethanol (TFE)[4] shows a pattern consistent with poor cation solvation and good solvation of anions. This is a consequence of the electron-withdrawing ability of the CF_3 group, which causes diminished basicity and nucleophilicity of the alcohol oxygen but increased acidity of the proton.

This characteristic of the fluorinated alcohols makes them one extreme in a spectrum of ion–solvent interactions. In contrast to the fluoro alcohols, the dipolar aprotic solvents interact strongly only with cations. Between these two extremes lie the hydrocarbon alcohols, amides, and water which possess both acidic and basic sites, leading to effective solvation of both cations and anions.

In view of the interesting behavior exhibited by trifluoroethanol, we have studied the conductance of tetraalkylammonium salts in 1,1,1,3,3,3-hexafluoro-2-propanol (HFP).

Experimental Section

1,1,1,3,3,3-Hexafluoro-2-propanol (Halocarbon Products Corp.) was distilled from molecular sieve 3 Å,' V16 in pellets, through a 2-ft Vigreux column, only the middle fraction being retained. The density of the distillate was found to be 1.6040 g/ml in good agreement with value of 1.6046 g/ml reported by Kivinen and Murto.[5] The solutions resulting from the conductance runs were saved and the solvent recovered by distillation in approximately 2-l. batches. The density of each batch was checked and found to be in agreement with the value given above. Because of the high vapor pressure (bp 59°) and the strong, unpleasant odor this solvent is difficult and disagreeable to work with. The tetraalkylammonium salts were recrystallized from suitable solvents and dried under vacuum.[6]

The electrical equipment, conductance cells, and techniques were the same as previously described.[7,8] The conductance of the hygroscopic salts, Me_4NCl and Bu_4NCl, were determined using a weight buret. The overall quality of this data is not as good as that for the other salts probably reflecting difficulties associated with handling this volatile solvent. In all other cases increments of salt were added to the Kraus-type conductance cells[9] using a Hawes–Kay dispensing device,[10] enabling the entire run to be carried out in a closed system.

Results

The measured equivalent conductance and corresponding electrolyte concentrations in moles per liter appears in the microfilm edition of this volume of the journal.[11] The density of the most concentrated solution used in each conductance run was measured. The density was assumed to follow the relationship $d = d_0 + Am$, where m is the moles of salt per kilogram of solution. The value 16.7 was used for the dielectric constant[12] of HFP and 1.619 cP for the viscosity.[12]

Conductance data were analyzed both by the Fuoss–Onsager equations[13]

(1) Supported in part by the Research Participation for College Teachers Program of the National Science Foundation.
(2) Supported by the Central Ohio Heart Association.
(3) Supported by the Undergraduate Research Participation Program of the National Science Foundation.
(4) D. F. Evans, J. A. Nadas, and M. A. Matesich, *J. Phys. Chem.*, **75**, 1708 (1971).
(5) A. Kivinen and J. Murto, *Suom. Kemistilehti B*, **40**, 6 (1967).
(6) D. F. Evans and P. Gardam, *J. Phys. Chem.*, **72**, 3281 (1968).
(7) C. G. Swain and D. F. Evans, *J. Amer. Chem. Soc.*, **88**, 383 (1966).
(8) D. F. Evans, C. Zawoyski, and R. L. Kay, *J. Phys. Chem.*, **69**, 3878 (1965); R. L. Kay, C. Zawoyski, and D. F. Evans, *ibid.*, **69**, 4208 (1965).
(9) H. M. Daggett, E. J. Bair, and C. A. Kraus, *J. Amer. Chem. Soc.*, **73**, 799 (1951).
(10) J. L. Hawes and R. L. Kay, *J. Phys. Chem.*, **69**, 2420 (1965).
(11) The measured equivalent conductance and corresponding electrolyte concentrations in moles per liter will appear following these pages in the microfilm edition of this volume of the journal. Single copies may be obtained from the Business Operations Office, Books and Journals Division, American Chemical Society, 1155 Sixteenth St., N.W., Washington, D. C. 20036. Remit check for money order for $3.00 for photocopy or $2.00 for microfiche, referring to code number JPC-73-366.
(12) J. Murto, A. Kivinen, S. Kivimaa, and R. Laakso, *Suom. Kemistilehti B*, **40**, 250 (1967).
(13) R. M. Fuoss and F. Accascina, "Electrolyte Conductance," Interscience, New York, N. Y., 1959.

TABLE I: Conductance Parameters in Hexafluoro-2-propanol at 25° Calculated from Eq 1 and 2

Salt	Λ_0	K_A	a	$\sigma\Lambda$
Me_4NCl	36.33 ± 0.03	56.83 ± 12.01	6.73 ± 0.40	0.03
Me_4NBr	36.72 ± 0.02		4.89 ± 0.03	0.03
Me_4NI	37.69 ± 0.03		4.81 ± 0.04	0.05
Me_4NClO_4[a]	38.63 ± 0.11	55.64 ± 14.93	5.41 ± 0.27	0.02
Et_4NBr	35.28 ± 0.03		5.94 ± 0.06	0.04
Pr_4NBr	30.62 ± 0.02		6.36 ± 0.07	0.03
Pr_4NI[a]	31.67 ± 0.04		6.13 ± 0.09	0.06
Bu_4NCl	27.11 ± 0.03		7.36 ± 0.14	0.06
Bu_4NBr	27.85 ± 0.03		6.44 ± 0.09	0.04
Bu_4NI	28.97 ± 0.01		6.42 ± 0.04	0.02
Bu_4NClO_4	29.86 ± 0.01		6.47 ± 0.04	0.02
i-Am_3BuNI[a]	27.90 ± 0.09		6.36 ± 0.15	0.15
$Hept_4NI$[a]	25.10 ± 0.04		6.58 ± 12	0.07

[a] Average value from two or more runs.

$$\Lambda = \Lambda_0 - Sc^{1/2} + Ec \log c + (J - B\Lambda_0)c \quad (1)$$

$$\Lambda = \Lambda_0 - S(c\gamma)^{1/2} + Ec\gamma \log(c\gamma) + (J - B\Lambda_0)c\gamma - K_A f_{\pm}^2 c\gamma\Lambda \quad (2)$$

and the modified equations proposed by Justice[14]

$$\Lambda = \gamma[\Lambda_0 - S(c\gamma)^{1/2} + Ec\gamma \log c\gamma + J_{(r)}c\gamma + J_{3/2(r)}(c\gamma)^{3/2}] \quad (3)$$

$$K_A = (1 - \gamma)/\gamma^2 c f_{\pm}^2 \quad (4)$$

$$\ln f_{\pm} = -\beta(c\gamma)^{1/2}/(1 + kq\gamma^{1/2}) \quad (5)$$

based on Bjerrum's critical distance q[15]

$$q = e^2/2\epsilon kT \quad (6)$$

In the Justice equations $r = q = 16.8$ Å for HFP was used to calculate J_r and $f_{\pm}$. The terms beyond the Onsager limiting law are those given by Justice.[14]

Conductance parameters in Table I were calculated from eq 1 and 2 using Kay's least-squares programs.[16] Equation 2 for associated electrolytes gave a better fit for all the runs, as would be expected for a three-parameter equation, but resulted in negative association constants as large as −150. For these salts conductance parameters calculated from eq 1 have been listed in Table I, since negative association constants are physically meaningless. As discussed in detail below, negative values of K_A in a solvent of this low a dielectric constant are quite unexpected.

Conductance parameters in Table II were calculated from eq 3-5.[14] The three adjustable parameters were Λ_0, K_A, and $J_{3/2}$. Positive association constants were obtained for all the salts. The value of $a_{3/2}$ calculated from the adjusted $J_{3/2}$ terms can be compared to q, 16.8 Å in HFP. Close agreement would not be expected in this situation for at least two reasons. First, the $J_{3/2}$ term is forced to carry uncertainties due to neglect of higher order concentration terms in the conductance equation and any other approximations. Second, as is developed in more detail below, in HFP the split between the J and K terms is difficult to achieve even with precise data. Considering these limitations, the agreement is satisfactory.

As is evident from a comparison of Tables I and II, Λ_0 values are nearly the same in the two treatments. Some indication of the precision of the measurements can be judged from the consistency of the following Kohlrausch differences as calculated by eq 3: $R_4NI - R_4NBr = 1.03 \pm 0.08$, $R_4NClO_4 - R_4NI = 0.96 \pm 0.01$, and $Me_4NX - Bu_4NX = 9.12 \pm 0.16$.

TABLE II: Conductance Parameters in Hexafluoro-2-propanol at 25° Calculated from Eq 3-5

Salt	Λ_0	K_A	$a_{3/2}$	$\sigma\Lambda$
Me_4NCl	36.39 ± 0.03	194 ± 6	15.0 ± 0.6	0.02
Me_4NBr	37.00 ± 0.03	208 ± 4	15.2 ± 0.2	0.02
Me_4NI	37.94 ± 0.02	216 ± 2	15.0 ± 0.1	0.01
Me_4NClO_4[a]	38.90 ± 0.05	249 ± 10	14.6 ± 0.4	0.04
Et_4NBr	35.26 ± 0.04	141 ± 5	16.1 ± 0.3	0.02
Pr_4NBr	30.67 ± 0.01	142 ± 2	15.5 ± 0.1	0.005
Pr_4NI[a]	31.66 ± 0.02	145 ± 5	15.5 ± 0.3	0.02
Bu_4NCl	26.99 ± 0.02	89 ± 6	16.8 ± 0.4	0.02
Bu_4NBr	27.82 ± 0.01	139 ± 1	15.2 ± 0.1	0.003
Bu_4NI	28.97 ± 0.01	136 ± 2	15.8 ± 0.1	0.006
Bu_4NClO_4	29.94 ± 0.02	154 ± 4	14.5 ± 0.4	0.01
i-Am_3BuNI[a]	27.83 ± 0.10	135 ± 10	15.3 ± 0.4	0.02
$Hept_4NI$[a]	25.09 ± 0.03	138 ± 6	14.8 ± 0.5	0.01

[a] Average value from two or more runs.

Discussion

In order to understand electrolyte behavior in HFP, it is helpful to compare the properties of this solvent to those of TFE and 2-PrOH, the hydrocarbon analog of HFP. Pertinent data are summarized in Table III. As compared to TFE and 2-PrOH, HFP exhibits lower viscosity, boiling point, and entropy of vaporization, all of which point to considerably less intermolecular hydrogen bonding in HFP. However, not only is HFP more acidic, but formation of a hydrogen-bonded complex between acetone and HFP is far more exothermic than acetone–TFE, a difference of 2.2 kcal/mol. In view of its greater effectiveness as a hydrogen bond donor, the minimal degree of intermolecular hydrogen bonding in HFP attests to its unsuitability

(14) J. C. Justice, *Electrochim. Acta*, **16**, 701 (1971); C. Treiner and J. C. Justice, *J. Chim. Phys.*, **68**, 56 (1971); J. C. Justice, private communication, to be published in Journal of Solution Chemistry. We thank Professor Justice for analyzing our results with his equations.
(15) N. Bjerrum, *Kgl. Dan. Vidensk. Selsk.*, 7, 9 (1926).
(16) R. L. Kay, *J. Amer. Chem. Soc.*, **82**, 2099 (1960).

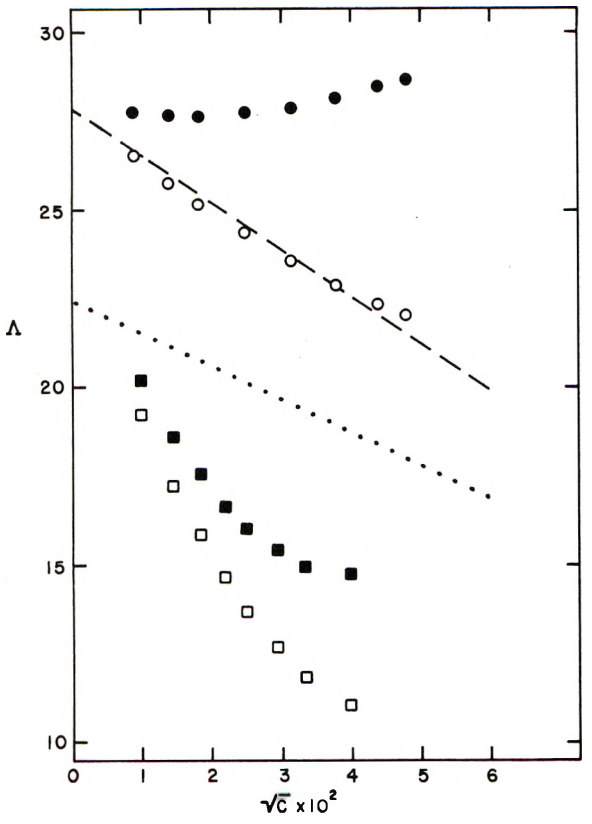

Figure 1. Conductance of *i*-Am_3BuNI in HFP and 2-PrOH: O, equivalent conductance in HFP; □, equivalent conductance in 2-PrOH; ●, $\Lambda + S\sqrt{c}$ in HFP; ■, $\Lambda + S\sqrt{c}$ in 2-PrOH. The dashed lines give the Onsager slope for (----) HFP and (····) 2-PrOH.

as a hydrogen bond acceptor. This is also reflected in the fact that although the compound is highly acidic in water, its autoprotolysis constant is low enough not to interfere with conductivity measurements, the specific conductance of HFP being at most 7×10^{-9} cm^{-1} ohm^{-1}.

Given the low dielectric constant of HFP, extensive ionic association is predicted by both the Fuoss[17]

$$K_A = (4\pi Na^3/3000)\ \exp(e^2/a\epsilon kT) \qquad (7)$$

and Bjerrum[15] theories

$$K_A = (N/1000)\int_a^q 4\pi r^2\ \exp(e^2/r\epsilon kT)dr \qquad (8)$$

In fact, for this dielectric constant the Fuoss treatment predicts a minimum association constant of 71 at an interionic separation of 11.2 Å between the centers of two ions in actual contact. The Bjerrum predictions decrease from 300 to 80 as this contact distance increases from 5 to 12 Å. Ordinarily, association constants of this magnitude are evaluated easily by any of several different conductance equations. With this solvent, however, such an analysis proved difficult. In order to illustrate this in detail, data for a typical run, *i*-Am_3BuNI, are analyzed in detail below. The values for concentrations and equivalent conductances are given in Table IV, as well as the $\Delta\Lambda$ values for each point for eq 1, 2, and 3. The $\Delta\Lambda$ values are the differences between the measured Λ and that calculated by eq 1, 2, or 3 and the parameters in Table V. Also shown in Table V for comparison are the corresponding parameters for *i*-Am_3BuNI in 2-PrOH.[18]

TABLE III: Properties of HFP, TFE, and 2-Propanol

	HFP	TFE	2-PrOH
ρ^{25}	1.605[a]	1.383[f]	0.781[j]
ϵ	16.7[a]	26.7[g]	19.4[k]
D, Debyes	2.05[b]	2.03[b]	1.68[l]
η, cP	1.62[a]	1.78[g]	2.08[j]
pK_A, water	9.30[c]	12.37[h]	~17[m]
ΔH form, acetone complex in CCl_4, kcal/mol	−5.94[d]	−3.72[d]	
Boiling point, °C	58.6[a]	73.75[f]	82.5[j]
Entropy of vaporization, Gibbs	26.2[e]	28.0[i]	28.3

[a] Reference 12. [b] A. Kivinen, J. Murto, and L. Kilpi, *Suom. Kemistilehti B*, **40**, 336 (1967). [c] W. J. Middleton and R. V. Lindsey, Jr., *J. Amer. Chem. Soc.*, **86**, 4948 (1964). [d] A. Kivinen, J. Murto, and L. Kilpi, *Suom. Kemistilehti B*, **40**, 301 (1967). [e] Calculated from data in J. Murto and A. Kivinen, *ibid.*, **40**, 258 (1967). [f] Reference 4. [g] J. Murto and E. Heino, *Suom. Kemistilehti B*, **39**, 263 (1966). [h] P. Ballinger and F. A. Long, *J. Amer. Chem. Soc.*, **81**, 1050 (1959); **92**, 795 (1960). [i] Pennsalt Chemicals Corp., "Trifluoroethanol," Booklet No. DC-1254, Philadelphia, Pa., 1956. [j] Reference 18. [k] W. Dannhauser and L. W. Bahe, *J. Chem. Phys.*, **40**, 3058 (1964). [l] Taken from NBS Circular No. 537. [m] Estimated, see ref 18.

TABLE IV: Equivalent Conductances and Corresponding Concentrations for *i*-Am_3BuNI in HFP

10^4C	Λ	$\Delta\Lambda$ (eq 1)	$\Delta\Lambda$ (eq 2)	$\Delta\Lambda$ (eq 3)
0.8218	26.566	−0.013	0.060	0.008
1.9560	25.772	−0.052	−0.027	−0.012
3.3276	25.156	−0.038	−0.051	−0.006
6.0423	24.345	0.024	−0.026	0.011
9.9331	23.562	0.080	0.022	0.009
14.439	22.906	0.076	0.041	−0.009
19.424	22.360	0.007	0.017	−0.008
23.030	22.035	−0.084	−0.035	0.007

In Figure 1 Λ as a function of $c^{1/2}$ for *i*-Am_3BuNI in HFP and in 2-PrOH has been plotted. Also included for both solvents are the Onsager slopes and the resulting values of $\Lambda + Sc^{1/2}$ for each measured concentration. The 2-PrOH data show a pattern typical of electrolyte solutions in solvents of dielectric constant below 20. All the measured points lie well below the Onsager slope due mainly to the high degree of ionic association. This is in sharp contrast to the HFP case where deviations from the Onsager slope are quite small and both positive and negative. The upper curve, $\Lambda + Sc^{1/2}$, would be a horizontal line equal to Λ_0 if the Onsager limiting behavior persisted throughout this concentration range. The deviations are accounted for by the higher order terms in the conductance equation and by ionic association.

The higher order terms in the Fuoss–Onsager eq 1, Ec ln c and Jc, are opposite in sign and for HFP both are large in magnitude. At highest concentration shown in Figure 1, Ec ln c is −7.81 and Jc is +8.57. Substraction of these terms from $\Lambda + Sc^{1/2}$, in other words solving eq 1 for Λ_0, gives a value of 27.88, deviating from the limiting Λ_0 by 0.08. This is the $\Delta\Lambda$ of Table IV. Although these values are small, it is the curvature evident in these deviations that is accounted for by ionic association in eq 2. However, this requires a negative association constant of

(17) R. M. Fuoss, *J. Amer. Chem. Soc.*, **70**, 5059 (1948).
(18) M. A. Matesich, J. A. Nadas, and D. F. Evans, *J. Phys. Chem.*, **74**, 4568 (1970).

TABLE V: Conductance Parameters for i-Am_3BuNI in HFP and 2-PrOH

Eq	Λ_0	K_A	a	$\sigma\Lambda$
		i-Am_3BuNI in HFP 25°		
1	27.95 ± 0.04		6.32 ± 0.09	0.06
2	27.83 ± 0.05	−44 ± 15	5.4 ± 0.3	0.05
3	27.94 ± 0.01	144 ± 3	14.9 ± 0.2	0.02
		i-Am_3BuNI in 2-PrOH 25°		
2	22.53 ± 0.01	1690 ± 10	8.0 ± 0.03	0.007
3	22.56 ± 0.01	1772 ± 5	12.4 ± 0.05	0.004

−44 with a value of $\gamma = 1.07$ at the highest concentration. Such a situation is physically absurd.

We have also analyzed the data in HFP with the Fuoss-Hsia equation[19] in which the $Jc^{3/2}$ is retained. The values of Λ_0 show little change from those given in Tables I and II. The values of a were greater by 1–3 Å then those shown in Table I. In every case, positive association constants were obtained, however, they ranged from 0.5 to 105. Only Me_4NBr and Me_4NClO_4 gave values of K_A equal to or larger than those predicted by eq 7.

The Justice treatment, on the other hand, gives association constants (Table II) that agree rather well with the degree of association predicted from Coulombic theories. This is reassuring since these theories should provide a good estimate of the minimum degree of ionic association to be expected under any circumstances, given the solvent properties. Such effects as dielectric saturation and multiple-step association increase the amount of ion pairing with large ions in a dielectric constant of 16.7; increases in a due to solvation leave K_A relatively unchanged.

The satisfactory fit of the conductance data by the Justice equation results from putting very large values of a (comparable to the Bjerrum critical distance q) into the J and $J_{3/2}$ terms. The resulting net increase in J is then compensated for by a corresponding increase in K_A. What is worrisome is that one gets out as K_A essentially what was put in as q, leading one to wonder whether the calculated K_A values are an artifact of the theory. On the other hand, in the original Fuoss-Onsager treatment, a corresponds to the contact distance between two hard-sphere ions moving through a continuum. With this model, the hydrodynamic and electrical boundary conditions are defined in an internally consistent way,[20] but the parameters evaluated are unsatisfactory.

In this situation, one is faced with the question of what criterion to use in determining the degree of ionic association from conductivity data. One approach is to invoke ionic association when it is impossible to fit the experimental data satisfactorily using an equation which, like eq 1, does not take association into account. Alternatively, one can begin by assuming that the minimum degree of association predicted by continuum theories (eq 7 and 8) must be present, and the selection of an appropriate equation is governed in part by that requirement.[21] There is a danger that the latter approach will give rise to artifacts of the analysis, particularly when the quality of experimental data is not good.

In spite of the unexpected difficulty in evaluating association constants, the results of this study reveal some very interesting characteristics of electrolyte behavior in 1,1,1,3,3,3-hexafluoro-2-propanol. The degree of ionic association is incredibly small for a series of salts in a solvent of such low dielectric constant. In examining the properties of HFP for an explanation of this behavior, its hydrogen-bonding ability is the most striking. The formation of tightly solvated complexes between HFP and anions seems very likely. When these solvated anions encounter tetraalkylammonium ions, the interionic contact distance is quite large, perhaps as large as 10 Å, the coulomb attraction is correspondingly diminished, and the ion pair dissociates readily.

One way of testing this is to add a small amount of HFP to a salt solution in an aprotic solvent. For Bu_4NBr and Bu_4NI in acetone, eq 2 shows Λ_0 values of 185 and 184, respectively, and association constants of 285 and 155. For the same salts in a 10% solution of HFP in acetone, preliminary experiments show a decrease of 30–35% in mobility[22] and negative association constants using eq 2. This clearly is consistent with extensive solvation of the anions, leading to greatly diminished ionic association.

Thus, electrolyte behavior in HFP closely parallels that observed in 2,2,2-trifluoroethanol for the same salts. It was unfortunately not possible to study the alkali halides in HFP due to their low solubility. This observation indicates that HFP is even less effective in solvating cations than TFE, which is consistent with its other properties.

In conclusion, 1,1,1,3,3,3-hexafluoro-2-propanol and trifluoroethanol are members of a solvent class distinctly different from other hydrogen-bonding solvents which interact with both cations and anions, and opposed to dipolar aprotic solvents which solvate cations preferentially. These properties of the polyfluorinated alcohols should make them a useful class of solvents in many practical applications.

Acknowledgment. This work was supported by Contract No. 14-01-001-1281 and 14-30-2615 with the Office of Saline Water, U. S. Department of the Interior.

(19) R. M. Fuoss and K.-L. Hsia, *Proc. Nat. Acad. Sci. U. S.*, **57**, 1550 (1967).
(20) See, however, the discussion in E. Pitts, B. E. Tabor, and J. Daly, *Trans. Faraday Soc.*, **65**, 849 (1969).
(21) The latter approach is exemplified by a recent study by C. DeRossi, B. Sesta, M. Battistini, and S. Petrucci, *J. Amer. Chem. Soc.*, **94**, 2961 (1972), of the conductance of KCl in mixed solvents in the dielectric constant range 18.8–71. No association was determined with eq 2; eq 1 fitted the data well within the experimental precision; and association was obtained with all equations when $\mathring{a}$ was set equal to q. However, since only four or five data points per set were determined, no definitive conclusions can be made since statistical analysis of a three-parameter equation with four points is questionable.
(22) This decrease in mobility is due at least in part to an increase in solution viscosity.

Effect of Urea Concentration upon the Activation Parameters for Fluidity of Water

J. C. MacDonald,* J. Serphillips, and J. J. Guerrera

Department of Chemistry, Fairfield University, Fairfield, Connecticut 06430 *(Received June 27, 1972)*

The effect of urea concentration over the range 0–7 M on the fluidity of aqueous solutions has been evaluated in terms of the parameters of the Arrhenius and Eyring equations, and in relation to the structural properties of water. The results confirm previous findings of others that urea is a structure breaker, that urea clustering begins at about 2 M urea, and that urea does have a concentration-dependent effect upon some properties of aqueous solutions. It may be generally true that nonlinearity of free energy of activation for fluidity plotted *vs.* concentration of added solute indicates formation of solute–solvent aggregates which become the principal kinetic entity for fluid flow.

The effect of aqueous urea concentration upon the Arrhenius activation parameters for viscous flow were previously reported.[1] Those data were in conjunction with measurements of polarographic diffusion coefficients of Zn^{2+} and the data suggested some change in solution structure at 2–3 M urea. Since those solutions necessarily contained 0.4 M KNO_3 as inert electrolyte for the polarographic measurements and the observed effects may not have been due solely to urea, viscosity measurements have now been made and from these data, activation parameters have been calculated for aqueous solutions of varying concentrations of urea only.

The effects of added urea upon the properties of water continue to be investigated, since explanation of protein denaturation, *e.g.*, by urea, is intimately connected with local liquid structure.[2] Since the previous report,[1] for example, there have appeared studies of heats of solution and nmr spectra of urea solutions,[3] nmr studies of rates of protolysis of urea,[4] interaction studies of urea and lysozyme,[5] ultrasonic studies of urea solutions,[6,7] solubility studies in urea solutions,[8] and partial molal volume studies in urea solutions.[9] Some of these studies[4,6] were over a range of urea concentrations and confirm the previous suggestion[1] that urea does indeed have a concentration-dependent effect upon liquid structure and that measurements of at least some properties of aqueous urea solutions at a single concentration are insufficient for definitive conclusions as to the effect of urea.

Experimental Section

All solutions were prepared in distilled water using reagent grade chemicals without further purification. Viscosity measurements were made with the use of an Ostwald viscometer calibrated using distilled water. Density measurements were made using a Westphal balance calibrated using distilled water. By using a Sargent Thermonitor for temperature control (±0.01°) and a Fisher thermometer having 0.1° subdivisions for temperature measurements, the viscosity measurements were reproducible to ±0.5% and the density measurements were more precise, ±0.1%.

Calculations

The temperature dependence of reciprocal viscosity ($1/\nu$) or fluidity (ϕ) was evaluated in terms of the parameters of an Arrhenius equation, $(1/\nu) = \phi = A \exp(-E_\phi/RT)$, it being assumed that the relationship of log (ϕ) *vs.* $1/T$ is linear over the temperature range of the measurements, 25–40°, and in terms of the Eyring equation[10]

$$\phi = (V/hN) \exp(-\Delta G^*/RT) = (V/hN) \exp(-\Delta H^*/RT) \exp(\Delta S^*/R)$$

The Arrhenius activation energy, E_ϕ, was taken as equal to ΔH^*, the Eyring energy of activation, and the Arrhenius A coefficient was equated with $(V/hN) \exp(\Delta S^*/R)$ to obtain ΔS^*, the entropy of activation; h and N are Planck's constant and the Avogadro number, respectively, V is the molar volume of the solvent, R is the gas constant in cal deg^{-1} mol^{-1}, T is the absolute temperature, and ν is viscosity in poise. Free energy of activation, ΔG^*, was then calculated from the Gibbs equation at 25°.

Results and Discussion

The calculated activation parameters using the APL language and 1130 computer are in Table I for both the data of urea in water, and of urea in 0.4 M aqueous KNO_3. Experimental reproducibility of these results was incorporated into the APL program by calculating standard deviations of all experimental viscosities from the linear least-squares regression line of the logarithmic form of the Arrhenius equation. The magnitudes of the deviation of experimental viscosities from a regression line using the Arrhenius data of Table I are confounded by the changing values of viscosity with temperature as well as by the logarithmic compression. However, since the viscosities ranged over 0.66–1.38 cP, and the maximum standard deviation in Table I is 0.0056 cP, then in the worst of cases

(1) J. C. MacDonald and J. J. Guerrera, *J. Chem. Eng. Data*, **15**, 546 (1970).
(2) W. P. Jencks, "Catalysis in Chemistry and Enzymology," McGraw-Hill, New York, N. Y., 1969, pp 332–338.
(3) S. Subramanian, T. S. Sarma, D. Balasubramanian, and J. C. Ahluwalia, *J. Phys. Chem.*, **75**, 815 (1971).
(4) R. L. Vold, E. S. Daniel, and S. O. Chan, *J. Amer. Chem. Soc.*, **92**, 6771 (1970).
(5) J. R. Warren and J. A. Gordon, *J. Biol. Chem.*, **245**, 4097 (1970).
(6) K. Arakawa, N. Takenaka, and K. Sasaki, *Bull. Chem. Soc. Jap.*, **43**, 636 (1970).
(7) O. Nomoto and H. Endo, *Bull. Chem. Soc. Jap.*, **43**, 2718 (1970).
(8) R. E. Lindstrom, *J. Pharm. Sci.*, **59**, 1695 (1970).
(9) W. A. Hargraves and G. C. Kresheck, *J. Phys. Chem.*, **73**, 3249 (1969).
(10) S. Glasstone, K. J. Laidler, and H. Eyring, "Theory of Rate Processes," McGraw-Hill, New York, N. Y., 1941, Chapter 9, pp 477–516.

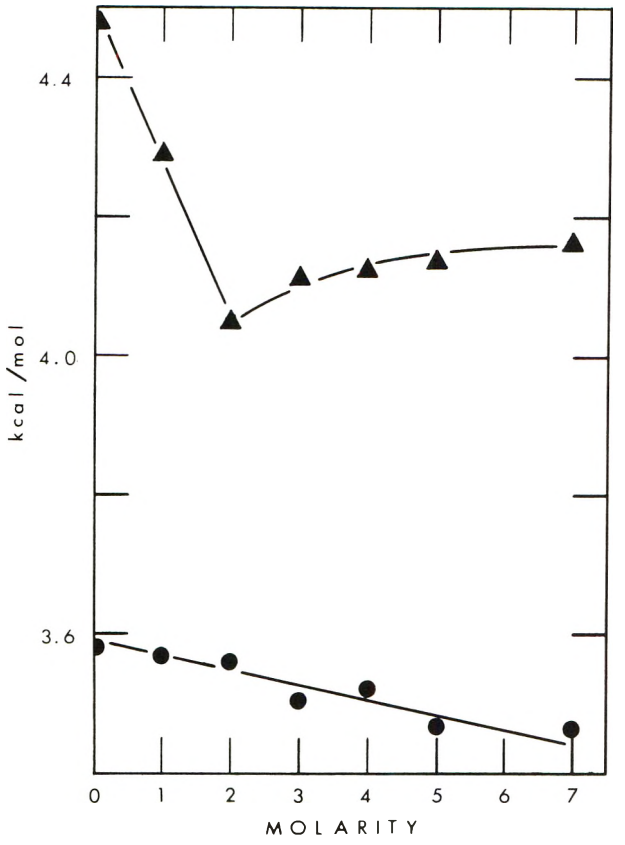

Figure 1. Energy of activation for fluidity *vs.* urea concentration. The circles represent the urea–water system; the triangles represent the urea–water–KNO_3 system.

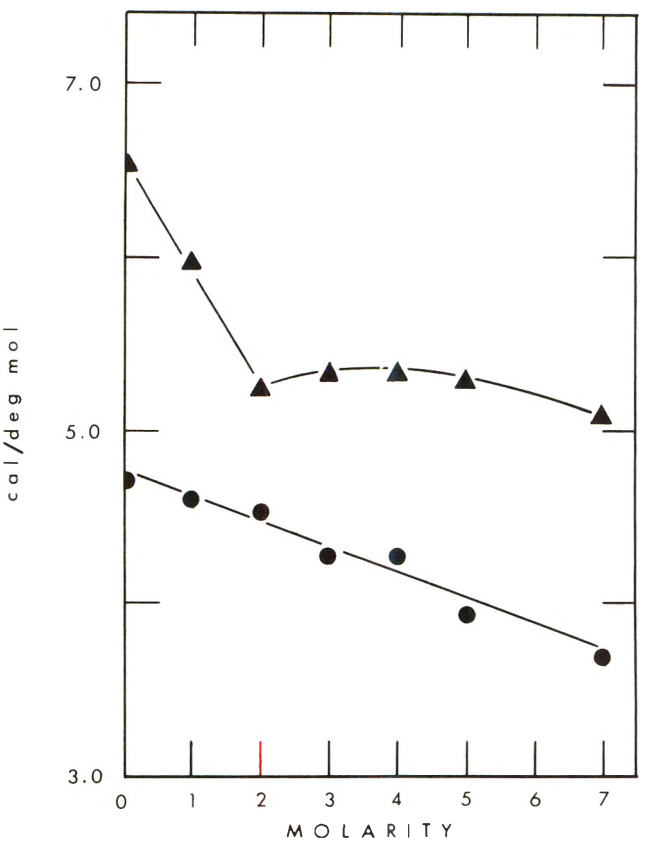

Figure 2. Entropy of activation for fluidity *vs.* urea concentration. The circles represent the urea–water system; the triangles represent the urea–water–KNO_3 system.

TABLE I: Activation Data for Fluidity

Urea, *M*	KNO_3, *M*	ΔH^*, kcal mol^{-1}	ΔS^*, cal deg^{-1} mol^{-1}	ΔG^*, kcal mol^{-1}	Arrhenius std dev,[a] cP
0	0	3.59	4.68	2.19	0.0006
1	0	3.57	4.60	2.19	0.0021
2	0	3.56	4.52	2.21	0.0024
3	0	3.50	4.24	2.24	0.0010
4	0	3.52	4.23	2.26	0.0016
5	0	3.46	3.89	2.30	0.0009
7	0	3.46	3.66	2.37	0.0014
0	0.4	4.48	6.51	2.37	0.0032
1	0.4	4.29	5.97	2.36	0.0045
2	0.4	4.05	5.22	2.36	0.0048
3	0.4	4.11	5.31	2.39	0.0029
4	0.4	4.12	5.27	2.42	0.0039
5	0.4	4.14	5.23	2.45	0.0030
7	0.4	4.16	5.04	2.53	0.0056

[a] The standard deviation of experimental viscosities from the linear least-squares regression line of the logarithmic form of the Arrhenius equation.

the data fit an Arrhenius equation with a relative standard deviation of about 0.9%.

The intent was to investigate the nonlinear variation of activation parameters in the three-component water–urea–KNO_3 solutions by determining activation parameters in the two-component water–urea system. The data at 25° for both the two- (ΔH_2^*, ΔS_2^*, ΔG_2^*) and three- (ΔH_3^*, ΔS_3^*, ΔG_3^*) component systems are in Figures 1–3.

ΔH_2^* and ΔS_2^* both decrease with increasing urea concentration confirming some previous findings[9,11,12] that urea is a structure breaker, although the concept of structure in water is only partly satisfactory.[13,14] ΔH_2^* measures the energy barrier to fluid motion and the decrease in ΔH_2^* with concentration indicates more fluidity, and thus less structure. The qualitative similarity of ΔH_2^* and ΔS_2^* results since ΔH_2^* here depends on resistance to shear and this is a function of system structure. ΔH_3^* and ΔS_3^* are also similar for the same reasons but the concentration dependence is qualitatively different from that of the two-component mixture, likely due to interactions involving KNO_3. ΔH_3^* and ΔS_3^* both decrease more sharply than for the two-component system, up to about 2 *M* urea, followed by essentially no further change in ΔS_3^* and by a small increase in ΔH_3^*. The ΔH_3^* and ΔS_3^* measurements are explainable below 2 *M* urea as due at least to results of solvent interactions of individual KNO_3 and urea molecules; both KNO_3,[15] and urea (Figures 1 and 2) in water individually decrease ΔH^* and ΔS^* for fluidity; further, urea adduct formation with KNO_3 may be affecting the activation parameters. The sharper slopes for the combined system of urea–KNO_3–water are not then unexpected although there is no proof from available data as to whether the sharper slopes are due to the combined effects of urea–water and of KNO_3–water interac-

(11) G. C. Kresheck and L. Benjamin, *J. Phys. Chem.*, **68**, 2476 (1964).
(12) H. S. Frank and F. Franks, *J. Chem. Phys.*, **48**, 4746 (1968).
(13) A. Holtzer and M. F. Emerson, *J. Phys. Chem.*, **73**, 26 (1969).
(14) L. G. Hepler, *Can. J. Chem.*, **47**, 4613 (1969).
(15) W. Good, *Electrochim. Acta*, **11**, 759 (1966).

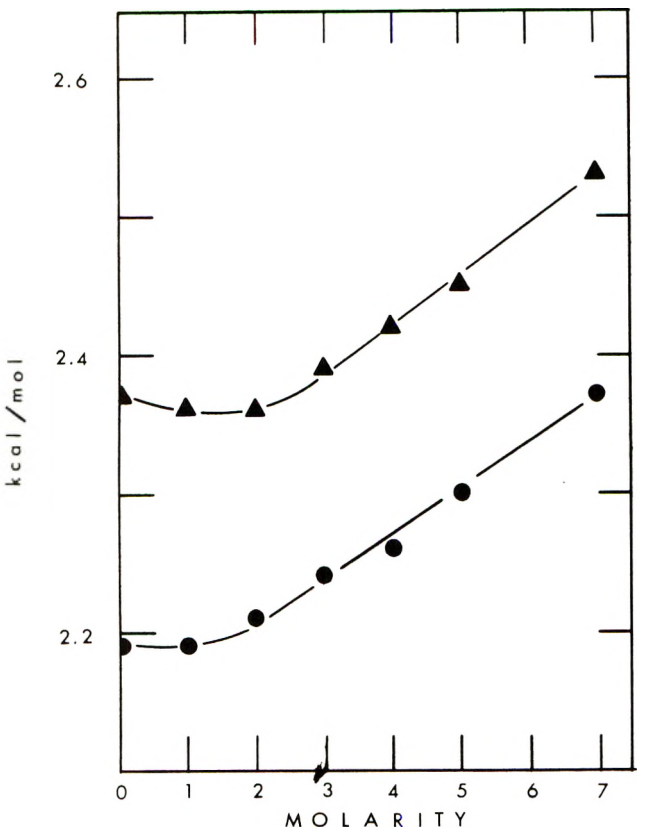

Figure 3. Free energy of activation for fluidity *vs.* urea concentration. The circles represent the urea–water system; the triangles represent the urea–water–KNO_3 system.

tions rather than a concerted urea–KNO_3–water interaction. The directional changes in ΔH_3^* and ΔS_3^* at about 2 *M* urea can be explained using two recent findings: (1) nmr studies of rates of protolysis of urea[4] show a concentration dependence of rate laws that suggests formation of urea aggregates above 2 *M* urea; (2) ultrasonic absorption coefficients in aqueous urea solutions[6] are concentration dependent with the observed structure breaking effect being greatest only above 2 *M* urea. The effect at higher urea concentrations likely then involves clusters of urea molecules and interactions of these clusters with KNO_3. Despite the qualitative difference in Figures 1 and 2 of $\Delta H_2^* - \Delta H_3^*$ and of $\Delta S_2^* - \Delta S_3^*$, ΔG_2^* and ΔG_3^* in Figure 3 are qualitatively similar. ΔG_2^* shows little change until a concentration of about 2 *M* urea beyond which there is a linear increase in ΔG_2^* with urea concentration, corresponding to a slope of 30 cal mol^{-2}; ΔG_3^* passes through a very shallow minimum between 1–2 *M* urea and then increases to a constant slope of 40 cal mol^{-2}. The similar slopes indicate minimal effect of KNO_3 upon ΔG^* following urea cluster formation and thus this cluster formation is more favored energetically than is urea–KNO_3 adduct formation. The ΔG_2^* and ΔG_3^* then appear to measure, as do also ΔH_3^* and ΔS_3^*, different physical processes above and below 2 *M* urea the concentration above which urea clustering may affect experimental results. ΔG_2^* is essentially constant until urea clustering apparently begins at about 2 *M* urea. Since ΔG_2^* controls the rate of flow, which is governed by the slowest step in the fluid process, the data suggest that below 2 *M* urea there is essentially no affecting of the fluid process by urea, in spite of the decrease in ΔH_2^* and ΔS_2^* both of which indicate structure breaking; the concept of structure is thus only partly satisfactory.[13,14] The calculation of ΔG_2^* at 25° from ΔH_2^* and ΔS_2^* showed ΔG_2^* to be independent of urea concentration below about 2 *M* urea. However, above 2 *M* urea, although ΔH_2^* and ΔS_2^* both give linear plots over 0–7 *M* urea, ΔG_2^* in Figure 3 calculated from the Gibbs equation increases with urea concentration. The slowest step in the fluid motion is dependent on the ease with which translation of the principal kinetic entity occurs. The data suggest this entity to be likely water itself below 2 *M* urea and that above 2 *M* urea the principal kinetic entity for fluid flow is likely an aggregate of urea and water. This is consistent with present concepts of protein denaturation by urea where the effect is thought to be due in part to the formation of water–urea aggregates, yielding less water–protein interaction, and subsequent unwinding of the protein chain.[2] The same concept was used to explain the above mentioned nmr[4] and sonic data.[6] The similarity of ΔG_2^* and ΔG_3^* plotted *vs.* urea concentration then suggests that 0.4 *M* KNO_3 has minimal effect upon the principal kinetic entity in solutions varying in urea concentrations. Indeed, over a range of at least 0–4 *M* KNO_3, this ionic solute has no effect on ΔG^* for fluidity.[15]

Finally, it is of interest that plots of ΔG^* for fluidity of aqueous solutions of electrolytes *vs.* electrolyte concentration[15-18] always were essentially linear, and the less the slope the less was the effect of solute upon fluid flow; however, a plot of ΔG^* for fluidity of dimethyl sulfoxide–water solutions *vs.* concentration[19] is nonlinear and the formation of an aggregate is suggested not only by that ΔG^* data but also by other experimental data.[20,21] It may be generally true that nonlinearity of ΔG^* for fluidity plotted *vs.* concentration indicates formation of solute–solvent aggregates which become the principal kinetic entity for fluid flow.[22]

(16) W. Good, *Electrochim. Acta*, **9**, 203 (1964).
(17) W. Good, *Electrochim. Acta*, **10**, 1 (1965).
(18) W. Good, *Electrochim. Acta*, **11**, 767 (1966).
(19) S. A. Schichman and R. C. Amy, *J. Phys. Chem.*, **75**, 98 (1971).
(20) R. K. Wolford, *J. Phys. Chem.*, **68**, 3392 (1964).
(21) J. R. Jezorek and H. B. Mark, Jr., *J. Phys. Chem.*, **74**, 1627 (1970).
(22) Listings of experimental viscosities and densities will appear following these pages in the microfilm edition of this volume of the journal. Single copies may be obtained from the Business Operations Office, Books and Journals Division, American Chemical Society, 1155 Sixteenth St., N.W., Washington, D. C. 20036. Remit check or money order for $3.00 for photocopy or $2.00 for microfiche, referring to code number JPC-73-370.

Dielectric Constants of Amide–Water Systems

Peter Rohdewald* and Manfred Moldner

Institut für pharmazeutische Chemie, Westfälische Wilhelms-Universität, 44 Münster, Germany *(Received June 27, 1972)*

Dielectric constant measurements were carried out on mixtures of unsubstituted, *N*-monoalkylated, and *N,N*-dialkylated aliphatic amides with water over the whole concentration range. The formamide–water and acetamide–water systems show positive deviations from ideal behavior of mixtures, while in mixtures of *N*-monoalkylated and *N,N*-dialkylated amides the deviations are negative. The positive deviations of $\Delta\epsilon$ are qualitatively attributed to a "build-in" of the components of the mixture in the structure of the respective solvent. The decreasing values of $\Delta\epsilon$ in the amide-rich region of the aqueous mixtures of the alkylated amides are explained by an interstitial solvation of water into the structure of the amides, whereas in the water-rich region the decrease in $\Delta\epsilon$ should result from the breaking of amide aggregates and the hydrophobic solvation of the alkyl moieties.

Introduction

Extending Hildebrand's solubility parameter theory[1] to semipolar and polar systems and observing an empirical equation which links the dielectric constant ϵ and the solubility parameter δ, $\delta = 7.5 + 0.2\epsilon$, Paruta and coworkers[2] postulated that "a maximum solubility of a given solute should occur within a particular narrow dielectric constant range, regardless of whether this dielectric constant is that of a pure solvent or that of an appropriate mixture of two solvents." Experimentally this hypothesis proved to be at first particulary successful,[2-4] but later the same author concluded that the observed dependence of peak solubility on the dielectric constants of binary mixtures is restricted to the given solvent system and not independent of the solvent system used.[5] The influence of the dielectric constant of binary or tertiary mixtures on the solubility of drugs was studied with the aid of an "approximated dielectric constant" (ADC). Assuming that the DC of a mixture of two or more solvents is directly proportional to the concentration of the individual solvents, Moore[6] calculated the ADC as follows

$$\mathrm{ADC} = [\Sigma(\%\ \mathrm{solvent}_1)(\epsilon_1) + (\%\ \mathrm{solvent}_2)(\epsilon_2) + \ldots (\%\ \mathrm{solvent}_x)(\epsilon_x)]/100$$

Although the results of Moore[6] first indicated the usefulness of the ADC to predict the solubilities of drugs in solvent mixtures, a recent paper showed that ADC had only a very limited ability to predict the solubilities.[7]

The aliphatic amides cover a very wide range of dielectric constants (from 20 to 190), therefore these substances seem to be an optimal class of water-miscible solvents for use in an extended study of the interrelations between the solubility of drugs and the dielectric constants of the pure amides and also of their aqueous mixtures. A knowledge of the dielectric constants of aqueous amide mixtures is not only important for the possible elucidation of the importance of the DC in solubility problems but also in the use of aqueous amide systems as electrolytic solvents or as polar solvents for kinetic investigations.

As far as we know, the dielectric constants of binary aqueous amide systems have not been the subject of a systematic investigation. Only the dielectric constants for the systems *N,N*-dimethylformamide–water[8,9] and *N*-butylacetamide–water[9] have been reported.

In our investigations we have included the unsubstituted amides formamide (FA), acetamide (AA), and propionamide (PA). In the series of FA and AA derivatives the length of the *N*-alkyl groups was changed for both the mono- and the dialkylated derivatives. The influence of the acid alkyl groups was investigated in the series of *N*-monomethylated amides going from *N*-methylformamide (NMF) to *N*-methylpropionamide (NMP).

The dependence of the dielectric constants of the binary systems on the nature of the amide substituents should give some indications of the liquid structure of the amide–water systems.

Experimental Section

N-Isopropylformamide (NIPF) was prepared from isopropylamine and methyl formate. The other commercially available liquid amides were treated with powdered CaO for 5–6 days, further dried by passage through a column of molecular sieve (4 Å, previously heated at 400°), and distilled under vacuum in an atmosphere of dry nitrogen. The middle fraction comprising 60% was retained. *N*-Methylacetamide (NMA) was azeotroped with toluol. AA was recrystallized twice from absolute ethanol and once from $CHCl_3$; mp 81°. PA was recrystallized twice from benzene; mp 80.5°. Purified water with a conductivity of 1–2 μohms cm^{-1} was obtained after deionization and double quartz distillation.

Refractive index measurements were made with an Abbe refractometer at 25 ± 0.05°; the densities were obtained using specific gravity bottles, capacity 25 ml at 25 ± 0.01°. The amide–water mixtures were prepared volumetrically using the Multidosimat F 415 from Methrom A.G., accuracy $\pm 10^{-2}$ ml.

(1) J. H. Hildebrand and R. L. Scott, "The Solubility of Nonelectrolytes," 3rd ed, Dover Publications, New York, N. Y., 1964, p 150.
(2) A. N. Paruta, B. J. Sciarrone, and N. G. Lordi, *J. Pharm. Sci.*, **53**, 1349 (1964).
(3) A. N. Paruta, B. J. Sciarrone, and N. G. Lordi, *J. Pharm. Sci.*, **54**, 838 (1965).
(4) A. N. Paruta, B. J. Sciarrone, and N. G. Lordi, *J. Pharm. Sci.*, **54**, 1325 (1965).
(5) A. N. Paruta and S. Irani, *J. Pharm. Sci.*, **56**, 1565 (1967).
(6) W. E. Moore, *J. Amer. Pharm. Ass., Sci. Ed.*, **47**, 855 (1958).
(7) C. Sunwoo and H. Eisen, *J. Pharm. Sci.*, **60**, 238 (1971).
(8) G. Douheret and M. Morenas, *C. R. Acad Sci., Ser. C*, **264**, 729 (1967).
(9) R. Reynand, *C. R. Acad. Sci., Ser. C*, **266**, 489 (1968).

TABLE I: Physicochemical Data of Some Aliphatic Amides

Amide	$n^{25}D$	ρ_4^{25}, g cm^{-3}	κ_{25}, cm^{-1} ohm^{-1}	ϵ_{25}
1-Chloro-*N,N*-dimethylacetamide	1.4753	1.1746	2×10^{-5}	49.4
N,N-Diethylformamide (DEF)	1.4320	0.9017	4.8×10^{-7}	28.4
	1.4352[a]	0.9057[b]		29.6[c]
		0.9061[c]		
N,N-Diethylacetamide (DEA)	1.4370	0.9080	7.5×10^{-7}	30.4
	1.4396[b]	0.9045[b]		32.1[c]
		0.9080[c]		
1-Chloro-*N,N*-diethylacetamide	1.4675	1.0848	5×10^{-6}	39.2
	1.4694[d]			
N,N-Diethylacetoacetamide (DEDEA)	1.4685	0.9905	9×10^{-7}	40.8
N,N-Diisopropylformamide (DIPF)	1.4316	0.8978	1.7×10^{-5}	24.2
	1.4371[e]			
N,N-Dipropylacetamide (DPA)	1.4416	0.8844	4×10^{-7}	23.2
	1.4411[e]	0.8891[c]		24.5[c]
N-Methylformamide (NMF)	1.4305	0.9985	7×10^{-6}	186.9
	1.4310[f]	0.9976[f]	5×10^{-5} [f]	182.4 [f]
N-Ethylformamide (NEF)	1.4289	0.9451	2×10^{-5}	101.5
	1.4320	0.9447		102.7 [g]
N-Isopropylformamide (NIPF)	1.4274	0.9081	1.7×10^{-5}	65.7
	1.4289[h]	0.9115[h]	8.5×10^{-7} [h]	68.3[h]

[a] H. Böhme and F. Soldan, *Chem. Ber.*, **94**, 3109 (1961). [b] B. V. Joffe, *Zh. Obsch. Khim.*, **25**, 902 (1955), values at 20°. [c] Reference 13. [d] M. Neemann, *J. Chem. Soc.*, 2525 (1955). [e] J. H. Robson and G. Reinhart, *J. Amer. Chem. Soc.*, **77**, 498 (1955), values at 20°. [f] Reference 15. [g] Reference 12. [h] D. Wagner, Dissertation, 1946, Stuttgart, values at 30°.

The dielectric constants were measured using the cells MFl_2-MFL_4, volume 50 ml, together with the Multidekameter from WTW. Measurements were made at 10 mHz and 25 ± 0.02°. The cells used were calibrated with purified NMA, water, *N,N*-dimethylformamide (DMF), acetone, benzyl alcohol, and ethylenechloride as standard liquids. The accuracy of the dielectric constants is ±0.3–0.5%. To avoid air bubbles in the mixtures the measurements were carried out 5 hr after mixing; freshly distilled liquids were used. Precautions were observed at all times to minimize the atmospheric contamination of the amides.

Results and Discussion

The dielectric constants of amides used in our investigations are listed in Table I together with their refractive indices, densities, and conductivities. Some comparisons with literature data are given only in cases of (small) deviations from literature data or for differences in the temperature used by other authors.

For NMA we obtained a DC value of 179 in agreement with the value of Dawson, *et al.*, of 178.9 [10] for 30°. The further purification by zone refining seems to be unnecessary in view of the instability of the highly purified NMA, DC 191.3,[11] in the presence of moisture, considering the following investigation of amide–water mixtures. The dielectric constants for the other amides used were in perfect agreement with the literature data.

From Table I it will be seen that the introduction of chloro atoms or the CH_3CO group into the dialkylated amides causes an increase of the DC of about 10 units as would be expected from the higher polarity of these amides. In contrast the monoalkylated amide *N*-methyl-2-chloroacetamide possesses a very low DC of 92.3 [12] when compared to the value for NMA cited previously. The steric hinderance to chain association seems to be responsible for the lowering of the DC in the monosubstituted amides[12] whereas the dialkylated amides are only slightly associated[13,14] and therefore an increase in the dipole moment contributes to the increase in the DC.

The results of the DC measurements on the amide–water systems are expressed as the excess in the DC. $\Delta\epsilon = \epsilon_{obsd} - \epsilon_{id}$, where $\epsilon_{id} = \epsilon_1 X_1 + \epsilon_2 X_2$, X is the mole fraction of the component.

All amide–water mixtures deviate widely from the behavior of ideal mixtures (Figures 1–4). The dielectric constant curves for mixtures of the unsubstituted amide and water (Figure 1) show a certain parallelism. The curve of AA is extrapolated to $\epsilon = 74$ for pure AA, obtained from mixtures of AA and FA.[15] The less soluble PA seems to exhibit a deviation from linearity toward lower DC values like the other two amides, although the DC of pure PA is not known.

In the systems FA–H_2O and AA–H_2O nearly the same positive deviations from ideal behavior appear, with a well-marked maximum between 45 and 50 mol % amide (Figure 2).

In Figures 3 and 4 the negative deviations, $\Delta\epsilon$, for the mono- and dialkylated amides are shown. The minima grow more pronounced with increasing chain lengths of the *N*-alkyl groups of the disubstituted amides, whereas for the monosubstituted amides no simple correlation between chain lengths and $\Delta\epsilon$ could be observed. The results are summarized in Table II. It is obvious that the magnitude of the minima in $\Delta\epsilon$ is related to the chain length of the *N*-alkyl and the acyl groups of the amides, except for the differences between the *N*-methyl and *N*-ethyl groups. The $\Delta\epsilon$ values of the formamides are generally lower than those of the corresponding acetamides.

(10) L. R. Dawson, P. G. Sears, and R. H. Graves, *J. Amer. Chem. Soc.*, **77**, 1986 (1955).
(11) O. D. Bonner and G. B. Woolsey, *J. Phys. Chem.*, **75**, 2879 (1971).
(12) P. G. Sears and W. C. O'Brien, *J. Chem. Eng. Data*, **13**, 112 (1968).
(13) M. Steffen, *Ber. Bunsengesell. Phys. Chem.*, **74**, 505 (1970).
(14) S. J. Bass, W. I. Nathan, R. M. Maighan, and R. H. Cole, *J. Phys. Chem.*, **68**, 509 (1964).
(15) G. R. Leader and J. F. Gormley, *J. Amer. Chem. Soc.*, **73**, 5731 (1951).

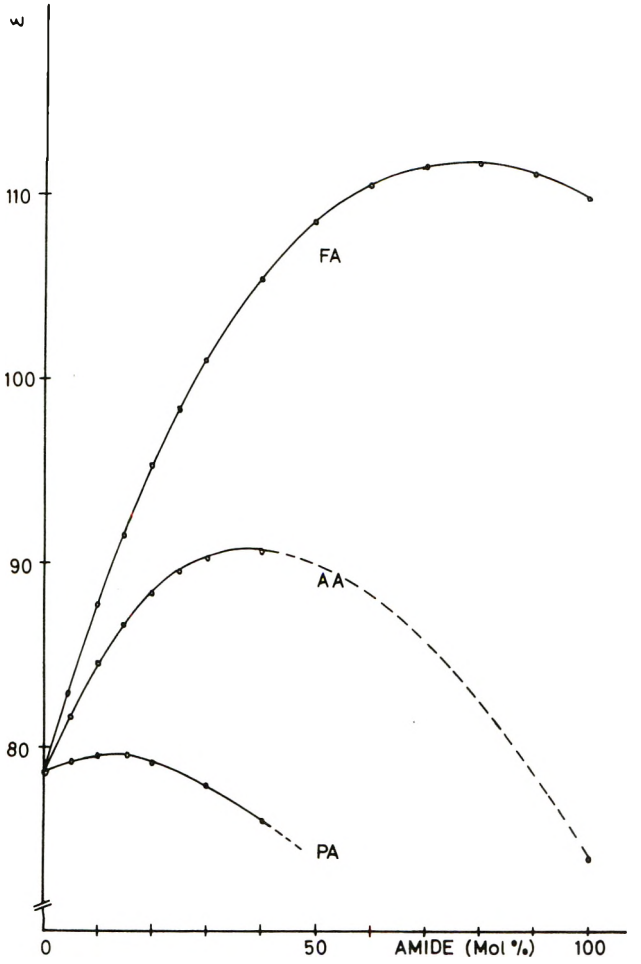

Figure 1. Dielectric constants of the amide–water systems for the unalkylated amides, as a function of the amide concentration. The dielectric constant curve for acetamide is extrapolated to the value of 74 for pure AA;[15] AA and PA are not completely soluble in water.

The position of the minima in $\Delta\epsilon$ is nearly independent of the length of the acyl or *N*-alkyl groups of the *N*-monoalkylated amides; only in the case of NIPF–H_2O is the minimum markedly shifted to a lower amide concentration, corresponding to a molar ratio of 1 amide:2 H_2O.

For the dialkylated amides the molar ratio at the minimum is changed regularly with each additional CH_2 group from 1:1 for DMA–H_2O to 1:3 for DPA–H_2O.

The results demonstrate clearly that the use of "approximated" dielectric constants of amide–water mixtures will lead to erroneous results especially for amides with larger alkyl groups; in this case the deviation from additivity in the minima is between 20 and 40% (Table II). The remarkable contrast between the unalkylated amides with positive $\Delta\epsilon$ values on the one hand and the mono- and dialkylated amides with negative $\Delta\epsilon$ values on the other hand requires some reflection.

Accepting the existence of a large number of cyclic associates in the pure unalkylated amides,[16] the $+\Delta\epsilon$ values could be interpreted as a "breaking-up" of cyclic amide associates through the formation of water–amide bonds. The diminuition of the number of cyclic associates where the dipoles are more or less antiparallel should lead to an increase in the dielectric constant of the amide–water systems.

The high dielectric constant of FA is in disagreement with a preferential cyclic association and its low electric

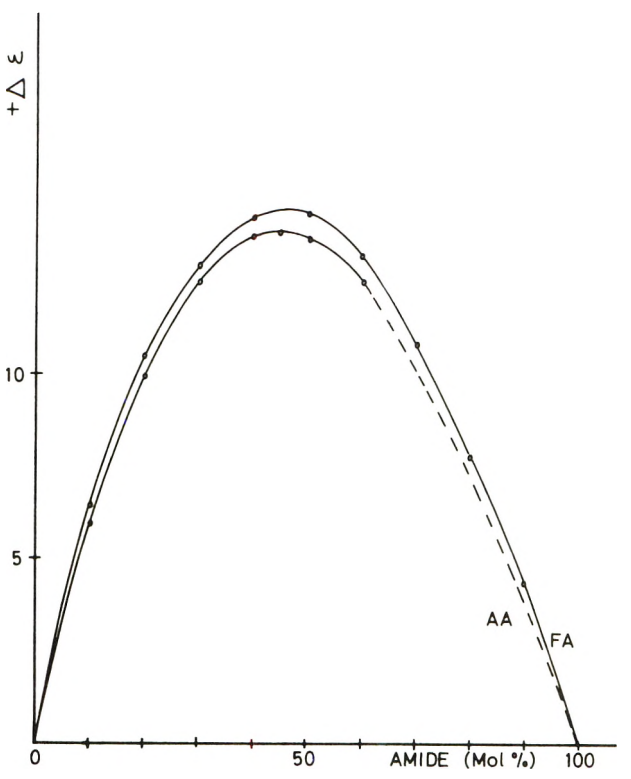

Figure 2. Positive $\Delta\epsilon$ values of the unalkylated amides as a function of the amide concentration.

TABLE II: Positions of the Maxima of $\Delta\epsilon$ and the Per Cent Deviation between the Observed DC and the ADC

Amide	Mol % amide at $\Delta\epsilon$ max	$\Delta\epsilon$, $\epsilon_{obsd} - \epsilon_{id}$	ADC − DC, %
AA	45	+13.9	+14.9
FA	46	+14.5	+18.8
NMF	60	−11.8	−8.1
NMA	50	−18.4	−14.1
NMP	57	−33.5	−25.2
NEF	60	−4.8	−5.2
NIPF	30	−8.5	−10.1
NEA	50	−16.4	−16.0
DMF	46	−8.8	−14.8
DEF	33	−16.5	−26.6
DMA	44	−9.8	−16.3
DEA	33	−14.8	−23.5
AEDEA	33	−13.5	−20.5
DPA	25	−26.4	−40.7

moments. Starting from the crystal structure of AA[16] it is possible to construct highly polar double chains of the unalkylated amide with a parallel ordering of the individual dipoles. Such chain associated unalkylated amides are in agreement with the high dielectric constant of FA and with the results of Tyuzyo[17] from measurements of the enthalpy of vaporization. Following the interpretation of Reynand[9] that the "break-up" of the associated chains of the *N*-monoalkylated amides is responsible for the minimum in $\Delta\epsilon$, one must expect minima also in the aqueous mixtures of FA and AA.

For the pure disubstituted amides dipolar head-to-tail

(16) M. Davies and H. E. Hallam, *Trans. Faraday Soc.*, **47**, 1170 (1951).
(17) K. Tyuzyo, *Bull. Chem. Soc. Jap.*, **30**, 851 (1957).

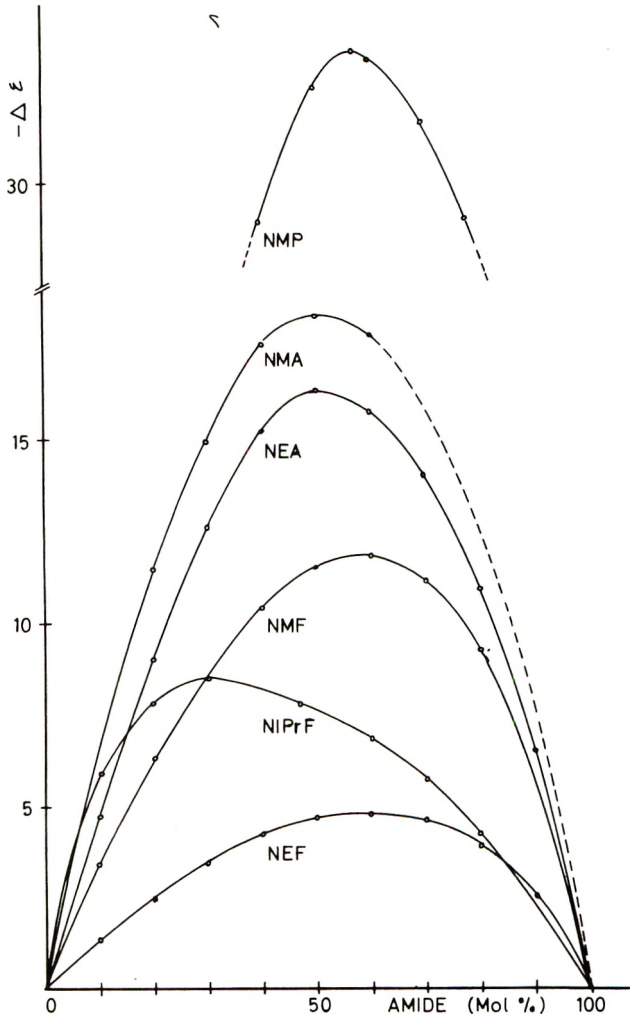

Figure 3. Negative $\Delta\epsilon$ values of the *N*-monoalkylated amides as a function of the amide concentration.

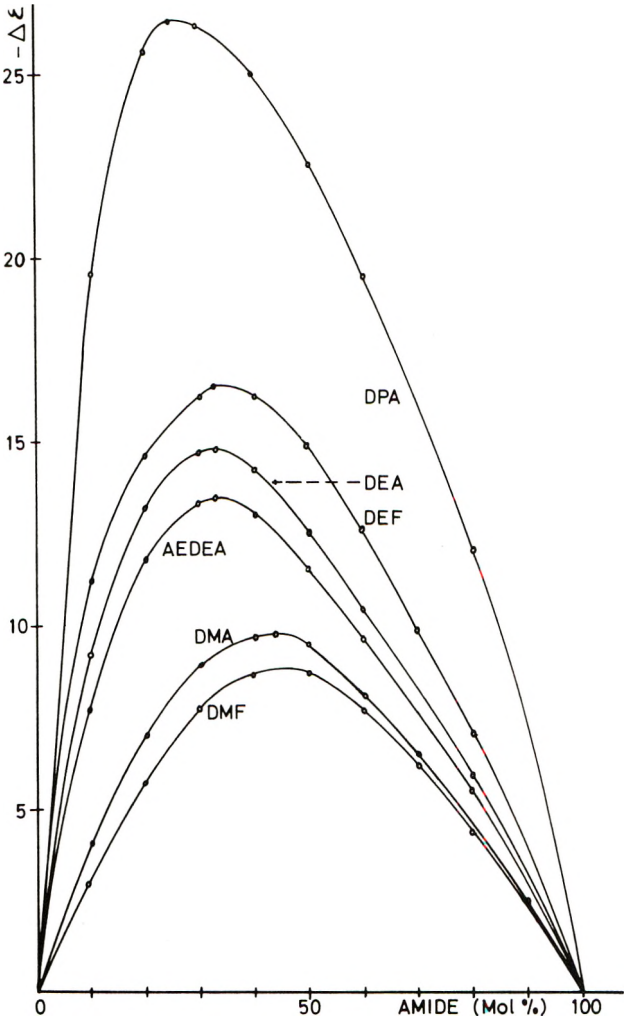

Figure 4. Negative $\Delta\epsilon$ values of the *N,N*-dialkylated amides as a function of the amide concentration.

associations with antiparallel dipoles are proposed[18] in accordance with the low dielectric constants. From this structure model an increase in the dielectric constant should occur in water mixtures because the weak bonding of the amide associates will be disturbed. If one considers only the amide structures there are the following possibilities for the changes in $\Delta\epsilon$ after mixing with water. (1) If the unalkylated amides consist mainly of cyclic associates, the unalkylated and the dialkylated amides will show positive $\Delta\epsilon$ values. (2) If the unsubstituted amides are primarily chain associated, the *N*-monoalkylated and the unalkylated amides should have negative $\Delta\epsilon$ values. The experimental results are in disagreement with the above possibilities.

We prefer to take under consideration the different modes of the changes in density and viscosity of the amide–water systems. The FA–H_2O system shows an increase in volume,[19] whereas in aqueous mixtures of the mono- and disubstituted amides a decrease in volume is observed.[20] The viscosities of aqueous formamide and acetamide solutions are abnormally low;[21] in contrast, aqueous mixtures of *N*-mono- and disubstituted amids show large viscosity maxima.[20]

We suggest that, from the quite different behavior of the unalkylated amides on the one hand and the *N*-alkylated amides on the other hand, the change in liquid structure is responsible for the divergent signs of $\Delta\epsilon$. Avoiding the terms structure breaking or structure forming, the mixing of the unalkylated amides with water leads to a loose liquid structure whereas with aqueous mono- and dialkylated amide solutions a more dense liquid structure is obtained. We believe that these different liquid structures are reflected by the different signs of $\Delta\epsilon$.

Similar possibilities for the formation of H-bonded networks exist for the amide and the water molecules because both molecules can act as H donors as well as H acceptors. We assume that the unalkylated amides are built-in *via* H bonding into the water structure and *vice versa*. The strengthening of the H bonds in the binary system and the increase in the dielectric constant should be the result of a more parallel ordering of the individual dipoles in the mixtures, resulting from the planar structure of the amide molecules.

The dense liquid structure in systems with high amide content can be explained by the interstitial solvation of water molecules in the amide structure. With increasing water content of the mixture, the alkyl groups of the amides are more and more exposed to the water and a denser

(18) T. Yonezawa and I. Morishima, *Bull. Chem. Soc. Jap.*, **39**, 2346 (1966).
(19) G. J. Burrows, *J. Roy. Soc. New South Wales*, **53**, 74 (1919).
(20) P. Assarsson and F. R. Eirich, *J. Phys. Chem.*, **72**, 2710 (1968).
(21) J. A. Rupley, *J. Phys. Chem.*, **68**, 2002 (1964).
(22) F. Franks in "Hydrogen-bonded Solvent-Systems," A. K. Covington and P. Jones, Ed., London, 1968, p 42.

packing of the water molecules around the hydrocarbon moieties occurs. Both effects lead to a more dense liquid structure compared with the water structure, followed by volume decrease and viscosity increase. Insulated water molecules possesses after all a lower dielectric constant than the H-bonded water molecules in pure water.

Even if the changes in the sign of $\Delta\epsilon$ may be qualitatively explained by the loose or dense structures of the amide–water systems, a quantitative agreement between the maxima or minima of the density and viscosity and the $\Delta\epsilon$ values is nonexistent. Irrespective of the structure of the *N*-mono- or *N,N*-dialkylated amides, the minima in ΔV occur at 40 mol % amide.[20] The viscosity maxima for NMA and NEA are found at 50 mol %. The dialkylated amides show viscosity maxima close to 25 mol % amide without a change in the position of the maximum with increasing length of the *N*-alkyl group, going from the methyl to the propyl substituents.[20]

The displacement of the minimum in $\Delta\epsilon$ toward lower amide concentration with increasing number of *N*-alkyl groups, as in the case of the *N,N*-dialkylated amides, supports the hypothesis of an interstitial solvation of water in the amide structure. The minimum in the system NIPF–H_2O at 30 mol % amide can be interpreted in the same manner.

In the more parallel arranged chains of the *N*-monoalkylated amides the steric conditions for the formation of cavities should be almost independent of the length of the acyl or *N*-alkyl groups, except for chain branching or the simultaneous presence of longer alkyl groups (exceeding three C atoms) in the acyl and *N*-alkyl position. Also no shift in the minimum of $\Delta\epsilon$ is observed when going from the *N,N*-dialkylated formamides to the respective acetamides. Even the introduction of the aceto group into DEA does not change the position of the minimum of $\Delta\epsilon$ (Table II). That the presence of one more H-accepting group in the molecule does not alter the position of the minimum seems to be an indication that the hydration of the polar group is of little consequence for the $\Delta\epsilon$ values. From another point of view, the differences in the signs of $\Delta\epsilon$ should not be the result of an interstitial solvation of the small molecules in water. Even though the isomers AA and NMF have the same steric requirements for an interstitial solvation, the signs of their $\Delta\epsilon$ values are opposite.

Certainly the formation of H bonds between the amide molecules and water also influences the structure of the liquid and the dielectric constant of the system. No information is available on the number or conformation of these mixed associates, so that speculations on a change of the dielectric constant resulting from the structure of definite aggregates could not be established. The discrepancy of the positions of maxima or minima of different excess functions of aqueous amide mixtures is not unique. The reviewed results of investigations on the system dioxane–water[22] reflect most clearly that we are far from a perfect understanding of the structure of aqueous solvent systems.

With regard to all the possible interactions of amide–water systems, the postulation of definite hydrates does not seem to be justified according to the present results.

Krafft Points of Calcium and Sodium Dodecylpoly(oxyethylene) Sulfates and Their Mixtures

Masakatsu Hatō*

Research Institute for Polymers and Textiles, Sawatari-4, Kanagawa-ku, Yokohama, Japan

and Kōzō Shinoda

Department of Chemistry, Faculty of Engineering, Yokohama National University, Ooka-2, Minami-ku, Yokohama, Japan

(Received June 23, 1972)

The Krafft points of pure calcium and sodium dodecylpoly(oxyethylene) sulfates ($C_{12}H_{25}(OCH_2CH_2)_nSO_4M$, n = 0, 1, 2, and 3) have been determined. The Krafft points were depressed with an increase in oxyethylene chain length. It is noteworthy that the Krafft points of the calcium salts can be depressed effectively by an increase in oxyethylene chain length, and therefore such surfactants can be used in hard water. In order to gain an insight into the solubility and the Krafft point of $C_{12}H_{25}(OCH_2CH_2)_nSO_4Na$ in hard water, the Krafft points of binary surfactant mixtures of different gegenions or ethylene oxide chain length were studied over the entire range of composition. The Krafft points of binary surfactant mixtures can be explained semiquantitatively based on the model that the Krafft point is the melting point of the hydrated solid agent.

Introduction

The Krafft points of calcium salts of ionic surfactants are generally higher than room temperature, and therefore they are usually far less soluble than corresponding sodium salts and do not form micelles around room temperature. It is clear from our recent work on fluorinated surfactants[1] that the Krafft point is affected by the gegenion(s), structure of the lipophilic group, mixing of two kinds of surfactants, etc., just as the melting points of corresponding organic compounds are. These phenomena can be explained by the theory[2] that the Krafft point is the melting point of the hydrated solid agent. If the Krafft point of the calcium salt of an ionic surfactant is lowered by introducing the oxyethylene group into the molecule, such a surfactant may be used in hard water as well as soft. In the present paper, the relation between Krafft points and the structures of ionic surfactants has been studied in order to find ionic surfactants useful in hard water, *i.e.*, the Krafft points of sodium and calcium dodecylpoly(oxyethylene)sulfates ($C_{12}H_{25}(OCH_2CH_2)_nSO_4Na$ or $\frac{1}{2}Ca$, n = 0, 1, 2, 3) and the solubilities of sodium dodecylpoly(oxyethylene) sulfates in the presence of a bivalent salt have been studied.

Experimental Section

Materials. Pure poly(oxyethylene) dodecyl ethers were obtained from the Nikko Chemicals Co. The purity of these materials was more than 99% according to gas chromatographic analysis. A series of dodecylpoly(oxyethylene) sulfuric acids were synthesized by introducing SO_3 vapor into the poly(oxyethylene) dodecyl ethers at 30–35°.[3] Sodium salts were obtained by neutralizing these acids with sodium hydroxide and repeatedly recrystallizing from a mixture of 2-propanol and ethanol (3:1 by volume) after extracting the unreacted ethers with petroleum ether.[3] $C_{12}H_{25}(OCH_2CH_2)_3SO_4Na$ (average oxyethylene chain length given) was obtained through the kindness of Dr. Tokiwa of the Kao-Soap Co. Calcium salts ($C_{12}H_{25}(OCH_2CH_2)_nSO_4{}^1\!/_2Ca$, n = 1, 2, 3) were obtained by adding a 2-propanol solution of calcium chloride to 2-propanol solutions of the respective acids. The compounds were washed with 2-propanol to remove the hydrogen chloride produced and purified in the same way as the sodium salts. The compounds were identified by infrared spectroscopy[4] and elementary analysis (C,H). Sodium dodecyl and tetradecyl sulfates were obtained from the Kao-Soap Co. through the kindness of Dr. Arai. These salts were recrystallized three times from water after extraction of possible impurities with petroleum ether. Calcium dodecyl and tetradecyl sulfates have been obtained by metathesis in water between calcium chloride and the sodium salts, and were purified in the same way as above.

Procedures. Provided composition of a mixed micelle is constant, a solubility curve above the Krafft point shifts to lower temperature to the same extent (compared with the solubility curve of a pure compound).[5] It is also time consuming to determine the Krafft points of surfactant mixtures from the phase diagram. Thus, for the systems $C_{12}H_{25}SO_4{}^1\!/_2Ca$ + $C_{12}H_{25}(OCH_2CH_2)_nSO_4{}^1\!/_2Ca$, $C_{12}H_{25}OCH_2CH_2SO_4{}^1\!/_2Ca$ + $C_{12}H_{25}OCH_2CH_2SO_4Na$, and $C_{14}H_{29}SO_4{}^1\!/_2Ca$ + $C_{14}H_{29}SO_4Na$, the Krafft points of the mixtures were estimated from the solution temperatures of the surfactants at 1 wt % (0.031–0.035 equiv/10^3 g of H_2O) or, for the mixture $C_{12}H_{25}SO_4{}^1\!/_2Ca$ + $C_{12}H_{25}SO_4Na$, the Krafft point was estimated from the solubilities of 3 wt % (0.11 equiv/10^3 g of H_2O) solutions. The Krafft point estimated by this efficient method agrees within 1° with that determined by the phase diagram. The critical micelle concentrations (cmc) at 25° have been determined from electrical conductivity measurements. The electrical con-

(1) K. Shinoda, M. Hatō, and T. Hayashi, *J. Phys. Chem.*, **76**, 909 (1972).
(2) K. Shinoda, *et al.*, "Colloidal Surfactants," Academic Press, New York, N.Y., 1963, pp 7–8.
(3) F. Tokiwa and K. Ohki, *J. Phys. Chem.*, **71**, 1343 (1967).
(4) D. Hummel, "Identification and Analysis of Surface-Active Agents," Spectra Vol. No. 46, Interscience, New York, N.Y., 1962
(5) H. Nakayama, K. Shinoda, and E. Hutchinson, *J. Phys. Chem.*, **70**, 3502 (1966).

ductivity of water was 1.1 μmho/cm at 25°. The detailed procedures are described in the preceding paper dealing with fluorinated surfactants.[1] The calcium salts as well as the sodium salts behave as strong electrolytes below the cmc.

Results and Discussion

(1) Effect of Oxyethylene Chain Length of Surfactants on the cmc Values and Krafft Points. The cmc values at 25° and the Krafft points have been listed in Table I.[6] The Krafft point of $C_{12}H_{25}(OCH_2CH_2)_2SO_4Na$ is below 0° and was estimated from the solubility in a sodium chloride solution, whereas no precipitation was observed for $C_{12}H_{25}(OCH_2CH_2)_2SO_4{}^1/_2Ca$ even in a 0.5 *M* calcium chloride solution at 0–1°. It is clear from Table I that the cmc values of calcium and sodium dodecylpoly(oxyethylene) sulfates decrease with the increase in oxyethylene chain length. This results from the decrease in electrical repulsion due to the decrease in charge density on the micelle surface[7] with an increase in oxyethylene chain length. Figure 1 shows the change in Krafft point with oxyethylene chain length. The data for $C_{16}H_{33}(OCH_2CH_2)_nSO_4Na$ and $C_{18}H_{37}(OCH_2CH_2)_nSO_4Na$ obtained by Weil, *et al.*[8] (1 wt %), are included. It is clear from Table I that the Krafft points of calcium and sodium dodecylpoly(oxyethylene) sulfates are depressed with an increase in oxyethylene chain length. It is noteworthy that the Krafft points of the calcium salts are effectively depressed by introducing one oxyethylene group. The Krafft points of $C_{12}H_{25}(OCH_2CH_2)_2SO_4{}^1/_2Ca$ and $C_{12}H_{25}(OCH_2CH_2)_3SO_4{}^1/_2Ca$ are below 0°, thus these surfactants dissolve well in the presence of bivalent cations such as Ca^{2+} and can be used in hard water.

(2) Effect of Mixing Two Surfactants of Different Gegenions on the Krafft Point. The Krafft points of binary surfactant mixtures ($C_mH_{2m+1}SO_4{}^1/_2Ca$ + $C_mH_{2m+1}SO_4Na$, m = 12, 14, and $C_{12}H_{25}OCH_2CH_2SO_4{}^1/_2Ca$ + $C_{12}H_{25}OCH_2CH_2SO_4Na$) are shown in Figure 2 as a function of the fraction of calcium ions in the system, *i.e.*, $X_{Ca}{}^0 = 2N_{Ca}/(N_{Na} + 2N_{Ca})$. It is evident from Figure 2 that there exists a minimum in the Krafft point at a certain composition. This phenomenon is usually observed in the melting point *vs.* composition curve.

(3) Effect of Added Salts on the Krafft Point. It is well known that the Krafft points as well as solubilities of ionic surfactants are affected by the addition of salts.[9] In order to find the effect of added salts on the Krafft points and the solubilities of sodium dodecylpoly(oxyethylene) sulfates, the temperatures above which 1 wt % (0.024–0.035 *M*) of sodium dodecylpoly(oxyethylene) sulfates dissolves have been measured and are shown in Figure 3 as a function of the ratio of bivalent cation to surface active anion ($2M^{2+}/R^-$). The solubilities of calcium dodecylpoly(oxyethylene) sulfates as a function of the ratio $2M^{2+}/R^-$ are also shown by the filled circles. It is found from Figure 3 that the Krafft point is initially depressed by the addition of different gegenions, just as in the case of mixing of two surfactants (Figure 2), then increases rapidly up to the Krafft point of the added bivalent salt, until the ratio $2M^{2+}/R^-$ reaches nearly 1. Above this concentration, at which the sodium ion may be almost completely replaced

TABLE I: Cmc at 25° and Krafft Point of $C_{12}H_{25}(OCH_2CH_2)_nSO_4M$

Compound	Cmc, *m*	Krafft point, °C
$\{C_{12}H_{25}SO_4\}_2Ca$	0.0012[a]	50
$\{C_{12}H_{25}OCH_2CH_2SO_4\}_2Ca$	0.00046	15
$\{C_{12}H_{25}(OCH_2CH_2)_2SO_4\}_2Ca$	0.00037	<0
$\{C_{12}H_{25}(OCH_2CH_2)_3SO_4\}_2Ca$	0.00031	<0
$C_{12}H_{25}SO_4Na$	0.0081	9
$C_{12}H_{25}OCH_2CH_2SO_4Na$	0.0042	5
$C_{12}H_{25}(OCH_2CH_2)_2SO_4Na$	0.0031	−1[b]
$C_{12}H_{25}(OCH_2CH_2)_3SO_4Na$[c]	0.0028[d]	<0

[a] The value at 55°. [b] The extrapolated value from the solubility in aqueous NaCl solution. [c] Average oxyethylene chain length of this compound was 3. [d] Reference 6.

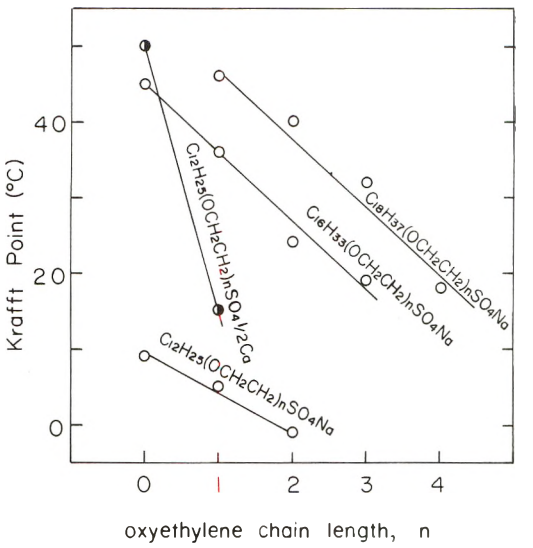

Figure 1. Effect of oxyethylene and hydrocarbon chain length on the Krafft points of $C_mH_{2m-1}(OCH_2CH_2)_nSO_4M$.

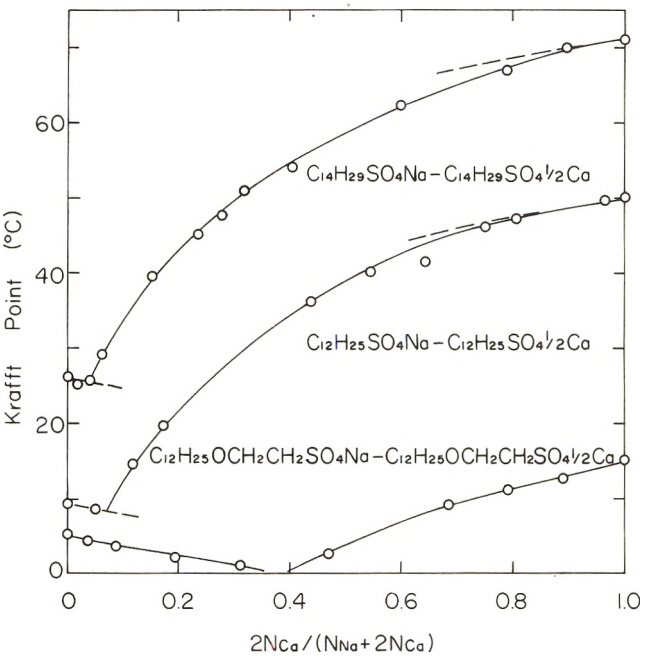

Figure 2. Krafft points of surfactant mixtures of sodium and calcium salts as a function of the fraction of calcium ions of the system.

(6) F. Tokiwa, *J. Phys. Chem.*, **72**, 1214 (1968).
(7) K. Shinoda, "Colloidal Surfactants," Academic Press, New York, N.Y., 1963, Chapter 1, pp 41 and 51.
(8) J. K. Weil, R. G. Bistline, Jr., and A. J. Stirton, *J. Phys. Chem.*, **62**, 1083 (1958).
(9) H. Nakayama and K. Shinoda, *Bull. Chem. Soc. Jap.*, **40**, 1797 (1967).

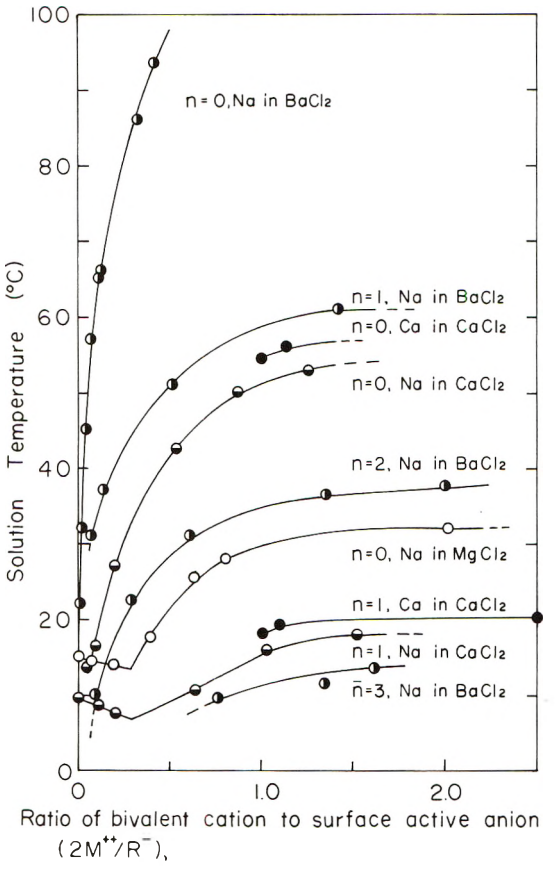

Figure 3. Effect of added salts on the dissolution temperature (≈ Krafft point) of 1 wt % $C_{12}H_{25}(OCH_2CH_2)_nSO_4Na$.

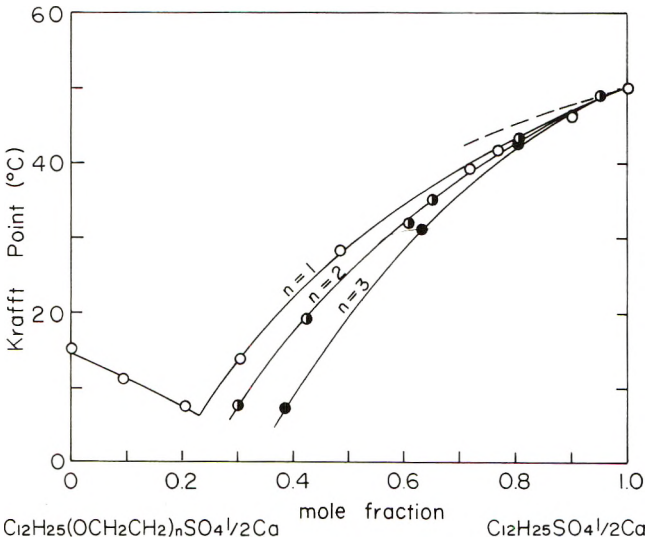

Figure 4. Krafft points of surfactant mixtures of different oxyethylene chain length as a function of the mole fraction of the system.

by the bivalent ion, the Krafft point is raised only a little.[9] The change in Krafft point with the change in concentration of an added salt can be semiquantitatively explained from the results in Figure 2.

(4) Effect of Mixing Two Surfactants of Different Oxyethylene Chain on the Krafft Point. Figure 4 shows the Krafft points of the mixtures $C_{12}H_{25}SO_4{}^1/_2Ca$ + $C_{12}H_{25}(OCH_2CH_2)_nSO_4{}^1/_2Ca$, n = 1, 2, 3, as a function of the mole fraction of the components. As the micelle formation is akin to phase separation[10] and the Krafft point is considered to be the melting point of a hydrated solid surfactant,[2,10] the change in the Krafft points of binary surfactant mixtures is considered to correspond to the freezing point depression of binary mixtures of ordinary substances. It is interesting to examine whether the Krafft point of surfactant mixture can be explained by this model[2] or not. Just as for the phase diagrams of solid–liquid equilibria of binary mixtures, the curves in Figures 2 and 4 illustrate the temperatures at which a solid phase appears from the liquid phase (mixed micelle). In order to find whether the solid phase is composed of a pure compound or a solid solution, the composition of the solid phase was analyzed for the mixtures $C_{12}H_{25}SO_4{}^1/_2Ca$ + $C_{12}H_{25}SO_4Na$ and $C_{12}H_{25}SO_4{}^1/_2Ca$ + $C_{12}H_{25}OCH_2CH_2SO_4{}^1/_2Ca$. The aqueous solutions of surfactant mixtures of given mole ratio ($X_1{}^0$ = 0.7, 0.5, 0.3) were kept at 15 ± 0.2° for 2–3 days, and the composition of the solid precipitate was estimated from the Krafft point depression, which was less than 0.3° (compared with the Krafft point of a pure compound) for both systems. The purity of solid phase was more than 98%. If the mixing in the micelle behaves ideally and the solid phase in equilibrium with the mixed micelle is pure, the change in Krafft point of a binary surfactant mixture may be expressed by the familiar equation for the freezing point depression of a binary mixture[11]

$$\mathrm{d} \ln a_1{}^m = (\Delta H_1{}^f/RT^2)\mathrm{d}T \tag{1}$$

where $a_1{}^m$ is the activity (first component) in the mixed micelle, $\Delta H_1{}^f$ is the heat of fusion (from the hydrated solid to the micelle) of the first component, R is the gas constant, and T is the absolute temperature. Supposing that ideal mixing is allowed between two types of cations (or anions) whereas cations and anions do not mix with each other, the activity $a_1{}^m$ is expressed as

$$a_1{}^m = (X_{1+}{}^m)^{\nu+}(X_{1-}{}^m)^{\nu-} \tag{2}$$

where

$$X_{1+}{}^m = z_{1+}N_{1+}/(z_{1+}N_{1+} + z_{2+}N_{2+})$$
$$X_{1-}{}^m = z_{1-}N_{1-}/(z_{1-}N_{1-} + z_{2-}N_{2-}) \tag{3}$$

where $X_{1+}{}^m$ and $X_{1-}{}^m$ are the fractions of cations and anions (surface active ions), respectively, of the first component in the mixed micelle; and ν_+ and ν_- are the numbers of cations and anions, respectively, in the molecule. $N_{1\pm}$ and $N_{2\pm}$ are the numbers in the micelle and $z_{1\pm}$ and $z_{2\pm}$ are the valence of cations (or anions) of the first and the second components, respectively. Assuming $\Delta H_1{}^f$ is independent of temperature, eq 1 is integrated to give

$$\ln (X_{1+}{}^m)^{\nu+}(X_{1-}{}^m)^{\nu-} = -(\Delta H_1{}^f/R)(1/T - 1/T_1{}^0) \tag{4}$$

where $T_1{}^0$ is the Krafft point of the pure first component and $\Delta H_1{}^f$ is obtained by calorimetry or calculated from the slope of the cmc and the solubility curve as a function of temperature.[12] By introducing $T_1{}^0$, $\Delta H_1{}^f$, and $X_1{}^m$ into eq 4, the change in Krafft point can be calculated. $T_1{}^0$ and $\Delta H_1{}^f$ are summarized in Table II. The calculated values are shown by dotted lines in Figures 2 and 4 as a function of $X_1{}^0$. $X_1{}^0$ (the composition of the system) was calculated from $X_1{}^m$ (the composition of the mixed micelle) by making a correction for selective adsorptivity. The selective

(10) K. Shinoda and E. Hutchinson, *J. Phys. Chem.*, **66**, 577 (1962).
(11) W. J. Moore, "Physical Chemistry," Prentice-Hall, Englewood Cliffs, N.J., 1962, p 134.
(12) K. Shinoda, S. Hiruta, and K. Amaya, *J. Colloid Interface Sci.*, **21**, 102 (1966).

TABLE II: Krafft Point, Heat of Fusion, and Molal Krafft Point Depression Constant of Hydrated Solid Agent

Compound	Krafft point, °K	Heat of fusion, kcal/mol	K,[a] deg/mol Calcd	K,[a] deg/mol Obsd
$\{C_{12}H_{25}SO_4\}_2Ca$	323	18[b]	6.6 ± 1	7.5 ± 1
$\{C_{14}H_{29}SO_4\}_2Ca$	344	~22[b]	6.7 ± 1	8.0 ± 1
$C_{12}H_{25}SO_4Na$	282	12.0[c]	3.8 ± 0.1	3.6 ± 1
$C_{14}H_{29}SO_4Na$	299	13.8[c]	4.1 ± 0.1	4.5 ± 2
NaCl[f]	1074[d]	7.2	19.4[e]	
$CaCl_2$[f]	1038[d]	6.1	39.2[e]	

[a] Molal Krafft point depression constant. [b] Calculated from the solubility and cmc curves. [c] Direct calorimetry.[12] [d] Melting point. [e] Molal freezing point depression constant. [f] Reference 17.

adsorptivity of Ca^{2+} to Na^+ was estimated[13] from the cmc of the mixture $C_{12}H_{25}SO_4{}^1/_2Ca$ + $C_{12}H_{25}SO_4Na$.[14] In the mole fraction ranges of $X_{Ca}{}^m > 0.8$ or $X_{Ca}{}^m < 0.2$, the correction was less than 0.5° in the Krafft point. The selective adsorptivity of $C_{12}H_{25}(OCH_2CH_2)_nSO_4^-$ to $C_{12}H_{25}SO_4^-$ was calculated from the ratio of the cmc at the same concentration of gegenions.[15] As the selective adsorptivity was 3–5 and more than 92% of surfactant molecules were in the micellar state at 1 wt % (0.030–0.035 equiv/l.), $X_{1-}{}^m$ and $X_{1-}{}^0$ agreed within experimental error. The initial slope of the calculated Krafft point *vs.* composition curve agrees with the experimental results. Thus, the presence of the minimum in the Krafft point *vs.* the composition curve can be explained by the entropy of mixing. The Krafft points of the mixtures of sodium alkyl sulfates ($C_{12}H_{25}SO_4Na$ + $C_mH_{2m+1}SO_4Na$, m = 10, 14, 16, 18)[16] agree with the calculated values. Calculated and observed molal Krafft point depression constants (K) have been listed in the fourth and fifth columns in Table II. Molal freezing point depression constants of several inorganic salts[17] are also listed. The molal Krafft point depression constant is $^1/_5$-$^1/_{10}$ of the molal freezing point depression constant. This results from (1) the heat of fusion of hydrated solid agents being *ca.* two to three times larger (12–22 kcal/mol) than that of inorganic salts (6–7 kcal/mol), and (2) the Krafft points being about $^1/_3$-$^1/_4$ of the melting points of inorganic salts.

(13) K. Shinoda, and K. Ito, *J. Phys. Chem.*, **65**, 1499 (1961).
(14) H. Lange, *Kolloid, Zh.*, **121**, 66 (1951).
(15) Reference 2, p 80.
(16) M. Raison, *Proc. Int. Congr. Surface Activ. 2nd, 1957*, 374 (1957).
(17) G. J. Janz, C. Solomons, and H. J. Gardner, *Chem. Rev.*, **58**, 461 (1958).

Viscosity Studies of Aqueous Solutions of Alcohols, Ureas, and Amides[1]

Theodore T. Herskovits* and Thomas M. Kelly

Department of Chemistry, Fordham University, New York, New York 10458 *(Received August 18, 1972)*

The relative viscosities, η/η_0, and the viscosity B and C coefficients in the equation, $\eta/\eta_0 = Bm + Cm^2$, of 25 aqueous alcohol, urea, and amide solutions have been determined at 25°. The C coefficient seems to be necessary for accurate description of the data at the higher molality ranges tested (from 0 to about 1.1 m and for several of the ureas from 0 to 1.5 m) where curvature in the data is apparent. Plots of the B coefficients *vs.* the partial molal volumes, $M_2\bar{V}_2$ (expressed in ml per mole), gave straight lines for each of the three series of compounds, with essentially the same slopes of 4.7 ± 0.1 × 10^{-3}. For the alcohols, $B = 4.7 \times 10^{-3}M_2\bar{V}_2 - 0.087$ and for both the ureas and amides, $B = 4.7 \times 10^{-3}M_2\bar{V}_2 - 0.174$. The slopes of these lines are appreciably higher than the 2.6 ± 0.2 × 10^{-3} values predicted by the Einstein and Simha equations for the viscosity behavior of spherical and ellipsoidal particles having the dimensions of these compounds. The larger viscosity increments, in excess of the Einstein–Simha volume contributions, and the constant negative decrements observed for each of these classes of compounds are attributed to the water structure-forming and structure-breaking influence of the nonpolar hydrocarbon portion and the polar hydroxyl and $-CONH_2$ portions of these compounds. Thus, the viscosity B coefficients for the alcohols are described satisfactorily by the equation, $B = 2.5 \times 10^{-3}M_2\bar{V}_2 + 0.055n - 0.087k$, which contains all three of these contributing terms. In this equation, n represents the number of CH_2 or $-CH_3$ units in the particular alcohol, and k is equal to 1. With somewhat less success, the same equation can also be used to predict the B values of the ureas and amides, where n represents the number of carbons in each of these two series of solutes and k has a value of 2. The effectiveness of these three classes of compounds as protein and nucleic acid denaturants is briefly examined.

Introduction

Various neutral solutes of the aliphatic alcohol, urea, and amide series are effective protein[2] and nucleic acid denaturants.[3] Recent investigation from our and other laboratories[2,3] have shown that the effectiveness of these denaturants increases with increasing hydrocarbon con-

(1) Work supported in part from a Grant No. GM 14468 from the National Institute of Health, U. S. Public Health Service and a faculty research grant from Fordham University.

tent and alkyl substitution. The importance of hydrophobic contributions to the solvent–amino acid side-chain interactions is most pronounced in the cases of the higher hydrocarbon-rich members of these three homologous series.[2a-e] Corresponding effects exhibiting solvent–solute interactions and reflecting changes in the structure of the supporting solvent, water, have been observed in model studies on small molecules[4] and detergent micelles.[5] However, while the effects of electrolytes on the structure of water have gained considerable attention in recent years,[6] partly as a result of their effects on the conformation of biopolymers,[7] relatively little related work has been published dealing with the solution properties and hydrodynamic behavior of neutral solutes of the alcohol, urea, and amide classes in aqueous solution.[4e-g,8,9] The viscosity B parameter and the deviation of this parameter from values predicted for noninteracting hard spheres have been used by various workers as a qualitative measure of the effects of electrolytes[6,10] and neutral solutes[6b,9-11] on the structure of water. In order to see what sort of correlation can be made between these parameters of the various alcohols, ureas, and amides, and their effectiveness as protein[2] and nucleic acid[3] denaturants, we have examined their viscosities in the 0–1.5 m ranges at 25.0°. This paper presents the results and analyses of the data obtained on aqueous solutions of these three homologous series of compounds.

Experimental Section

All of the reagents, alcohols, glycols, ureas, and amides, used were analytical grade, or of the purest commercially available quality. In addition, the alcohols and liquid amides were freshly distilled before use, with the central fractions being retained for experimental work. The solid amides and ureas were recrystallized from hot ethanol, and dried under vacuum. The water used was distilled in an all glass Corning still.

Cannon-Fenske viscometers of relatively long flow times (292–450 sec) were used so as to minimize the kinetic energy corrections. At least three readings of the flow times with variations not exceeding ±0.2 sec were taken for each solution. The viscosities were calculated from the average flow times, t, and densities, ρ, based on the equation

$$\eta = \alpha\rho t - \beta\rho/t \qquad (1)$$

where $\alpha = \pi ghr^4/8lV$ and $\beta = m'V/8\pi l$, with g being the gravitational constant, h the height of the liquid column (the distance between the upper and lower levels of the liquid in the vertically secured viscometer), V the volume of the bulb, r and l the radius and length of the viscometer capillary, respectively, and m' a characteristic constant depending on the shape of the end of the capillary.[12a] The viscometer which was used for most of our measurements had a $m' = 1.11$ (with $V = 3.1$ ml and $l = 6.85$ cm), comparable to the value of 1.15 reported by Hall and Fuoss[12a] for one of their viscometers. Viscosity and density measurements were made on solutions equilibrated in a 25.0° constant temperature bath controlled to ±0.02°. The α and β constants were determined from measurements at 25.0 and 35.0° and the literature values of the viscosity of water at these temperatures. All reported viscosities are relative viscosities, η/η_0, run on water prior to measurements on the binary solutions (given as supplementary material in the microfilm edition of this journal[13]).

Densities were measured with 10-ml pycnometers, calibrated with distilled water at 25.0°. Experimentally determined densities were used to evaluate the partial specific volume, $\bar{V}_2$, by the formula[12b]

$$\bar{V}_{app.} = (1/\rho) - (1/w_2)[(\rho - \rho_0)/\rho_0] \qquad (2)$$

and the related apparent molal volumes, $\Phi(V_2) = M_2\bar{V}_2$, where ρ is the density of the solution, ρ_0 is the density of pure water, and w_2 and M_2 are respectively the concentrations in grams per ml, and the molecular weights of the solute. The $\bar{V}_2$ values reported and used (Tables I and II) were evaluated by extrapolation to infinite dilution of $\bar{V}_{app}$ *vs.* solute concentration plots. The $\bar{V}_2$ values obtained are found to agree closely with the available literature data[14] and the calculated $\bar{V}_2$ values based on Traube's rule[12b,15] (data given in parentheses in column 4 of Table I). According to Traube's rule, in aqueous solutions the atomic and group contributions in ml per mole are as follows: C(9.9), O(2.3), N(1.5), H(3.1), $-NH_2$(7.7), CH_2(16.1), –CONH–(20.0), –COOH(18.9), plus a covolume of 13 ml per mole for each solute.

(2) (a) E. E. Schrier, R. T. Ingwall, and H. A. Scheraga, *J. Phys. Chem.*, **69**, 298 (1965); (b) P. H. Von Hippel and K.-Y. Wong, *J. Biol. Chem.*, **240**, 3909 (1965); (c) T. T. Herskovits, B. Gadegbeku, and H. Jaillet, *ibid.*, **263**, 2588 (1970); (d) T. T. Herskovits, H. Jaillet, and B. Gadegbeku, *ibid.*, **243**, 4544 (1970); (e) T. T. Herkovits, H. Jaillet, and A. T. DeSena, *ibid.*, **243**, 6511 (1970); (f) L. S. Kaminski and A. J. Davison, *Biochemistry*, **8**, 4631 (1969); (g) S. Y. Gerlsma, *Eur. J. Biochem.*, **14**, 150 (1970); (h) J. R. Warren and J. A. Gordon, *J. Biol. Chem.*, **245**, 4097 (1970).

(3) (a) T. T. Herskovits, S. J. Singer, and E. P. Geiduschek, *Arch. Biochem. Biophys.*, **94**, 99 (1961); (b) T. T. Herskovits, *ibid.*, **97**, 474 (1962); *Biochemistry*, **2**, 335 (1963); (c) L. Levine, J. A. Gordon, and W. P. Jenck, *ibid.*, **2**, 168 (1963); (d) T. T. Herskovits and J. P. Harrington, *ibid.*, **11**, 4800 (1972).

(4) (a) W. Kauzman, *Advan. Protein Chem.*, **14**, 1 (1959); (b) C. Tanford, *J. Amer. Chem. Soc.*, **84**, 4240 (1962); (c) D. B. Wetlaufer, S. K. Malik, L. Stoller, and R. L. Coffin, *ibid.*, **86**, 508 (1964); (d) E. E. Schrier, M. Pottle, and H. A. Scheraga, *ibid.*, **86**, 3444 (1964); (e) H. Schneider, G. C. Kresheck, and H. A. Scheraga, *J. Phys. Chem.*, **69**, 1310 (1965); (f) J. J. Kozak, W. S. Knight, and W. Kauzmann, *J. Chem. Phys.*, **48**, 675 (1968); (g) D. B. Dahlberg, *J. Phys. Chem.*, **76**, 2045 (1972).

(5) (a) W. Bruning and A. Holtzer, *J. Amer. Chem. Soc.*, **83**, 4865 (1961); (b) A. Wishnia, *Proc. Natl. Acad. Sci., U. S.*, **48**, 2200 (1962); (c) M. J. Schick and A. H. Gilbert, *J. Colloid Sci.*, **20**, 464 (1965); (d) M. F. Emerson and A. Holtzer, *J. Phys. Chem.*, **71**, 3320 (1967); (e) W. B. Gratzer and G. H. Beaven, *ibid.*, **73**, 2270 (1970); (f) A. Ray and G. Nemethy, *ibid.*, **75**, 804, 809 (1971).

(6) (a) R. W. Gurney, "Ionic Processes in Solution," McGraw-Hill, New York, N. Y., 1953, Chapter 9; (b) R. A. Robinson and R. H. Stokes, "Electrolyte Solutions," 2nd ed, Butterworths, London, 1959.

(7) (a) D. R. Robinson and W. P. Jencks, *J. Amer. Chem. Soc.*, **87**, 2470 (1965); (b) P. Von Hippel and T. Schleicher in "Structure and Stability of Billogical Macromolecules," S. N. Timasheff and G. D. Fasman, Ed., Marcel Dekker, New York, N. Y., 1969, p 417.

(8) F. Francks in "Physico-Chemical Processes in Mixed Aqueous Solvents," F. Francks, Ed., American Elsevier, New York, N. Y., 1967, p 50.

(9) J. A. Rupley, *J. Phys. Chem.*, **68**, 2002 (1964).

(10) R. H. Stokes and R. Mills, "Viscosity of Electrolytes and Related Properties," Pergamon Press, Oxford, 1965.

(11) (a) J. M. Tsangaris and R. B. Martin, *Arch. Biochem. Biophys.*, **112**, 267 (1965); (b) L. S. Sandell and D. A. I. Goring, *Macromolecules*, **3**, 50 (1970).

(12) (a) H. T. Hall and R. M. Fuoss, *J. Amer. Chem. Soc.*, **73**, 265 (1951); (b) E. J. Cohen and J. T. Edsall, "Proteins Amino Acids and Peptides," Reinhold, New York, N. Y., 1943, Chapter 9.

(13) Listings of the relative viscosity and density data of the alcohols, glycols, amides, and ureas in aqueous solutions as a function of solute concentration at 25.0° will appear following these pages in the microfilm edition of this volume of the journal. Single copies may be obtained from the Business Operations Office, Books and Journals Division, American Chemical Society, 1155 Sixteenth St., N.W., Washington, D. C. 20036. Remit check or money order for $3.00 for photocopy or $2.00 for microfiche, referring to code number JPC-73-381.

(14) (a) L. G. Longsworth in "Electrochemistry in Biology and Medicine," T. Shedlowski, Ed., Wiley, New York, N. Y., 1955, Chapter 12; (b) L. G. Longsworth, *J. Phys. Chem.*, **67**, 689 (1963); (c) L. Onsager, *Annu. N. Y. Acad. Sci.*, **46**, 241 (1945).

(15) J. Traube, *Samml. Chem. U. Chem-Tech. Vortrage*, **4**, 255 (1899).

TABLE I: Summary of the *B* and *C* Coefficients and Related Parameters of the Alcohols, Glycols, Amides, Ureas, and Other Solutes

				Viscosity increment		
	B	C	$\bar{V}_2$	$1000B/(M_2V_2)$	Simha (Eq 7 and 8)	$10^6C/(M_2V_2)^2$
			Alcohols and Glycols			
Methanol	0.087	−0.002	1.19 (1.17)	2.28	2.52 ± 0.05	
Ethanol	0.170	0.014	1.20 (1.20[a])	3.07	2.53	4.6
1-Propanol	0.250	0.022	1.19 (1.16)	3.50	2.55	4.4
2-Propanol	0.273	0.019	1.18 (1.16)	3.85	2.51	3.8
1-Butanol	0.300	0.029	1.17 (1.16)	3.46	2.62	3.9
2-Butanol	0.311	0.057	1.17 (1.16)	3.59	2.55	7.6
tert-Butyl alcohol	0.373	0.036	1.19 (1.18[a])	4.23	2.50	4.6
Ethylene glycol	0.143	0.006	0.90 (0.88[a])	2.56	2.66	1.9
Glycerol	0.225	0.019	0.79 (0.78[a])	3.09	2.58	3.6
			Amides			
Formamide	0.019	−0.001	0.87 (0.86[a])	0.49	2.56	
Acetamide	0.111	0.003	0.95 (0.94[a])	1.98	2.62	0.8
Propionamide	0.188	0.004	0.97 (0.98[a])	2.65	2.60	0.8
n-Butyramide	0.264	0.013	1.00 (1.00[a])	3.03	2.57	1.7
N,N-Dimethylformamide	0.171	0.001	1.04 (0.98)	2.25	2.6	0.2
N,N-Dimethylacetamide	0.267	0.007	1.02 (1.00)	3.00	2.6	0.9
			Ureas			
Urea	0.035	0.007	0.75 (0.74[a])	0.78	2.56	3.5
Methylurea	0.142	0.002	0.84 (0.84[a])	2.28	2.60	0.4
Ethylurea	0.155	0.052	0.91 (0.86)	1.93	2.70	8.1
n-Propylurea	0.300	0.016	0.93 (0.91[a])	3.16	2.77	1.8
Isopropylurea	0.289	0.029	0.97 (0.90)	3.04	2.72	3.0
n-Butylurea	0.328	0.071	1.00 (0.93)	2.82	2.81	5.3
1,3-Dimethylurea	0.265	0.003	0.93 (0.91[a])	3.24	2.64	0.5
Tetramethylurea	0.384	0.034	0.99 (0.93)	3.34	2.59	2.6
1,1-Diethylurea	0.370	0.036	0.99 (0.93)	3.22	2.59	2.7
1,3-Diethylurea	0.428	0.057	1.00 (0.93)	3.69	2.79	4.2
			Others			
Sucrose	0.8786[b]		0.62[c]	4.2	2.7 ± 0.1[d]	
Glycine	0.131 (30°)[b]	0.022	0.76[c]	3.0	2.6[d]	11.6
Glycylglycine	0.250 (30°)[b]	0.26	0.81[c]	3.2	2.9[d]	43.6
Triglycine	0.385 (30°)[b]	0.17	0.84[c]	3.4	3.5[d]	13.2

[a] Computed using the partial molal volume data of ref 14a and 14b. The rest of the values given in parentheses were calculated on the basis of Traube's rule.[12b,15] [b] Date taken from ref 11a and 25. [c] Values based on the apparent molal volume data of ref 14a and 6b (sucrose). [d] Estimates based on the a/b values of ref 21; for sucrose it was assumed that a/b is the same as that for the disaccharide, cellobiose.

Results

Viscosity data of nonelectrolytes and macromolecules are usually represented and analyzed on the basis of equations having the form first developed by Einstein in 1906[16] for the viscous flow of spherical particles at infinite dilution, moving in a continuous medium. The viscosity, η, relative to that of the solvent medium, η_0, in terms of the volume fraction, Φ, occupied by the particles is given as

$$\eta = \eta_0(1 + 2.5\Phi) \tag{3}$$

This equation is valid for Φ values usually less than 0.03. Guth, Simha, and coworkers and others[17] have extended the hydrodynamic theory of spherical particles to higher solute concentrations and have obtained equations with higher Φ terms. The square terms of Φ have varying coefficients of 4.32 to 14.1.[17] The relative viscosity, η/η_0, for values equal to or less than 0.25 can be sufficiently accurately represented by the equation

$$\eta/\eta_0 = 1 + 2.5\Phi + C'\Phi^2 \tag{4}$$

where the coefficient C' represents the contribution of solute–solute interactions to the relative viscosity. At moderate to high solute concentrations, m, the form of eq 4 employed by several authors,[9,11,18] is

$$\eta/\eta_0 = 1 + Bm + Cm^2 \tag{5}$$

and with the volume fraction Φ equal to $mM_2\bar{V}_2/1000$ [19] we can write this equation as

$$\eta/\eta_0 = 1 + 1000B/(M_2\bar{V}_2)\Phi + (1 \times 10^6)C/(M_2\bar{V}_2)^2\Phi^2 \tag{6}$$

The coefficients B and C of eq 5 can be evaluated from the intercept and slope of $(\eta/\eta_0 - 1)/m$ *vs.* m plots. The B and C parameters listed for the various alcohols, gly-

(16) A. Einstein, *Ann. Phys.*, **19**, 289 (1906); **34**, 591 (1911).
(17) E. Guth and R. Simha, *Kolloid-Z.*, **74**, 147, 266 (1936); (b) E. Guth and O. Gold, *Phys. Rev.*, **53**, 322 (1938); (c) R. H. Ewart, *Advan. Colloid Sci.*, **2**, 197 (1946); (d) H. Eilers, *Kolloid-Z. M.*, **97**, 313 (1941); (e) J. M. Peterson and M. Fixman, *J. Chem. Phys.*, **39**, 2516 (1963); (f) D. G. Thomas, *J. Colloid Sci.*, **20**, 267 (1965).
(18) D. Eagland and G. Pilling, *J. Phys. Chem.*, **76**, 1902 (1972).
(19) M. F. Emerson and A. Holtzer, *J. Phys. Chem.*, **73**, 26 (1969).

TABLE II: *B* Coefficients and Hydration Parameters of Alcohols, Ureas, and Amides Based on Eq 10 and 13

	B coefficient			Hydration parameters	
	Exptl	Calcd from eq 13[a]	$M_2\bar{V}_2$[b]	$hM_1\bar{V}_1$[c]	h[d]
		Alcohols and Glycols			
Methanol	0.087	0.063	38.1	−3.6	−0.2
Ethanol	0.170	0.161	55.3	11.8	0.7
1-Propanol	0.250	0.257	71.5	26.6	1.5
2-Propanol	0.273	0.255	70.9	37.9	2.1
1-Butanol	0.300	0.350	86.8	27.7	1.5
2-Butanol	0.311	0.350	86.3	35.1	2.0
tert-Butyl alcohol	0.373	0.353	88.3	60.9	3.4
Ethylene glycol	0.143	0.163	55.9	−2.1	−0.1
Glycerol	0.225	0.262	73.5	13.1	0.8
		Ureas			
Urea	0.035	−0.007	45.0	−31.4	−1.7
Methylurea	0.142	0.092	62.2	−7.6	−0.4
Ethylurea	0.155	0.192	80.2	−22.8	−1.3
n-Propylurea	0.300	0.283	94.9	13.4	0.7
Isopropylurea	0.289	0.294	99.0	7.3	0.4
n-Butylurea	0.328	0.391	116.1	−0.6	0
1,3-Dimethylurea	0.265	0.196	81.9	18.5	1.0
Tetramethylurea	0.384	0.388	114.9	33.3	1.9
1,1-Diethylurea	0.370	0.388	114.9	27.9	1.6
1,3-Diethylurea	0.428	0.391	116.1	37.3	2.1
		Amides			
Formamide	0.019	−0.021	39.2	−35.0	−2.0
Acetamide	0.111	0.076	56.1	−13.7	−0.8
Propionamide	0.188	0.168	70.9	2.4	0.1
n-Butyramide	0.264	0.266	87.1	15.6	0.9
N,N-Dimethylformamide	0.171	0.171	76.0	−10.7	−0.6
N,N-Dimethylacetamide	0.267	0.268	88.8	13.8	0.8
		Others			
Sucrose			211.0[b]	114.4	6.4
Glycine			43.5[b]	6.9	0.4
Glycylglycine			77.2[b]	11.0	0.6
Triglycine			113.5[b]	−3.5	−0.2

[a] Parameters used with eq 13 were alcohols and glycols, n = 1–4 and k = 1; ureas, n = 1–5 and k = 2; amides, n = 1–5 and k = 2. [b] The value for sucrose is taken from ref 6b while those for glycine, glycylglycine, and triglycine are from ref 14a. [c] Based on eq 10, $hM_1\Delta_1 = 1000B/\nu - M_2V_2$. [d] Calculated by use of the relationship based on eq 10, $h = (1000B/\nu - M_2\bar{V}_2)/18$.

cols, ureas, and amides of this study in Table I were computed by means of a least-squares program representing such plots. The solid lines drawn through the data points of the relative viscosity plots of Figures 1–3 have been made on the basis of these two parameters and the data given as supplementary material in the microfilm edition of this volume of the journal.[13] We have also included in Table I the related $\bar{V}_2$, and the $1000B/(M_2\bar{V}_2)$ and $(1 \times 10^6)C/(M_2\bar{V}_2)^2$ coefficients, based on eq 6. Based on the Einstein eq 3, the first coefficient, the so called viscosity increment designated as ν, should be equal to 2.5. Deviation from the Einstein ν value of 2.5 has been attributed to various causes, including the small size of some of the solutes relative to the solvent, the effects of hydration, structure formation, and structure breaking of the solvent (water) by the solute.[6,9,19] These effects will be considered in detail in the Discussion of this paper. An additional factor influencing ν is the deviation of the particle from sphericity. Simha[20] treated the problem of the viscosity of ellipsoidal particles and has derived equations for prolate (elongated) and oblate (disk-like) particles in terms of the axial ratios, a/b of the particle, with viscosity increments respectively given as

$$\nu = \frac{(a/b)^2}{15[\ln 2(a/b) - (3/2)]} + \frac{(a/b)^2}{5[\ln 2(a/b) - (1/2)]} + (14/15) \quad (7)$$

$$\nu = (16/15)[(a/b)/\tan^{-1}(a/b)] \quad (8)$$

where a is the semimajor axis and b is the semiminor axis of the ellipsoid. For comparison, we have also included in this table ν values estimated graphically from plots of molecular axial ratios, a/b against ν based on eq 7 and 8. Estimates of the axial ratios were obtained from measurements on Courtauld space-filling molecular models of the solutes, as described by Edwards.[21] The ν values vary only

(20) R. Simha, *J. Phys. Chem.*, **44**, 25 (1940).
(21) J. T. Edwards, *J. Chem. Educ.*, **47**, 261 (1970).

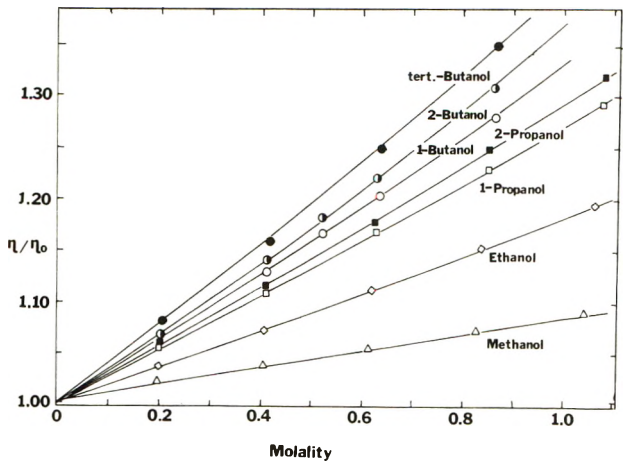

Figure 1. Relative viscosity–concentration curves for the alcohols. The solid lines drawn through the data points were calculated using eq 5 and the B and C parameters of Table I.

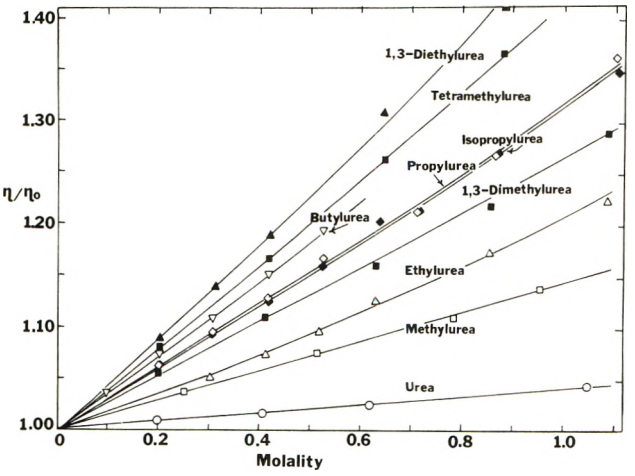

Figure 2. Relative viscosity–concentration curves for the ureas. The solid lines drawn through the data points were calculated using eq 5 and the B and C parameters of Table I. The filled symbols represent the data of branched and alkyl substituted ureas.

slightly from the Einstein 2.5 value since the molecules considered have relatively low a/b ratios, ranging from 1.06 for *tert*-butyl alcohol to about 1.85 for butylurea. Emerson and Holtzer[19] were first to point this out. This is also clearly apparent from the viscosity increments of glycine, glycylglycine, and triglycine of 3.0, 3.2, and 3.4, despite the greater variation in the calculated ν for the latter compounds, having axial ratios of about 1.4 to 2.8.[21]

From the data given in columns 4 and 6 of Table I it is also apparent that while the Einstein ν coefficients are in most cases not very substantially different from the theoretical 2.5 value. The second-order C' coefficient of eq 4 and 6 ($= 10^6C/(M_2V_2)^2$) shows considerably greater variation from the expected 4.32 to 14.1 value. The hard-sphere calculations of Peterson and Fixman[17e] have resulted in the lower estimate of 4.32. Eiler's earlier experimental estimate of 4.94[17d] is relatively close to this value. However, the more generally accepted recent estimate,[17f,18,23] based on Thomas' statistical analysis of various viscosity data taken from the literature places it at 10.05.[17f] Our computed values of this coefficient probably reflect both the greater experimental uncertainty of the computation of this term, and its sensitivity to the effects of particle

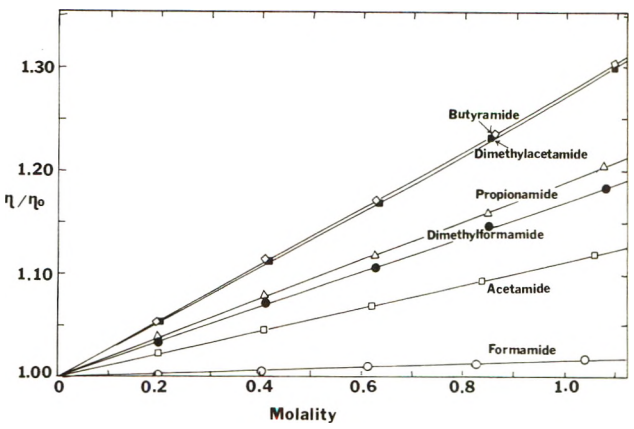

Figure 3. Relative viscosity–concentration curves for the amides. The solid lines drawn through the data points were calculated using eq 5 and the B and C parameters of Table I.

shape[22] and solvent properties. It is perhaps worth noting that the C' coefficient for *tert*-butyl alcohol, the most spherical of the various solutes tested in this study, has a value of 4.63 which is within 7% of Eiler's estimate of 4.94.[17d]

The studies of Breslau and Miller[23] have shown that there is a close correlation between the B coefficients of viscosity and the effective molar volume of electrolytes. Based on eq 4 and 6, the first coefficient of Einstein spheres should lead to the relationship

$$B = (2.5 \times 10^{-3})M_2\bar{V}_2 = (2.5 \times 10^{-3})(4/3\pi r^3 N) \quad (9)$$

However, because the apparent molal volumes of solutes in aqueous solutions contain a covolume contribution,[12b,15] over the atomic or group contributions, there is also an apparently constant term that has to be subtracted from the $M_2\bar{V}_2$ term of the solute. The plots of the B coefficients *vs.* $M_2\bar{V}_2$ for the alcohols, ureas, and amides, shown in Figure 4 give also satisfactory straight lines with essentially the same slope of $4.7 \pm 0.1 \times 10^{-3}$. The slopes of these lines fall between the values of 2.9×10^{-3} and 6.06×10^{-3} obtained by Breslau and Miller[23] for various monovalent and divalent electrolytes, when the effective molar volume is expressed in ml per mole. All the curves are displaced to the right by a constant volume increment, corresponding to about 18 to 36 ml per mole. A rough correlation is also observed between the experimental viscosity increment, $1000B/(M_2\bar{V}_2)$ plotted against the molar volume or the molecular radius, r_w. The latter plots are shown in Figure 5.

Rupley[9] obtained B coefficients for methanol, ethanol, 1-propanol, and several amides based on data of the International Critical Tables that in most cases represent viscosity results obtained at relatively high solute concentrations. Strict agreement for this reason can not be expected with our results of Table I. In addition, the slight curvature of the data at higher concentration seen in Figures 1–3 would tend to overestimate the apparent B values, unless this is taken into account by including a higher quadratic term in concentration characterized by the C coefficient in eq 5. The trend of our data is the same as far as the increasing molal volume and hydrocarbon content of these compounds is concerned. The same trend in the viscosity data is also seen in the case of our urea re-

(22) R. Simha, *J. Appl. Phys.*, **23**, 1020 (1952).
(23) B. R. Breslau and I. F. Miller, *J. Phys. Chem.*, **74**, 1056 (1970).

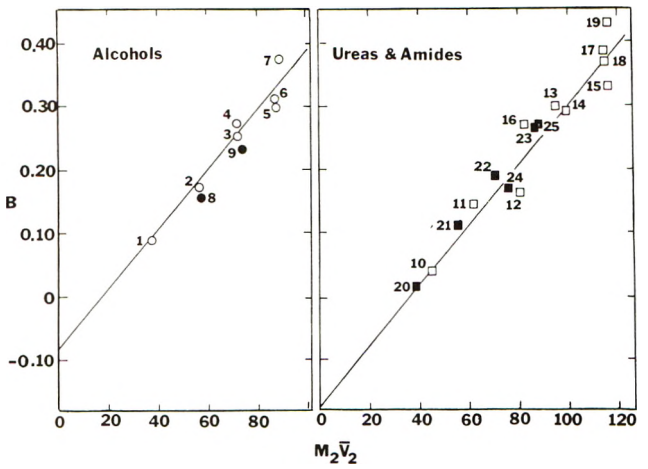

Figure 4. Plots of the viscosity B coefficients *vs.* the partial molal volume, $M_2\bar{V}_2$, for the alcohols, ureas, and amides. The numbers in the figure designate the following compounds: 1, methanol; 2, ethanol; 3, 1-propanol; 4, 2-propanol; 5, 1-butanol; 6, 2-butanol; 7, *tert*-butyl alcohol; 8, ethylene glycol; 9, glycerol; 10, urea; 11, methylurea; 12, ethylurea; 13, *n*-propylurea; 14, isopropylurea; 15, *n*-butylurea; 16, 1,3-dimethylurea; 17, tetramethylurea; 18, 1,1-diethylurea; 19, 1,3-diethylurea; 20, formamide; 21, acetamide; 22, propionamide; 23, *n*-butylamide; 24, *N,N*-dimethylformamide; 25, *N,N*-diethylacetamide.

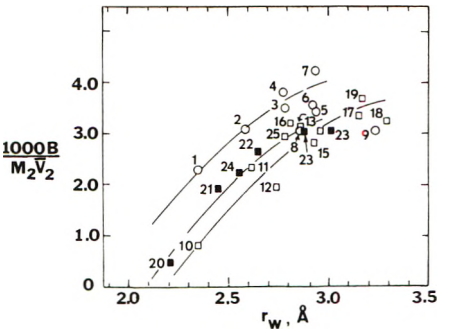

Figure 5. The variation of the viscosity increment, $1000B/(M_2\bar{V}_2)$, with the van der Waals radius, r_w. Numbers designate the same compounds as in Figure 4. The r_w values were taken from the tabulated values given by Edwards[21] or calculated using the relationship, $r_w = (abc)^{1/3}$, where a, b, and c are the dimensions of the three axes of Courtauld molecular models measured at right angles to each other.[21]

sults (Figure 2), and the data of Nagy[24] on several of the ureas studied in the higher 0.5–3.5 M ranges. A B coefficient of 0.0378 was obtained for urea by Jones and Talley,[25] which is in sufficiently close agreement with our value of 0.035.

Discussion

The most significant finding of this study based on the viscosity behavior of the aliphatic alcohols, ureas, and amides listed in Table I is that the viscosity increments of most of these solutes are in the ranges predicted by the Einstein and Simha equations for rigid spherical or ellipsoidal particles. Thus of the 25 compounds listed in Table I, 16 have ν values within ±0.6, and an additional 6 within ±1.0 of the theoretical value of 2.5 to 2.8. Emerson and Holtzer[19] have discussed critically the factors which contribute to the observed viscosity increment of solutions as well as the ambiguities that attend the interpretation of viscosity data of solutes that are small in relation to the dimensions of the solvent. Deviation of the B coefficients and the related viscosity increments from the Einstein and Simha values have been interpreted in terms of both the hydration of the hydrodynamic unit or solute[6b] and the effects of the hydrodynamic unit on the structure of the solvent, water.[6,9,26]

Based on eq 4 and 6, the B coefficient of viscosity can be expressed in terms of the effective hydrodynamic volume, v_h, or the partial molal volume of the particle $M_2\bar{V}_2$ plus that of the associated or bound solvent $M_1\bar{V}_1$.[6b] This may be expressed as

$$B = \nu \times 10^{-3}V_h = \nu \times 10^{-3}(M_2\bar{V}_2 + hM_1\bar{V}_1) \quad (10)$$

with h representing the moles of solvent bound per mole of solute. Alternatively, with the weight of bound solvent given in grams w_1 bound per gram of solute, B can be expressed in the more familiar form[19,27]

$$B = \nu \times 10^{-3}M_2(\bar{V}_2 + w_1/\rho_0) \quad (11)$$

If hydration was the sole effect to be considered, the deviation of B from the Einstein-Simha value (given in column 5 of Table I) should lead to a moderate estimate of bound water for the more polar lower members of the urea and amide family of compounds, glycol, glycerol, and the glycine homologues, and relatively little hydration for highly branched and largely spherical compounds such *tert*-butyl alcohol and dimethyl-, tetramethyl-, and 1,3-diethylurea. As it turns out, calculations based on eq 10, given in the last two columns of Table I, give untenable negative estimates of bound water for all the lower members of the urea and amide series and methanol, ranging from −0.2 to −2.0 mol per mol of solute, rather low or negative estimates for the glycine series, and relatively high estimates for the branched and more hydrophobic higher homologs of all three series of compounds. Taken literally, the latter estimates obtained would represent as much as 40 wt % of bound solvent to the average hydrodynamic unit.

Clearly an alternative interpretation, based at least in part on the possible effects of the solute on structure of water, is in order especially if we are to attempt to explain the linear correlation of B as a function of the partial molal volumes found for the three groups of solutes of this study, having essentially the same slopes (Figure 4). Cast in the same general form as eq 10, the correlation data of Figure 4 may be expressed as

$$B = \nu' \times 10^{-3}(M_2\bar{V}_2 - kM_1\bar{V}_1) \quad (12)$$

The negative, second term of this equation represents the displacement of all the data points of three families of compounds by a nearly constant amount to the right. This suggests that all the solutes of a given family behave as if in the course of viscous flow their molar volumes were lowered by a constant amount corresponding to 1 or 2 mol of solvent per mol of solute. One of two explanations may be offered in relation to these findings and the negative $kM_1\bar{V}_1$ terms. These are (1) the assumption that the solvent can be considered a continuum, as required by Einstein's treatment of the viscosity of hard spheres,[16] is not strictly valid for solutes of relatively small dimensions approaching that of the solvent; or (2) for a given series of

(24) Data of B. Nagy cited by W. P. Jencks, *Fed. Proc.*, **24**, 5–50 (1965).
(25) G. Jones and S. K. Talley, *J. Amer. Chem. Soc.*, **55**, 624 (1933).
(26) R. L. Kay, T. Vituccio, C. Zawoyski, and D. F. Evans, *J. Phys. Chem.*, **70**, 2336 (1966).
(27) Chapter 21 of ref 12b.

solutes, the polar, structure-breaking portion of the molecules reduces the microscopic viscosity of the neighboring solvent during the course of viscous flow.[28] Since the same OH, or $-CONH_2$, is present in each of the homologous series studied, the decrease in viscosity and the corresponding decrement in B will be by a constant amount for each of the series of compounds. Actually the experimental ν's are found to be higher than the theoretically predicted values based on the Einstein or Simha equations with ν equal to 4.7 ± 0.1 for most of the alcohols, ureas, and amides (Figure 4). However, the observed increase in B for each additional $-CH_2$ or $-CH_3$ unit is remarkably constant, with a total increment of 16 to 18 ml per methylene unit as shown in Figure 4. This increment per carbon unit for the alcohols is about 5 to 6 ml in excess of the Einstein value of $2.5V_h$, where V_h is the effective molecular volume of the hydrodynamic unit. Since the volume contribution of the solute is specified by the Einstein or Simha νV_h term, one feels justified in assigning the excess contribution as being due to the change in the microscopic viscosity of the solvent in the vicinity of the hydrocarbon portion of the solute, assuming that each methylene unit will contribute a more or less constant increment to B. With n representing the number of methylene units, and ignoring at this level of approximation any end contributions or chain length effects observed in the viscosity behavior of pure liquids,[29] the B coefficient of viscosity can be expressed as

$$B = 2.5 \times 10^{-3}(M_2\bar{V}_2 + 22n - 35k)$$
$$= 2.5 \times 10^{-3}M_2\bar{V}_2 + 0.055n - 0.087k \quad (13)$$

The data of the first two columns of Table II present a comparison of the experimentally determined and calculated B coefficients based on eq 13. The partial molal volumes, $M_2\bar{V}_2$, used for these calculations were based on the $\bar{V}_2$ data of Table I and are listed in column 3. For the urea and amide calculations we have somewhat arbitrarily assumed that the first members of these series, urea and formamide, are characterized by the same volume increments per carbon or amido unit (*i.e.*, that $n = 1$ for these two compounds) as the $-CH_2$ or $-CH_3$ group contributions of the alcohols.

The close agreement between the observed and calculated B parameters for the alcohols suggests that both the volume contributions and the water structure-forming and structure-breaking influences of the solute have been satisfactorily taken into account. The less satisfactory accord between the calculated and experimental data of the ureas and amides could be attributed to the greater difficulty of formulating a realistic view of the B contributions of the heteroatomic end groups of these two families of compounds, without undue arbitrariness. We have not attempted to improve the agreement between the calculated and observed B values for these compounds by introducing further constant terms into eq 13. It is apparent that the discrepancies are most serious in cases of the lower members of these two families of compounds. In fact, these so called "end effects" are most probably related to the small size of the solutes relative to water alluded to earlier. The diffusion studies of Longsworth and others[14b,c] have suggested that the 6π factor in the Stokes–Einstein equation (which in some ways is analogous to the Einstein–Simha viscosity increment, ν, in eq 3, 7, and 8) is inappropriate for relatively small molecules, and is experimentally not approached until the solute to solvent volume ratios are about 5 to 1.

The structure-breaking influence of urea and related polar compounds such as formamide may be questioned. Recently, however, Finer, *et al.*,[30] have presented evidence based on nmr studies on aqueous urea solutions showing that urea causes a breakdown of the ordered structure of water which is not replaced by extended structures involving urea molecules. The relatively large negative contributions of the urea and amido groups to the viscosity increment of the ureas and amides seen in Figure 4 are consistent with the findings of Finer, *et al.*[30] The denaturation of several proteins by the various alcohols,[2a-c,f,g] ureas,[2d,h] and amides[2e,f] has been attributed largely to hydrophobic interactions between the nonpolar hydrocarbon portion of the denaturant and the various nonpolar amino acid side chains. Such bonding or interactions formed in the aqueous media are generally attributed to entropic factors associated with the ordering of the solvent water in the vicinity of the nonpolar portions of the solute or amino acid side chain.[4,31] It is reasonable to assume that the hydrophobic influence of the solute on the structure of water should also contribute to the viscosity increment of aqueous solutions, and that the observed contributions should be most noticeable in cases of the higher homologs of the alcohols, ureas, and amides.

By our criteria, water structure formation by the solute would require the dominance of the second positive term in eq 13, relative to the magnitude of the constant negative last term of this equation. Dominance of the latter term would mean the net loss of water structure and a corresponding decrease in the viscosity increment, $1000B/M_2\bar{V}_2$, below the Einstein–Simha value, in the neighborhood of 2.5. In fact, this interpretation of the viscosity data of solutions was first suggested by Rupley.[9] However, the fact that the observed deviation of this viscosity increment is usually not very large and the uncertainties concerning the effects of the relative size of the solute on the viscosity increment of the solution are largely unknown, the interpretation of viscosity data based on the trend and relative magnitude of the viscosity B coefficients and the related $1000B/M_2\bar{V}_2$ parameters must be interpreted with caution. For example, while there is an apparent correlation between the B or $1000B/(M_2\bar{V}_2)$ values of the alcohols and their effectiveness as protein[2a-c,f,g] and nucleic acid[3] denaturing agents, this "trend" or correlation of the data can not be extended to glycerol, sucrose, or glycine. Both sucrose and glycerol are known to stabilize proteins against thermal denaturation,[32] while glycine is not known to be a protein denaturant. Sucrose also stabilizes the micellar form of the nonionic detergent Triton X-100.[3,33] Table III presents a comparison of the viscosity increments, $1000B/(M_2\bar{V}_2)$, obtained with the alcohols, glycols, and several of the ureas and amides, with the relative effectiveness of these compounds as protein

(28) Rupley[9] made the observation that the methanol and ethanol have higher activation energies of viscous flow than urea and acetamide. ΔE_{vis} of activations of 7500 and 4500 cal/mol at 10° for 20% ethanol and 15% urea solutions were given as examples of the influence of these solutes on the structure of water.

(29) (a) T. E. Thorpe and J. W. Rodgers, *Proc. Roy. Soc., London, Ser. A*, **60**, 152 (1896); (b) E. C. Bingham, *Phys. Rev.*, **35**, 407 (1912).

(30) E. G. Finer, F. Francks, and M. J. Tait, *J. Amer. Chem. Soc.*, **94**, 4424 (1972).

(31) (a) H. S. Frank and M. W. Evans, *J. Chem. Phys.*, 507 (1945); (b) H. S. Frank and W. Y. Wen, *Discuss. Faraday Soc.*, **24**, 133 (1957).

(32) (a) R. B. Simpson and W. Kauzmann, *J. Amer. Chem. Soc.*, **75**, 5139 (1953); (b) S. Y. Gerlsma, *J. Biol. Chem.*, **243**, 957 (1968).

(33) It should be noted, however, that both glycerol and sucrose destabilized dodecysulfate micelles,[5d] and glycerol also destabilizes DNA[3c] (see the last column of Table III).

TABLE III: Viscosity, *B*, Protein and Nucleic Acid Denaturation and Related Parameters of the Alcohols, Glycols, and Some of the Ureas and Amides

Solute or denaturant	$1000B/(M_2\bar{V}_2)$	ΔF_{tr} of alkyl side chains[a] at 25°, cal/mol	Setschenow constants, K_s, at 25°		Denaturation midpoints	
			Indole[b]	Adenine[c]	Cytochrome c at 25°,[d] *M*	T4 bacteriophage DNA at 73°,[d] *M*
Alcohols, Glycols, and Others						
Methanol	2.28	−700	−0.075	−0.015	12.5	3.5
Ethanol	3.07	−1000	−0.112	−0.090	7.4	1.2
1-Propanol	3.50	−1350	−0.170	−0.200	4.0	0.54
2-Propanol	3.85	−1450	−0.137	−0.160	4.6	0.90
1-Butanol	3.46	−1900	−0.220	−0.355		0.33
2-Butanol	3.59	−2020	−0.178	−0.310	0.7	0.62
tert-Butyl alcohol	4.23	−1720	−0.140	−0.200	3.6	0.60
Ethylene glycol	2.56	−610	−0.079	−0.064	13.9	2.2
Glycerol	3.09		(−0.041)[e]			1.8
Sucrose	4.2					
Glycine	3.0					2.2
Ureas						
Urea	0.78		−0.093	−0.10	6.6	1.0
Methylurea	2.28	−700	−0.167	−0.21	5.6	
Ethylurea	1.93	−1000	−0.215	−0.25	4.7	0.6
n-Propylurea	3.16	−1350	−0.270	−0.36	2.3	
n-Butylurea	2.82	−1900	−0.409	−0.55	0.7	
1,3-Dimethylurea	3.24		(−0.301)[e]		4.9	1.0
Amides						
Formamide	0.49		−0.107	0	8.8	1.9
Acetamide	1.98	−700	−0.117	−0.127	8.3	1.1
Propionamide	2.65	−1000	−0.149	−0.165	4.7	0.62
n-Butyramide	3.03	−1350	−0.201	−0.292	2.6	0.46
N,N-Diethylformamide	2.25		(−0.312)[e]	−0.255	5.1	0.60

[a] Values for the straight chain alkyl groups taken from ref 2a and 4d are based on Scheraga-Nemethy theory of hydrophobic bonding; values for the branched alkyl groups taken from ref 2c are based on the free energies of transfer of amino acid side chains from water to 95 or 100% ethanol. [b] Data taken from ref 2c–e. [c] The alcohol and glycol values are taken from ref 3d, whereas the urea values are based on the unpublished data of J. J. Bowen obtained in our laboratory. The amide values are based on the solubility data of Levine, *et al.*,[3c] obtained at 37°. The latter values were calculated using the relationship, $K_s = 1/c_2 \log (S_0/S)$, where S_0 is the solubility of adenine in water and S the solubility in the particular urea solution having the concentration c_2 in moles per liter. [d] Cytochrome c data taken from ref 2c–e; T4 bacteriophage DNA data taken from ref 3c. [e] Values of K_s of *N*-acetyl-L-tryptophan ethyl ester taken from ref 2c–e.

and deoxyribonucleic acid denaturants. The denaturation data are expressed in moles per liter of denaturant required to produce 50% denaturation or change in a physical or biological parameter selected to follow the denaturation transition.[2a-g,3c] The data obtained on cytochrome c[2c-e] were included for reasons suggested by Dickerson and coworkers,[34] namely, that in comparison with other proteins cytochrome c represents the best example of the so-called "hydrophobic drop or oil drop" model for globular proteins, with most of the nonpolar amino acid side chains packed in the interior hydrophobic region of the protein fold. In addition to the denaturation data of T4 bacteriophage DNA obtained by Levine, *et al.*[3c], we have also included in this table three other indices of hydrophobicity used in discussions of protein and nucleic acid stability:[2a-g,3c,4a-d,7] estimates of the free energy of transfer of alkyl portion of the denaturants based on the Scheraga-Nemethy theory of hydrophobic bonding[2a,4d] or solubility measurements[4b] (for estimates of ΔF_{tr} of the branched alkyl groups[2c]), and the Setschenow constants, K_s, of indole[2c-e] and adenine.[35]

(34) (a) R. E. Dickerson, M. L. Kopka, J. Weinzierl, J. Varnum, D. Eisenberg, and E. Margoliash, *J. Biol. Chem.*, **242**, 3015 (1967); (b) R. E. Dickerson, T. Takano, D. Eisenberg, O. B. Kallai, L. Samson, A. Cooper, and E. Margoliash, *ibid.*, **246**, 1511 (1971).

(35) The alcohol and glycol values given were taken from ref 3d; the urea values are those of J. J. Bowen obtained in our laboratory. The values for the amides were calculated from the solubility data of adenine at 37° given in ref 3c.

Bulk Properties of Synthetic Polymer–Inorganic Salt Systems. Melting Behavior of Salted Poly(caproamide)[1]

B. Valenti, E. Bianchi, G. Greppi, A. Tealdi, and A. Ciferri*

Chemistry Department, University of Genoa, Genoa, Italy *(Received June 30, 1972)*

Publication costs assisted by The National Research Council

Mixtures of nylon 6 and one of the salt LiBr, LiCl, or KCl (composition range 0–12% w/w) were prepared by melting, under vacuum at 260°, an intimate blend of the two components. The equilibrium melting temperature, T_m, of the mixtures was determined by differential scanning calorimetry using the treatment of Hoffman and Weeks. T_m of pure nylon 6 is continuously depressed by increasing salt content, the order for increasing salt effectiveness being KCl < LiCl < LiBr. Salts could be extracted from mixtures with hot water, with complete recovery of the fusion temperature of pure nylon 6. A study of the thermal stability of nylon 6 in the presence of salts indicated some alterations of molecular weight unable to account for the melting behavior. X-Ray analysis indicated that LiBr and LiCl tend to favor the crystallization of the γ form of nylon 6 with respect to the more common α form. Preliminary data on the effect of salts on the kinetics of crystallization and the melt viscosity of nylon 6 are also presented. The crystallization rate of nylon 6 is drastically slowed by LiBr and LiCl. The melt viscosity of pure nylon 6 at 250° is considerably increased in the presence of LiCl. The body of results presented suggests the occurrence of a strong interaction (*i.e.*, binding), possibly between the amide group of the amorphous polymer and salts such as LiCl and LiBr. A similar interpretation is used for explaining the role of aqueous salt solutions on the conformational stability of biological polymers. Salt additives appear to have technological interest since they may represent a very effective tool for the control of the melt viscosity and of the rate and temperature of crystallization, without the softening effects normally associated with the use of conventional, liquid diluents.

(1) Introduction

The idea of investigating the bulk properties of synthetic polymer-inorganic salt mixtures in absence of water (or any conventional diluent) derives from our previous work on the effect of aqueous salt solutions on the conformational stability of biological polymers.[2-9] In particular, we were looking for a final proof for the occurrence of a direct interaction (*i.e.*, binding) between the salts which are known to be strong denaturants of biopolymers (the so-called salting-in agents) and the polar polymeric substrate. The hypothesis of a direct interaction, as the principal mechanism for lyotropic effects, has already received a number of compelling verifications.[2b,6-9] However, the alternative suggestion of an indirect role of the salts, mediated through the effect of salts on water, caused debates in the scientific literature of the early twenties[10] and it is still advocated in terms of the now fashionable water structure concept.[11]

As reported in a preliminary comunication,[12] a strong interaction between a typical polar polymer such as nylon 6 (polycaproamide) and salting-in agents such as LiBr, LiCl, $CaCl_2$ does indeed occur in the absence of water. For instance, transparent, amorphous samples of nylon 6 can be obtained when LiCl is as low as 4% w/w. Extraction of salt with hot water allows the sample to recover the crystallinity typical of nylon 6. In fact, the use of salt additives may have technological importance, particularly for the processing of high melting polar polymers.[13] Moreover, a number of interesting possibilities for altering and for studying physical properties of bulk polar polymers have now arisen. These facts have considerably widened our original aim of elucidating the biopolymers case.

In this paper we consider in detail the role of LiBr, LiCl, and KCl on the equilibrium melting, the thermal stability, and the structure of nylon 6.

(2) Experimental Section

Materials. Nylon 6 samples were supplied as unfractionated polymers by Snia Viscosa and by Montecatini-Edison. Although preliminary investigations did not reveal any difference in the behavior of these samples, the Snia Viscosa sample was preferably used. Nylon 6 was chosen because it contains amide groups and has a melting point above which the polymer is still relatively stable. All nylon used was dissolved in 85% HCOOH, and reprecipitated in the form of a fine powder by addition of CH_3OH. The sample thus obtained, monomer free, had

(1) Dedicated to the memory of Professor A. Katchalsky.
(2) (a) T. A. Orofino, A. Ciferri, and J. J. Hermans, *Biopolymers*, **5**, 773 (1967); (b) A. Ciferri, R. Garmon, and D. Puett, *ibid.*, **5**, 439 (1967).
(3) D. Puett and L. V. Rajagh, *J. Macromol. Chem.*, **A2**, 111 (1968).
(4) E. Bianchi, G. Conio, A. Ciferri, D. Puett, and L. V. Rajagh, *J. Biol. Chem.*, **242**, 1361 (1967).
(5) A. Ciferri, "Treatise on Skin," H. R. Elden Ed., Interscience, New York, N. Y., in press.
(6) J. Kurtz and W. F. Harrington, *J. Mol. Biol.*, **17**, 440 (1966).
(7) D. R. Robinson and W. P. Jenks, *J. Amer. Chem. Soc.*, **87**, 2402 (1965).
(8) L. Mandelkern and W. E. Steward, *Biochemistry*, **3**, 1135 (1964).
(9) A. Katchalsky and A. Oplatka, *Proc. Int. Congr. Rheology, 4th*, 1 (1965).
(10) J. W. McBain, "Colloid Science," D. C. Health, Boston, Mass., 1950.
(11) P. H. von Hippel and K. Y. Wong, *J. Biol. Chem.*, **240**, 3909 (1965).
(12) A. Ciferri, E. Bianchi, F. Marchese, and A. Tealdi, *Makromol. Chem.*, **150**, 265 (1971).
(13) Italian Patent No. 12767-A/71.
(14) K. Hoshino and M. Watanabe, *J. Chem. Soc. Jap., Pure Chem. Sect.*, 24 (1949).

an intrinsic viscosity in *m*-cresol at 25° of 1.46 dl/g, corresponding to a molecular weight[14,15] of about 20,000.

Salts used were analytical grade KCl, LiCl, and LiBr. Mixtures of polymer and salts were prepared in the following way. To a glass tube containing the polymer powder, an adequate amount of a solution of salt in CH_3OH was added as to wet the entire polymer and to give polymer samples containing quantities of salt variable between 2 and 12% w/w. CH_3OH was eliminated by maintaining the glass tubes at 50° for about 24 hr. Last traces of solvent and any adsorbed water were then eliminated by maintaining the tubes at 100° under vacuum for about 5 hr. The tubes were then sealed under vacuum and maintained in an oven at 260° for varying lengths of time (t_f) in order to achieve fusion and optimum homogenization. After the time t_f had elapsed, the tubes were quickly brought to a lower temperature (T_c) to achieve isothermal crystallization for variable lengths of time (t_c). After the time t_c had elapsed, glass tubes were removed from the oven, allowed to cool at room temperature, and then broken. Occurrence of some volatile material was noticed upon breaking the tubes. Samples were stored in a moisture-free atmosphere for lengths of time not exceeding a few days. A control polymer sample without salt was also prepared following the same procedure.

As previously indicated,[12] salts could be removed from the polymer–salt mixture by extraction in H_2O at 100° for about 10 hr, with recovery of the crystallinity and of the fusion temperature of salt-free nylon 6. The amount of material which could be extracted with hot water, after the thermal treatment, approximately coincided with the weight loss resulting from dissolution of samples in 85% HCOOH (after thermal treatment) followed by precipitation with CH_3OH. For materials having t_f = 5 hr and t_c = 48 hr at 200°, about 3% (w/w) weight loss (in addition to the loss due to extraction of salt) was observed, essentially independent of salt content. This loss is smaller than that previously observed[12] for samples having t_f = 72 hr.

Viscosity Measurements. Samples were dissolved in *m*-cresol at room temperature for 24 hr, polymer concentration, *c*, being about 0.4 g/100 ml. Solutions were filtered through a sintered-glass filter, although no evidence of insoluble material or gels was noticed. Specific reduced viscosity, η_{sp}/c, was measured at 25°, according to conventional techniques,[3] using Ubbelhode type viscometers at no less than four different polymer concentrations between 0.4 and 0.1 dl/g. Efflux time of solvent was never less than 200 sec. It is to be noted that preliminary viscosity measurements performed in 85% HCOOH did not prove to yield reproducible results very likely due to occurrence of aggregation phenomena, as has also been observed by others.[16] Such effects were observed even for the original nylon 6 sample (with no salt) not subjected to any thermal treatment. Measurements in *m*-cresol were completely free from such complications.

Preliminary melt viscosity data were obtained at 250° using a capillary extrusion rheometer (shear rate 100 sec^{-1}) or a glass capillary viscometer operating under vacuum.

Thermal Analysis. A Perkin-Elmer differential scanning calorimeter DSC-1B was used operating with heating rates between 8 and 64°/min.

The melting parameters, T_f and ΔH_f, respectively the fusion temperature and the fusion enthalpy, were obtained using the following thermal treatments of the samples. (1) Direct determination of T_f and ΔH_f by melting the samples crystallized in the oven at temperature T_c for a length of time t_c, as indicated above. (2) Securing a new thermal history for the samples by melting in the DSC apparatus at 260° for 12 min and then quickly cooling by manual operation of the instrument at a crystallization temperature T_c where samples were kept for a length of time t_c. After the t_c time had elapsed, the fusion profile was registered by increasing the temperature above T_c.

ΔH_f and T_f were obtained from the area and the position of the endothermal peaks of fusion, exploring the effect of changes in the heating rate at 8, 16, 32, and 64°/min.

A preliminary study of crystallization kinetics was performed using the DSC instrument. The technique consisted in selecting the crystallization time t_c' (using the indicated thermal treatment 2) required for obtaining a fusion enthalpy ΔH_f of about 7.5 (±1.5) cal/g. Taking as a correct figure of the melting enthalpy ΔH_m the value of 35–55 cal/g of crystalline polymer reported in the literature,[17-19] the above ΔH_f value corresponds to about 15% crystallinity. This determination could be easily done for polymer–salt mixtures exhibiting a considerable degree of crystallinity. In the case of nylon 6 + 4% LiCl, however, the low crystallization rate only permitted a reliable determination of the time t_c'' corresponding to a $\Delta H_f \simeq 2$ cal/g.

X-Ray Measurements. X-Ray films were obtained at room temperature using a Debye-Scherrer camera and Fe Kα radiation filtered through a thin Al film. The samples used were finely subdivided and enclosed in a quartz capillary of 0.5 mm diameter. Exposure time was 8 hr. No low-angle X-ray patterns were obtained in the present study.

(3) Results

Viscosity Data. The effect of the thermal treatment on the intrinsic viscosity $[\eta]$ of the nylon 6–salt mixtures is illustrated in Figure 1. The corresponding η_{sp}/c *vs.* *c* plots were accurately linear and the extrapolation of $[\eta]$ could be made within ±1%. The thermal history of the samples investigated included, beside the time t_f of permanence at 260° shown on the abscissa of Figure 1, a period of 48 hr of isothermal crystallization at T_c = 200° for pure nylon 6; T_c = 180° for nylon 6 + 2% LiCl; and T_c = 150° for nylon 6 + 4% LiCl. It was found, however, that the determining effect on the value of $[\eta]$ was the length of the time t_f; rather small variations (±5°) around 260° produced a significant alteration of $[\eta]$. The results indicate that the intrinsic viscosity of nylon 6, maintained under vacuum in a closed container at 260°, increases up to t_f values of about 5 hr, decreasing upon further increase of t_f. A similar trend is exhibited by nylon 6–salt mixtures, although increasing amounts of salt result in a gradual reduction of $[\eta]$. (This effect is not primarily due to the presence of salt in solution, as ascertained by extracting the salt with H_2O at 100° before the viscosity measurements.[12])

The results of the melt viscosity measurements indicate that the melt viscosity of nylon 6 is considerably increased by small amounts of LiCl. The ratio of the melt viscosity

(15) R. Bennewitz, *Faserforsch. Textiltech.*, **5**, 155 (1954).
(16) L. Simek, V. Klepal, and O. Vilin, *Past. Hmoty Kauc.*, **6(9)**, 273 (1969).
(17) M. Dole and B. Wunderlich, *Makromol. Chem.*, **34**, 29 (1959).
(18) K. H. Illers and H. Haber Korn, *Makromol. Chem.*, **142**, 31 (1971).
(19) G. W. Urbanczyk, *J. Polym. Sci.*, **45**, 161 (1960).

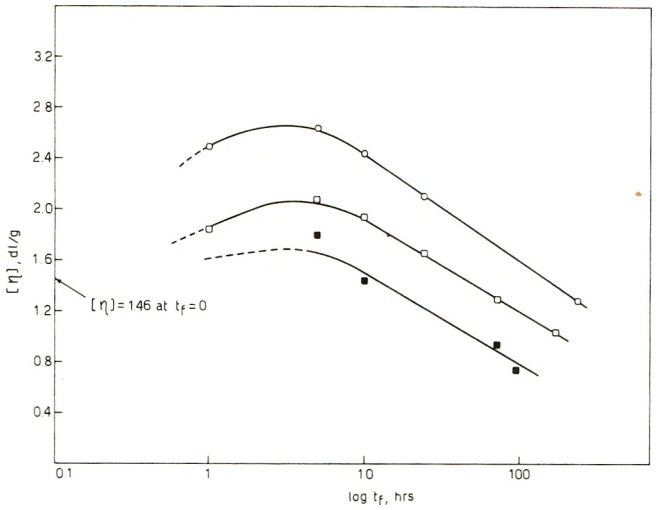

Figure 1. Variation of the intrinsic viscosity of nylon 6–salt systems with the time, t_f, during which they were allowed to stay at 260° in sealed glass tubes: ○, pure nylon 6; □, nylon 6 + 2% LiCl; ■, nylon 6 + 4% LiCl (T = 25°).

of a nylon 6 + 4% LiCl mixture, to the corresponding value measured for pure nylon 6, was between 2 and 3, depending upon the method of measurement and the fusion time t_f.

Thermal Analysis. Typical thermal profiles in the fusion range, and under a variety of conditions, are collected in Figure 2. Data represent samples for which the fusion time t_f was 5 hr. This value of t_f was generally used (unless otherwise specified) for the DSC experiments since preliminary studies indicated that under these conditions homogenization had already been reached. Included in Figure 2 are profiles obtained using methods 1 and 2 (*cf.* Experimental Section) for the thermal treatment preceding the determinations of the melting profile. They can be recognized by the value of t_c; for samples crystallized in the DSC instrument t_c never exceeded 4 hr, while for samples crystallized in the oven t_c was invariably equal or greater than 48 hr.

Typical values of the fusion enthalpy ΔH_f deduced from the thermal profiles are collected in Table I. Values of ΔH_f reported for pure nylon 6 should offer an idea of the degree of crystallinity resulting after the two thermal treatments employed. The values of ΔH_f reported for nylon 6-salt systems also reflect intrinsic alterations brought about by the salt (binding, shift in α/γ ratio, *cf. seq.*, etc.) plus the effect of salts in reducing the rate of crystallization. Often the profiles reveal the occurrence of two ill-resolved peaks corresponding to fusion temperatures T_f^b and T_f^a (*cf.* Figure 2). However, upon increasing the crystallization time t_c, the height corresponding to the low fusion peak gradually increased relatively to the height of the high fusion peak. A similar effect was observed upon increasing the rate of heating from 8 to 64°/min. Above a certain crystallization temperature the two peaks could no longer be resolved irrespective of the time t_c. The effect of increasing the fusion time t_f from 5 to 72 hr was negligible for pure nylon while in the case of nylon 6 + 2% LiCl the high fusion peak disappeared even at low T_c. The occurrence of multiple peak (usually double) of the type illustrated in Figure 2 has been noticed by several investigators[18,20-22] even in the cases (including α or γ nylon 6) in which only one crystalline modification was present. The work of Roberts,[22] in particular, clearly

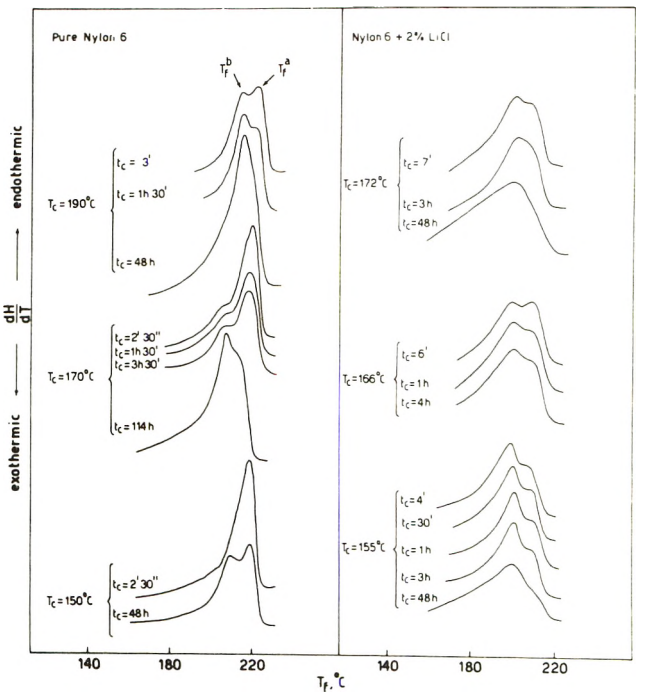

Figure 2. Typical fusion profiles registered at the DSC for nylon 6 samples and for nylon 6 + 2% LiCl systems. The crystallization temperature, T_c, and the crystallization time, t_c, are indicated. Weight of samples varied between 10 and 13 mg. Heating rate was 16°/min.

TABLE I: Selected Values of the Fusion Enthalpy ΔH_f (cal/g) for Nylon 6–Salt Systems

	T_c, °C					
Salt, w/w %	150	160	170	180	190	200
0%	10.6[a]	9.6	9.5	9.2	8.5	7.2
	10.6		14.7	15.6	16.2	18.0
3.5% KCl			9.1	8.5	7.6	
7% KCl			9.6	8.7	7.7	
2% LiBr	9.9	10.0	9.6	8.1	6.5	
	16.9					
4% LiBr	8.3	7.5	5.4			
		16.9				
6% LiBr	5.4	4.5				
2% LiCl	7.5	7.0	6.4	5.1		
	12.0		13.6		14.4	14.0
2.6% LiCl	6.1	5.4	4.7	4.0		
4% LiCl	~1					
	10.7	9.1	11.6			

[a] When two values of ΔH_f are reported, the first one corresponds to thermal treatment 2 (t_c between 1 and 15 min; except for 4% LiCl when t_c = 180 min) and the second one to thermal treatment 1 (t_c = 48 hr; except for 2% LiCl at 200° and 4% LiCl at 170° when t_c = 96 hr).

indicates that the high melting peak should be associated with the recrystallization, during the melting run, of crystals formed at a given T_c. The experimental evidence cited above clearly suggests that the peak characterized by the fusion temperature T_f^b is the one which appropriately corresponds to the fusion of crystals formed at the relevant T_c.

(20) I. Abu-Isa, *J. Polym. Sci., Part A-1*, **9**, 199 (1971).
(21) F. N. Liberti and B. Wunderlich, *J. Polym. Sci., Part A-2*, **6**, 883 (1968).
(22) R. C. Roberts, *J. Polym. Sci., Part B-8*, 381 (1970).

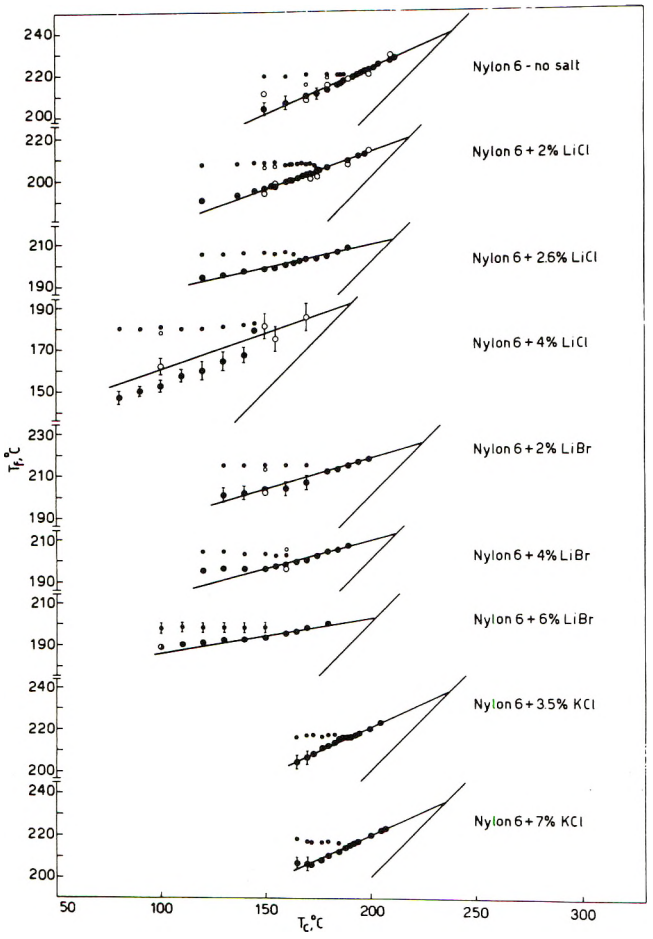

Figure 3. Variation of the fusion temperature with crystallization temperature for several nylon 6–salt systems: black dots, data corresponding to thermal treatment 2; open circles, data corresponding to thermal treatment 1 (*cf.* text). The difference in size of dots serves to indicate values of T_f^b and T_f^a (*cf.* Figure 2), larger dots corresponding to T_f^b. Experimental indetermination on T_f values is indicated in the few cases in which it was larger than usual. Heating rate was 16°/min.

TABLE II: Equilibrium Melting Temperatures for Nylon 6–Salt Systems

Salt, w/w %	Molar fraction	T_m, °C (±2°)
0	0	240
3.5% KCl	0.052	238
7.0% KCl	0.103	236
2.0% LiBr	0.026	226
4.0% LiBr	0.052	213
6.0% LiBr	0.077	203
2.0% LiCl	0.052	220
2.6% LiCl	0.067	212
4.0% LiCl	0.100	192

Plots of T_f^a and T_f^b as a function of T_c are reported in Figure 3. Fusion temperatures (*cf.* Figure 3) did not exhibit systematic variations in correspondence to differences in ΔH_f values (*cf.* Table I) resulting from differences in t_c or in the rate of crystallization. Likewise, no significant effect of t_f was observed on the fusion temperatures. Longer t_c values (using thermal treatment 1) were particularly used for nylon 6 + 4% LiCl when the rate of crystallization was low, in order to compare data at a similar degree of crystallinity. Careful analysis of the effect of

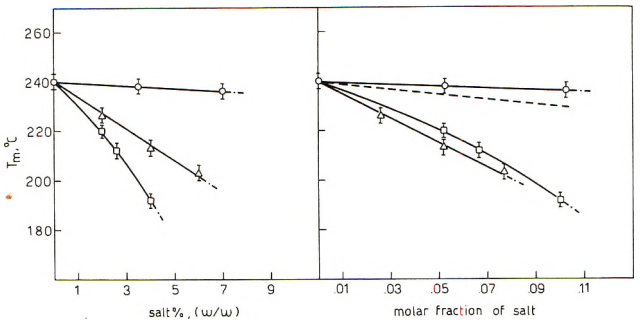

Figure 4. Variation of the equilibrium melting temperature, extrapolated from the data in Figure 3, with salt concentration: □, LiCl; Δ, LiBr, O, KCl. The dashed line represents the theoretical variation of T_m with diluent content calculated according to eq 4 with $\chi_1 = 0.2$, $X = 4.2$, and $\Delta H_u = 5100$ cal/mol.

rate of heating indicated no alterations of T_f (±1°) between 16 and 64°/min. A possible exception was the case in which crystallization was very fast (*i.e.*, pure nylon 6 at low T_c) when an increase of T_f of 2–3° occurred between 16 and 64°/min. Since the determination of T_f was more precise at 16°/min than at 64°/min, the former rate was generally used. T_f *vs.* T_c plots yielded the same extrapolated T_m value (*cf.* seq.) when data at 16 or 64°/min were used. The data in Figure 3 indicate that upon increasing T_c, T_f also increases. However, when two peaks are present, T_f^a is not essentially affected by variations in T_c. It is seen that the experimental points do not lie on the $T_f = T_c$ line; however, the data can be extrapolated (within ±2°) to obtain a value of fusion temperature on the $T_f = T_c$ line. The T_f *vs.* T_c line was drawn following the T_f^b points, and the T_f points at high T_c, when only one peak was observed. In terms of the Hoffman and Weeks[23] treatment, the extrapolated value corresponds to the equilibrium melting temperature T_m. Values of T_m thus extrapolated are reported in Table II and in Figure 4 as a function of salt composition expressed both as w/w and molar fraction of salt (referred to the ε-caprolactam unit). The data indicate that on increasing salt concentration the melting temperature is depressed. A noticeable difference exists among the effects of different salts, the order for increasing depression at a given molar fraction of salt being

$$KCl < LiCl < LiBr \quad (1)$$

The results of the analysis of the crystallization kinetics are collected in Figure 5. The time necessary to the development of about 15% crystallinity at a given molar fraction of salt and supercooling, $\Delta T = T_m - T_c$, is seen to increase in the order

$$KCl < LiBr < LiCl \quad (2)$$

increasing concentrations of a given salt (LiBr and LiCl) producing increasing reduction of crystallization rate. Particularly evident is the effect of 4% LiCl for which, due to the extremely low crystallization rate, only the t_c'' time could be determined. The data suggest that supercoolings of the order of 60° are required in order to obtain relatively fast crystallization rates. Due to the slowness of crystallization, no measurements were taken when salt concentration was greater than 4% LiCl and 6% LiBr.

(23) J. D. Hoffman and J. J. Weeks, *J. Res. Nat. Bur. Std., Sect. H*, **66**, 13 (1962).

TABLE III: X-Ray Data for Nylon 6–Salt Systems

Salt, w/w %	Thermal treatment t_f, hr	Thermal treatment t_c, hr	Thermal treatment T_c, °C	Spacings, Å	Observations
0	5	48	190	4.4, 3.7	α
3.5% KCl	72	48	150	4.4, 3.7, 3.1, 2.2	α + KCl
7% KCl	72	48	150	4.4, 3.7, 3.1, 2.2	α + KCl
7% KCl	5	220	180	4.4, 3.7, 3.1, 2.2	α + KCl
4% LiBr	5	48	160	4.4, 3.7, 4.1	$\alpha + \gamma$, $\%\alpha/\%\gamma \sim 1$
4% LiBr	5	220	160	4.4, 3.7, 4.1	$\alpha + \gamma$, $\%\alpha/\%\gamma \sim 1$
6% LiBr	5	48	100	4.4, 3.7, 4.1	$\alpha + \gamma$, $\%\alpha/\%\gamma < 1$
2% LiCl	5	48	170	4.4, 3.7, 4.1	$\alpha + \gamma$, $\%\alpha/\%\gamma > 1$
4% LiCl	5	48	140	4.4, 3.7, 4.1	$\alpha + \gamma$, $\%\alpha/\%\gamma < 1$
4% LiCl	5	220	160	4.4, 3.7, 4.1	$\alpha + \gamma$, $\%\alpha/\%\gamma < 1$

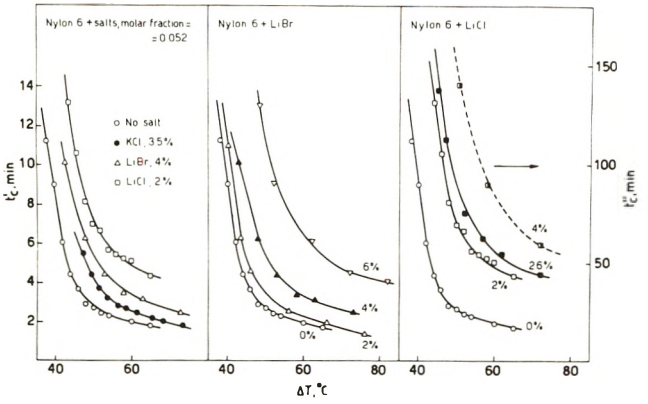

Figure 5. The time t_c' necessary to develop about 15% crystallinity (corresponding to a ΔH_f value about 7.5 cal/g) plotted as a function of the supercooling $\Delta T = T_m - T_c$ for nylon 6–salt system. Salt composition is given as w/w. On the diagram to the left, the compositions given correspond to a constant molar fraction of KCl, LiBr, and LiCl equal to 0.052. The dashed curve on the right correspond to the time t_c'' necessary to develop a ΔH_f of about 2 cal/g.

X-Ray Data. Wide angle X-ray patterns for pure nylon 6 (*cf.* Table III) exhibited spacings at 4.4 and 3.7 Å irrespective of the values of the parameters characterizing the thermal treatment (T_c, t_c, and t_f). Only in the case of the original powder, not subjected to any thermal treatment, a faint reflection at 4.1 Å was noticed in addition to the 4.4- and 3.7-Å spacings. The latter spacings are characteristic of the α form (200 and 002 planes) according to Bunn and coworkers,[24,25] while the 4.1-Å spacing is characteristic of the γ form (001 and $\bar{2}01$ planes) according to Ota, *et al.*[26-30] In the presence of LiCl and LiBr coexistence of α and γ was indicated, although no appreciable effect of T_c, t_c, and t_f was, again, found. On increasing LiCl or LiBr concentration the content of γ form appeared to increase. While the data were inadequate for a quantitative assessment, the ratio per cent α/per cent γ appeared to be of the order of $\sim$1 for 4% LiBr and >1 for 2% LiCl (in both cases the molar fraction of salt being 0.052). In the presence of KCl, only the α form was observed. In this case, beside the reflections of the α form, also the reflections typical of KCl were observed. By contrast, no reflection of LiCl or LiBr could be observed under the conditions investigated.

The reflections observed in the presence of LiCl and LiBr were considerably sharper than in the case of pure nylon 6 (at given t_f, t_c, and supercooling ΔT), suggesting the occurrence of more perfect crystals when salt is present (the low degree of crystallinity not withstanding).

(4) Discussion

The behavior of the intrinsic viscosity *vs.* fusion time (*cf.* Figure 1) is similar to that recently reported by Peebles and Huffman[31] in their study and critical review of thermal degradation of nylon 66. They noticed that thermal degradation follows a different course depending upon whether or not volatile products of degradation are allowed to escape. In sealed tube experiments, similar to our own, the intrinsic viscosity was found to first pass through a maximum, then a minimum, followed by abrupt formation of insoluble, cross-linked material. On the other hand, when volatile products were allowed to escape, rapid gelation occurred even in absence of oxygen. An extensive list of degradation products (volatile and not, several of them soluble in H_2O or HCOOH solutions) was compiled by Peebles and Huffman. They suggested that in the region in which an initial climb of intrinsic viscosity is observed, polymerization of unreacted ends, and some deamination, is prevailing. A similar interpretation seems to be valid for our data, at least up to fusion times of about 5 hr. Note that 5 hr was just the fusion time adopted in our present thermal analysis investigation. Therefore, although our samples were not stabilized[32,33] and a change of molecular weight occurred during the preferred thermal treatment, conditions adopted were such as to exclude occurrence of alterations capable of significantly contributing to the observed melting behavior. Even though salts might have favored some depolymerization (by ammonolysis and hydrolysis reactions[31]) or favored the occurrence of side chain branching,[31] relative to nylon 6 containing no salt, the results of our extraction studies (*cf.* Materials and also ref 12) clearly support the foregoing conclusion. In fact, the material which could be

(24) C. W. Bunn and E. V. Garner, *Proc. Roy. Soc., Ser. A*, **189**, 39 (1947).
(25) D. R. Holmes, C. W. Bunn, and D. J. Smith, *J. Polym. Sci.*, **17**, 159 (1955).
(26) T. Ota, O. Yoshizaki, and E. Nagai, *Chem. High Polym.*, **20**, 225 (1963).
(27) D. Vogelsong, *J. Polym. Sci., Part A-1*, 1055 (1963).
(28) Y. Kinoshita, *Makromol. Chem.*, **33**, 1 (1959).
(29) H. Arimoto, *J. Polym. Sci., Part A-2*, 2283 (1964).
(30) E. M. Bradburry, L. Brown, A. Elliot, and D. A. D. Parry, *Polymer*, **6**, 465 (1965).
(31) L. H. Peebles and M. W. Huffman, *J. Polym. Sci., Part A-1*, **9**, 1807 (1971).
(32) J. R. Schaefgen and P. J. Flory, *J. Amer. Chem. Soc.*, **70**, 2709 (1948).
(33) E. Turska and S. Gogolewski, *Polymer*, **12**, 616, 629 (1971).

extracted (about 3% w/w, beside the salt) could not have affected the melting temperature, in terms of eq 4, *cf. seq.*, by more than 5° and, moreover, the polymer resulting from such an extraction had a fusion temperature indistinguishable from that of the original nylon 6.

Before entering into the discussion of more plausible interpretations of the observed melting behavior, it is appropriate to critically discuss the extrapolation of T_m values from the data in Figure 3. The extrapolation proposed by Hoffman and Weeks[23] is based on the application of the Thompson formula

$$T_f = T_m[1 - (2\sigma_e/\Delta h_f l)] \quad (3)$$

where l is the thickness of larger, mature lamellae crystallized at temperature T_c, σ_e is the end surface free energy, and Δh_f is the enthalpy of fusion per unit volume. One of the crystal dimensions, that corresponding to the step height for chain-folded crystals, is assumed to depend only on crystallization temperature; growth of the crystal occurred prevalently in the directions perpendicular to l. However, it has now been recognized that thickening processes in chain-folded crystal, as well as recrystallization processes during the melting run, do occur and may cast doubts on the extrapolation of the true melting temperature.[34-37] These effects may be assumed to represent only a minor complication when, as in the present case (*cf.* Results), greatest reliance is placed on T_f values corresponding to small supercooling ΔT, fast melting rates are used, and the effect of alteration of t_c is negligible. Other limitations of the theory, particularly those connected with more elaborate ways for accounting for the surface free energy[38-41] and the degree of perfection of the crystal,[42] could however be relevant, particularly for the nylon 6–salt systems. It would, therefore, be desirable to attempt other determinations of T_m, in particular through the direct use of eq 3 and the measured lamellae thickness.

Our reported value for T_m of pure nylon 6 (240°) is somewhat smaller than the value reported by others[18,42] following a similar approach. Occurrence of some degradation products resulting from the thermal treatment (*cf.* Materials) may justify part of the difference. The depression of T_m due to the addition of 4% w/w of LiCl is of order of 50°. The depression observed may be compared with that expected for weakly interacting polymer–diluent systems for which random mixing occurs. The latter depression is given by the well-known equation[43]

$$(1/T_m) - (1/T_m^0) = (R/\Delta H_u)X(v_1 - v_1^2\chi_1) \quad (4)$$

where T_m^0 is the melting temperature of pure polymer, ΔH_u the melting enthalpy per crystallizable polymer unit, X the ratio of molar volumes of the polymer unit and of the diluent, v_1 the volume fraction of diluent, and χ_1 an interaction parameter. The equation is plotted in Figure 4 using a value of $X = 4.2$ (corresponding to the LiCl molar volume), $\chi_1 = 0.2$ (a reasonable value for a thermodynamically good diluent[43]), and $\Delta H_u = 5100$ cal/mol, as deduced from literature.[17] It is seen that the above theory predicts a negligible melting point depression in the composition range investigated. The behavior observed in the presence of LiCl or LiBr cannot therefore be rationalized in terms ot this theory, unless extremely high (negative) values of the polymer–diluent interaction parameter are considered. These results, and the order of salt effectiveness according to series 1, are in line with the ranking of the salts for their ability to bind to denatured biopolymers in water solutions and to depress the corresponding denaturations points.[2b,3] In the case of water solutions, no binding ability or depression effects were observed with KCl[2b,3] (generally regarded as a salting-out agent), while the melting point depression observed with strongly interacting salting-in agents was described in terms of a free energy of binding[2a,8,43,44] having the form $\Delta G = -pRT \ln (1 + Ka_s)$, where K is the binding constant between salt and amorphous polymer, a_s is the salt activity, and p the number of binding sites per polymer unit. A plausible interpretation of the present results is that the binding ability of salts to amorphous polymers persists even in the absence of water.

The specific site of interaction is, likely, the amide group. Stoichiometric complexes have been observed between model peptides and LiBr in aqueous solutions.[6] Complexes between amide groups and iodine for both γ and α nylon 6 have been discussed by Abu-Isa[20] on the basis of infrared evidence and it is remarkable that occurrence of these bound species tends to favor the crystallization of the γ form (*cf. seq.*), as is the case of LiCl and LiBr observed here. Another evidence for the ability of LiCl and LiBr to interact with nylon 6 is offered by the absence of reflections due to the salt in the diffraction patterns of the mixtures. By contrast, when KCl is present, reflections of the salt were observed (KCl, in fact, may have insignificant diluent power for nylon 6). The possibility that salting-in agents interact with polar polymers even in complete absence of water seems in contrast with observations by Sherebrin and Oplatka[45] and by Alexander[46] who investigated the effect of limited amounts of water on the denaturation of collagen and keratin fibers in presence of LiBr. These authors suggested that Li ions must be partly hydrated (three–ten water molecules per Li ion) in order to induce denaturation. While under the experimental conditions adopted here it is unlikely that this amount of water was present in our samples, we have observed that equilibration of nylon 6 + 4% LiCl mixtures, having low degree of crystallinity, with normal atmospheric moisture at room temperature, resulted in an additional regression of crystallinity (as judged by ΔH_f and transparency of the samples). Although the evolution of crystallinity with moisture needs further investigation, we feel that the most critical factor in observing salt effects in the bulk state is an intimate homogenization of polymer and salt.

Before an interpretation based on binding between salt and *amorphous* nylon 6 is accepted, other alternatives should be considered. A possibility is that the melting behavior should be attributed to the occurrence of crystalline modifications of nylon 6. The crystallographic modifi-

(34) J. J. Weeks, *J. Res. Nat. Bur. Std., Sect. A*, **67**, 441 (1963).
(35) J. D. Hoffman and J. J. Weeks, *J. Chem. Phys.*, **42**, 4301 (1965).
(36) E. Hellmuth and B. Wunderlich, *J. Appl. Phys.*, **36**, 3039 (1965).
(37) R. A. Fava, *J. Polym. Sci., Part D-5*, 1 (1971).
(38) T. Kawai, *Kolloid-Z. Z. Polym.*, **201**, 15 (1965).
(39) C. M. L. Atkinson and M. J. Richardson, *Trans. Faraday Soc.*, **65**, 1774 (1969).
(40) M. G. Broadhurst, *J. Res. Nat. Bur. Std., Sect. A*, **70**, 481 (1966).
(41) A. Peterlin and H. G. Zachmann, *J. Polym. Sci., Part C-34*, **11** (1971).
(42) T. Arakawa and F. Nagatoshi, *J. Polym. Sci., Part B-8*, **41** (1970).
(43) P. J. Flory, "Principles of Polymer Chemistry," Cornell University Press, Ithaca, N. Y., 1953.
(44) J. A. Schellman, *J. Phys. Chem.*, **62**, 1485 (1958).
(45) M. H. Sherebrin and A. Oplatka, *Biopolymers*, **6**, 119 (1968).
(46) P. Alexander, *Annu. N. Y. Acad. Sci.*, **53**, 653 (1951).

cations of nylon 6 which have been reported in the literature are summarized by Liberti and Wunderlich.[21] The α form[24,25] consists of extended sheets where hydrogen-bonded chains are arranged in an antiparallel fashion with the amide groups parallel to the draw direction. Although there is still some controversy[26-30] on the detailed structure of the γ form first suggested by Kinoshita,[28] it appears that the structure consists of pleated sheets containing hydrogen-bonded, parallel chains with the plane of the amide group roughly perpendicular to the draw direction. Beside the α and γ forms, a β form was suggested by Bunn and coworkers[24,25] and observed by Ziabicki and Kedzierska[47] by melt-spinning nylon 6 at very high speed. The β form appeared to be less stable than the α form into which it could be transformed by annealing. Vogelsong[27] suggested however that the β and γ forms of nylon 6 were identical and now only different α and γ forms appear to be considered.[30] The $\alpha \rightarrow \gamma$ transition was achieved by treatment with a iodine–potassium iodide solution, followed by removal of iodine with aqueous solutions of sodium thiosulfate.[20,28,29] Reversal $\alpha \rightarrow \gamma$ transition may be obtained by drawing[48,49] or by treatment with aqueous phenol solutions.[28] Abu-Isa,[20] working with isolated α or γ forms, recently showed that no $\alpha \rightarrow \gamma$ or $\gamma \rightarrow \alpha$ transition can be induced by thermal treatment, the two forms are quite stable unless hydrogen bonding is broken by melting, mechanical, or chemical treatments. The fusion of the two forms occurs in the same temperature region (~210–220°) and multiple peaks are exhibited by both forms. Thus, the stability of the two forms appears to be very near the same, although the melting entalphies may be slightly different.[49] The iodine complex of the α nylon 6 was indistinguishable, by infrared techniques, from the complex of γ nylon 6 and exhibited no melting between 30 and 250°. The temperature of the washing solution, used to remove the iodine, determined whether α nylon 6 (high-temperature wash) or γ nylon 6 (low-temperature wash) would crystallize upon iodine removal.

On the basis of the above analysis it is plausible to suggest that, although salting-in agents such as LiCl and LiBr seem to favor the occurrence of a certain amount of γ form, it is not likely, in view of the similarity of the fusion temperatures of the two forms, that this effect may be regarded as responsible for the large depressions of the melting temperature brought about by these salts. There also seems to be no evidence indicating that LiCl or LiBr become part of new crystalline forms having melting points different from those of pure α or γ forms.

In addition to the large depression of the melting temperature, salting-in agents have the property of strongly reducing the crystallization rate of nylon 6, as evidenced from the decrease of ΔH_f with increasing salt concentration at given t_c and ΔT (*cf.* Figure 5 and Table I; note also the interesting inversion of the order of LiBr and LiCl in series 1 and 2).

In connection with the behavior of the melt viscosity at 250° it is interesting to observe that the reported increase, due to the presence of salt, occurs in spite of the fact that the intrinsic viscosity of nylon 6–LiCl mixtures is lower than that of pure nylon 6. Partial results[12] on the effect of salts on the glass transition temperature T_g of nylon 6 (~60°) did not reveal a pronounced effect of LiCl on T_g; the problem, however, requires further investigation.

The possibility of obtaining transparent nylon 6–LiCl or LiBr samples, with (controlled) low or negligible degree of crystallinity,[12,50] is based on the occurrence of the reduction of both T_m and crystallization rate, coupled with the practical necessity of significant supercoolings and the relatively high T_g value. In particular, even with slow cooling, it was found to be extremely difficult to crystallize mixtures containing 8% LiCl or 12% LiBr. The difficulty can better be appreciated considering that for a nylon 6 + 8% LiCl mixture, after about 800 hr at T_c = 80°, the only faint and broad fusion peak, which could be detected at $T \sim 105°$, had an area corresponding to a ΔH_f of no more than 0.5 cal/g. Available evidence thus suggests that when LiCl or LiBr concentration is increased beyond the limits within which melting temperature and crystallization rate may be conveniently measured, the depression of both these quantities is further increased. The mixtures may then easily remain, below T_g, in the state of frozen liquids.

Acknowledgment. The cooperation of Drs. R. Marazza and Daniela Rossi in obtaining the X-ray data is gratefully acknowledged. We express our appreciation to Professor G. Wegner for clarifying discussions.

This investigation was supported by the Italian National Research Council, through its Technological Committee, research contract No. 71.01157.11.115.A.16.

(47) A. Ziabicki and K. Kedzierska, *J. Appl. Polym. Sci.*, **2**, 14 (1959).
(48) H. Arimoto, *Kobunshi Kagaku*, **19**, 212 (1962).
(49) K. Miyasaka and K. Ishikawa, *J. Polym. Sci., Part A-2*, **6**, 1317 (1968).
(50) V. A. Kargin, T. I. Sogolova, N. Ya. Rapoport, V. A. Vorotnikova, and N. A. Slovokhotova, *Vysokomol. Soedin., Ser. A*, XIII, 1779 (1971).

Kinetics of Spherulite Growth in Cholesteryl Esters[1]

Fraser P. Price* and A. Keith Fritzsche

Polymer Science and Engineering, University of Massachusetts, Amherst, Massachusetts 01002 *(Received May 12, 1972)*

Publication costs assisted by the National Institutes of Health

The growth rates of crystalline spherulites developing from the smectic phases of cholesteryl myristate and cholesteryl nonanoate and from the cholesteric phase of cholesteryl acetate have been measured over a range of temperatures. Within experimental error these growth rates showed no temperature dependence. The growth rates were used, in conjunction with previously determined kinetics of gross transformation, to calculate nucleation rates and the temperature coefficients of the nucleation rates for the crystallization of the three esters. The critical nuclei were ascertained to be disk-like with reasonable surface energies but surprisingly small size.

Introduction

The thermodynamic behavior of compounds and mixtures of compounds which exhibit mesophase behavior has been the subject of much investigation.[2-4] However, relatively little has been done to delineate the energy barriers which separate the various mesophases. In this laboratory we have been engaged in the study of kinetics of transformation between mesophases, from the isotropic to various mesophase states, and from various mesophase states to the solid crystalline state.[5-7] We have been concerned primarily with the long-chain fatty acid esters of cholesterol. High-precision dilatometry has been the technique of choice. Such gross transformation studies yield information about the overall transformation rate which includes both the nucleation and the growth of the transforming regions. To separate the nucleation and growth processes, it is necessary to measure one or the other by an independent technique. The present paper is concerned with the measurement of the growth rates at various temperatures. The spherulites which are known to appear from the liquid crystal phases of cholesteryl myristate, nonanoate, and acetate have been studied. Combining information about the spherulite growth rates and their temperature coefficients with the gross transformation rates we shall be able to gain information about the nucleation rate of the transformations into the solid state.

Experimental Section

Samples of cholesteryl myristate and nonanoate were the same ones used in the previous investigations.[5-7] The myristate and acetate had been purified by recrystallization from *n*-pentanol. The nonanoate was used as obtained. The source of these materials was the Aldrich Chemical Co., Milwaukee, Wisc. for the acetate and the nonanoate, while the myristate was a product of the Eastman Organic Chemical Co., Rochester, N. Y.

Apparatus. The crystallization was carried out on the hot stage of a Zeiss polarizing microscope. This hot stage was equipped with electric heaters so that it could be heated to temperatures above the isotropic melting point of the various liquid crystal forming substances and then by circulating thermostated water through it rapidly quenched down to the temperature at which it was desired that the crystallization take place. The temperature control at the crystallization temperature was ±0.1°. The temperature was measured by a copper–constantan thermocouple imbedded at the hot stage near the sample. The developing spherulites were photographed on Polaroid type 57 ASA 3000 film. Usually multiple exposure photographs were made.

Experimental Procedure. Samples of the material under investigation were placed between microscope cover slips. Each sample was heated to the isotropic state for at least 30 min prior to quenching to the crystallization temperature. In the cases of cholesterol myristate, acetate, and nonanoate these temperatures were respectively 95, 120, and 98°. Several minutes were required for establishment of the final crystallization temperature after the circulating water was turned on. The growth rates of the developing spherulites were recorded by making multiple exposures at appropriate time intervals. In many cases it was not possible to see the initiation of the spherulites. The motion of the spherulitic front during the various time intervals was used to calculate the spherulite growth rate. At least three exposures were made of each developing spherulitic system. In some cases in order to facilitate the interpretation of the multiple exposure photograph portions of the developing spherulite were successively blocked out by inserting an opaque object at appropriate positions in the optical train. The photograph thus obtained for the spherulite showed a stepped edge with the height of the steps being a measure of the distance the spherulite had grown between successive exposures. The magnification calibrated by photographing a stage micrometer was approximately 160×. All the growth rate data were obtained from a minimum of three to a maximum of ten such measurements on a particular developing spherulite.

(1) This research was supported by the National Institutes of Health, Grant No. HE 13188.
(2) (a) G. H. Brown, J. W. Doane, and V. D. Neff, *Crit. Rev. Solid State Sci.*, **1**, 303 (1970); (b) R. S. Porter, E. M. Barrall, II, and J. F. Johnson, *Accounts Chem. Res.*, **2**, 53 (1969).
(3) G. J. Davis and R. S. Porter, *Mol. Cryst. Liquid Cryst.* **6**, 337 (1970).
(4) G. J. Davis and R. S. Porter, *Mol. Cryst. Liquid Cryst.*, **10**, 1 (1970).
(5) F. P. Price and J. H. Wendorff, *J. Phys. Chem.*, **75**, 2389 (1971).
(6) F. P. Price and J. H. Wendorff, *J. Phys. Chem.*, **75**, 2849 (1971).
(7) F. P. Price and J. H. Wendorff, *J. Phys. Chem.*, **76**, 276 (1972).

Results and Discussion

All samples upon cooling when viewed between crossed polars changed in appearance from opaque to a sandy birefringent background. This birefringent background was indicative of the smectic state in the cholesteryl myristate and nonanoate and of some texture of the cholesteric state in the cholesteryl acetate. The particular texture (focal-conic or Grandjean) from which the spherulites were developing was not noted. This would have been possible with the smectic myristate and nonanoate but probably not with the cholesteric acetate, because of its transient existence. In any event, the extremely small energy difference between textures of a given mesophase probably preclude effects of texture upon either nucleation or growth rates of the spherulites. No attempt was made to record the temperatures of the transformations from the isotropic phase to mesophase because of the rapid cooling through this temperature range to the temperature of crystallization. In the cholesteryl myristate in very thin films the smectic phase turned opaque with scattered birefringent regions. The spherulites of the crystalline material which developed seemed to grow around these birefringent regions. In thicker samples of the myristate, the disappearance of the birefringent smectic phase did not occur nor was the structure the same. However, the growth rates in both thick and thin samples of the myristate were identical. Measurements made of doubly purified and the unpurified myristate samples yielded no detectable differences in spherulite growth rates. The results of this study are summarized in Table I. Herein is displayed the very surprising result that there seems to be no effect of temperature upon the growth rate of spherulites developing from mesophases into the solid crystalline state. The precision measures attached to the growth rate are the average deviations of the growth rates. The fact that the spherulite growth rates do not depend upon the temperature whereas the gross transformation rates do means that the temperature dependence of the gross transformation process resides solely in that of the nucleation of the developing regions. This will be discussed more fully later. It is noteworthy that in a recent investigation[8] of the transformation to the crystalline state of cholesteryl nonanoate it was assumed that the temperature coefficient of the growth rate was negligible compared to that of the nucleation rate and that the temperature coefficient of the rate of the appearance of turbidity reflected only the temperature sensitivity of the nucleation rate. The present work validates the assumption of these investigators and further, it indicates a very similar temperature dependence of the nucleation rate for the nonanoate.

Now, we turn to some of the peculiarities of the individual esters during the crystallization process. In the myristate, which was studied most extensively, it was noted that the long annealing period above 95° did not alter the growth rate of the spherulites. In two experiments, one at 47.6° and the other at 57.5°, samples were annealed for only 5 min prior to quenching to the crystallization temperature. The growth rates at these temperatures were 0.0012 and 0.0011 cm/sec. Whereas, the growth rate seems not to be altered either by purification or by time of annealing, the latter does markedly affect both the number of spherulites finally appearing and the intensity of the background smectic phase from which the spherulites develop. It is possible that the effect of prolonged annealing on the number of spherulites may be due to decreases in sample thickness with concommitant increases in the influence of the glass surfaces. However, it is believed that this is improbable because (a) previous dilatometric experiments[5] wherein the wall spacings were fixed showed effects similar to those noted here and (b) recent experiments with dilatometers containing tiny (0.05 mm diameter) glass beads showed the smectic–solid transformation rates of the myristate to be enhanced by the presence of the beads. Increasing the annealing time decreases the intensity difference between the spherulite and the background, markedly increases the induction period prior to the initial appearance of spherulites, and decreases the total number of spherulites finally appearing. In the nonanoate the cloudy smectic state seemed to become transparent when the spherulites formed.

TABLE I: Spherulite Growth Rates of Crystalline Phases of Several Fatty Acid Esters of Cholesterol

Ester	Crystallization range, °C	No. of temperatures studied	Growth rate, cm/sec
Myristate	37.5–57.5	8	$1.1 \pm 0.1 \times 10^{-3}$
Nonanoate	35.0–41.5	3	$0.40 \pm 0.03 \times 10^{-3}$
Acetate	60.0–74.0	3	$4.6 \pm 0.6 \times 10^{-3}$

We now turn to the problem of calculation of the energetic parameters involved in the nucleation of the various solid crystalline phases. We have previously determined the Avrami[9] constants n and K for the transformation to the solid compounds cholesteryl myristate,[5] cholesteryl nonanoate,[7] and cholesteryl acetate.[6] In these situations the value of n was invariably 4, indicating the development of spheres nucleated sporadically in time. The habit of the developing regions indeed turns out to be spherical and we are therefore not particularly surprised that the number of these spheres should increase with time. Now, knowing the values of the growth rate, G, and the constant, K, we now calculate the nucleation rate, $\dot{N}$, from the equation $K = (\frac{1}{3})\pi G^3 \dot{N}$ for the various temperatures at which the gross transformation was studied. The nucleation rate is related to the temperature[10] through

$$\ln \dot{N} = \ln N_0 - (E^{\pm}/RT) - (\Delta F^*/RT) \qquad (1)$$

where N_0 is an essentially temperature independent parameter depending upon the shape of the developing nucleus and upon molecular parameters, $E^{\pm}$ is the energy required for transport of material across the interface between the developing nucleus and the surrounding melt, ΔF^* is the energy required to produce a nucleus of a particular size and shape having the thermodynamic properties of the bulk developing phase at the temperature under investigation, and R and T have their usual significance. The quantity ΔF^* depends upon either the first or the second power of the reciprocal of the supercooling depending on whether the developing nucleus can enlarge respectively in two or three directions. Thus plots of the $\ln \dot{N}$ *vs.* $1/T\Delta T^m$ (ΔT is the supercooling) for values of $m = 1,2$ are sufficient to determine if the developing nucleus is enlarging in only two directions ($m = 1$) and is a disk or

(8) J. M. Pochon and H. W. Gibson, *J. Amer. Chem. Soc.*, **93**, 1279 (1971).
(9) M. Avrami, *J. Chem. Phys.*, **7**, 1103 (1939); **8**, 212 (1940).
(10) F. P. Price in "Nucleation," A. C. Zettlemoyer, Ed., Marcel Dekker, New York, N. Y., 1970, Chapter 8.

TABLE II: Values of Interfacial Energies and Critical Sizes of Nuclei in the Crystallization of Cholesteryl Esters

Ester	Temp range, °C	T_T, °C	T_T transition	ΔH, cal/g	h, Å	σ, ergs/cm^2	r^*, Å
Myristate	40.3–50.6	70.5	Solid–smectic	18.7	37.4	6.5	9.5–14.3
Nonanoate	26.0–55.0	78.8	Solid–cholesteric	10.2	31.6	3.8	6.5–14.6
Acetate	79.8–90.6	112.8	Solid–isotropic	10.7	22.7	4.2	10.2–14.1

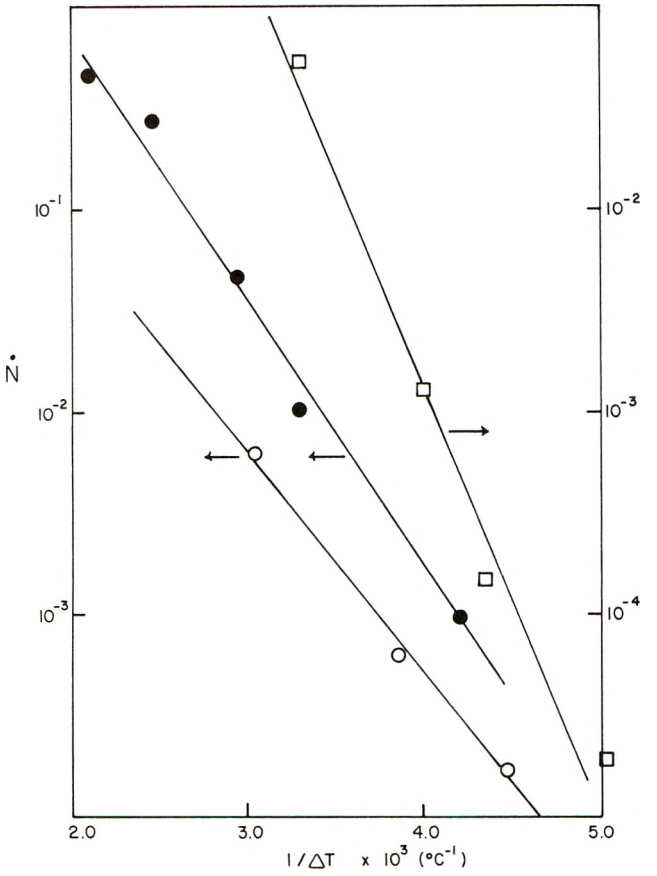

Figure 1. Plots of the logarithm of the nucleation rate *vs.* the reciprocal of the super cooling for (○) cholesteryl acetate, (●) cholesteryl nonanoate, and (■) cholesteryl myristate.

is enlarging in three directions ($m = 2$) and is a sphere. In our particular case, since the approximately 10% error in the growth rate introduces about a 30% error in the nucleation rate, it is sufficient to plot ln $\dot{N}$ *vs.* $1/\Delta T$ or $1/\Delta T^2$ rather than *vs.* $1/(T\Delta T)$ or $1/(T\Delta T^2)$. Such plots are shown in Figure 1 wherein are displayed the plots of $\dot{N}$ of the three compounds under consideration against $1/\Delta T$. It is clear from the linearity of these plots that the inverse second power plot will be curved. Therefore, the nucleation process produces disk-like nuclei. The formation of a disk-like region of transformed material in contact with the melt from which it grows requires the free energy with respect to the mother phase given by

$$\Delta F = -\pi r^2 h \Delta G_v + 2\pi r^2 \sigma_e + 2\pi r h \sigma \qquad (2)$$

Here r is the radius of the disk and h is its height, the interfacial energies σ_e and σ are those associated with the flat and the curved surfaces, respectively, and ΔG_v is the free energy of transformation per unit volume of the material at the temperature under consideration. In situations such as in the myristate where the transformation to the crystalline phase takes place from a low lying enantiotropic phase we will approximate ΔG_v by

$$\Delta G_v = \Delta H(T_T - T)/T_T = \Delta H(\Delta T)/T_T \qquad (3a)$$

where ΔH is the enthalpy of transition into the crystalline state at the equilibrium transition temperature, T_T, and T is the temperature at which the transformation is occurring. However, when the transformation to the crystalline state takes place from a low lying monotropic phase, such as the cholesteric phase in the case of acetate and the smectic phase in the case of the nonanoate, account must be taken of the diminution of ΔG_v due to the transformation into that monotropic phase. Here

$$\Delta G_v = (\Delta H \Delta T/T_T) - (\Delta H' \Delta T'/T_T') = (\Delta H \Delta T/T_T)(\alpha) \qquad (3b)$$

where $\Delta H'$ is the enthalpy of the transition into the monotropic phase at its equilibrium temperature $T_{T'}$, $\Delta T' = T' - T$ and $\alpha = 1 - (\Delta H'/\Delta H)(T_T/T_{T'})[1 - (\delta T/\Delta T)]$ where $\delta T = T_T - T_{T'}$. The values of the quantities ΔF^* and r^* associated with the maximum in the curve of ΔF *vs.* r are obtained by setting $\partial \Delta F/\partial r$ equal to zero and solving for r. Substituting this expression for r^* back into eq 2 yields ΔF^*. The values of the quantities at the extremum are

$$r^* = (\sigma T_T/\Delta H \Delta T)\{1/[1 - (2\sigma_e/h\Delta G_v)]\} \qquad (4a)$$

$$\Delta F^* = \{\pi h \sigma^2 T_T/\Delta H[1 - (2\sigma_e/h\Delta G_v)]\}(1/\Delta T) \qquad (4b)$$

and if it is assumed that the quantity $2\sigma_e/h\Delta G_v$ is much less than unity, an assumption which is probably somewhat tenuous, we arrive at

$$r^* = \sigma T_T/\alpha \Delta H \Delta T \qquad (5a)$$

$$\Delta F^* = \pi h \sigma^2 T_T/\alpha \Delta H \Delta T \qquad (5b)$$

Here α is unity in the case of the myristate and is somewhat less than unity for the nonanoate and the acetate. By substituting eq 5b into eq 1 we get $(\pi h \sigma^2 T_T)/(\alpha R \bar{T} \Delta H)$ as an explicit expression for the slopes of the curves in Figure 1. Here $\bar{T}$ is the average crystallization temperature. In order to calculate σ and r^* a knowledge of h must be had. We have assumed that quantity h was equal to the extended length of the particular ester under consideration. The results of these calculations are displayed in Table II. The temperature ranges indicated in the second column are those over which measurements of gross transformation rates yielded $n = 4$ and seemed to behave as if sporadic nucleation of spheres was occurring. For the myristate eq 3a was used to calculate ΔG_v. Equation 3b was used to calculate ΔG_v for the nonanoate and the acetate where $T_{T'}$ is 74.8° (cholesteric–smectic) and 91.6° (isotropic–cholesteric), respectively, and $\Delta H'$ is 0.13 cal/g [3] and 0.17 cal/g,[4] respectively. When these figures are used in eq 3b the magnitude of α was between 0.88 and 0.90 for the nonanoate and between 0.95 and 0.99 for the acetate. Thus, regardless of whether eq 3a or 3b is used, the differ-

ence in the calculated values of σ and r^* will not be very great. The third column indicates the temperature at which the crystalline phase can be in equilibrium with a particular higher temperature phase while the fourth column shows what the higher temperature phase is. The values of ΔH given in the fifth column of Table II should be in error by at most 10%.[3,4] The sixth column lists the extended lengths of the various esters which were assumed to be equal to h. The penultimate column of this table gives the values of the interfacial energies derived using in conjunction with eq 5, either eq 3a or 3b, whichever is appropriate. The interfacial energies are not unreasonable in magnitude. It should be noted here that the assumptions made in going from eq 4 to eq 5 may not be valid. If the quantity $2\sigma_e/h\Delta G_v$ is not negligible in comparison to unity then σ will be somewhat reduced. The values of the radius of the critical sized nucleus shown in the final column seem surprisingly small. It should be noted that, because of the functional dependence of the interfacial energies and the critical nuclei sizes upon the quantity $2\sigma_e/h\Delta G_v$, that if this latter quantity, should be say 0.1, the value of σ would be reduced by 5% but the value of the critical radius would remain unchanged. In the absence of any more direct knowledge about the possible magnitude of σ_e in comparison to ΔG_v it is not deemed profitable to speculate further about the effects of this quantity upon the changes in magnitude of σ and r^*. One further mention of this quantity σ_e in comparison to ΔH_v is worth making and that is the greater the supercooling the smaller is the ratio $\sigma_e/\Delta G_v$ so that the greater the supercooling, the more likely this term is to be negligible in comparison to unity.

Conclusions

The development of crystalline regions in the solid phases of cholesteryl myristate, nonanoate, and acetate takes place in the form of spherulites. This is consistent with the observation that the n in the Avrami equation for transformations into these crystalline states is 4. This magnitude indicates the nucleation of spheres developing sporadically in time. The growth rates of the spherulites of these three esters of cholesterol are independent of temperature over the ranges from 37 to 58° for the myristate, from 35 to 42° for the nonanoate, and from 60 to 74° for the acetate. This independence of the spherulite growth rates coupled with the high-temperature dependence of the growth transformation rates permits calculation of the temperature coefficients of the nucleation rates of the transforming crystalline regions. The interfacial energies calculated to exist between the developing nuclei and the surrounding mother phase are reasonable in magnitude. The values of the critical nuclei radii are much smaller than are usually encountered. The volume of the critical nucleii probably corresponds to only a few unit cells.

Light Scattering and Microscopic Investigations of Mesophase Transition of Cholesteryl Myristate.[1] I. Morphology of the Cholesteric Phase

S. A. Jabarin and R. S. Stein*

Polymer Research Institute, University of Massachusetts, Amherst, Massachusetts 01002 *(Received July 13, 1972)*

Publication costs assisted by the National Institutes of Health

Cholesteryl myristate exhibits a smectic and cholesteric mesophase, both when heated from the solid and when cooled from the isotropic melt. The morphology of the cholesteric phase obtained upon heating from the smectic phase can be described as having disk-like non-random orientation correlation. The isotropic–cholesteric phase transition, occurring on cooling, on the other hand, occurs in two steps. The first is a rapid transformation to a turbid "blue" homeotropic texture, while the second is a much slower transition to a more macroscopically ordered focal-conic spherulitic texture. The light scattering is similar to that observed for a spherulitic polymer and is shown to arise from fluctuation in the orientation direction of anisotropic structures. Spherulite sizes and orientation of optic axes are discussed.

I. Introduction

Cholesteryl myristate exhibits a smectic and cholesteric mesophase both when heated from the solid and when cooled from the isotropic melt.[2a] The thermal properties and the heat of transitions of cholesteryl myristate and other esters of cholesterol have been studied and are well documented.[2] Stein and coworkers[3,4] have studied the light scattering from a series of cholesteryl esters. The results indicate that the scattering arises from regions having correlated orientation of optic axes with dimensions

(1) Supported in part by a Grant from the National Institutes of Health.
(2) (a) G. W. Gray, "Molecular Structure and Properties of Liquid Crystals," Academic Press, New York, N. Y., 1962; (b) G. J. Davis, R. S. Porter, and E. M. Barrall, *Mol. Cryst. Liquid Cryst.*, **11**, 319, (1970).
(3) R. S. Stein, M. B. Rhodes, and R. S. Porter, *J. Colloid Interface Sci.*, **27**, 336 (1968).
(4) M. B. Rhodes, R. S. Porter, W. Chu, and R. S. Stein, *Mol. Cryst. Liquid Cryst.*, **10**, 731 (1970).

comparable to the wavelength of light. In this paper we shall describe a study of the morphology, size, and the orientation of the ordered regions in the cholesteric mesophase of cholesteryl myristate as well as the effect of thermal history on this morphology. In a following paper we shall discuss the kinetics of the isotropic–cholesteric phase transiton. The methods used are the light scattering, microscopy, and the depolarized light transmission techniques.

II. Experimental Section

A. Material. Cholesteryl myristate was obtained from Applied Science Laboratories, State College, Pa., lot 648-38. The laboratory had purified the sample by column chromatography and proved the purity to be better than 99% by thin layer chromatography. The purity of a similar sample was confirmed by Barrall, *et al.*,[5] using spectrometric analysis. However, more recent work by Davis and Porter[6] indicated that the purity was 98.1% as determined by the shape of the differential scanning calorimetric curves. This latter value is probably more accurate since the melting point depression reflects impurities, probably isomers, not detected by chromatography.

The temperatures of transitions for this material as determined by microscopy are 73.6, 79.7, and 84.0° for the solid–smectic, smectic–cholesteric, and cholesteric–isotropic transitions, respectively. These values agree well with the published literature values.[2b]

B. Preparation of Samples and Treatment of Cover Slips. Samples of thin films for both light scattering and microscopy were studied between microscope cover slips. A small amount of the powdered samples was placed on a microscope cover slide and then heated slowly to the isotropic melting point. Another cover slip was placed on top with a minimum amount of disturbance, then the temperature was raised to 90°, and held at this temperature for 0.5 hr, after which the sample was cooled to the desired temperature.

The cover slips were cleaned prior to use with potassium permanganate–sulfuric acid solution, rinsed several times with distilled water, and then dried between lens paper in a desiccator.

C. Microscopy. The photomicrographs were obtained with samples between crossed polaroids using a Carl Zeiss polarizing microscope (Standard WL) equipped with a camera in combination with a Metler FP2 hot stage. Kodak Plus-X Pan black and white panchromatic film (24 × 36 mm) was used.

D. Depolarized Light Intensity Measurements. The depolarized light intensity was measured using a four-stage Zeiss photometer in which the light intensity is indicated as a microammeter reading. The angular aperture of the photometer is 9° for the 0.16 numerical aperture objective lens used in this study.

E. Photographic Light Scattering. The light scattering pictures were obtained by using the small angle photographic light scattering apparatus which has been described elsewhere.[7] This consists of a Spectra-Physics Model 130 helium–neon gas laser (λ_0 6358 Å), a rotatable analyzer (Type HN 36 plastic mounted polaroid), and a photographic film holder. Stray radiation is eliminated by passing the incident laser beam through a 2-mm pinhole located about 1 cm below the sample. The exposure time was regulated by a camera type shutter. The patterns were recorded on 4 × 5 in. Polaroid Land Film Type 57.

III. Results and Discussion

When a sample of cholesteryl myristate is cooled very quickly from the isotropic melt to the cholesteric phase and kept under isothermal conditions, the field of view as seen in a polarizing microscope (between crossed polaroids) becomes a pale blue color almost immediately after temperature equilibrium is achieved. This color lasts for a few seconds and sometimes for several minutes depending on the temperature when the observation is made, the time being longer at higher temperatures within the range of the cholesteric phase. This transformation is seen to be followed by another slow transformation, to a more macroscopically ordered texture. When observing the transmission of light between crossed polaroids, only a small increase of transmission is seen upon forming the "blue" texture while a much larger increase in transmission occurs when the more macroscopically ordered texture is formed. These two changes were observed throughout the entire temperature range of the cholesteric phase using samples of varying thicknesses.

The appearance of the blue texture is believed to result from the scattering of visible light by structures of sizes smaller than its wavelength.[8] In this paper, the morphology of the phase resulting from the second slow transformation will be described.

The experimental procedure was as follows. The sample was heated to 90° and held at that temperature for 0.5 hr in the hope that this would ensure complete randomization in the isotropic melt. The sample was then cooled very quickly to the desired temperature. After temperature equilibrium was achieved (within 1 to 2 min), photomicrographs and light scattering pictures were taken at successive time intervals. Figure 1 shows the microscopic pictures at 80° for a 0.5-mil thick sample. Here one can see circular structures containing well-defined maltese crosses where the dark bands are parallel to the polarization directions similar to spherulitic structures obtained with crystallizing high polymers in which optic axes have average orientation parallel or perpendicular to the radius. The spherulites grow radially at a constant rate except when they impinge with each other. The corresponding Hv (polarizer vertical and analyzer horizontal) light scattering patterns are given in Figure 2. The Hv pattern taken 15 min after temperature equilibrium has a small four-leaf clover appearance typical for spherulites of high polymers. This pattern becomes smaller and more intense with time but another diffuse pattern surrounding the initial one appears which becomes more intense at longer times. This outer pattern, however, has 90° orientation, *i.e.*, with its intensity maxima oriented along the polarization directions.

Figure 3 shows the growing structures at successive times at 80° for a 1.5-mil thick sample. It is apparent from these photomicrographs that not all of the nuclei appear at the same time and that initially the spherulite appears to be internally uniform. As the spherulite grows, internal structure is seen to develop. The corresponding Hv light scattering patterns are given in Figure 4. These appear to be a composite of two patterns, at least at short times. As previously discussed, the very small central pat-

(5) E. M. Barrall, R. S. Porter, and J. F. Johnson, *J. Phys. Chem.*, **70**, 385 (1966).
(6) G. J. Davis and R. S. Porter, *Mol. Cryst. Liquid Cryst.*, **10**, 1 (1970).
(7) W. Chu, Ph.D. Thesis, University of Massachusetts, Amherst, 1969.
(8) T. Asada and R. S. Stein, *Mol. Cryst. Liquid Cryst.*, in press.

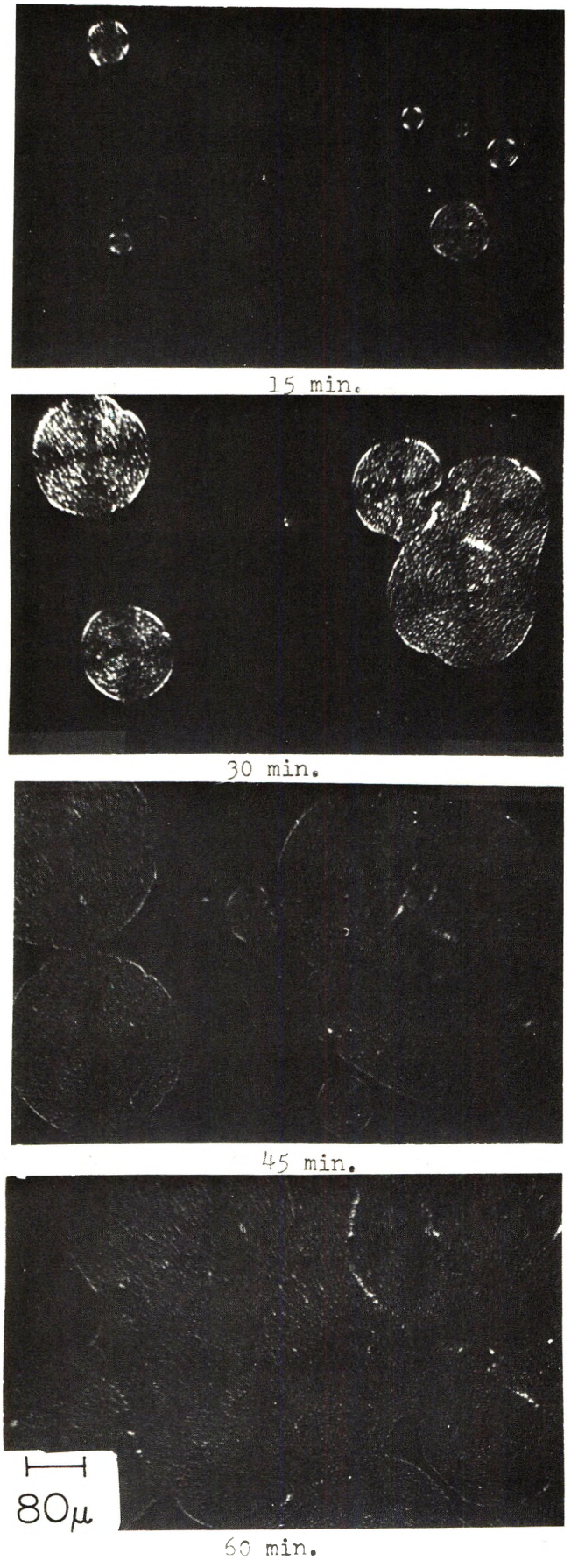

Figure 1. Photomicrographs of a 0.5-mil cholesteryl myristate sample at 80° at various time intervals.

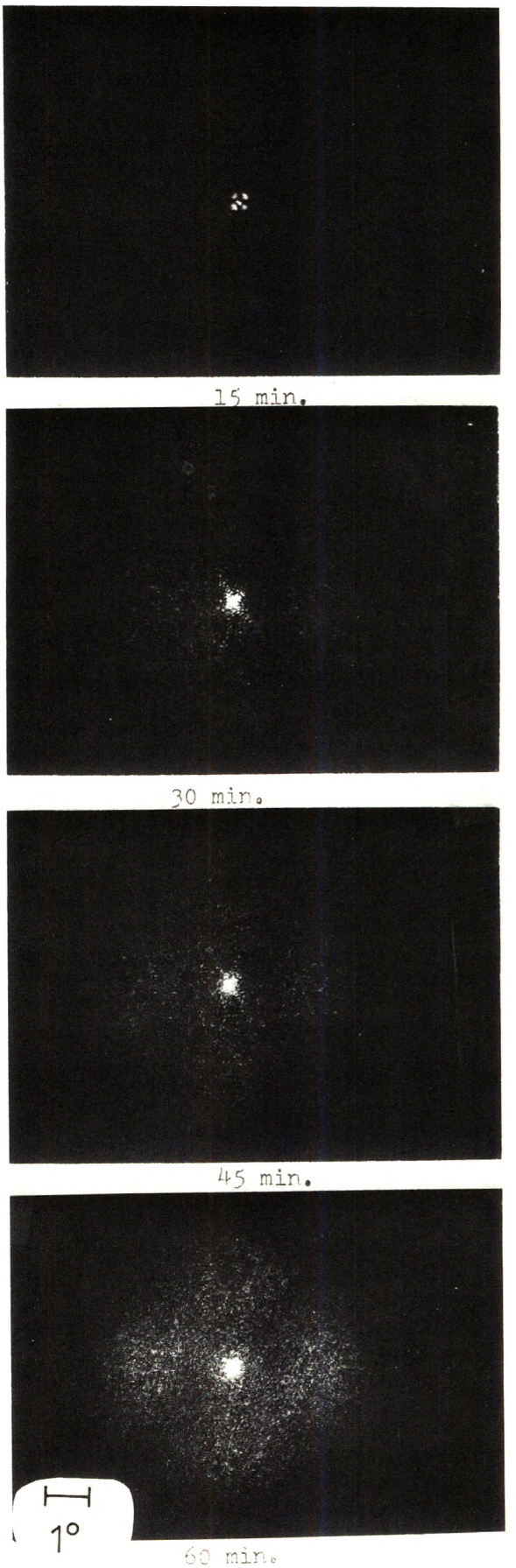

Figure 2. Hv Light scattering patterns of 0.5-mil cholesteryl myristate sample at 80° at various time intervals.

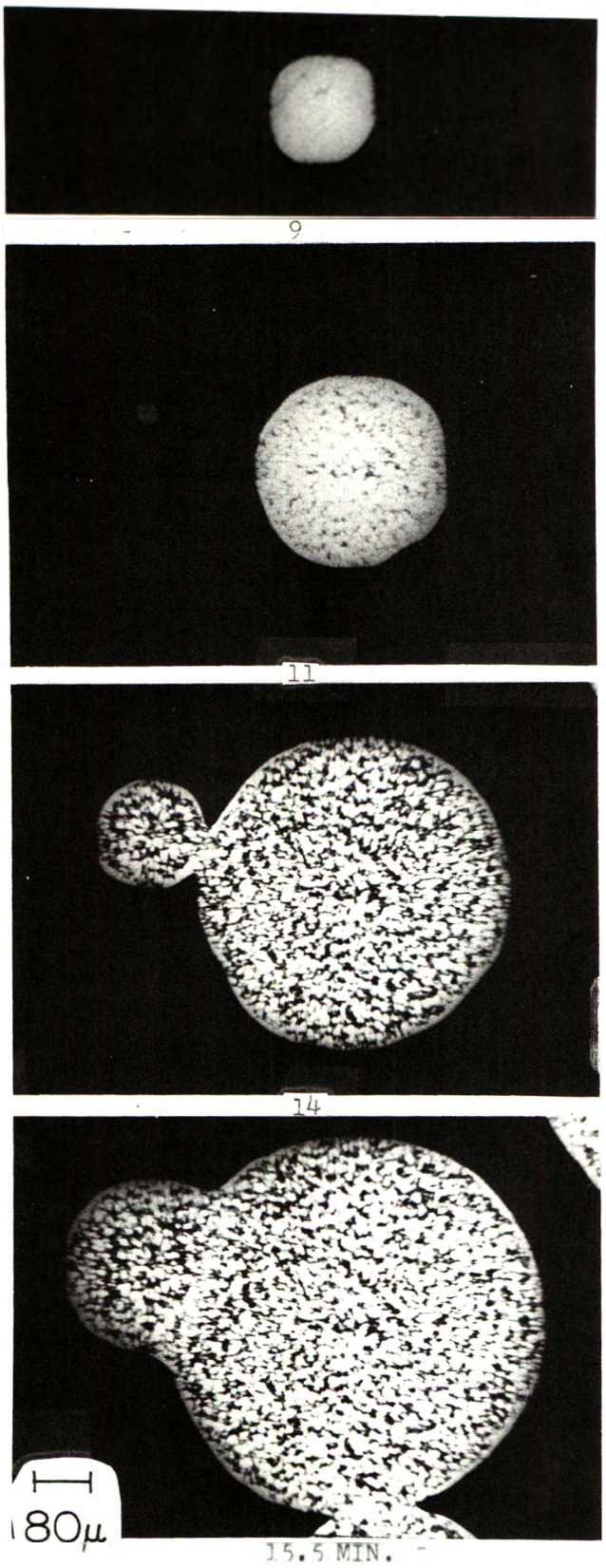

Figure 3. Photomicrographs of a 1.5-mil cholesteryl myristate sample at 80° at various time intervals.

tern has 45° orientation, while the outer larger one has 90° orientation. Similar results were obtained at 79.8, 80.5, and 81°. These observations are independent of the part of the sample which is studied.

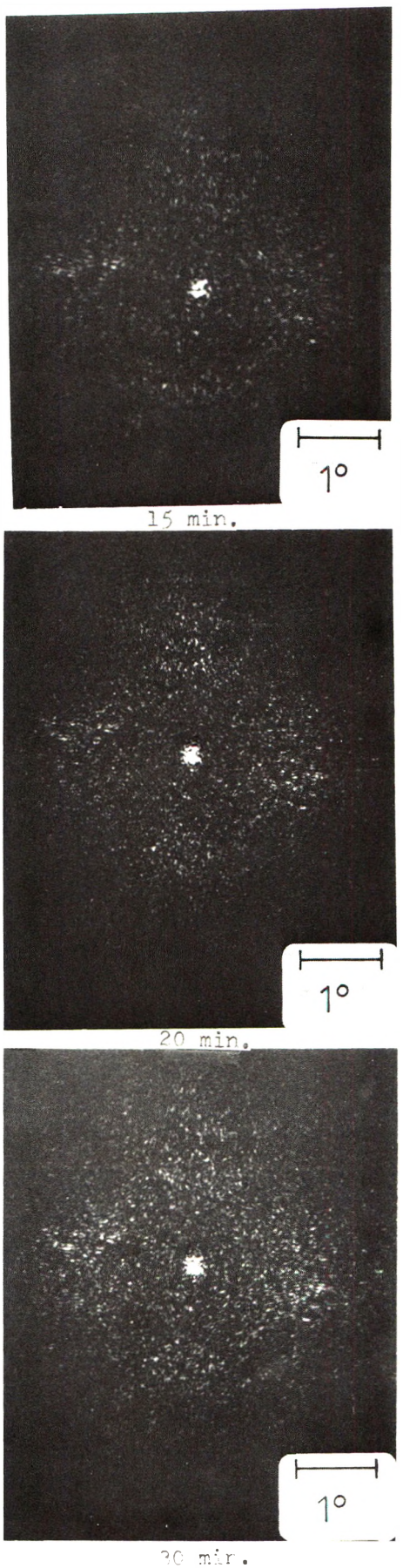

Figure 4. Hv scattering patterns of 1.5-mil cholesteryl myristate sample at 80° at various time intervals.

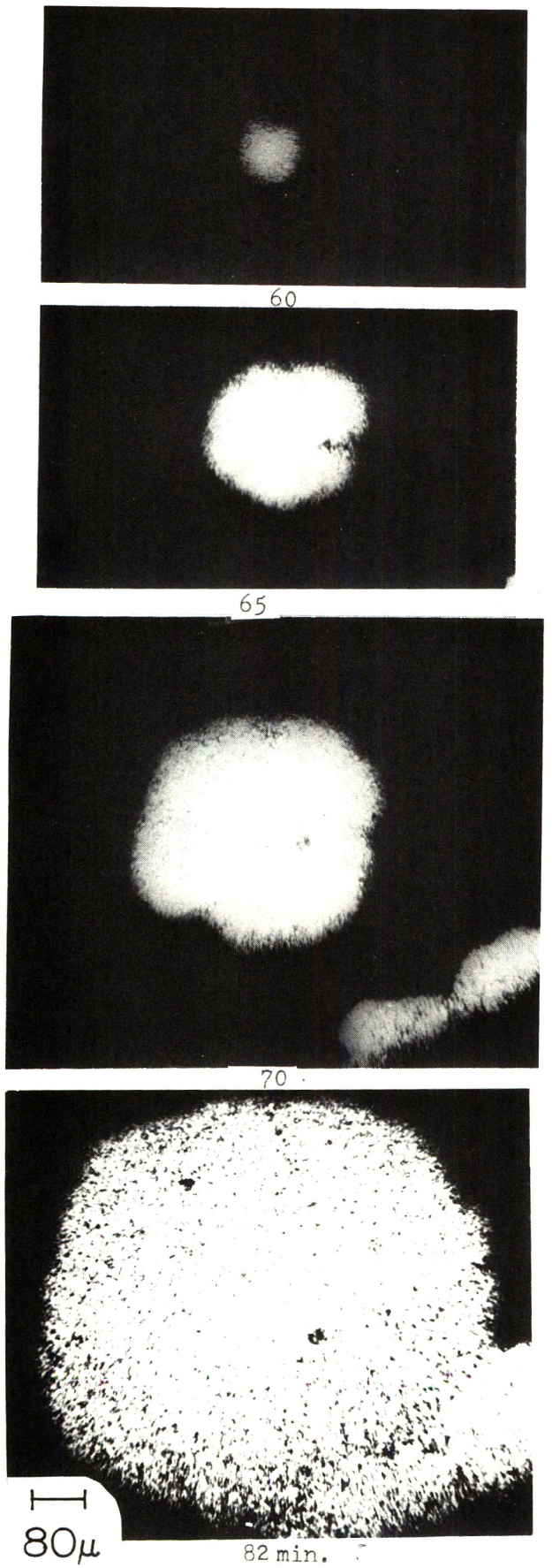

Figure 5. Photomicrographs of a 1.5-mil cholesteryl myristate sample at 82° at various time intervals.

Figure 5 shows the variation at 82°. Similar results were obtained at 81.5°. At these two temperatures the morphology is very similar, but differs from that observed at lower temperatures in that the growing centers contain elongated microstructures, while at lower temperatures, the internal structures are more like spherical small grains.

The difference in the internal morphology of the spherulites in the low- and high-temperature range of the cholesteric phase is more clearly demonstrated in the photomicrographs of Figure 6, which have a higher magnification. The light scattering patterns also bear out the difference. Figure 7 gives the Hv and Vv patterns at temperatures between 79.8 and 81° taken 1 hr after the sample reached equilibrium. Figure 8 shows the light scattering patterns at 82°. The initial Hv pattern at 82° is the typical 45° oriented pattern obtained at lower temperatures. It is seen from Figures 7 and 8 that the Hv pattern for the entire temperature range is composed of two parts as before. The corresponding Vv pattern is composed of a central part which is very intense and an outer part of lower intensity and 45° orientation. One can also see that the Hv pattern obtained in the lower temperature range has a definite minimum in the variation of intensity with scattering angle along the 0 and 90° direction, but in the higher temperature range, no such minimum is detected. This is most clearly shown in Figure 8 at 82°. Figure 8 should be compared with Figure 6, where the internal structure of the growing object is more rod shaped.

Interpretation of the Light Scattering Patterns. The nature of the light scattering patterns can be explained in terms of theories which have been developed to explain the scattering from spherulitic polymers. The scattering from isolated homogeneous spheres having different radial and tangential polarizabilities, α_r and α_t, imbedded in a homogeneous medium of polarizability, α_s, have been calculated.[9] The equations for I_{Vv} and I_{Hv} are given by

$$I_{Vv} = K'V_0^2(3/U^3)^2\{(\alpha_t - \alpha_s)(2\sin U - U\cos U - \mathrm{Si}\,U) + (\alpha_r - \alpha_s)(\mathrm{Si}\,U - \sin U) - (\alpha_t - \alpha_r)\cos^2(\theta/2)\cos^2\mu\,[4\sin U - U\cos U - 3(\mathrm{Si}\,U)]\}^2 \quad (1)$$

$$I_{Hv} = K'V_0^2(3/U^3)^2\{(\alpha_t - \alpha_r)\cos^2(\theta/2)\sin\mu \times \cos\mu\,[4\sin U - U\cos U - 3(\mathrm{Si}\,U)]\}^2 \quad (2)$$

where V_0 is the volume of the sphere, K' is an optical constant, $U = (4\pi R/\lambda)\sin(\theta/2)$, where R is the radius of the sphere, λ is the wavelength of the light in the medium, and θ is the polar scattering angle between the incident and scattered rays. The azimuthal scattering angle is μ. Figure 9 gives the relationship between these two angles. In the above equations, it is assumed that α_t, α_r, and α_s are sufficiently close together so that the light wave is not affected appreciably on passing through the sphere boundary, so that the Rayleigh-Gans approximation can be used for calculation of the scattering. Si U designates the integral

$$\mathrm{Si}\,U = \int_0^U (\sin x/x)\,dx \quad (3)$$

It is seen that I_{Hv} arises entirely from anisotropy of the

(9) R. S. Stein and M. B. Rhodes, *J. Appl. Phys.*, **31**, 1873 (1960).

spherulite and depends strongly upon the azimuthal angle μ. I_{Vv}, on the other hand, contains three terms, the last of which arises from anisotropy and is dependent upon μ. The first two terms in I_{Vv} depend upon the difference between the spherulite polarizabilities and that of the surroundings, and they are independent of μ.

Equation 2 for Hv scattering predicts that at a particular μ the intensity of the scattering will pass through a maximum with increasing scattering angle θ. The intensity is zero at zero angle ($U = 0$) and at large angle ($U \rightarrow \infty$). The maximum intensity occurs at $U = 4.1$ which corresponds to a scattering angle θ_m given by

$$(4\pi R/\lambda) \sin (\theta_m/2) = 4.1 \quad (4)$$

Therefore, the determination of the angular position of the scattering maximum serves to characterize the average size of the spherulites. While the above results have been obtained for isolated spherulites, more recent calculations in which interspherulitic interference is considered lead to the same conclusions.[10]

The scattering from thin anisotropic disks of radius R oriented normally to the incident beam was also calculated and is described by the equations[11]

$$I_{Vv} = K^2V^2(2/w^2)^2\{(\alpha_t - \alpha_s)[wJ_1(w) + J_0(w) - 1] + (\alpha_r - \alpha_s)[1 - J_0(w)] + (\alpha_t - \alpha_r)[2 - 2J_0(w) - wJ_1(w)] \cos^2 \mu\}^2 \quad (5)$$

and

$$I_{Hv} = K^2V^2(2/w^2)^2\{(\alpha_t - \alpha_r)[2 - 2J_0(w) - wJ_1(w)] \sin \mu \cos \mu\}^2 \quad (6)$$

where $w = kR \sin \theta = (2\pi/\lambda)R \sin \theta$ and J_0 and J_1 are Bessel functions of the first kind with order zero and one, respectively.

The above equations apply to the case where the principle polarizability of the disk is at 0 or 90° to the radius and predict that Vv scattering patterns having maximum intensity in the polarization direction and Hv scattering patterns with maximum intensity at 45° to the polarization direction.

A more general theory has been developed for the scattering from two-dimensional spherulites,[12] where the optic axis lies in the plane of the disk but tilted at an angle β to the radius. In this case the intensity of the scattered beam for I_{Vv} and I_{Hv} is essentially similar to eq 5 and 6, respectively, except that the angle μ is replaced by $\xi = \mu + \beta$. Thus the light scattering pattern will be rotated through the azimuthal angle by the amount β. The variation of such spherulitic patterns with θ exhibits a maximum corresponding to

$$w = (2\pi/\lambda)R \sin \theta_m = 3.9 \quad (7)$$

The applicability of the sphere or the disk theories depends upon the relative values of the radius of the sphere or disk and the thickness of the sample film. In any case, the qualitative features of the two theories are very similar and it is difficult to distinguish between the two on the basis of scattering patterns obtained with normal incident light. Unpublished calculations by T. Hashimoto (Kyoto University) demonstrate that the two cases may be distinguished by tilting the samples in that the pattern for disks becomes dependent upon the tilt angle.

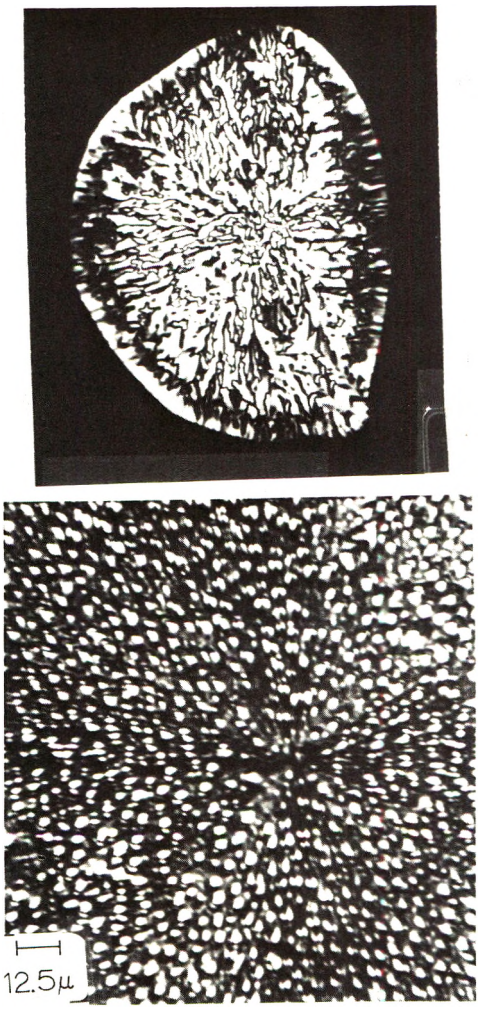

Figure 6. Photomicrographs of 1.5-mil cholesteryl myristate sample at 82 (top) and 80° (bottom).

The photomicrographs given above indicate spherulite-type growth in the cholesteric phase of cholesteryl myristate. At the onset of "crystallization," one can see well-defined maltese crosses in the photomicrographs and suggest the applicability of the above theories. The corresponding Hv light scattering patterns show well-defined four-leaf clover patterns with 45° orientation characteristic of these spherulites. At longer time intervals of crystallization the appearance of another four-leaf clover Hv light scattering pattern with 90° orientation suggests the development of a new structure. The calculated values of the sizes of these two structures obtained from the angles of intensity maxima of the Hv scattering patterns can be compared directly with the sizes measured from the microscopic pictures.

The results of such calculations for the central Hv light scattering pattern and the measured values from the microscopic pictures are given in Table I. The agreement between the two methods is very good. Therefore, one can conclude that the central Hv pattern arises from scatter-

(10) R. Prud'homme, D. Yoon, and R. S. Stein, *Bull. Amer. Phys. Soc.*, **17**, 296 (1972).
(11) R. S. Stein, *Electromagn. Scattering, Proc. Interdisciplinary Conf., 1962*, 439 (1963).
(12) S. Clough, J. J. VanAartsen, and R. S. Stein, *J. Appl. Phys.*, **36**, 3072 (1965).

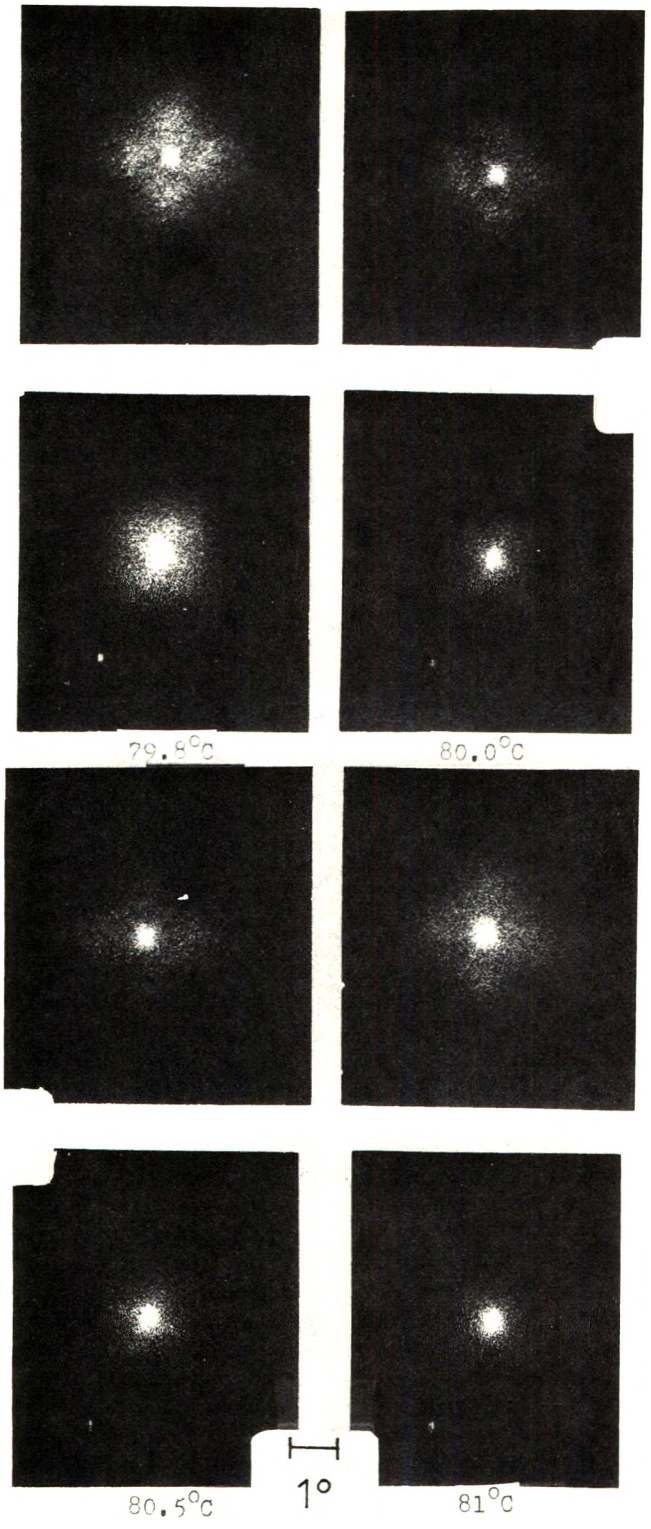

Figure 7. Hv (top photomicrograph of each temperature) and Vv (bottom photomicrograph of each temperature) light scattering patterns for 1.5-mil cholesteryl myristate sample at different temperatures.

ing from the spherulites. It should be noted here that the diameters of these spherulites are large and in fact approach three or four times the thickness of the sample. Therefore, they must be considered as two-dimensional spherulites, *i.e.*, disks.

The outer Hv pattern with 90° orientation, on the other hand, represents scattering at larger angles which must

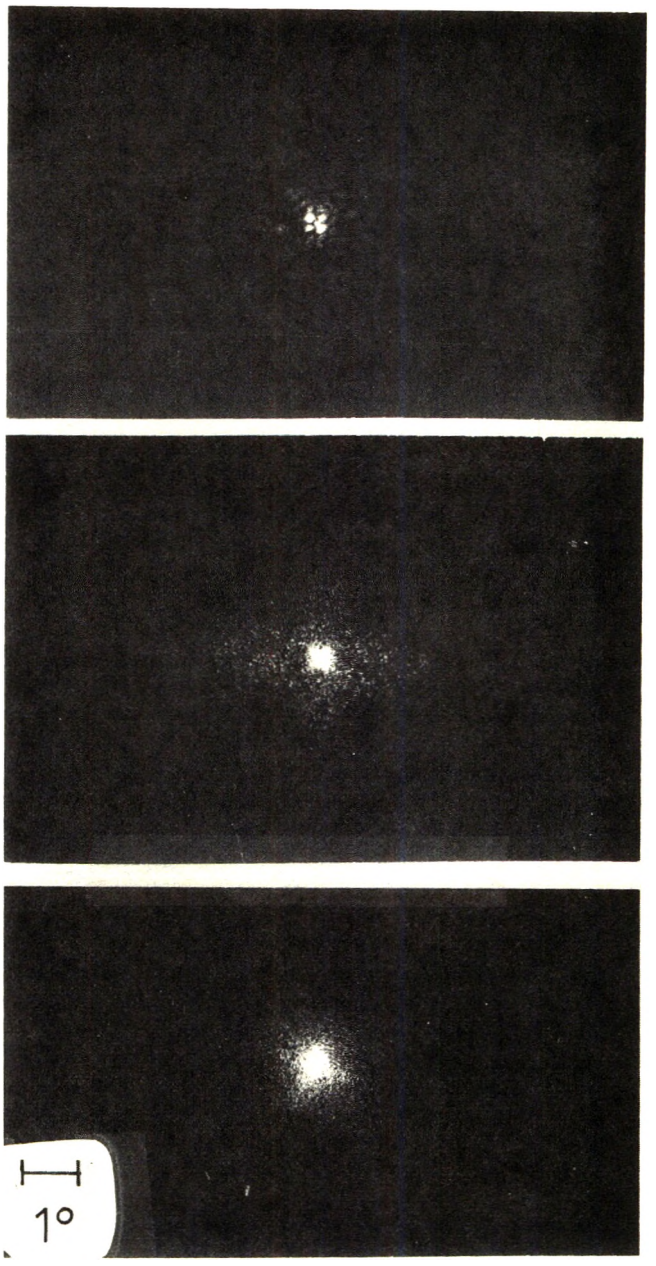

Figure 8. Hv (top two photomicrographs) and Vv (bottom photomicrograph) light scattering patterns for 1.5-mil cholesteryl myristate sample at 82°. (Hv on top is at 27 min, in middle is at 50 min, Vv is at 50 min.)

consequently result from smaller structures which we believe to be the microstructures within the spherulites. For example, from Figure 2, the calculated diameter from light scattering at 80° using eq 2 is 8 μ while the size of the structures inside the spherulte is estimated from micrographs to be about 10 μ. Similarly, for the 1.5-mil sample, the calculated diameter at 80° from light scattering is 25 μ and the estimated size from photomicrographs is also 25 μ.

As previously discussed, the outer Hv light scattering pattern exhibits a definite maximum in the intensity along the 0 and 90° direction (see Figures 2 and 4), which does not change with time, but which increases in intensity, indicating that the size of the microstructure giving rise to this scattering remains constant with time and only their number increases. This fact can be seen by investigating the photomicrographs in Figures 1 and 3.

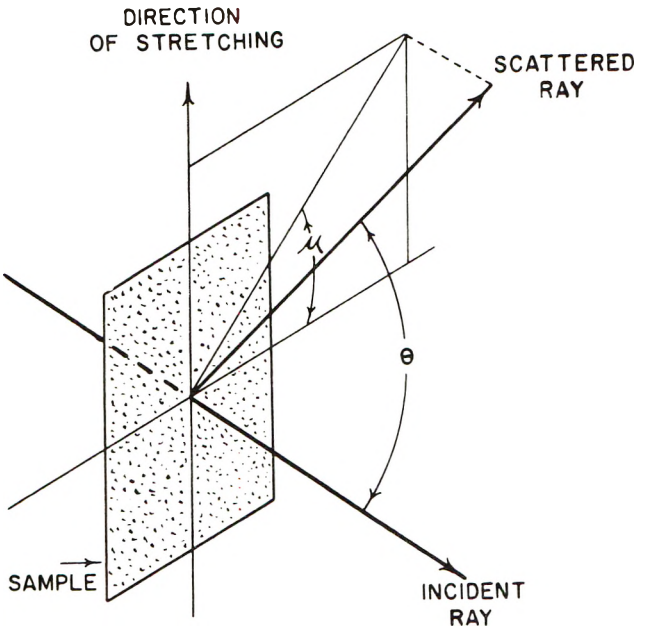

Figure 9. Coordinate system used in describing the scattering from an anisotropic spherulite.

TABLE I: Spherulite Size as Obtained from Light Scattering and from Microscopy

Sample thickness, mils	T, °C	Time of crystallization, min	Diameter, μ	
			Light scattering	Microscopy
0.5	80	15	76	80
1.5	80	15	400	450
3.0	82	23	200	200

The presence of a maximum in the outer Hv pattern indicates that the microstructures of the spherulites have spherical shape. Such maxima would not occur with scattering from rod-like structure, for example.[13] However, at higher temperatures, such as at 82°, the intensity decreases monatonically along the 0 and 90° directions, indicating that the scattering results from rod-type aggregates.[13] This is in agreement with the photomicrographs shown in Figure 6. The Vv scattering pattern has the ±45° orientation as shown in Figures 7 and 8. Therefore, one can conclude that at temperatures below 81°, the internal structure of the big spherulites is composed of microstructural units which exhibits spherical shape in which the optic axes are at 45° to the radius. At higher temperatures, the internal structure of the spherulites consists of rods with optic axes of the molecules are at 45° to the long axis of the rods as indicated by the qualitative[13] and quantitative[14a] considerations of Stein and Rhodes[13] and Kawai, *et al.*[14a]

It should be noted that within one of these microstructures, the optic axis must be at either +45 or −45° to the radius, but not a random mixture of the two. However, there must be an approximately equal number of such +45 and −45° structures, as has been noted for spherulites of polytetrafluoroethylene.[14b] The problem arises of how to account for the 0 or 90° orientation of the optic axis in the large spherulites and yet construct these

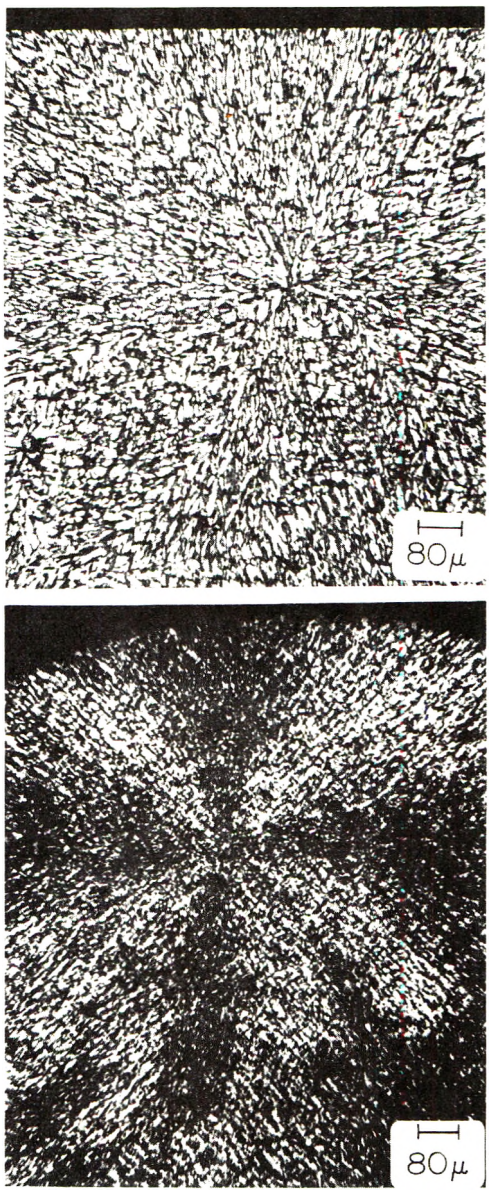

Figure 10. Photomicrographs of a 1.5-mil cholesteryl myristate sample at 80° when cooling from the isotropic melt (top) and when heating from the smectic phase (bottom).

from the microstructures having ±45° orientation. This is possible if, over dimensions comparable with the large structure, there are an equal number of small structures having +45 and −45° orientation. In this case, the scattering of the large spherulite will be determined by the average optic axis orientation angle over the larger regions of the spherulite which is 0°. A recent, yet unpublished, theory of scattering from spherulites having internal structure with different principal polarizability orientation than that of the average principal polarizability of the spherulite itself has been developed by Hashimoto, Murakami, Todo, Hayashi, and Kawai (Kyoto University, Japan).[14a]

Morphological Differences Occurring During Heating and Cooling Cycles. The morphology of cholesteryl myristate described above is obtained when cooling the sample

(13) M. B. Rhodes and R. S. Stein, *J. Polym. Sci.*, **62**, S84 (1962).
(14) (a) M. Moritani, N. Hayashi, A. Utsuo, and H. Kawai, *Polym. J. (Japan)*, **2**, 74 (1972); (b) M. B. Rhodes and R. S. Stein, *J. Polymer Sci., Part B-1*, 663 (1963).

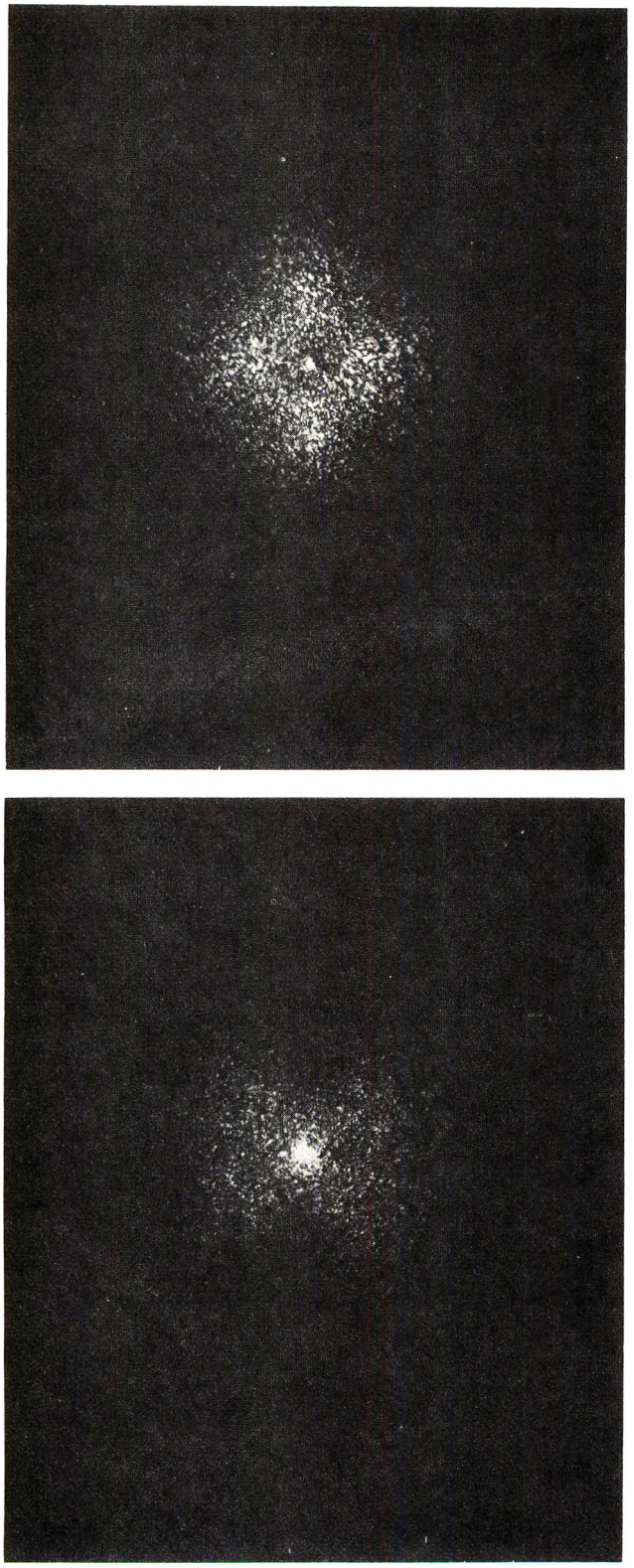

Figure 11. Hv light scattering patterns at 80° of 1.5-mil cholesteryl myristate sample when cooling (top) from isotropic melt and when heating (bottom) from the smectic phase.

from the isotropic melt to the cholesteric phase. However, upon heating to the cholesteric phase from the smectic phase a different morphology is obtained. The difference can be observed by microscopic pictures as illustrated in Figure 10. This difference in morphology is revealed by a light scattering experiment as shown in Figure 11. On cooling, one obtains an Hv pattern with 90° orientation and a very bright spot in the center. On the other hand, the pattern obtained for the sample when heated from the smectic phase is an Hv pattern with 45° azimuthal angle orientation. The intensity of the scattered light decreases monatonically along the ±45° direction. This result is in agreement with previous experiments,[4] where upon heating cholesteryl myristate from the smectic to the cholesteric phase an Hv pattern with 45° orientation was obtained. In view of these results, one must conclude then that the morphology of the cholesteric phase is dependent on whether the sample is cooled from the isotropic melt or heated from the smectic phase.

IV. Comparisons and Conclusions

Liquid crystals are known to adopt a variety of morphologies within mesophases. These morphologies are referred to as textures. The particular texture adopted by a mesophase depends on a variety of conditions. Among these are the nature of the compound, the way in which the mesophase is produced, and the nature and cleanliness of the supporting surface employed to mount the specimen.

The textures of the cholesteric mesophase and the conditions under which they are produced may be summarized as follows. When a cholesteric phase is produced by cooling the isotropic melt of the substance, confined between a slide and a cover slip, it usually appears as a fine cloud, the particles of which grow on further cooling to give a confused and usually fine-grained structure. The fine cloud texture often exhibits a weak blue or violet color when viewed between crossed polars.[2a,15-17] This is called the homeotropic cholesteric texture.

Another texture which is commonly obtained in the cholesteric mesophase between glass surfaces is the focal-conic texture. Under the microscope, the preparation appears to contain an arrangement of fine dark lines. These lines are ellipses and hyperbolas or portions of these. The lines appear in pairs and are related to each other in a focal-conic geometry.[2a] The ellipse is the locus of the vertices of cones of revolution passing through the hyperbola. The ellipses do not intersect one another and meet only tangentially giving rise to the so-called focal-conic "domains." The tangential arrangement of the ellipses is referred to as polygonal texture.[2a] The mesophase in this texture is composed of cones whose bases are ellipses and whose apices are the meeting points of a number of hyperbolas. The domain of the cone of revolution for a circle and a line, which are related as focal-conic, may be divided into series of curved, parallel strata which will entirely fill the cone. The molecules in the strata lie at right angles to the lines drawn between points on the ellipse and points on the hyperbolas, thus they lie parallel to the strata.[2a,18] This arrangement causes the optic axis to continuously change throughout the domain of the focal-conic group, as is theoretically confirmed by Bragg.[19] The ellipses and hyperbolas are considered to be lines in the neighborhood of which the optic axial direction changes suddenly. Thus they represent optical discontinuities, ei-

(15) I. G. Chistyakov and L. A. Gusokova, *Sov. Phys.-Crystallogr.*, **14**, 132 (1969).
(16) R. D. Ennulat, *Mol. Cryst. Liquid Cryst.*, **3**, 405 (1968).
(17) G. Friedel, *Ann. Phys. (Paris)*, **18**, 273 (1922).
(18) G. H. Brown and W. G. Shaw, *Chem. Rev.*, **57**, 1049 (1957).
(19) Sir W. Bragg, *Nature (London)*, **133**, 445 (1934).

ther within a domain in the case of a hyperbola or between domains in the case of an ellipse. As a ray of light passing close to such discontinuity is deviated, the discontinuity in the direction of the optic axis is seen as a black line. The same reasoning applies for crystalline spherulites.

When the homeotropic or the focal-conic texture is disturbed by causing small movements of the cover slip over the preparation, it gives rise to the planar texture. In some cases the change occurs very fast but it rarely forms spontaneously by just cooling.[2a] In the planar texture, the optic axis is normal to the plane of the preparation, and the optical sign is negative.[2a] The planar cholesteric texture is very strongly optically active. The optical effects of this texture were first explained by deVries[20] and have been studied by Fergason.[21,22] When the sample is introduced into a wedge-shaped space provided by tilted glass or mica plates, the planar texture is formed spontaneously on cooling the melt to the cholesteric phase. The optical patterns appear as bright and dark lines which follow the shape of the wedge. The separation between them corresponds to a constant change of thickness of the wedge. These lines were originally interpreted by Grandjean as planes of discontinuity perpendicular to the surface and have been called Grandjean planes.[2a] However, recent work[23] showed that the Grandjean texture in a thin wedge is due to the orientation influence of the supporting surface.

It should be pointed out that the polygonal regions of the focal-conic texture discussed above represent a simple case and are only observed under very favorable conditions. In many cases in which the polygonal arrangement arises, the ellipses are not in the planes of the surfaces of the preparation, and the cones lie with their bases in various planes of inclination to the surface.[2a]

In the present study concerning cholesteryl myristate morphology, it was shown that the isotropic-cholesteric phase transition occurs in two steps. The first is a rapid transformation to a turbid blue homeotropic texture, which is in agreement with the dilatometric results.[24] The second step is a much slower transition, to a more macroscopically ordered texture. The analyses of the light scattering patterns and the microscopic observations indicate that the macroscopic morphology is spherulitic, the microstructure of which is composed of small focal-conic groups which arrange themselves in a spherically symmetrical arrays to give the spherulitic texture.

As previously discussed, cholesteryl myristate in the cholesteric phase exhibits a blue homeotropic texture which subsequently changes to a new texture as studied, for example, by Friedel[17] and Gray[2a] who were concerned with textural changes at different temperatures. The present results are different from previous work in that the textural changes at constant temperatures were followed as a function of time. Chistyakov and Gusokova[15] found that when slowly cooling a cholesteryl myristate sample, they observed single-crystal cholesteryl-type regions appearing against a background of the homeotropic texture. The conclusion drawn from the results presented here is that the homeotropic cholesteric texture will always give rise to the more macroscopically ordered texture under isothermal conditions.

It has been demonstrated above that the scattering of light of the spherulitic state of cholesteryl myristate is similar to that observed for spherulitic polymers and arises from fluctuations in the orientation direction of anisotropic regions which have dimensions comparable with the wavelength of light. This conclusion is in agreement with the results of earlier studies made by Chatelain[25] on a nematic liquid crystal and more recently by Stein, *et al.*,[4] on some cholesteryl esters.

It is found in this study that the orientation of the optic axes in the spherulitic form of the cholesteric phase was dependent on whether the cholesteric phase is produced by cooling from the melt or heating from the smectic phase. On heating to the cholesteric phase, the orientation of the optic axis was perpendicular to the spherulite radius, while when cooling from the melt, the optic axis was oriented at 45° to the radius. The change in optic axis direction is due to different orientation of the focal-conic groups with respect to the radius of the spherulite. These differences are difficult to identify by microscopy; they are easily detected by light scattering experiments.

It should be pointed out that the organization of the focal conic groups into spherulites is greatly influenced by surfaces. It is seen from Table I that the spherulite size increases with increasing sample thickness. This is a consequence of the nucleation rate in the thicker films being less, as is shown by quantitative measurement in part II.[26] The spherulites grow until their size is limited by impingement with other spherulites. Consequently, lower nucleation rates lead to larger spherulites. The growth rate of the spherulite is much less affected by sample thickness and it is believed to not be primarily a surface effect.

The transformation from the homeotropic to a more macroscopic texture is observed in thick samples but spherulites are not usually seen to develop with these. Also the lifetime of the homeotropic state is greater for the thicker samples. It seems likely that spherulites may be a consequence of heterogeneous nucleation occurring at or near the surfaces of the thin samples. Once such nuclei form, they continue to grow radically outward through the accumulation of focal-conic-type substructures having a size characteristic of the temperature of growth. The focal conics are oriented with respect to the radial direction of growth, either by a secondary nucleation process (as found with polymers) or by flow associated with the mass transfer accompanying the transformation. This leads to the observed spherulite morphology with thin films.

For thicker samples, the focal-conic structures may nucleate homogeneously in profusion (or perhaps heterogeneously on advanticious impurities). This leads to phase transformation with a nonspherulitic texture before the more rapidly growing nuclei at the surface can produce an appreciable fraction of spherulitic material.

In some respects, the transformation occurring with thicker samples is simpler in that it is not complicated by surface effects. However, such samples cannot be readily studied by microscopy and we are currently applying light scattering techniques for this.

(20) A. deVries, *Acta Crystallogr.*, **4**, 219 (1951).
(21) J. L. Fergason, *Mol. Cryst. Liquid Cryst.*, **1**, 293 (1966).
(22) J. L. Fergason, N. N. Goldberg, and R. J. Nodalin, *Mol. Cryst. Liquid Cryst.*, **1**, 309 (1966).
(23) G. H. Brown, J. W. Doane, and V. D. Neff, *Crit. Rev. Solid State Sci.*, **1**, 303 (1970).
(24) F. P. Price and J. H. Wendorff, *J. Phys. Chem.*, **75**, 2839 (1971).
(25) P. Chatlelain, *Acta Crystallogr.*, **4**, 453 (1951).
(26) S. Jabarin and R. S. Stein, **77**, 409 (1973).

Light Scattering and Microscopic Investigations of Mesophase Transitions of Cholesteryl Myristate.[1] II. Kinetics of Spherulite Formation

S. A. Jabarin and R. S. Stein*

Polymer Research Institute and Department of Chemistry, University of Massachusetts, Amherst, Massachusetts 01002
(Received July 13, 1972)

Publications costs assisted by the National Institutes of Health

Cholesteryl myristate exhibits a transition from an isotropic melt to the cholesteric phase upon cooling. This transition ordinarily occurs in two steps. The first is a rapid transformation to a turbid "blue" homeotropic state while the second is a much slower transition to a more macroscopically ordered focal conic or spherulitic texture. The latter transformation may be described by nucleation and growth kinetics similar to those obeyed by crystalline polymers. The process may be followed by direct microscopic observation, by the depolarized light transmission technique, or by the low-angle light scattering procedure. The kinetics of transformation fit the Avrami equation giving an n value of 3. The analyses of the temperature dependence of the growth and nucleation rates yield very small interfacial energy products, $\sigma_1\sigma_2$, of 0.1 and 0.2 erg^2/cm^4 for growth and nucleation, respectively.

Introduction

It was shown in part I[2a] that cholesteryl myristate exhibits a transition from an isotropic melt to the cholesteric mesophase upon cooling. This transition was shown to occur in two steps. The first step is a rapid transformation to a turbid blue phase, while the second is a much slower transition to a macroscopically ordered spherulitic texture. In this paper the results of the investigation of spherulite formation will be presented.

The experimental methods are described in part I.[2a]

Results and Discussion

The experimental procedure is the same as was described earlier.[2a] The sample was heated to 90°, well above the cholesteric isotropic transition, kept at this temperature for at least 0.5 hr, then quickly cooled to the desired temperature and held at constant temperature. Photomicrographs and depolarized light intensity (DLI) measurements were taken at different time intervals. The radius and the number of the spherulites were then measured. Growth rates and nucleation rates were determined as functions of temperature and sample thickness.

Growth Rate. The variation of spherulite radii with time for a 1-mil thick sample at various temperatures is given in Figure 1 and is seen to be linear. Similar behavior is seen for spherulitic polymers.[2b,3] This indicates that the process is diffusion independent, since if it were not, the radius should depend upon the square root of time. The spherulite growth rate, G, is obtained from the slopes of the plots of spherulite radius *vs.* time.

Similar kinetic studies were carried out for different sample thicknesses. It was found that the growth is independent of diffusion for all cases as indicated by the linearity of the plots of radius *vs.* time. The growth rates and the degree of supercooling for various samples are given in Table I.

Nucleation Rate. The number of nuclei per unit volume at several temperatures was measured as a function of time. Typical data are plotted in Figure 2 for a 1-mil sample. It can be seen from the figure that the density of nucleation first increases steadily after which it levels off toward a constant value. It should be emphasized that the leveling off occurs with only 50 to 75% transformation completed so that it does not occur as a result of complete transformation. The number of spherulites counted in the field of view ranges from 35 at 80.0° to 25 at 81°. The results are the average of three observations.

The steady increase in the number of nuclei with time is indicative of sporadic nucleation. The nucleation rates, $\dot{N}$, are obtained from the initial slopes. The resulting data are given in Table II, along with the nucleation density, $\bar{N}$, at the leveling off for samples of 1- and 3-mil thicknesses. Such behavior has also been observed in some polymeric systems.[3-5] The results suggest sporadic heterogeneous nucleation with first power dependence of nucleation rate on time.

Heterogeneous nucleation is the process of birth of small crystalline regions on or near surfaces such as the container walls or adventitious impurities such as dust particles. Homogeneous nucleation, on the other hand, is a result of random fluctuation or order in the melt and it depends on the first power of time. A more general discussion can be found in an article by Price.[6]

Temperature Dependence of Nucleation Rate. The theory for nucleation in condensed systems for either homogeneous or heterogeneous nucleation has been developed by Turnbull and Fisher.[7] The nucleation rate per unit volume and time is given by

$$\dot{N} = N_0 \exp[-(\Delta E_D^* + \Delta F^*)/kT] \qquad (1)$$

where ΔE_D^* is the activation energy for transport across

(1) Supported by a Grant from the National Institutes of Health.
(2) (a) S. Jabarin and R. S. Stein, *J. Phys. Chem.*, **77**, 399 (1973); (b) A. Sharples, *Polymer*, **3**, 250 (1962).
(3) L. Mandelkern, "Crystallization of Polymers," McGraw-Hill, New York, N. Y., 1964.
(4) R. S. Stein, *et al.*, *J. Polym. Sci., Part A-3*, 3041 (1965).
(5) J. N. Hay, *J. Polym. Sci., Part A-3*, 433 (1965).
(6) F. P. Price, "Nucleation," A. C. Zettlemoyer, Ed., Marcel Dekker, New York, N. Y., 1970, Chapter 8.
(7) D. Turnbull and J. C. Fisher, *J. Chem. Phys.*, **17**, 71 (1949).

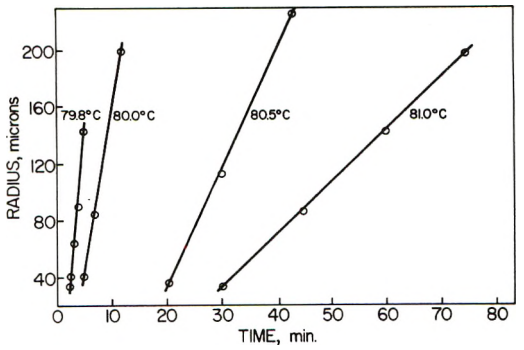

Figure 1. Dependence of radial growth on time at various growth temperatures for 1-mil sample.

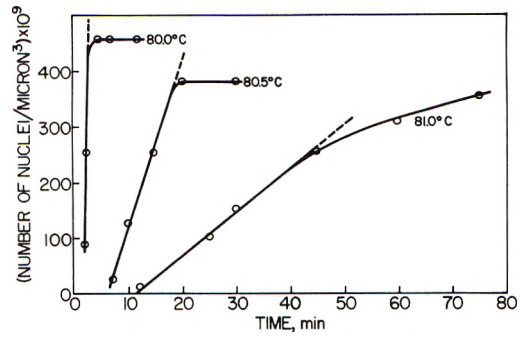

Figure 2. Number of nuclei per unit volume as a function of time at different temperatures for 1-mil sample.

TABLE I: Growth Rates at Various Temperature for Cholesteryl Myristate

T, °C	ΔT, °C, degree of supercooling	G, μ/min
	1.0-mil Sample	
79.8	4.2	37
80.0	4.0	23
80.5	3.5	4
81.0	3.0	3.6
	1.5-mil Sample	
74.8	4.2	32
80.0	4.0	29.4
80.5	3.5	17.7
81.0	3.0	8.0
	3.0-mil Sample	
79.8	4.2	30
80.0	4.0	27
80.5	3.5	19
81.0	3.0	12

the liquid-nucleus interface, N_0 is a constant, and ΔF^* is the free energy of the formation of the nucleus of critical dimensions. This quantity depends on the geometry of the nucleus and on the kind of nucleation process. k is Boltzmann's constant and T is the absolute temperature.

If the process is homogeneous, ΔF^* can be calculated for various nucleus shapes. For three-dimensional case, ΔF^* is given by[3]

$$\Delta F^* = A\sigma_1\sigma_2 T_T^{\,2}/(\Delta h_f)^2(\Delta T)^2 = A\sigma_1\sigma_2^{\,2}/(\Delta f_u)^2 \quad (2)$$

where A is a geometric factor equal to 8π for cylindrical nuclei and 32 for block-shaped nuclei. σ_2 and σ_1 are the

TABLE II: Nucleation Rate at Various Temperatures for 1- and 3-mil Cholesteryl Myristate Samples

T, °C	ΔT, °C	$\dot{N}$, μ^{-3} min^{-1}	$\bar{N}$, μ^{-3}
		1-mil Sample	
79.8	4.2	333×10^{-9}	762×10^{-9}
80.0	4.0	260×10^{-9}	457×10^{-9}
80.5	3.5	29×10^{-9}	381×10^{-9}
81.0	3.0	7.6×10^{-9}	375×10^{-9}
		3-mil Sample	
79.8	4.2	24×10^{-9}	82×10^{-9}
80.0	4.0	16.5×10^{-9}	64×10^{-9}
80.5	3.5	4.5×10^{-9}	55×10^{-9}

lateral interfacial energy and the end surface free energy per unit area, respectively. T_T is the transition temperature and ΔT is the degree of supercooling. Δh_f is the heat of transition per unit volume and Δf_u is the free energy of transition per unit volume.

In the most general case of heterogeneous nucleation, one considers a crystal phase in contact with a surface. If we define σ_s as the interfacial energy between the substrate surface and the melt, and σ_{os} as the interfacial energy between the substrate surface and the crystal, ΔF^* for a two-dimensional process is given by

$$\Delta F^* = 4b_0\sigma_1\sigma_2/\Delta f_u - (\Delta\sigma/b_0) \quad (3)$$

where

$$\Delta\sigma = \sigma_2 + \sigma_{os} - \sigma_s \quad (4)$$

where it is assumed that the lateral surface of the crystal is in contact with the substrate. b_0 is a fixed lattice spacing of the crystal.

By substituting eq 3 into 1, one obtains

$$\dot{N} = N_0 \exp(-\Delta E_D^*/kT) \exp(-4b_0\sigma_1\sigma_2 T_T/k\Delta h_f T\Delta T)\{1/[1 - (\Delta\sigma T_T/b_0\Delta T\Delta h_f)]\} \quad (5)$$

In this case a plot of ln N *vs.* $T_T/T\Delta T$ will not give a straight line. It can be seen from eq 5 that the maximum value of $\Delta\sigma T_T/b_0\Delta T\Delta h_f$ is unity. Therefore, it is possible to calculate an upper limit of $\Delta\sigma$ which is found to be 0.02 and 0.01 erg/cm² for 4.2 and 3.0° supercooling, respectively. These values are extremely small as compared to the values of $\sigma_1\sigma_2$ as will be shown below. To a first approximation the second term of the second exponential in eq 5 can be assumed to be unity. In this case then, eq 5 reduces to eq 6 for two-dimensional nucleation

$$\dot{N} = N_0 \exp(-\Delta E_D^*/kT) \exp(-4b_0\sigma_1\sigma_2 T_T/\Delta h_f kT\Delta T) \quad (6)$$

and for three-dimensional cylindrical case

$$\dot{N} = N_0 \exp(-\Delta E_D^*/kT) \exp(-8\pi_0\sigma_1\sigma_2^{\,2}T_T^{\,2}/(\Delta h_f)^2 kT(\Delta T)^2) \quad (7)$$

It can be seen from eq 6 and 7 that a plot of ln $\dot{N}$ *vs.* $T_T/T\Delta T$ or $T_T^2/T(\Delta T)^2$ for one of the two cases should yield a straight line. Such plots were constructed for cholesteryl myristate. This is given in Figure 3 for a 1-mil sample. It is seen that while ln $\dot{N}$ *vs.* $T_T/T\Delta T$ is linear, ln $\dot{N}$ *vs.* $T_T^2/T(\Delta T)^2$ is not, indicating two-dimensional nucleation. The same results were also found for a 3-mil sample.

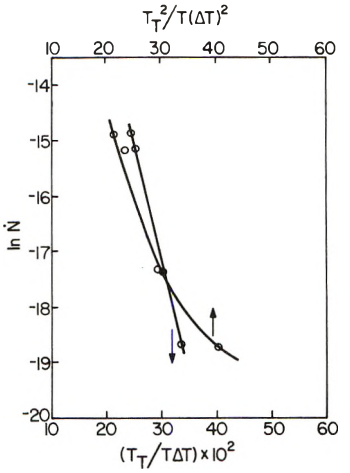

Figure 3. Temperature dependence of nucleation rate.

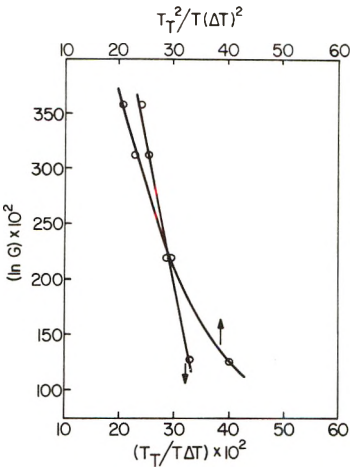

Figure 4. Temperature dependence of growth rate.

TABLE III: Interfacial Energies Obtained from Nucleation Rates of Cholesteryl Myristate

Sample thickness, mils	$(\sigma_1\sigma_2)_N$, erg^2/cm^4	σ_{av}, erg/cm^2	Range of r, Å
1.0	0.242	0.49	550–720
3.0	0.162	0.40	400–600

TABLE IV: Interfacial Energies Obtained from Growth Rates of Cholesteryl Myristate

Sample thickness, mils	$(\sigma_1\sigma_2)_G$, erg^2/cm^4	σ_{av}, erg/cm^2	Range of r, Å
1.0	0.140	0.37	400–550
1.5	0.084	0.29	320–430
3.0	0.056	0.24	200–280

The slope of the straight line for the two-dimensional case is $4b_0\sigma_1\sigma_2/\Delta h_f k$. Hence, $\sigma_1\sigma_2$ can be calculated. The value of maximum Δh_f is 0.41 cal/g.[8,9] Assuming b_0 is 10 Å which corresponds to approximately the short axis of cholesteryl myristate molecule, the calculated maximum values of $\sigma_1\sigma_2$ are given in Table III, along with $\sigma_{av} = (\sigma_1\sigma_2)^{1/2}$ and the range of the critical nuclei radii, which is obtained from $r = 2\sigma_{av}/\Delta f_u$. It should be noted that the choice of $b_0 = 10$ Å is arbitrary. The value of b_0 does not affect σ_{av} seriously since σ_{av} is proportional to $(b_0^{1/2})$.

It is interesting to note that the critical nucleus radius obtained here corresponds to the size of the structures of the "blue" phase in cholesteryl myristate.

Temperature Dependence of Growth Rate. When the linear growth rate of spherulites is characterized by a negative temperature coefficient, it is usually concluded that the growth of the spherulites is controlled by a secondary nucleation process. In other words, the spherulites grow when new crystallites are formed on the tips of the preexisting spherulites generated by the primary process.[3,6]

The growth rate, G, for spherulitic growth which is nucleation controlled is given by[8]

$$G = G_0 \exp[-(\Delta E_D^* + \Delta F^*)/kT] \qquad (8)$$

where G_0 is a constant and the other terms were defined above.

When the nucleation is two dimensional, ΔF^* is[3,10,11]

$$\Delta F^* = 4b_0(\sigma_1\sigma_2)_G/\Delta f_u \qquad (9)$$

and for cylindrical three dimensional

$$\Delta F^* = 8\pi(\sigma_1\sigma_2^2)_G/(\Delta f_u)^2 \qquad (10)$$

The subscript G is given here in order to deferentiate ΔF^* obtained from growth rate from that obtained from the nucleation rate.

By substituting eq 9 and 10 into eq 8, one obtains expressions similar to those in eq 6 and 7. Therefore, a plot of ln G *vs.* $T_T/T\Delta T$ or ln G *vs.* $T_T^2/T(\Delta T)^2$ should be linear. Such plots were constructed from the growth data for cholesteryl myristate. A typical plot is given in Figure 4 for a 1-mil sample. It is seen that a plot of ln G *vs.* $T_T/T\Delta T$ is linear while that for ln G *vs.* $T_T^2/T(\Delta T)^2$ is not. The same results were obtained for 1.5- and 3-mil thick samples. One must then conclude that the growth is two dimensional. The calculated values of $\sigma_1\sigma_2$ and the critical radius of the nuclei are given in Table IV.

By comparing the values of $(\sigma_1\sigma_2)_N$ in Table III obtained from nucleation rates with $(\sigma_1\sigma_2)_G$ in Table IV obtained from growth rates, we see that they are larger for the first case than for the latter. This indicates that more energy is required to produce the primary nucleus and less energy to cause it to grow into a two-dimensional spherulite.

The values of the interfacial energy obtained from nucleation or growth rates are very small. This indicates that very small forces hold the system together to produce a particular texture. This is reasonable in view of the observation that textures in liquid crystals are easily changed by small mechanical disturbance such as movement of cover slips.

The above results show that while the nucleation rate greatly decreases with sample thickness the growth rate is affected to a lesser degree and actually increases with thickness, especially the sample thickness exceeds 1.5 mil. A possible explanation of this dependence is that the glass surface orients the homeotropic phase, and it is more difficult to grow the spherulitic phase from this oriented state than from the randomly oriented mesophase.

(8) G. J. Davis, R. S. Porter, and E. M. Barrall, *Mol. Cryst. Liquid Cryst.*, **10**, 1 (1970).
(9) This is the enthalpy of transition from the cholesteric state to the isotropic melt. The enthalpy of transition from the spherulitic cholesteric state to the "blue" phase is undoubtedly less than this.
(10) F. P. Price, *Encycl. Polym. Sci. Technol.*, **8**, 63 (1968).
(11) F. Gornich and J. D. Hoffman, *Ind. Eng. Chem.*, **58**, 41 (1968).

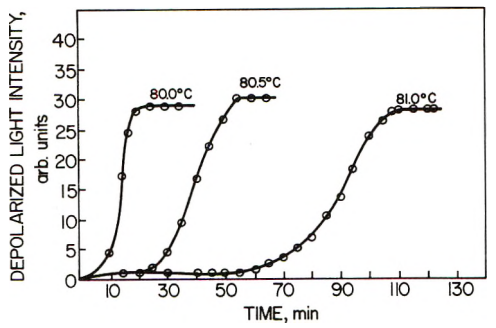

Figure 5. Depolarized light intensity *vs.* time at various temperatures for 3-mil sample.

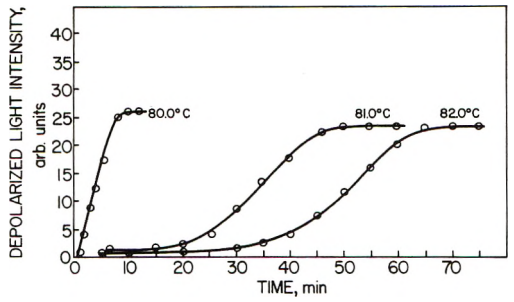

Figure 6. Depolarized light intensity *vs.* time at various temperatures for 6-mil sample.

TABLE V: Summary of Kinetic Data for Cholesteryl Myristate

T, °C	*n*	*K*, min^{-3}	$t_{1/2}$, min	*t*, min
		3.0-mil Sample		
80.0	2.94	100×10^{-5}	8	4
80.5	3.00	11×10^{-5}	20	18
81.0	2.92	27×10^{-5}	40	55
		6.0-mil Sample		
80.0	3.0	1420×10^{-5}	4.5	0.5
81.0	3.0	15.7×10^{-5}	20	15
82.0	3.1	2.11×10^{-5}	30	20

Overall Kinetic Rate Constant. The measurement of growth and nucleation rates by the microscopic technique is difficult for thicker samples because of the problem of focusing the microscope with such samples. Therefore, in order to follow overall rate kinetics in these cases, the depolarized light intensity (DLI) technique was chosen. This method has been used by many workers studying crystallization kinetics.[12-18]

The experimental procedure involves the measurement of the depolarized light intensity transmitted *vs.* time. The DLI *vs.* time plots are converted to fit the Avrami equation by using the following empirical equation

$$\theta_a = (I_\infty - I_t)/(I_\infty - I_0) = \exp(-Kt^n) \qquad (11)$$

where I_t is the transmitted intensity at time t and I_0 and I_∞ are the values of I_t at $t = 0$ and $t = \infty$, respectively. θ_a is the fraction of untransformed material. The parameters K and n in the equation describe the rate and mechanism of crystallization. At this point it should be pointed out that although the above equation seems to hold for many systems, the relationship between DLI and molecular structure is still not completely understood.[19,20]

The DLI *vs.* time was measured at several temperatures for 3- and 6-mil samples. The results are given in Figures 5 and 6. From these data, the Avrami exponent n and the rate constant K in eq 11 may be obtained by plotting ln $(-\ln \theta_a)$ *vs.* ln t. These plots are given in Figures 7 and 8. In constructing such plots, the induction period, τ, during which no transmission increase occurs, was subtracted from t. A summary of the results is given in Table V where it is seen that n equals 3. It is known from the nucleation data presented above that the process is sporadic. Therefore, $n = 3$ indicates that the growing objects are disk shaped (two-dimensional spherulites).

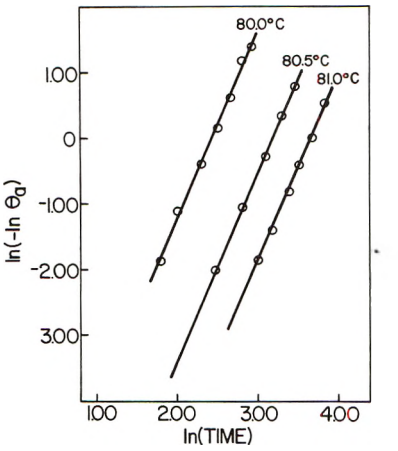

Figure 7. Avrami plot for 3-mil sample at various temperatures.

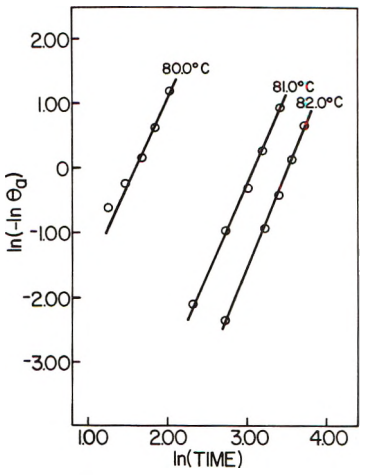

Figure 8. Avrami plot for 6-mil sample at various temperatures.

The mathematical formulation of the Avrami equation involves several assumptions and limitations which have been discussed.[21,22] It is useful to consider the rate constant, K, given in eq 11 which depends on the kind of nucleation (sporadic or instantaneous) and on the geometry

(12) F. P. Price, General Electric Research Lab Report No. RL-7741 (1952).
(13) J. Magill, *Brit. J. Appl. Phys.*, **12**, 618 (1961); *Polymer*, 2, 221 (1961).
(14) B. Levy, *J. Appl. Polym. Sci.*, **5**, 408 (1961).
(15) I. Kirshenbaum, *et al.*, *J. Polym. Sci., Part B-2*, 897 (1964).
(16) F. L. Binsbergen, *J. Macromol. Sci. B*, **4**, 837 (1970).
(17) F. L. Binsbergen and M. DeLange, *Polymer*, **11**, 309 (1970).
(18) E. M. Barrall, J. F. Johnson, and R. S. Porter, *Appl. Polym. Symp.*, **8**, 191 (1969).
(19) S. Clough, M. B. Rhodes, and R. S. Stein, *J. Polym. Sci. C*, No. 18, 1 (1967).
(20) R. S. Stein, M. B. Rhodes, and R. S. Porter, *J. Colloid Interface Sci.* **27**, 336 (1968).
(21) A. Sharples, "Introduction to Polymer Crystallization," Edward Arnold, London, 1966.
(22) F. P. Price, *J. Appl. Phys.*, **36**, 3014 (1965).

TABLE VI: Comparison of K as Obtained by Depolarized Light Intensity and Microscopy for 3-mil Cholesteryl Myristate Sample

T, °C	K (from DLI), min^{-3}	K (microscopy) Sporadic K, min^{-3}	K (microscopy) Instantaneous K, min^{-2}
79.8		162×10^{-5}	34.8×10^{-3}
80.0	100×10^{-5}	90×10^{-5}	32.1×10^{-3}
80.5	11×10^{-5}	13×10^{-5}	9.4×10^{-3}
81.0	2.7×10^{-5}		

of the growth. If the assumption is made that one primary nucleus gives rise to one disk or one spherulite, then by a direct measurement of both the rate of formation and the growth, crystallization rate constants can be calculated for both the sporadic and the instantaneous processes which can be compared with the corresponding values determined from the measurements of the overall rate of crystallization of the DLI technique as shown in Table VI. The agreement between the two methods is very good for the case of sporadic rate constant.

The above discussion has been concerned with the formation of the spherulitic texture. In the DLI measurements, a small increase of transmission is observed upon forming the blue phase, while a much larger increase occurs upon forming the spherulitic texture.[23] The small increase in DLI occurs very fast, within 1 to 2 min, while the second increase occurs more slowly and it takes 20 to 60 min to be completed.

Discussion and Conclusions

Price and Wendorff[24] have studied the transformation kinetics for the isotropic–cholesteric phase transition of cholesteryl myristate by the dilatometric method which they found to fit the Avrami equation giving a value of $n = 2$. It was concluded that the liquid–cholesteric transformation takes place by the formation of disk-like nucleii which subsequently grow into rods. At 2.2° supercooling, the half-time of the transformation was 1 min, while in the present study, the transition to the blue homeotropic texture occurs in periods of 1 to 2 min and lasts for 1 to 30 min, depending on the temperature, before the other texture appears.[23] This latter texture transformation is slow and it takes periods of few minutes up to 40 min. Upon comparing these results with the dilatometric results, it can be concluded that the dilatometric measurements are sensitive to the formation of the blue homeotropic texture while they are not sensitive to the second transition. In other words, there is a negligible volume change associated with the formation of the second texture. It appears that the usual thermodynamic studies of the transition by dilatometry and calorimetry deal primarily with the transformation to the blue state, and do not reflect the textural changes associated with the second transition.

It was concluded from the light scattering patterns and the microscopic pictures presented in part I,[2a] that while the spherulites grow with time, the focal-conic groups of the microstructure of the spherulite do not change in size but increase in number. Therefore, the growth rates reported above correspond to growth of spherulites by increasing the number of the microstructural entities (*i.e.*, focal-conic groups). The interfacial energies obtained from the growth rates correspond to the energies required to bring focal-conic groups to the surface of the growing spherulite.

(23) T. Asada and R. S. Stein, submitted for publication.
(24) F. P. Price and J. H. Wendorff, *J. Phys. Chem.*, **75**, 2389 (1971).

A Statistical Mechanical Theory of Solubility[1]

R. O. Neff* and D. A. McQuarrie

Department of Chemistry, Indiana University, Bloomington, Indiana 47401 *(Received October 10, 1972)*

Publication costs assisted by the Petroleum Research Fund

Results on perturbation theory applied to liquid mixtures by Leonard, Henderson, and Barker are applied to the problem of solubility of gases in liquids. A term due to the decrease in solvent–solvent attractions on adding one solute molecule is found to have a significant effect on the solubility. The Henry's law constant, molar heat of solution, and partial molar volume of solute are predicted for the system neon in argon. The van der Waals constant, a, is predicted from molecular parameters with use of the Percus–Yevick radial distribution function for mixtures. Terms due to the density dependence of the radial distribution function are included.

Introduction

Of the three states of matter, the liquid is the most complex. It has neither the extreme order of the solid state nor the extreme disorder of the gaseous state. A still more difficult problem is that of liquid solutions. Here the problem is more difficult due to the interactions between

(1) Supported by a Petroleum Research Fund Grant (No. 4722-AC6).

unlike molecules. A simpler system is that of dilute solutions, *e.g.*, predicting the solubility of small quantities of gases in liquids. A well-known experimental quantity which describes such systems is the Henry's law constant K_H

$$K_H \equiv \lim_{x_2 \to 0} p_2/x_2 \tag{1}$$

where p_2 is the partial pressure of solute above the solution and x_2 is the mole fraction of solute. From K_H, the molar heat of solution ΔH_s and the partial molar volume of solute $\bar{V}_2$ can be obtained from

$$\Delta H_s/RT = (1/T)[\partial \ln K_H/\partial(T^{-1})]_p \tag{2}$$

$$\bar{V}_2 = RT(\partial \ln K_H/\partial p)_T \tag{3}$$

This article deals with the ability of statistical mechanics to predict experimental values of these quantities.

A rigorous but formal theory of liquids is that of the radial distribution function.[2a] Unfortunately, this theory is not very easy to apply to real systems. One important contribution of the theory, nevertheless, has been in the understanding of simple, nonassociating liquids, particularly rigid spheres. Verlet, using computer simulation, calculated the structure factor $\hat{h}(k)$ for a hard-sphere system from radial distribution function theory, where

$$\hat{h}(k) = \rho \int \exp(i\vec{k} \cdot \vec{r})(g(r) - 1)\, d\vec{r} \tag{4}$$

where $g(r)$ is the radial distribution function. He showed that $\hat{h}(k)$ for hard spheres is quite similar to that obtained by experiment for real simple systems, *e.g.*, Kr(l).[2b] Since $\hat{h}(k)$ gives a very detailed description of the structure of a fluid, we can see that the structure of real liquids at high densities is not too different from that of a hard-sphere fluid. This seems to imply that the structure of a liquid is primarily determined by the repulsive part of the potential. The attractive, relatively longer range part of the potential provides a somewhat uniform background potential. This, now generally accepted, physical picture has formed the basis of a number of successful perturbation theories of liquids.

In 1954, Zwanzig[3] provided the formalism to relate the properties of a real liquid to those of the hard-sphere fluid with a perturbation theory of liquids. He divided the total potential energy of a liquid into two contributions, a reference part and a perturbation part. The perturbation part represents the difference between the reference and the real system. The task of calculating macroscopic properties of real fluids reduced to that of calculating properties for a reference system, hopefully well known, and perturbation or correction terms. Consistent with the work of Verlet, perturbation theory has been applied to single-component liquids using different repulsive potentials as the reference system and attractive potentials for the corrective terms.[4,5] Perturbation theory has also been applied to concentrated solutions and is discussed, along with other theories of concentrated solutions, in a recent review article.[6]

The rigorous statistical mechanical theory of dilute solutions is that of McMillan and Mayer.[7] They treat dilute solutions in a manner similar to imperfect gas theory. Here, instead of gas molecules *in vacuo*, there are solute molecules in the solvent. The solvent is treated as a uniform background about which the solute particles move. Predicting properties of dilute solutions then reduces to one of calculating the interaction of one solute molecule with the solvent, two solute molecules with each other *and* the solvent, etc.

Several papers have recently appeared on the solubility of gases in liquids. Pierotti presented a simple, physically intuitive approach[8] in which he pictures the process of adding one solute molecule to pure solvent as equivalent to first making a cavity in the pure solvent the size necessary to hold one solute molecule, and then "charging" the cavity to the proper intermolecular potential. The work of creating the cavity was predicted from scaled particle theory which predicts the work necessary to introduce a hard sphere into a collection of hard spheres.[9] The work of charging was determined by integrating over the pair-wise Lennard-Jones intermolecular potential for solute–solvent interaction. He predicts values of K_H, ΔH_s, and $\bar{V}_2$ for several solutes and solvents. In a later article, Snider and Herrington,[10] starting with a van der Waals type equation of state modified for mixtures, derive equations for the properties of dilute solutions. Where Pierotti actually starts with molecular, Lennard-Jones potential parameters, Snider and Herrington do not. They adjust the solute–solvent van der Waals constant (a_{12}) so that the theory predicts correct values of K_H for some solute and solvent. They then predict values of ΔH_s and $\bar{V}_2$ for simple systems. As it was later shown, the poor agreement of Snider and Herrington is due to mistaken values of K_H.[11]

In this paper we start with the Leonard, Henderson, and Barker perturbation theory for mixtures[12] and derive rigorous expressions for K_H, ΔH_s, and $\bar{V}_2$. The reference system is hard sphere and its properties are predicted by the Percus–Yevick theory. The correction terms result from statistical mechanical perturbation theory. It is shown that the work of Pierotti and Snider and Herrington can be obtained as special cases of the more rigorous expressions obtained here. We find terms tacitly left out by previous workers, and in addition, terms which result from the density dependence of van der Waals constant are included. To test our results we predict properties of very simple, experimental systems. All predictions are done from molecular properties.

Derivation

Consider a liquid solution of some solute (denoted by a subscript 2) in some solvent (subscript 1) which is in equilibrium with gaseous solute at a partial pressure p_2. From thermodynamics we know that at equilibrium the

(2) (a) T. L. Hill, "Statistical Mechanics," McGraw-Hill, New York, N. Y., 1956; (b) L. Verlet, *Phys. Rev.*, **165**, 201 (1968).
(3) R. Zwanzig, *J. Chem. Phys.*, **22**, 1420 (1954).
(4) J. A. Barker and D. Henderson, *Accounts Chem. Res.*, **4**, 303 (1971).
(5) J. D. Weeks, D. Chandler, and H. D. Anderson, *J. Chem. Phys.*, **54**, 5237 (1971).
(6) D. Henderson and P. J. Leonard in "Physical Chemistry, An Advanced Treatise," Vol. VIIIB, H. Eyring, D. Henderson, and W. Jost, Ed., Academic Press, New York, N. Y., 1971, pp 413–510.
(7) W. G. McMillan and J. E. Mayer, *J. Chem. Phys.*, **13**, 276 (1945).
(8) R. A. Pierotti, *J. Phys. Chem.*, **67**, 1840 (1963).
(9) H. Reiss, H. S. Frisch, and J. L. Lebowitz, *J. Chem. Phys.*, **31**, 369 (1959); H. Reiss, *Advan. Chem. Phys.*, **9**, 1 (1965).
(10) N. S. Snider and T. M. Herrington, *J. Chem. Phys.*, **47**, 2248 (1967).
(11) L. A. K. Staveley, *J. Chem. Phys.*, **53**, 3136 (1970).
(12) P. J. Leonard, D. Henderson, and J. A. Barker, *Trans. Faraday Soc.*, **66**, 2469 (1970).

chemical potential of the solute in the two phases must be equal, *i.e.*, that

$$\mu_2^{liq} = \mu_2^{gas} \tag{5}$$

If we assume that the gas phase is ideal

$$\mu_2^{gas} = \mu_2^*(T) + kT \ln(p_2/kT) \tag{6}$$

The chemical potential of the liquid phase can be obtained from the Helmholtz free energy by

$$\mu_2 = (\partial A/\partial N_2)_{V,T,N_1} \tag{7}$$

Leonard, Henderson, and Barker applied the Barker-Henderson theory for pure liquids to mixtures and obtained the following expression for the Helmholtz free energy of a mixture[12]

$$A/kT = (A_0/kT) - 4\pi\rho_1 N_2 d_{12}^3 g_0^{12}(d_{12})[d_{12} - \delta_{12}] + (2\pi/kT)\sum_{i,j}\rho_i N_j \int_{\sigma_{ij}}^{\infty} dr\, r^2 u_{ij}(r) g_0^{ij}(r) \tag{8}$$

where A is the Helmholtz free energy of the real liquid, A_0 corresponds to that property for a hard-sphere mixture reference fluid, ρ_i is the number density of component i, N_i is the number of i molecules, d_{ij} is the hard-sphere diameter between molecules i and j, $g_0^{12}(d_{12})$ is the two-body hard-sphere mixture radial distribution function between a solute and a solvent particle at the contact distance d_{12}, $u_{ij}(r)$ is some potential function for the interaction of an i and a j molecule which is used as a perturbation potential, σ_{ij} is the intermolecular distance where u_{ij} is zero, $g_0^{ij}(r)$ is the mixture two-body hard-sphere radial distribution function between i and j molecules

$$\delta_{12} = \int_0^{\sigma_{12}} \{1 - \exp[u_{12}(z)/kT]\}\, dz \tag{9}$$

$$d_{11} = \int_0^{\sigma_{11}} \{1 - \exp[u_{11}(z)/kT]\}\, dz \tag{10}$$

$$d_{22} = \int_0^{\sigma_{22}} \{1 - \exp[u_{22}(z)/kT]\}\, dz \tag{11}$$

The way one determines d_{12} depends on the reference system used. If the reference system properties are predicted without assuming that their diameters are additive, *i.e.* without assuming that

$$d_{12} = (d_{11} + d_{22})/2 \tag{12}$$

then d_{12} is an unspecified parameter. By setting

$$d_{12} = \delta_{12} \tag{13}$$

the second term on the right-hand side of eq 8, which contains the radial distribution function on contact, is then zero. Since in this paper the properties of the hard-sphere reference system will be predicted by results from Percus-Yevick theory *with* the assumption that the hard-sphere diameters are additive, we will use eq 12 for d_{12} and so must be sure to include the second term eq 8. In deriving these results Leonard, Henderson, and Barker omit terms in $1/T^2$ and higher powers of $1/T$. It also contains the assumption that the total potential of the $N_1 + N_2$ molecules is the sum of the two-body potentials, neglecting three-body and higher interactions.

Applying eq 7 to eq 8, one obtains

$$\mu_2^{liq}/kT = (\mu_2^{ref}/kT) - 4\pi\rho_1 d_{12}^2[d_{12} - \delta_{12}] \times \{g_0^{12}(d_{12}) + N_2(\partial g_0^{12}(d_{12})/\partial N_2)_{N_1,V,T}\} + (2\pi\rho_1 N_1/kT)\int_{\sigma_{11}}^{\infty} dr\, r^2 u_{11}(r)(\partial g_0^{11}(r)/\partial N_2)_{N_1,V,T} + (4\pi\rho_1/kT)\int_{\sigma_{12}}^{\infty} dr\, r^2 u_{12}(r)[g_0^{12}(r) + N_2(\partial g_0^{12}(r)/\partial N_2)_{T,V,N_1}] + (2\pi\rho_2/kT)\int_{\sigma_{22}}^{\infty} dr\, r^2 u_{22}(r)[2g_0^{22}(r) + N_2(\partial g_0^{22}/\partial N_2)_{N_1,V,T}] \tag{14}$$

In more condensed form, the above equation is

$$(\mu_2^{liq}/kT) = (\mu_2^{ref}/kT) + (\mu_2^{corr}/kT) \tag{15}$$

where the last four terms are all denoted by μ_2^{corr}/kT. Percus-Yevick theory with use of the compressibility equation predicts the following equation of state for a mixture of additive hard spheres[13]

$$p/\rho kT = \chi(\xi) = [(1 + \xi + \xi^2)/(1-\xi)^3] - [3\xi/(1-\xi)^3 \times [x_1x_2/(x_1d_{11}^3 + x_2d_{22}^3)](d_{11} - d_{22})^2 X \tag{16}$$

where

$$\xi = (\pi\rho/6)[x_1d_{11}^3 + x_2d_{22}^3] \tag{17}$$

$$X = d_{11} + d_{22} + \xi d_{11}d_{22}[(x_1d_{11}^2 + x_2d_{22}^2)/(x_1d_{11}^3 + x_2d_{22}^3)] \tag{18}$$

It has been shown[10] that the chemical potential predicted by this equation of state relative to the perfect gas is

$$(\mu_2/kT) = [\mu_2^*(T)/kT] + \ln\rho_2 - \ln(1-\xi) + [d_{22}^3/(x_1d_{11}^3 + x_2d_{22}^3)]\xi\chi(\xi) + (1/2)[3\xi/(1-\xi)]^2[d_{22}(x_1d_{11}^2 + x_2d_{22}^2)/(x_1d_{11}^3 + x_2d_{22}^3)]^2 + [3\xi/(1-\xi)]\{[d_{22}^2(x_1d_{11} + x_2d_{22})/(x_1d_{11}^3 + x_2d_{22}^3)] + [d_{22}(x_1d_{11}^2 + x_2d_{22}^2)]/[x_1d_{11}^3 + x_2d_{22}^3]\} \tag{19}$$

We will condense the above equation to

$$(\mu_2/kT) = (\mu_2^*/kT) + \ln\rho_2 + (\mu_2^{HS}/kT) \tag{20}$$

where the last four terms are denoted by μ_2^{HS}/kT. Using eq 20 for μ_2^{ref}/kT in eq 15

$$\mu_2^{liq}/kT = (\mu_2^*/kT) + \ln\rho_2 + (\mu_2^{HS}/kT) + (\mu_2^{corr}/kT) \tag{21}$$

Substituting eq 6 and 21 into eq 5 gives

$$\ln(p_2/x_2) = \ln(pkT) + (\mu_2^{HS}/kT) + (\mu_2^{corr}/kT) \tag{22}$$

Taking the limit as x_2 goes to zero of eq 22 as in eq 1

(13) J. L. Lebowitz, *Phys. Rev.*, **133**, 895 (1964).

$$\ln K_H = \ln RT/\bar{V}_1 + (\mu_2^{HS}/kT) + (\mu_2/kT) \quad (23)$$

where

$$\mu_2^{HS}/kT = -\ln(1-y) + y\chi(y)R^3 + (1/2)[3y/(1-y)]^2R^2 + [3y/(1-y)](R^2+R) \quad (24)$$

$$y = \pi\rho_1 d_{11}^3/6$$

$$R = d_{22}/d_{11}$$

$$\chi(y) = (1 + y + y^2)/(1-y)^3$$

$$\mu_2^{corr}/kT = (-2\rho_1 a_{12}/kT) + (2\rho_1 I_{11}/kT) - 4\pi\rho_1 d_{12}^3(d_{12} - \delta_{12})g_0^{12}(d_{12}) \quad (25)$$

$$a_{12} = -2\pi\int_{\sigma_{12}}^{\infty} dr\, r^2 u_{12}(r) g_0^{12}(r) \quad (26)$$

$$I_{11} = \pi N_1 \int_{\sigma_{11}}^{\infty} dr\, r^2 u_{11}(r)[\partial g_0^{11}(r)/\partial N_2]_{V,T,N_1} \quad (27)$$

The term with the derivative of $g_0^{11}(r)$ with respect to N_2 has not been included in previous work on predicting Henry's law constants. The term considers the effect on the solvent-solvent interactions of adding one solute molecule to the liquid.

We will now show that Pierotti's results can be obtained from eq 23. If one substitutes the Percus-Yevick compressibility expression for the hard-sphere pressure[14,15] into Pierotti's eq 11 and 12 for the free energy of cavity formation, they are the same as our reference terms. His expression for the free energy of charging can be obtained from our correction term by using the low-density limit of the radial distribution function in a_{12}, *i.e.*

$$g_0^{12}(r) = \lim_{\rho_1,\rho_2 \to 0} g_0^{12}(r) \begin{cases} = 0 & r < \sigma_{12} \\ = 1 & r \geq \sigma_{12} \end{cases} \quad (28)$$

Pierotti's method of derivation, although physically intuitive, did not allow him to find the term in I_{11}. I_{11} considers the change in $g_0^{11}(r)$ when one solute molecule is added. Although it is readily apparent that this change is small, the term is multiplied by an extra factor of Avogadro's number. Therefore the term cannot be neglected from inspection.

Since Snider and Herrington started with a van der Waals equation of state with the Percus-Yevick compressibility equation of state for the hard-sphere part, our hard-sphere terms are identical. The attractive terms in Snider and Herrington's equation for K_H are the same as our correction term in a_{12}. The term with I_{11} is omitted in their paper also. To determine the van der Waals constant a_{12} they assume that their equation predicts the proper K_H and calculate a_{12} from experimental values of K_H. The method is more empirical and less molecular then Pierotti's. Their empirical a_{12} may include the effects of our term in I_{11}. Since there was some confusion about the *experimental* values of K_H for the solubility of Ne in Ar at the time of their paper, Staveley[11] reworked their calculations using the proper experimental K_H. Staveley was able to predict K_H at different temperatures from a known value at one temperature. A difficulty with this method of predicting K_H is that one value must be known already.

As stated earlier one can easily obtain formulas for ΔH_s and $\bar{V}_2$ from the Henry's law constant. For ΔH_s, we obtain the following

$$\Delta H_s/RT = (\Delta H_s^{ref}/RT) + (\Delta H_s^{corr}/RT) + (\alpha T - 1) \quad (29)$$

where

$$\Delta H_s^{ref}/RT = (1/T)[(\partial\mu_2^{HS}/kT)/\partial(T^{-1})]_p = \alpha T\omega \quad (30)$$

$$\omega = [y/(1-y)]\{[(1+2y)^2/(1-y)^3]R^3 + 3[(1+2y)/(1-y)^2] \times R^2 + [3/(1-y)]R + 1\}$$

$$R = d_{22}/d_{11}$$

$$\Delta H_s^{corr}/RT = (1/T)[\partial(\mu_2^{corr}/kT)/\partial T^{-1}]_p \quad (31)$$

$$= -(2\rho_1 a_{12}/kT) - (2\rho_1 a_{12}\alpha T/kT) - (2\rho_1/kT) \times (\alpha T)\rho_1(\partial a_{12}/\partial\rho_1)_p + (2\rho_1/kT)I_{11} + (2\rho_1 L_{11}/kT)\alpha T + (2\rho_1/kT)\rho_1(\partial I_{11}/\partial\rho_1)_p\alpha T - 4\pi\rho_1 d_{12}^2(d_{12} - \delta_{12}) \times \alpha T[g_0^{12}(d_{12}) + \rho_1(\partial g_0^{12}(d_{12})/\partial\rho_1)_T]$$

$\alpha = (1/V)(\partial V/\partial T)_p$ (coefficient of thermal expansion). Pierotti's results for ΔH_s can be obtained from the above by omitting the term in R^3 from ω of $\Delta H_s^{ref}/RT$, which is the same as neglecting the pressure terms in his cavity expression, and omitting all terms but the first in $\Delta H_s^{corr}/RT$.

The first two terms of $\Delta H_s^{corr}/RT$ and all of $\Delta H_s^{ref}/RT$ are the same as the results of Snider and Herrington's work. The third term is omitted by them since they assume a_{12} is independent of density. The next three terms all arise from our new term with I_{11}. While Pierotti used experimental values for α, Snider and Herrington used a theoretical value which they obtained from their equation of state, eq 16

$$\alpha' T = (1-y^3)/(2y^3 + 4y^2 + 4y - 1) \quad (32)$$

For $\bar{V}_2$, we obtain

$$\bar{V}_2 = \beta RT + \bar{V}_2^{ref} + \bar{V}_2^{corr} \quad (33)$$

where

$$\bar{V}_2^{ref} = RT[\partial(\mu_2^{HS}/kT)/\partial p]_T = \beta RT\omega \quad (34)$$

$$\bar{V}_2^{corr} = RT[\partial(\mu_2^{corr}/kT)/\partial p]_T$$
$$= RT\beta(-2\rho_1 a_{12}/kT) + RT\beta[-(2\rho_1/kT)\rho_1(\partial a_{12}/\partial\rho_1)_T] + RT\beta(2\rho_1 I_{11}/kT) + RT\beta[(2\rho_1/kT)\rho_1(\partial I_{11}/\partial\rho_1)_T] - 4\pi\rho_1 d_{12}^2(d_{12} - \delta_{12})RT\beta[g_0^{12}(d_{12}) + \rho_1(\partial g_0^{12}(d_{12})/\partial\rho_1)]$$

$\beta = -(1/V)(\partial V/\partial\rho)_T$ isothermal compressibility (35)

This result reduces to Pierotti's if $\bar{V}_2^{corr}$ is omitted. The reference terms are the same as Snider and Herrington's but the last four terms in $\bar{V}_2^{corr}$ are not included. Pierotti used experimental values for β while Snider and Herrington used an expression derived from eq 16.

$$\rho kT\beta = (1-y)^4/(2y^3 + 4y^2 + 4y - 1) \quad (36)$$

Calculations

In our calculations we used the reference terms as written in eq 24, 30, and 34. Parameters used were the experi-

(14) M. S. Wertheim, *Phys. Rev. Lett.*, **10**, 321 (1963).
(15) E. Thiele, *J. Chem. Phys.*, **39**, 474 (1963).

TABLE I: Physical Properties of Argon[a]

Temp, °K	$\bar{V}_1$, cm³/mol	αT	$\rho k T \beta$
84.42	28.20	0.372	0.0513
87.29	28.66	0.392	0.0561
87.42	28.66	0.392	0.0564
115.8	33.23	0.811	0.171
129.93	37.5	1.43	0.406

[a] J. S. Rowlinson, "Liquids and Liquid Mixtures," Plenum Press, New York, N. Y., 1969, p 46.

TABLE II: Lennard-Jones 6–12 Potential Parameters

Atoms	ϵ/k, °K	$10^{-8}\sigma$, cm
Ar–Ar	117.7[a]	3.504[a]
Ne–Ar	64.5[b]	3.10[b]
Ne–Ne	35.8[c]	2.75[c]

[a] A. E. Sherwood and J. M. Prausnitz, *J. Chem. Phys.*, **41**, 429 (1964). [b] J. M. Parson, T. P. Shafer, F. P. Tully, P. E. Siska, Y. C. Wang, and Y. T. Lee, *J. Chem. Phys.*, **53**, 2123 (1970). [c] J. S. Rowlinson, *Annu. Rept. Progr. Chem.*, **56**, 22 (1959).

mental molar volume of solvent V_1 (Table I) and effective hard-sphere diameters d_{ij} determined by eq 10, 11, and 12. The Lennard-Jones 6–12 potential was used throughout as the perturbation potential with the parameters given in Table II.

All integrals over the radial distribution functions were written in terms of the Laplace transform of $rg_{ij}(r)$ and inverse Laplace transform of $ru_{ij}(r)$ according to Frisch, *et al.*[16]

$$\int_{d_{ij}}^{\infty} dr\ r^2 u_{ij}(r) g_0^{ij}(r) = \int_0^{\infty} ds\ U_{ij}(s) G_{ij}(s) \qquad (37)$$

where

$$G_{11}(s) = s[h - L_2(s)\exp(sd_{22})]/12\eta_1 D(s) \qquad (38)$$

$$G_{12}(s) = s^2 \exp(sd_{12})\{[0.75(\eta_2 d_{22}^3 - \eta_1 d_{11}^3) \times (d_{22} - d_{11}) - d_{12}(1 + 0.5\xi)]s - (1 + 2\xi)\}/D(s) \qquad (39)$$

$$D(s) = h - L_1(s)\exp(sd_{11}) - L_2(s)\exp(sd_{22}) + S(s)\exp(2sd_{12})$$

$$h = 36\eta_1\eta_2(a_{22} - d_{11})^2$$

$$L_1(s) = 12\eta_2[(1 + 0.5\xi) + 1.5\eta_1 d_{11}^2(d_{22} - d_{11})]d_{22}s^2 + [12\eta_2(1 + 2\xi) - hd_{11}]s + h$$

$$S(s) = h + [12(\eta_1 + \eta_2)(1 + 2\xi) - h(d_{11} + d_{22})]s - 18(\eta_1 d_{11}^2 + \eta_2 d_{22}^2)^2 s^2 - 6(\eta_1 d_{11}^2 + \eta_2 d_{22}^2)(1 - \xi)s^3 - (1 - \xi)^2 s^4$$

$$\eta_i = \pi\rho_i/6$$

$$\xi = \pi(\rho_1 d_{11}^3 + \rho_2 d_{22}^3)/6$$

$L_2(s)$ can be found from $L_1(s)$ by interchanging η_1, d_{11} with η_2, d_{22}, and

$$U_{ij}(s) = L^{-1}\{ru_{6-12}(r)\} = 4\epsilon_{ij}\sigma_{ij}^2\{[(s\sigma_{ij})^{10}/10!] - [(s\sigma_{ij})^4/4!]\} \qquad (40)$$

$G_{ij}(s)$ has been determined from the multicomponent Percus–Yevick equation by Lebowitz.[13] The integrals in eq 37 involving $G_{ij}(s)$ and $U_{ij}(s)$ were evaluated numerically using Gauss quadrature. For simple calculations this technique is limited to simple potentials such as Lennard-Jones and Kihara types. More accurate potential data are available for neon and argon[17] but the Laplace transform technique becomes numerically ackward. Terms with the density derivatives of the radial distribution function and the density derivative of terms with a radial distribution function were evaluated by differentiating $G_{ij}(s)$ with respect to the density and then integrating.

One should note that the integrals needed start at σ_{ij} and not d_{ij} as the Laplace transform method. A small integral from d_{ij} to σ_{ij}, which must be subtracted from the Laplace result, is not easy to calculate. Although the Laplace transform of the radial distribution function for mixtures can be inverted we used a simpler, more approximate technique to evaluate the small integrals. We evaluated the integrand at d_{ij} with an expression for the radial distribution function on contact from Lebowitz and at σ_{ij} (zero) and assumed a linear function for the integrand between these two points. Since these small integrals are only about 10% of the large integrals, we consider the approximation to be accurate enough.

As in Pierotti's work we used experimental values for the coefficient of thermal expansion and isothermal compressibility.

Discussion

In Table III we see that Pierotti's approach, even though simple enough to compute by slide rule, gives reasonable agreement near 87°K. Pierotti seems to have used a different reference term due to his interpretation of the pressure terms. In order to reproduce his results for Ne in Ar with the parameters he specified, we had to neglect these terms. One way in which the pressure terms in his eq 12 would be negligible is if real liquid values of the pressure were used. The hard-sphere pressure from the Percus–Yevick compressibility equation of state is about a factor of 10 larger than that of a real fluid. Other workers, in applying scaled particle theory to other systems, have interpreted the pressure this way.[18] From perturbation theory we see that the reference terms should correspond to the reference potential alone and using experimental or real fluid properties in the reference term is not consistent. The Pierotti approach underestimates (less negative) the charging or perturbation term by using the low-density limit of the radial distribution function. The two effects almost cancel for K_H but not so for the prediction of ΔH_s and its agreement is quite poor.

Leonard and Henderson reported the results of some calculations on K_H in a recent article.[6] They apparently used the same reference terms as Snider and Herrington and this work. They included a van der Waals constant predicted by "a preliminary second-order term" in the Leonard–Henderson–Barker expansion. The difference between our prediction of K_H and theirs is due to the new term in I_{11}.

(16) H. L. Frisch, J. L. Katz, E. Praestgaard, and J. L. Lebowitz, *J. Phys. Chem.*, **70**, 2016 (1966).
(17) P. E. Siska, J. M. Parson, T. P. Schafer, and Y. T. Lee, *J. Chem. Phys.*, **55**, 5762 (1971).
(18) E. Wilhelm and R. Battino, *J. Chem. Thermodyn.*, **3**, 379 (1971).

TABLE III: Solubility of Neon in Argon

	Experiment	Henderson[a] and Leonard	Pierotti[b]	Snider and Herrington; Staveley[c]	This work
$T = 84.42°K$					
K_H, atm	1140[d]	561			1520
ΔH_s, cal/mol					258
$\bar{V}_2$, cm^3/mol					32
$T = 87.29°K$					
K_H, atm	1085[d]				1300
ΔH_s, cal/mol	201[d]			284,294	235
$\bar{V}_2$, cm^3/mol	20–30[e]			29,30	32
$T = 87.42°K$					
K_H, atm	1064[d]	544	483		1310
ΔH_s, cal/mol	232[d]	291,[g] −296[f]	−88		236
$\bar{V}_2$, cm^3/mol			31		32
$T = 115.8°K$					
K_H, atm	651[d]			651,641	672
ΔH_s, cal/mol	597[d]			612,633	570
$\bar{V}_2$, cm^3/mol	40–50[e]			51,53	51
$T = 129.93°K$					
K_H, atm	450[d]	337			446
ΔH_s, cal/mol					914
$\bar{V}_2$, cm^3/mol					82

[a] Reference 6, p 503. [b] Reference 8. [c] Reference 11. [d] W. B. Streett, *J. Chem. Phys.*, **42**, 500 (1965). [e] W. B. Streett, *ibid.*, **46**, 3282 (1967). Reference 11. [f] With experimental αT. [g] αT predicted by eq 32.

The more empirical approach of Snider and Herrington gives comparable agreement with experiment for K_H and better for ΔH_s. The method they used in determining the van der Waals constant a_{12} probably included effects due to the I_{11} term and the term with the radial distribution function on contact. Although Snider and Herrington's results for ΔH_s agree better with experiment, we feel that eq 31 is more rigorous. In all theories discussed in this paper the density of the solvent is determined by experimental values of the solvent molar volume, including the reference terms. The best estimate of the temperature or pressure dependence of the density would be with the experimental values of α and β. Leonard and Henderson stated this in their review article. Although Snider and Herrington's approach gives good agreement with their theoretical values of α and β, they get very poor results with the experimental values. The good agreement of their work must be due to compensating errors.

The results of this work predict quite good values of K_H from intermolecular potential data and the solvent molar volume. Agreement is better than all previous work except that of Snider and Herrington at 115°K. Including a $1/T^2$, Barker–Henderson type term would improve agreement at temperatures around 84–87°K. The agreement at temperatures of 115.8 and 129.93°K is already very good.

Our predictions of ΔH_s are much better than previous predictions from potential parameters. Both Henderson and Leonard and Pierotti got the wrong sign for ΔH_s when they used experimental values of αT. Henderson and Leonard's agreement is not bad using the Snider and Herrington approximate value for αT. As the authors stated, this must be due to some cancellation of errors. As stated before all the results of this work are with experimental values of α and β, the most appropriate values.

The results of this work substantiate the idea that real fluids resemble a collection of hard spheres in a volume determined by the attractive potential. Perturbation theory is quite capable of predicting solubility in simple, real liquids. Possibly the most surprising result is that the decrease in solvent–solvent attraction when a solute molecule is added is an important effect in the solvation process, even in dilute solutions. Future studies planned in this area include extending predictions to more concentrated solutions, predicting solubility in more complex systems, and investigating other perturbation expansions.

Acknowledgment. Acknowledgment is made to the donors of The Petroleum Research Fund, administered by the American Chemical Society, for support of this research.

A Determination of the Rotational Barrier about the N–C Bond in Two Chalcogen Replaced *N,N*-Dimethylamides[1]

R. F. Hobson and L. W. Reeves*

Chemistry Department, University of Waterloo, Waterloo, Ontario, Canada *(Received September 25, 1972)*

Publication costs assisted by the National Research Council of Canada

Hindered rotation (HR) about the N–C amido bond in samples of 3-dimethylaminoacrylonitrile and (dimethylaminoethylene)malonitrile has been examined by proton magnetic resonance. Substitution of the $=CH_2$ moeity in place of chalcogens in the amide structure leads to a large decrease in the barrier to rotation about the amido N–C bond, but substitution of electronegative groups for hydrogen in $=CH_2$ then causes an increase in the barrier. The effects of CN substitution are manifest by stabilization of the carbanion resonance structure. In turn, the free energy of activation for HR is found to increase approximately with the square of the total mesomeric interacting potential of the substituents. Eight-site formulation of the chemical exchange for 3-dimethylaminoacrylonitrile requires consideration of parity in the signs of long-range couplings. Thus it is suggested that both of the $^4J(CH_3\text{-}H)$ and $^5J(CH_3\text{-}H)$ couplings have the same sign. This is substantiated by line shape analysis and the magnitudes of the averaged couplings in the fast exchange limit. The magnitudes of all couplings are reported and they are considered to be dependent upon the extent of π conjugation and/or configuration interaction.

Introduction

The subject of hindered rotation about N–C amido type bonds has been the object of several studies from this laboratory[2] and has, in the past, received considerable attention.[3] With a working knowledge of nuclear magnetic resonance (nmr) line shape analysis, it is possible to concentrate on special series of compounds which will lead to a partial separation of $\Delta G\ddagger(N\text{-}C_{BR})$ (where the subscript BR denotes bond rotation) into steric, resonance, and polar contributions thereby augmenting the general stereochemistry of the important peptide link. It is the purpose of this article to report the study of two amido structures where the carbonyl oxygen is replaced by a C=C double bond. In particular, since the cyanide group has been found to have a peculiar effect on $\Delta G\ddagger(N\text{-}C_{BR})$ in the compound $Ox(CN)$[2d,4] this substituent is worthy of more investigation. Previous variation of the doubly bonded Y substituent has been limited mainly to the chalcogens while replacement of the X substituent has been the subject of much more investigation.[2,3]

Experimental Section

The experimental precautions required to measure rates of hindered rotation by the nmr method have been adequately evolved and described in previous reports.[2] Spectra were recorded using a Varian HA 100 nmr spectrometer and temperatures were calibrated according to Van Geet.[5a]

3-Dimethylaminoacrylonitrile, CHCNx(H), and (dimethylaminoethylene)malonitrile, $C(CN)_2x(H)$, were purchased from Aldrich Chemical Co. and were used without further purification. The two nmr samples contained well-dried solutions of (in mole %) (a) 11.2% CHCNx(H), 87.7% CCl_4, and 1.1% hexamethylidisiloxane (HMDS); (b) 11.5% $C(CN)_2x(H)$, 85.5% *sym*-tetrachloroethane (TCE), and 3% HMDS.

Results

The spectrum of $C(CN)_2x(H)$ is referred to structure I. The important spectral features for kinetic analysis are contained in the A_3B_3 spectrum, with $J_{AB} = 0$. The larger four bond coupling, 0.3 ± 0.05 Hz, appeared at a lower field than the smaller, 0.2 ± 0.05 Hz. In previous cases of such couplings where the Y substituent has been a chalcogen, the larger coupling has been assumed[2,3] (and sometimes proven[5b]) to belong to the trans or A methyl. However, it has also been observed, for compounds with Y = chalcogen, that the largest of such couplings is displayed by the methyl feature which is also most temperature sensitive.[6] Thus the various coupling and chemical shift factors in $C(CN)_2x(H)$ are quite different. The difference in magnitude of these couplings is too small to include a determination of relative signs, so they are both assumed to be of the same sign.[5b] The kinetic results for $C(CN)_2x(H)$ were found to be E_a = 17.1 ± 0.5 kcal/mol, $\Delta H\ddagger(25°)$ = 16.5 ± 0.5 kcal/mol, $\Delta G\ddagger(25°)$ = 17.7 ± 0.5 kcal/mol, and $\Delta S\ddagger$ = −3.9 ± 2.0 cal deg^{-1} mol^{-1}. These results agree

(1) Research supported by operating grants made available to L. W. R. by the National Research Council of Canada.

(2) (a) L. W. Reeves and K. N. Shaw, *Can. J. Chem.*, **48**, 3641 (1970); (b) *ibid.*, **49**, 3671 (1971); (c) L. W. Reeves, R. C. Shaddick, and K. N. Shaw, *ibid.*, **49**, 3683 (1971); (d) E. A. Allan, R. F. Hobson, L. W. Reeves, and K. N. Shaw, *J. Amer. Chem. Soc.*, **94**, 6604 (1972); (e) R. F. Hobson and L. W. Reeves, *J. Phys. Chem.*, in press.

(3) (a) M. T. Rogers and J. C. Woodbrey, *J. Phys. Chem.*, **66**, 540 (1962); (b) L. W. Reeves, *Advan. Phys. Org. Chem.*, **3**, 187 (1965); (c) G. Binsch, *Top. Stereochem.*, **3**, 97 (1968); (d) G. Binsch, *J. Amer. Chem. Soc.*, **91**, 1304 (1969); (e) T. H. Siddall and W. E. Stewart, *Progr. Nucl. Magn. Resonance Spectrosc.*, **4**, 33 (1969); (f) W. E. Stewart and T. H. Siddall, III, *Chem. Rev.*, **70**, 517 (1970); (g) H. Kessler, *Angew. Chem., Int. Ed. Engl.*, **9**, 219 (1970).

(4) It has been convenient to refer to amides of the general formula, $Me_2N\text{-}C(=Y)\text{-}X$, by a functional notation, Yx(X).

(5) (a) A. L. Van Geet, *Anal. Chem.*, **40**, 2227 (1968); (b) A. J. R. Bourn and E. W. Randall, *Mol. Phys.*, **8**, 567 (1964).

(6) R. F. Hobson, Ph.D. Thesis, University of Waterloo, 1972.

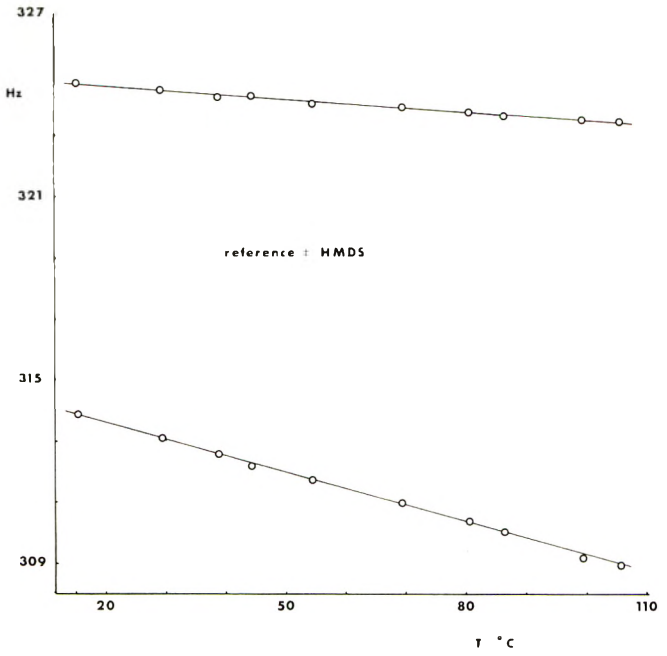

Figure 1. A plot of the *N*-methyl chemical shifts *vs.* temperature for $C(CN)_2x(H)$, reterenced internally to HMDS. The field increases with decreasing frequency.

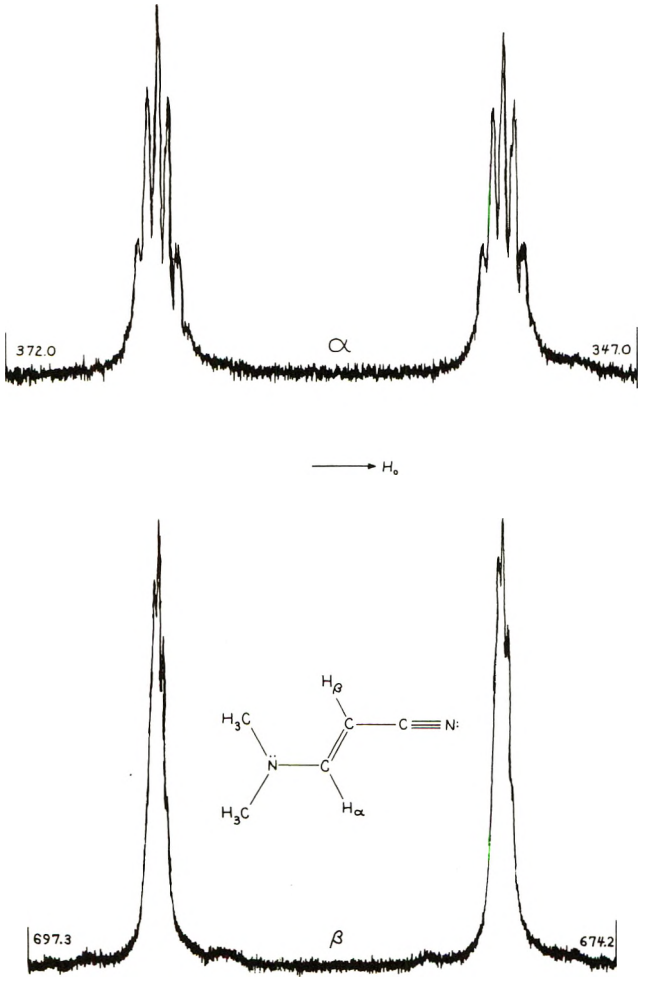

Figure 2. Spectrum of the protons M(α) and X(β) identified in structure II of the text (referenced to HMDS).

(where comparable) with a previous study by Mannschreck, *et al.*,[7] using coalescence temperature methods. The reported chemical shift difference $|\Delta\omega| = |\omega_A - \omega_B|$ in the absence of exchange for the latter work (the solvent was $CDBr_3$ but no concentrations were supplied) differs considerably from the present findings, Figure 1, implying that $\Delta\omega$ is quite solvent sensitive.

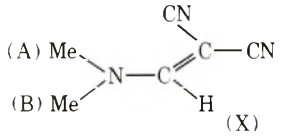

I

CHCNx(H) has an extra proton so that the spectrum becomes A_3B_3MX with $J_{AB} = 0$. The nonzero couplings have been assigned *(vide infra)* in magnitude as (±0.05 Hz) $J_{AM} = 0.5$ Hz, $J_{BM} = 0.3$ Hz, $J_{AX} = 0.12$ Hz, $J_{BX} = 0.2$ Hz, and $J_{MX} = 13.5$ Hz. The couplings were measured directly from the M and X spectra (Figure 2) in the slow exchange limit and checked with their fast exchange averages, which indicated that there was probably no temperature dependence. Structure II identifies the protons named in the spectrum. The protons M and X have a trans arrangement in the CHCNx(H) molecule studied here so their nmr spectra are dominated by the large trans coupling, J_{MX}. The upper spectrum in Figure 2, that of the M proton, can be assigned with two closely overlapping quartets in each doublet arising from coupling constants J_{AM} and J_{BM}. The longer range couplings from A and B protons are seen as barely resolved fine structure in the X spectrum. The A_3 and B_3 parts of the spectrum have four transitions each and exchange between A and B necessitates an eight-site exchange treatment.[2a]

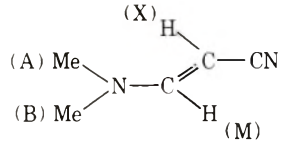

II

It is first necessary to decide which of the M and X couplings are associated with the A methyl and which with the B methyl. This has been accomplished with the aid of the slow exchange spectra. In the case where J_{AM} is the larger four-bond coupling and J_{AX} is the smaller five-bond coupling, the sum of the A couplings is 0.65 Hz while the sum of the B couplings is 0.5 Hz. Since the resolution was not sufficient to measure the A and B splittings explicitly, a line width argument was used to show that the above case is correct. The difference in sums of couplings is 0.15 Hz for this case while the other possible grouping leads to a 0.3 Hz difference. These differences are large enough to be differentiated between in the line width of a slow exchange spectrum. There is, of course, the possibility that $|J_{BM}| > |J_{AM}|$ in which case the above argument applies with A and B interchanged. In any case, the larger four-bond coupling appeared at high field, opposite to $C(CN)_2x(H)$, and the most temperature sensitive methyl feature was at low field. The temperature dependence of

(7) A Mannschreck and U. Koelle, *Tetrahedron Lett.*, **No. 10**, 863 (1967).

$\Delta\omega$ in the latter results in a decrease from 0.39 ppm at $-32°$ to 0.276 ppm at 55°, while in the former it increases with temperature (Figure 1).

The 8 × 8 rate matrix is symmetric because the exchange system is equal population and nontruncated.[8] It becomes possible to measure relative signs between J_{AX} and J_{BX}, and J_{AM} and J_{BM} if sufficient spectral resolution is available. Following the arguments used for the ABX case with $J_{AB} = 0$,[2b] the rate matrix has four possible constructions depending on the parity of the four coupling constants. Considering only the 4 × 4 off-diagonal submatrices K^P (where P represents the combined parity) the possible combined parities are ++, +−, −+, and −− according to the relative coupling signs. If, for example, J_{AX} and J_{BX} are of the same sign we specify a + parity, otherwise a − parity is appropriate. The submatrices become

$$K^{++} = \begin{vmatrix} -k & & & \\ & -k & & \\ & & -k & \\ & & & -k \end{vmatrix} \qquad K^{--} = \begin{vmatrix} & & & -k \\ & & -k & \\ & -k & & \\ -k & & & \end{vmatrix}$$

$$K^{+-} = \begin{vmatrix} 0 & -k & & \\ -k & 0 & & \\ & & 0 & -k \\ & & -k & 0 \end{vmatrix} \qquad K^{-+} = \begin{vmatrix} & & -k & 0 \\ & & 0 & -k \\ -k & 0 & & \\ 0 & -k & & \end{vmatrix}$$

The couplings J_{AM} and J_{BM} have been considered by Bourn and Randall[5b] and thought to be both negative while J_{AX} and J_{BX} by analogy with 1,3-butadienes are probably both positive.[9] The ++ parity was selected and yielded good line shape fits (Figure 3). The assignment $|J_{BX}| > |J_{AX}|$ supports the observed pattern in 1,3-butadienes where trans zig-zag paths lead to the largest couplings over five bonds.[9] The average couplings $\frac{1}{2}|J_{AM} + J_{BM}| = 0.4$ Hz and $\frac{1}{2}|J_{AX} + J_{BX}| = 0.16$ Hz measured in the fast exchange limit are also in agreement with the ++ parity.

The trans J_{MX} coupling in CHCNx(H) may be compared with similar couplings in some substituted vinyl compounds, $CH_2{=}CH_4$. In the series R = H, CN, $COCH_3$, Cl, and F, J_{MX} values have been reported as 18.95, 17.92, 17.8, 14.6, and 12.75 Hz, respectively.[10] It is apparent that this coupling decreases either with increased conjugation to the side chain or increased π-electron repulsion by the side chain. When R is a dimethylamino group J_{MX} is found to be 17.8 Hz, comparable to J_{MX} for R an acetyl group. The relatively small value of J_{MX} (13.5 Hz) obtained here for CHCNx(H) indicates that double trans substitution can enhance the effects of substitution on this coupling. It might be expected, then, that $\Delta G^{\ddagger}(N\text{-}C_{BR})$ and appropriately related trans couplings have a common origin in the structure.

The kinetic parameters for this study of CHCNx(H) are $E_a = 14.3 \pm 0.5$ kcal/mol, $\Delta H^{\ddagger}(25°) = 13.7 \pm 0.5$ kcal/mol, $\Delta G^{\ddagger}(25°) = 12.9 \pm 0.5$ kcal/mol, and $\Delta S^{\ddagger} = 2.7 \pm 1.1$ cal deg^{-1} mol^{-1}.

Discussion

The moeity $C{=}CH_2$ replacing a chalcogen requires a carbanion form $=C\text{-}CH_2^-$ in order to allow delocalization of π electrons in the N-C bond. This is expected to be much less stable than $=C\text{-}O^-$ so that the barrier in the compound $CH_2x(H)$ should be lower than the barrier in the model compound Ox(H). Indeed, the estimate of $\Delta G^{\ddagger}(N\text{-}C_{BR}) = 11.7$ kcal/mol for $CH_2x(H)$[6] is much lower than the average value found for Ox(H), 21.0 kcal/mol.[11] Substitution with cyano groups stabilizes the carbanion structure with dramatic increases in $\Delta G^{\ddagger}(N\text{-}C_{BR})$.

Steric interactions between x and Y in the compounds $CH_2x(H)$ and CHCNx(H) should be similar as the CN substituent is far removed from the important part of the molecule. Thus the estimated increase in $\Delta G^{\ddagger}(N\text{-}C_{BR})$ of 1.2 kcal/mol may be ascribed to conjugation or stabilization of the carbanion II or III. This brings out an interesting point about the results obtained for the compound Ox(CN).[2a] (They favor structure IV.) If conjugation as in III is dominant, then $\Delta G^{\ddagger}(N\text{-}C_{BR})$ in Ox(CN) should be less than $\Delta G^{\ddagger}(N\text{-}C_{BR})$ in Ox(H) while if structure IV is more representative, the reverse will be observed and the result can be realized by a carbanion type of intermediate

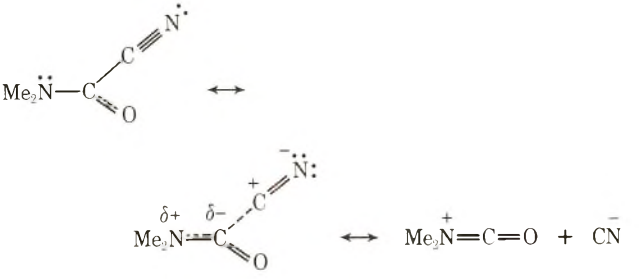

See also ref 12 for various CN and NC valence bond descriptions.

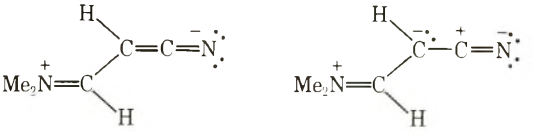

III IV

Addition of a second cyanide to the $C{=}CH_2$ moiety sharply increases $\Delta G^{\ddagger}(N\text{-}C_{BR})$. If the substituent effect were simply additive, we would expect $\Delta G^{\ddagger} \approx 14.0$ kcal/mol, so this is not the case. The compound $CHNO_2x(H)$ (with protons trans) has also been examined by nmr using approximate methods.[7] The quoted value of $\Delta G^{\ddagger}(N\text{-}C_{BR}) = 16.5$ kcal/mol should be within 1 kcal/mol of the $\Delta G^{\ddagger}(N\text{-}C_{BR})$ that would have been obtained by a detailed line shape study and is much larger than that found for CHCNx(H), but comparable to $\Delta G^{\ddagger}(N\text{-}C_{BR})$ for $C(CN)_2x(H)$. The mesomeric bonding potential of NO_2 compared with CN has been found to be greater by a factor $\sim$1.8.[6] This suggests that $\Delta G^{\ddagger}(N\text{-}C_{BR})$ in these compounds is proportional to the square of the total mesomeric bonding potential attached to the β carbon. A plot of $(h_Y)^2$ *vs.* $\Delta G^{\ddagger}(N\text{-}C_{BR})$ also shows a linear correlation, where the h_Y values are Hückel coulomb parameters which have recently been determined for this series including the unsubstituted compound $CH_2x(H)$.[6] Since

(8) S. O. Chan and L. W. Reeves, *J. Amer. Chem. Soc.*, in press.
(9) A. A. Bothner-By and R. K. Harris, *J. Amer. Chem. Soc.*, **87**, 3445 (1965); **87**, 3451 (1965).
(10) A. A. Bothner-By, *Advan. Magn. Resonance*, **1**, 258 (1965).
(11) P. T. Inglefield, E. Krakower, L. W. Reeves, and R. Stewart, *Mol. Phys.*, **15**, 65 (1968).
(12) C. P. Smyth, "Dielectric Behavior and Structure," McGraw-Hill, New York, N.Y., 1958, 312 ff.

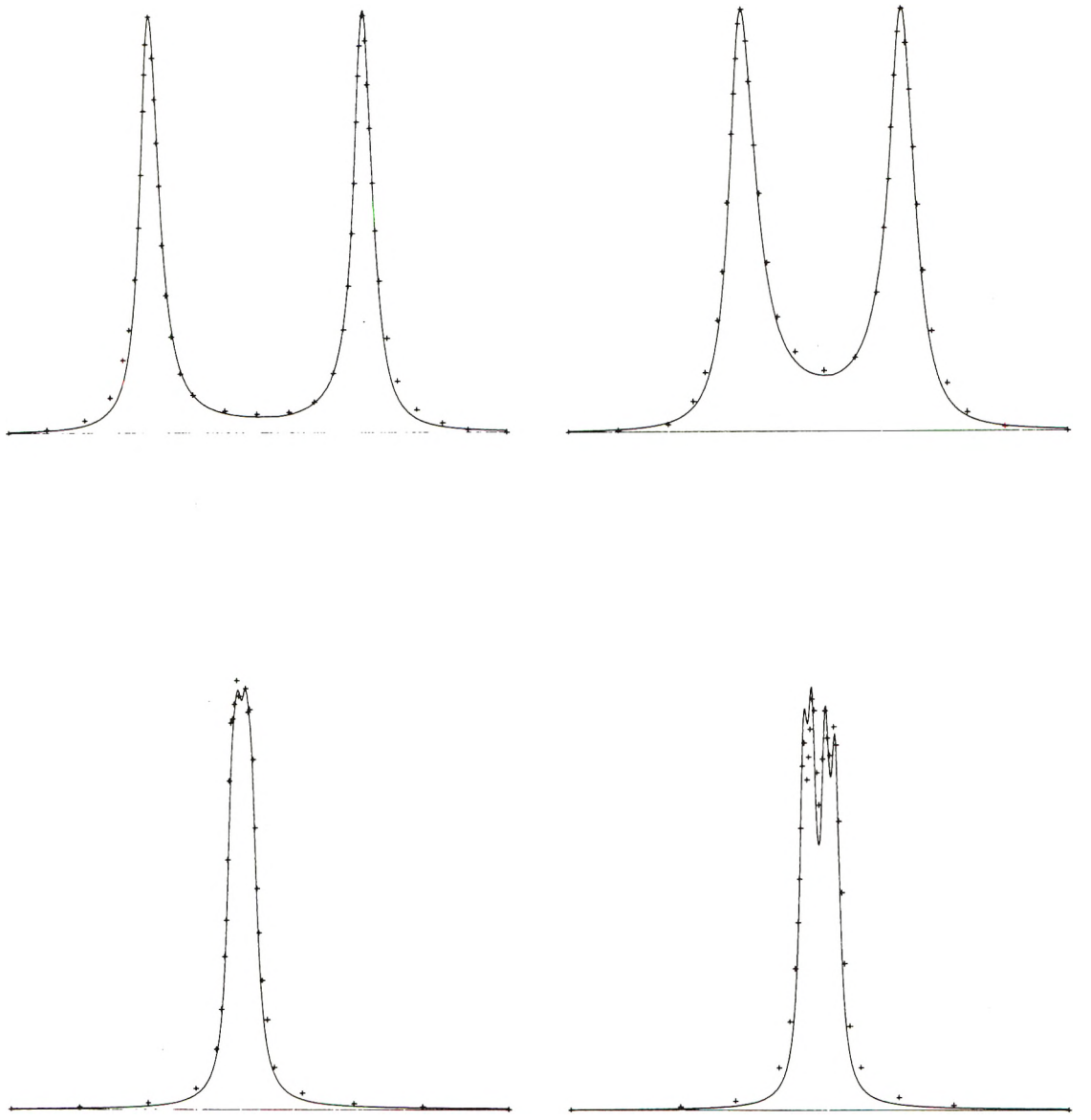

Figure 3. Fitted spectra for CHCNx(H) (experimental crosses over computer simulated spectrum): top left; k = 8.56 sec^{-1}, T = −32°, width = 79.0 Hz; top right, k = 12.4 sec^{-1}, T = −28.7°, width = 81.0 Hz; bottom left, k = 13,564.0 sec^{-1}, T = 50.3°, width = 14.65 Hz; bottom right, k = 24,950.0 sec^{-1}, T = 55.3°, width = 9.23 Hz.

steric effects may be present to some extent, a study of several compounds in the series X = H, Y = CZZ^1 where Z and Z^1 are varied among previously studied halogen and pseudohalogen substituents including hydrogen,[2] will enable more precise conclusions to be drawn about the resonance and steric contributions to $\Delta G\ddagger(N\text{-}C_{BR})$ in view of a recent parametric analysis of hindered rotation by Hückel molecular orbital and Taft substituent theories.[6]

Acknowledgment. The authors are grateful to Dr. K. N. Shaw for making available some of his computer programs.

COMMUNICATIONS TO THE EDITOR

Local Electric Field in Ice I

Sir: The relationship between the principal refractive indices and the molecular electronic polarizability of water molecules in crystalline ice I has recently been considered.[1] It was pointed out that hydrogen bonding in the crystal causes the water molecules to be effectively isotropically polarizable, and so the observed birefringence of ice I must result from anisotropies in the local electric field within the crystal lattice. A quantitative calculation of the local electric field predicted a slightly greater birefringence than has been experimentally observed. In this communication we wish to present a more general approach to the calculation of the local electric field in ice I, the results of which suggest that the previously noted discrepancy[1] is due to neglect of a small anisotropy in the time-averaged polarizability of water molecules in ice I.

The interpretation of the refractive indices of anisotropic media in terms of molecular polarizabilities is complicated by the anisotropy of the local electric field. In the case of anisotropic crystals the normal Lorenz–Lorentz equation is not valid, and account must be taken of the geometry of the crystal lattice. In an earlier paper[2] we have shown that the local electric field F_α in an anisotropic crystal may be written as

$$F_\alpha = E_\alpha + 4\pi L_{\alpha\beta} P_\beta \qquad (1)$$

where E_α is the macroscopic electric field in the crystal, $L_{\alpha\beta}$ is the Lorentz-factor tensor defined in ref 2 and P_β is the bulk polarization of the crystal. From eq 1 it is possible to derive Lorenz–Lorentz equations that are applicable to anisotropic crystals. For directions parallel to the principal axes of the optical indicatrix these may be written as

$$\alpha_{ii} + (n_i^2 - 1)(\alpha_{i\alpha} L_{\alpha i}) = (4\pi N)^{-1}(n_i^2 - 1) \qquad (2)$$

where i takes the values x, y, or z corresponding to the principal axes of the indicatrix, and a repeated greek suffix implies summation over all possible values of the suffix, *i.e.*, x, y, and z. The polarizability tensor of the molecule or atom in the crystal with respect to the indicatrix axes is $\alpha_{\alpha\beta}$, n_i are the principal refractive indices, and N is the number of molecules or atoms per unit volume. The tensor $L_{\alpha\beta}$ may be calculated exactly for any crystal structure by the method described earlier.[2] It has a trace of unity, and for isotropic crystals the tensor is diagonal with all components equal to one third. For uniaxial crystals the **L** tensor has components L_{zz} and $L_{xx} = L_{yy} = \frac{1}{2}(1 - L_{zz})$, the z direction corresponding to the optic axis; in this case eq 2 becomes

$$(n_i^2 - 1)/[1 + L_{ii}(n_i^2 - 1)] = 4\pi N \alpha_{ii} \qquad (3)$$

and the corresponding expression for the local field is

$$F_i = [1 + L_{ii}(n_i^2 - 1)]E_i \qquad (4)$$

We have calculated the components of the Lorentz-factor tensor for ice I and find that they are close to the isotropic value. Using our calculated components, one can evaluate the polarizability components of a water molecule in ice I from eq 3; our results are summarized in Table I.

TABLE I: Refractive Indices,[a] Lorentz-Factor Tensor Components and Polarizability of Ice I at −3°

	n_i (Na D line)	L_{ii}	α_{ii}
$i = z$ (optic axis)	1.3104	0.344	1.49×10^{-24} cm^3
$i = x, y$	1.3090	0.328	1.50×10^{-24} cm^3

[a] Reference 3.

From our results it would appear that the primary cause of birefringence in ice I is the anisotropy of the local electric field, as concluded by Minton.[1] In the ice I lattice each oxygen atom is surrounded tetrahedrally by four hydrogen atoms, and the oxygen atoms form a three-dimensional hexagonal lattice. In a plane perpendicular to the optic axis the hexagons of the lattice have a chair conformation, while in planes parallel to the optic axis the conformation of the hexagons of oxygen atoms is of the boat form. Since atoms are on the average closer together in the boat form than the chair form the local electric field, as determined by the Lorentz-factor tensor component, would be expected to be greater for a direction parallel to the optic axis, and this is shown by our results. A small anisotropy in the effective polarizability of water molecules in ice I is predicted by our results. We suggest that the long-range anisotropy of the lattice causes the local environment of water molecules in the crystal to be anisotropic, and this induces an anisotropy in the polarizability.

Since the components of the Lorentz-factor tensor in ice I are close to one third, we may replace L_{ii} in eq 3 by $L_{ii} = \frac{1}{3} + \delta_i$ where δ_i is the small anisotropy correction. Expanding the resulting equation as a power series in δ_i gives

$$(n_i^2 - 1)/(n_i^2 + 2) = (4\pi N \alpha_{ii}/3)[1 + 4\pi N \alpha_{ii}\delta_i + O(\delta_i^2)] \qquad (5)$$

The theory proposed by Minton gives an expression of the form

$$(n_i^2 - 1)/(n_i^2 + 2) = (4\pi N \alpha/3)[1 + \alpha f_i + O(\alpha^2 f_i^2)] \qquad (6)$$

where α is an isotropic polarizability and f_i is a structure factor. Comparing the first-order correction terms of eq 5 and 6 for the z direction, and using our calculated δ_z we find that $f_z = 4.22 \times 10^{21}$ cm^{-3}. This compares with the

(1) A. P. Minton, *J. Phys. Chem.*, **76**, 886 (1972).
(2) D. A. Dunmur, *Mol. Phys.*, **23**, 109 (1972).
(3) D. Eisenberg and W. Kauzmann, "The Structure and Properties of Water," Clarendon Press, Oxford, 1969, p 115.

value of $3.2 \pm 0.7 \times 10^{21}$ cm^{-3} calculated by Minton from his dipole lattice sum. Agreement is satisfactory in view of the slow convergence of the direct dipole summation used by Minton. Our technique for calculating dipole lattice sums uses transformations to rapidly convergent summations over the lattice and reciprocal lattice.

We conclude that our representation of the local electric field in ice I indicates that the birefringence is due mainly to the anisotropy of the local field. However, we predict a small anisotropy in the effective molecular polarizability of water molecules in ice I, which we suggest is due to interactions between the water molecules and their anisotropic environment.

Acknowledgment. Valuable correspondence with Dr. A. P. Minton is acknowledged, and one of us (P. G. C.) thanks the United Kingdom Science Research Council for a Research Studentship.

Department of Chemistry
The University
Sheffield S3 7HF, U. K.

P. G. Cummins
D. A. Dunmur*

Received July 7, 1972

Temperature Dependence of the Magnetic Susceptibility of Mercury Tetrathiocyanatocobalt

Publication costs assisted by Kernforschungsanlage Julich Zentralbibliothek

Sir: Magnetic susceptibilities are generally measured by the Gouy or Faraday method. Since both methods are relative ones, calibration substances with accurately known susceptibilities have to be used. As a very convenient calibration agent $HgCo(SCN)_4$ has been suggested[1] and has found wide application.[2] Mercury tetrathiocyanatocobalt has a gram susceptibility of 16.44 ($\pm$0.08) $\times 10^{-6}$ emu/g at 20°. The temperature dependence has been measured down to 80°K[3] and follows within this range the Curie-Weiss law $\chi_g = C/T - \Theta$. By extrapolation to $1/\chi_g = 0$ the authors find for the Weiss constant a value of $\Theta = -10$°K.

Since this substance might also be useful for calibrations at low temperatures we extended the investigations to 5°K. We used a commercial helium flow type cryostat (Leybold) to establish temperatures between 5 and 300°K. Helium gas at a pressure of 10 Torr served as heat exchanger between the sample and the cold plate of the cryostat. The temperature was measured by means of a calibrated carbon resistor and a gold (+0.03% Fe)-alumel thermocouple. We employed the Faraday method and calibrated our system at room temperature with conductivity water ($\chi_g = -0.720 \times 10^{-6}$ emu/g) and mercury ($\chi_g = -0.1667 \times 10^{-6}$ emu/g). Since calibrations with water can be falsified by dissolved oxygen due to its high paramagnetic susceptibility, we drove it off quantitatively by bubbling helium through it for some time. Hereafter the water was enclosed in small quartz bulbs, which served as sample holders. Our vacuum balance (Sartorius) allowed us to observe changes in weight of 1 μg. With our magnetic system, fields up to 15 kG could be applied.

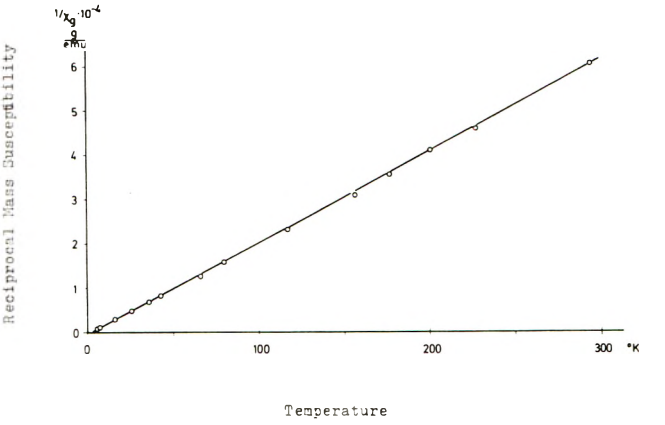

Figure 1. Reciprocal of the measured mass susceptibility *vs.* temperature.

The mercury tetrathiocyanatocobalt was prepared as recommended,[1] and introduced into quartz sample holders whose diagmagnetic susceptibility showed no temperature dependence. We measured eight different samples weighing between 2 and 25 mg and found no field dependence at room temperature or at 5°K. Above 15°K the reproducibility of the different measurements was always better than 1%, whereas below this temperature we observed larger deviations due to temperature fluctuations.

TABLE I

Temperature, °K	293	227	203	177	157	117	80
Susceptibility, 10^6 emu/g	16.45	21.85	24.54	28.47	32.40	43.60	63.3
Temperature, °K	66	43	36.5	26	16.5	7.2	5.8
Susceptibility, 10^6 emu/g	79.8	121.3	144.1	206.1	341.7	879.7	1237

The results of a typical run are given in Table I. In Figure 1 the reciprocal of the measured mass susceptibility is plotted against temperature, and is found to follow the Curie-Weiss law down to the lowest temperature. For room temperature we find the same value as the above-mentioned authors;[1] however, the Weiss constant determined is $\Theta = +2$°K, indicating that the former extrapolation from 80°K has lead to an erroneous result.

(1) B. N. Figgis and R. S. Nyholm, *J. Chem. Soc.*, 4190 (1958).
(2) L. N. Mulay, *Anal. Chem.*, **34**, 343 (1962); W. Bronger and H. Schuer, *Chem. Ing. Tech.*, **40**, 961 (1968); H. Kessler and M.-J. Sienko, *J. Chem. Phys.*, **55**, 5414 (1971).
(3) B. N. Figgis and R. S. Nyholm, *J. Chem. Soc.*, 338 (1959).

Institute for Physical Chemistry
517 Julich 1, Germany

H.-St. Rade

Received September 28, 1972

Radiolytic Yields of Hydrated Electrons at 30 to 1000 Picoseconds after Energy Absorption

Publication costs assisted by U.S. Atomic Energy Commission

Sir: The yield of hydrated electrons (e_{aq}^-) has been studied by numerous experiments at microsecond times.[1] Under homogeneous conditions, when e_{aq}^- escapes the spur, most experiments agree that the yield is 2.7 ± 0.1 e_{aq}^- per 100-eV absorbed energy.[2] The initial tight cluster of reactive species (spur) is formed by the ionizing radiation and an unknown fraction of these species recombines before the spur relaxes into a homogeneous distribution. The initial yield of e_{aq}^- before it escapes the spur is an extremely critical parameter of the diffusion kinetic theories of the spur.[3,4] It is also important in deciding between mechanisms which give rise to the yields of radiation products in concentrated solutions and the unusual competition behavior at these high concentrations.[5]

Direct measurements of electron absorption to determine the initial G value of the hydrated electron before it expands from the spur are difficult since one requires time resolution to better than 1 nsec, and a dose measurement in the same spatial region as that where the absorption spectrum is being measured. Signal-to-noise limitations preclude spreading and scattering the electron beam to make it uniform over a large irradiation cell.

We have directly measured $G(e_{aq}^-)$ by two entirely different techniques at times shorter than 1 nsec and at 30 psec and obtain a value 4.0 ± 0.2. In Table I we list the G values with the different techniques and dosimeters.

Only a simplified sketch of the experimental techniques will be given here, and complete details of the two measurements will be published later in separate papers. The stroboscopic pulse radiolysis (SPR) apparatus at Toronto[6] was used to give the value 4.0 ± 0.2 at 30 psec. The details of the SPR system are described in other papers.[6-8] This system observes the kinetics of e_{aq}^- between the linac fine structure pulses spaced at 350-psec intervals. The 40-MeV electron beam both irradiates the sample, and forms its own analyzing light. At Argonne a single fine structure pulse was used, coupled with fast detection equipment. The measurement for times less than 1 nsec used a sampling oscilloscope (SO) with a rise time of 25 psec (Tektronix 7000 series with a S-4 sampling head) and a F4014 photoidode (ITT), with either a S-4 or S-20 photocathode. Two pulsed-ion lasers were used to analyze the signals at wavelengths of 514.5 or 647.1 nm. The data were accumulated by using a multichannel analyzer. The photodiode has a risetime of less than 100 psec (some overshoot makes the settling time longer, but less than 1 nsec).

The most vexing problem with the determination of $G(e_{aq}^-)$ was measuring the dose which produced the observed optical absorption. Four different dosimeters were used, two with SO-PR system and two with the SPR system. Table I shows the excellent agreement between all four methods. This consistency underscores the confidence in the measured value of $G(e_{aq}^-)$.

With the SO-PR system, 0.01 M air-saturated thiocyanate[9] and the oxygen-saturated "super Fricke" dosimeters were used.[10] For the thiocyanate dosimeter, the same analyzing light beam (argon ion laser at 514.5 nm) was used to measure both $(SCN)_2^-$ and e_{aq}^-. The super Fricke was irradiated in a cell comparable to the dimensions of the electron beam.

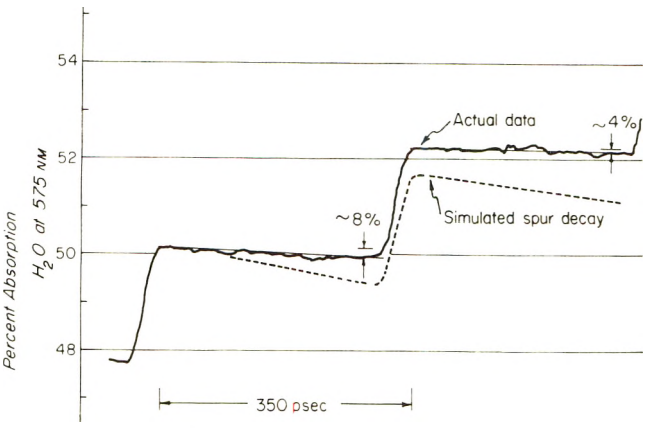

Figure 1. The e_{aq}^- signal in H_2O using the stroboscopic pulse radiolysis (SPR) technique is shown. There is little decay of the signal during the time window from 30 to 350 psec which agrees with the observed decay rate of 10^8 sec^{-1} indicated by the expression, $G(e_{aq}^-) = 2.7 + 1.4 \exp(-10^8 t)$. A simulated spur decay[12] using the calculations of Kuppermann[3] shows that a large discrepancy occurs. The 8 and 4% are the percentage deviations from flatness referred to one step as 100%, and are *not* 8 and 4% decay of the total e_{aq}^- concentration. As seen in the numbers at left the total absorption is about 50%. Further, in any step the decay is a composite of the decays of electrons of different ages (see ref 6-8).

With the SPR system, both the hydrated electron dosimeter and a Perspex dosimeter[11] were used. The solvated electron dosimetry was done by conventional PR using a He-Ne laser as an analyzing light source through the same irradiation volume (delineated by 3-mm apertures). The e_{aq}^- absorption was measured at 100 nsec and a G value of 2.7 was assumed. The Perspex dosimetry was done by irradiating a block of six Perspex slabs spaced to correspond to the length and density of the sample cell. Again 3-mm apertures delineated the analyzing volume and were used with the spectrophotometer to determine the change in absorbance and hence the dose.

The yield after 30 psec (SPR) and before 1 nsec (SO-PR) can both be called *initial* yields since there is very little observable decay of e_{aq}^- between 30 and 1000 psec. Using SPR, there was no observed decay of e_{aq}^- over the 30-350-psec interval as shown in Figure 1.[12] The SO tech-

(1) E. M. Fielden and E. J. Hart, *Radiat. Res.*, **32**, 564 (1967).
(2) E. J. Hart and M. Anbar, "The Hydrated Electron," Wiley-Interscience, New York, N. Y., 1970.
(3) A. Kuppermann, "Radiation Research," G. Silini, Ed., North Holland Publishing Co., Amsterdam, 1967.
(4) H. A. Schwarz, *J. Phys. Chem.*, **73**, 1928 (1969).
(5) P. L. T. Bevan and W. H. Hamill, *Trans. Faraday Soc.*, **66**, 2533 (1970).
(6) M. J. Bronskill, W. B. Taylor, R. K. Wolff, and J. W. Hunt, *Rev. Sci. Instrum.*, **41**, 333 (1970).
(7) M. J. Bronskill, R. K. Wolff, and J. W. Hunt, *J. Chem. Phys.*, **53**, 4201 (1970).
(8) J. E. Aldrich, P. Foldvary, J. W. Hunt, W. B. Taylor, and R. K. Wolff, *Rev. Sci. Instrum.*, **43**, 991 (1972).
(9) E. M. Fielden and N. W. Holm, "Manual on Radiation Dosimetry," N. W. Holm and R. J. Berry, Ed., Marcel Dekker, New York, N. Y., 1970, p 288.
(10) H. Fricke and E. J. Hart, "Radiation Dosimetry," Vol. 2, F. H. Attix and W. C. Roesch, Ed., Academic Press, New York, N. Y., 1966, p 226.
(11) R. I. Berry and C. H. Marshall, *Phys. Med. Biol.*, **14**, 585 (1969).
(12) R. K. Wolff, M. J. Bronskill, J. E. Aldrich, and J. W. Hunt, *J. Phys. Chem.*, submitted for publication.

TABLE I: Initial Yields of Hydrated Electrons

Pulse radiolysis techniques	Dosimetry Type	Dosimetry krads	λ, nm	Earliest times	G
(a) Sampling (SO-PR)					
1. Absolute	$(SCN)_2^-$	(1) 2.18	514.5	<1 nsec	4.06 ± 0.1
		(2) 2.40	514.5	<1 nsec	4.16 ± 0.1
			514.5	<1 nsec	4.0 ± 0.2
2. Relative	Super Fricke G = 2.9 at 30 nsec	0.3–3	514.5	<1 nsec	4.1 ± 0.2
(b) Stroboscopic (SPR)					
1. Absolute	HX-Perspex		633	30 psec	4.0 ± 0.2
2. Relative	G = 2.7 at 0.1 μsec		633	30 psec	4.0 ± 0.3

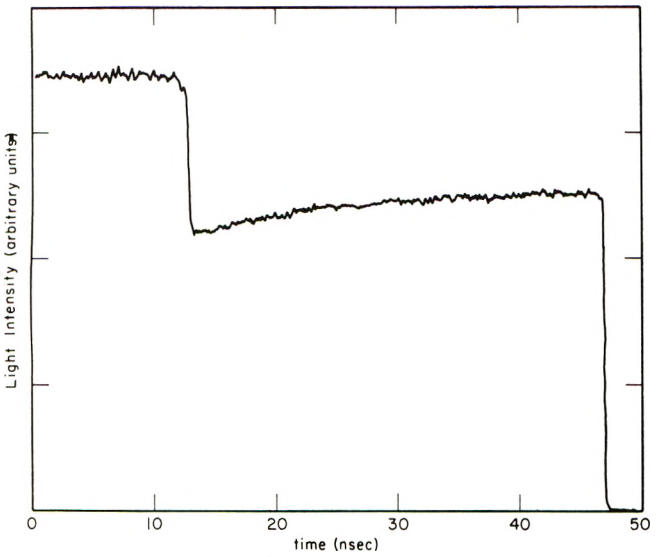

Figure 2. Transmission of irradiated water at 514.5 nm showing 100% light (far left), absorption by hydrated electron (center), and zero light (far right). This observation made with the SO-PR technique. A similar experiment with 2-nsec total sweep showed no decay from ~100 to 1000 psec within experimental error. The initial photodiode ringing was about 5% (peak-to-peak) of total absorption. These electrons all have the same age ± ~25 psec.

nique with its extended time range showed that the e_{aq}^- absorption decreased from its initial value of 4.1 to an apparent plateau of 2.9 after 30 nsec with an initial rate of 3×10^7 sec^{-1} relative to the total concentration of e_{aq}^- (Figure 2). At longer times, this decay agrees with the observations made previously by Thomas and Bensasson[13] and also more recently by Buxton,[14] and can be empirically fit by the equation $G(e_{aq}^-) = 2.7 + 1.4 \exp(-10^8 t)$. Previous yields obtained with apparatus of a few nanoseconds rise time and extrapolated to zero time must be viewed with caution as the specific electronics used will modify the appearance of the early kinetics.

The form of the decay of the hydrated electron in the time from 10^{-11} to 10^{-8} sec is quite different from that predicted by diffusion models.[3,4] Schwarz[4] predicted a $G^\circ(e_{aq}^-)$ of 4.8 and a very fast initial decay (in the time region where we find little decay) to about 3.5 at 1 nsec and to 3.0 at 10 nsec. With this in mind, it is not surprising that the initial $G(e_{aq}^-)$ we measure is not the same as the $G^\circ(e_{aq}^-)$ diffusion theory finds necessary to predict experimental scavenger data. At present we have not attempted to correlate our measurements with the data which the diffusion model fits well; however, preliminary analysis of data from several e_{aq}^- scavenger experiments shows that the form of product yield *vs.* concentration can be predicted quite nicely. This is not a confirmation of our measurements, of course, but a piece of evidence which is consistent with our data.

We now consider possible explanations of these results. A trivial explanation could be that the observed nanosecond traces are simply the result of spectral shifts with time. However, the G values and kinetics are the same using the red laser (647.1 nm) as the green one (514.5 nm). In addition, the spectrum of e_{aq}^- in psec times is the same as μsec times,[7] so spectral shifts are not the explanation. Another possibility is that there are two different components in the spur, so that the decay according to spur diffusion theory is balanced for a certain period of time by the formation of new e_{aq}^- species formed from excited states. A third possibility is that the initial spatial distribution of electrons is much wider than expected and the spur contains more reacting species. In any case, further diffusion kinetic calculations are needed to fit these results.

Acknowledgment. This communication is based on work supported by the U. S. Atomic Energy Commission and by the Medical Research Council of Canada and the National Cancer Institute of Canada.

(13) J. K. Thomas and R. V. Bensasson, *J. Chem. Phys.*, **46**, 4147 (1967).
(14) G. V. Buxton, *Proc. Roy. Soc., Ser. A*, **328**, 9 (1972).

Department of Medical Biophysics
University of Toronto
and Physics Division
Ontario Cancer Institute
Toronto, Canada
John W. Hunt
R. K. Wolff
M. J. Bronskill

Chemistry Division
Argonne National Laboratory
Argonne, Illinois 60439
Charles D. Jonah
E. J. Hart
Max S. Matheson*

Received November 19, 1972

The ADVANCES IN CHEMISTRY Series...

Excellent Reviews in Book Form of Specialized Chemical Topics

For comprehensive reviews of all the important aspects of a chemical subject... read the books in the ADVANCES IN CHEMISTRY Series.

Ranging up to 750 pages in length, ADVANCES volumes include...

- Authoritative, thought-provoking articles by as many as several dozen scientists per volume.
- Carefully compiled collections of data.
- Groups of related papers presented at important national and international symposia.
- Invited reviews of current work written by researchers eminent in the field discussed.

With the ADVANCES you learn about brand-new chemical subjects... and bring yourself up to date on familiar chemical topics. The numerous scientists contributing to each volume provide you with stimulating reading enriched by a variety of viewpoints. And the ADVANCES bring material together under one cover which would otherwise be scattered among many journals... *or not available at all.*

... Put chemical topics of interest to you in proper perspective. Read the ADVANCES IN CHEMISTRY Series.

Listed here are the 26 most recent titles in the ADVANCES IN CHEMISTRY SERIES.

No.	Title	Price	Cost
103	**Origin and Refining of Petroleum**	230 pp (1971)	$10.00
102	**Molecular Sieve Zeolites--II**	459 pp (1971)	$16.00
101	**Molecular Sieve Zeolites--I**	526 pp (1971)	$16.00
101	**and 102 ordered together**		$30.00
100	**Bioinorganic Chemistry**	436 pp (1971)	$14.00
99	**Multicomponent Polymer Systems**	598 pp (1971)	$16.50
98	**Platinum Group Metals and Compounds**	165 pp	$9.00
97	**Refining Petroleum for Chemicals**	293 pp (1970)	$11.50
96	**Engineering Plastics and Their Commercial Development**	128 pp (1969)	$7.50
95	**Cellulases and Their Applications**	470 pp (1969)	$14.50
94	**Dietary Chemicals vs. Dental Caries**	186 pp (1970)	$9.00
93	**Radionuclides in the Environment**	529 pp (1970)	$15.00
92	**Epoxy Resins**	230 pp (1970)	$10.50
91	**Addition and Condensation Polymerization Processes**	767 pp (1969)	$19.50
90	**Fuel Cell Systems--II**	446 pp (1969)	$17.50
89	**Isotope Effects in Chemical Processes**	278 pp (1969)	$13.00
88	**Propellants Manufacture, Hazards, and Testing**	395 pp (1969)	$12.00
87	**Interaction of Liquids at Solid Substrates**	212 pp (1968)	$9.50
86	**Pesticidal Formulations Research. Physical and Colloidal Chemical Aspects**	212 pp (1969)	$9.50
85	**Stabilization of Polymers and Stabilizer Processes**	332 pp (1968)	$12.00
84	**Molecular Association in Biological and Related Systems**	308 pp (1968)	$10.50
83	**Chemical Marketing: The Challenges of the Seventies**	199 pp (1968)	$9.50
82	**Radiation Chemistry--II**	558 pp (1968)	$16.00
81	**Radiation Chemistry--I**	616 pp (1968)	$16.00
81	**and 82 ordered together**		$30.00
80	**Chemical Reactions in Electrical Discharges**	514 pp (1969)	$15.00

Prices postpaid in U. S. and Canada, plus 35 cents elsewhere. For copies and/or information on these or on 74 other titles in this series, address

Special Issues Sales, Dept. 201

American Chemical Society
1155 Sixteenth St., N. W.
Washington, D. C. 20036

Good students need the best texts . . .

PHYSICAL CHEMISTRY, Third Edition

Gordon Barrow
1973, 928 pages (tent.), (003823-6), $16.95
An Instructor's Manual will be available.

In this edition, the author responds to progress in the field by updating molecular-level material and by reorganizing and tightening the interrelation of this material with macroscopic features. Requiring only a background in college-level general chemistry and introductory mathematics, this volume provides tools and information of value in interpreting thermodynamic properties, states of matter, and kinetic results. This revision offers rewritten, reorganized, and updated material in a number of areas, as in the sections on atomic and molecular structure, crystal structures, and elementary reactions. There are also new treatments of molecular energies, chemical kinetics, and the deduction of thermodynamic properties from molecular quantities. The discussion of multicomponent solutions has been recast so that more use is made of the earlier thermodynamic results.

ANALYTICAL CHEMISTRY

James G. Dick, Sir George Williams University, Montreal, Canada
1973, 640 pages (tent.), (016786-9), $13.95 (tent.)
An Instructor's Manual will be available.

Unusually clear and easy to read, this text seeks to introduce students to gravimetric, volumetric, and instrumental techniques while emphasizing the theory underlying their development. The precision, accuracy, and inherent limitations of each technique are debated in order to stress the need for proper evaluation of data and results. An extensive treatment of chemical equilibria is offered, as are discussions of titration theory, titration curves, and the interpretation of analytical data. In all cases, however, general principles are emphasized in order to encourage the student's awareness of similarities (as well as differences) among diverse chemical groups and techniques. A complete laboratory manual is included as the final chapter of the text; experiments have been carefully chosen to provide experience in both classical and modern methods and to expose students to analysis of inorganic, organic, pharmaceutical, and biochemical materials.

DIGITAL COMPUTERS IN SCIENTIFIC INSTRUMENTATION: Applications in Chemistry

Sam P. Perone, Purdue University, and David O. Jones, Independent Consultant, Chemical Instrumentation
1973, 420 pages (tent.), (049319-7), $7.95 (tent.) Soft cover

This text seeks to teach laboratory computer techniques and digital instrumentation to graduate and upper-level undergraduate students. It is valuable for general reference or as a supplemental text for general courses in scientific instrumentation. Topics covered include fundamentals of small computer programming, digital logic, experimental interfacing, time-sharing, and utilization of hierarchical computer structures.

FUNDAMENTALS OF MOLECULAR SPECTROSCOPY, Second Edition

C. N. Banwell, University of Sussex, England
1972, 360 pages, (084007-5), $9.95 Soft cover

This text explains the principles of spectroscopy in pictorial rather than mathematical terms. SI units are now used throughout (except for the wavenumber), and additions include brief discussions of photoelectron spectroscopy, Mössbauer spectroscopy, Fourier transform techniques as applied to infra-red and n.m.r. spectroscopy, the use of lasers in Raman spectroscopy, and the mechanism of lasers.

. . . like the ones we publish. McGraw-Hill

(clip here)

To order simply fill out this coupon and return to:

Norma-Jeanne Bruce / Dept. PC / College Division, 27
McGRAW-HILL BOOK COMPANY
1221 Avenue of the Americas / New York, New York 10020
☐ Barrow (003823-6) ☐ Banwell (084007-5) ☐ Dick (016786-9) ☐ Perone-Jones (049319-7)

Within 10 (ten) days of receipt of book(s) I will remit full price of book(s) plus local sales tax, postage, and handling. (McGraw-Hill pays postage and handling if I remit in full with this coupon.) I will return unwanted book(s) postpaid.

Name_____ Affiliation_____

Address_____ City_____ State_____ Zip_____

Prices subject to change without notice. Offer good in USA only.

62 Rev N1/2010762

23 W.A. 25%